Quantum Ratchets

Quantum Ratchets

Proefschrift

ter verkrijging van de graad van doctor
aan de Technische Universiteit Delft,
op gezag van de Rector Magnificus prof. dr. ir. J. T. Fokkema,
voorzitter van het College voor Promoties,
in het openbaar te verdedigen op vrijdag 16 september 2005 om 10.30 uur
door

Joël PEGUIRON

Physicien diplômé,
Université de Neuchâtel,
geboren te Neuchâtel, Zwitserland.

Preface

This thesis is the result of four years of research. It has greatly benefited from the contributions of many people. Furthermore, my life during my time in Delft and later in Regensburg would not have been as happy as it has been without the presence and the support of many relatives, friends, and colleagues. Let me express here my gratitude to them.

First of all, this thesis would not have been possible without my "daily" supervisor Milena Grifoni and my "official" supervisor Gerrit Bauer.

Dear Milena, you have been a wonderful supervisor, and you have also been much more than a supervisor! Among your scientific qualities, I have admired your perpetual enthusiasm, your tireless perseverance and your amazing intuition which I have never been able to fault. I have appreciated your mathematical rigor as well as your flexible and at the same time exigent attitude towards my work. Even in your busiest days you have found time and patience to discuss when necessary. You probably remember as well as I do that my research project has not been easy every day, as it is normal I guess in such an endeavor. Nevertheless, it has been a daily pleasure for me to go to work during these years. This is also due to your great human qualities. I have valued that, during our collaboration, we have been inclined to discover each other's interests outside professional life, for example at the occasion of our weekly jogging breaks or when you invited me at your place when we were moving to Regensburg. Thank you and your family for your hospitality at this occasion. On the whole, I have learned very much on a scientific and on a human point of view at your contact. I wish that we will keep a fruitful collaboration for a long time! Thank you very much Milena, good luck for the continuation of your career and all the best to your family.

Gerrit, your very flexible and friendly attitude as well as your total confidence in the administration of my thesis project have made it a simple and almost pleasant task. I have appreciated scientific discussions at the occasion of group seminars and yearly evaluations. From you I have also learned a lot about the politics of scientific research and I think that your group benefits very much from your engaged management. Thank you and all the best!

The work presented in this thesis has greatly benefited from collaborations and

The soul of the Delft group is its secretary, Yvonne Zwang, who among other tasks tirelessly takes care of the sacred coffee break. She has also been my main Dutch teacher and a successful one. She is known as "the best secretary of the world" and to my opinion definitely deserves it. Dear Yvonne, thank you for everything and all the best! The permanent staff of the group was completed at my time by Yuli Nazarov, Yaroslav Blanter, and Jos Thijssen. Yuli, I would not tell the full truth if I would not mention the vivid experience of your uncompromising attitude during group seminars. This attitude has given me a lot to think about, and still does, which probably already demonstrates its usefulness. The reason is that it was so orthogonal to my spontaneous feelings, but at same time I had to recognize its pertinence on a strictly scientific point of view. I have reached the conviction that your chief motivation at these occasions was a strong feeling of responsibility for the students of your group, and especially for their education, and I feel very grateful to you for that. Indeed I think I have learned important things from you. I also admire you for being one of the most brilliant scientists whom I have interacted with. Yaroslav, your broad range of interests has been the source of many instructive discussions. I have also enjoyed speaking French with you. Jos, it has been very nice to share your musical interests. My colleagues have rendered my time in Delft absolutely unforgettable. With Freek Langeveld, I have not only shared interesting scientific discussions, but also endless evenings devoted to gastronomy, beer tasting, music listening, and philosophizing. We have also enjoyed playing chamber music together and done many beautiful hiking tours. Dear Freek, thank you for these privileged moments and for having given me the chance to better discover your country, and all the best! With Daniel Huertas Hernando, everything has started with our common duty as computer administrators of the group. Due to the outstanding personality of Dani, this rather ungrateful task has soon turned into the development of a great friendship which we have pursued by many activities. Dear Dani, thank you for everything and all the best! From Gabriele Campagnano I have had the pleasure of learning and discovering many things in Jazz music, including his own playing and the secrets of custom-built trumpets. I have also appreciated his enthusiastic company as an office mate and his support in my work at some occasions. Thank you Gabriele and all the best! Many thanks also to the other members or guests of the group, Dima Bagrets, Miriam Blaauboer–your always positive attitude has been a great support!, Antonio DiLorenzo, Siggi Erlingsson–it was nice to meet you again in Basel!, Max Geerts, Sijmen Gerritsen, Wataru Izumida, Oleg Jouravlev–your laugh is agreeably contagious!, Markus Kindermann, Alex Kovalev, Takeshi Nakanishi, Elisabetta Paladino–it was nice of you to regularly bring us a piece of Sicilian sun!, Alessandro Romito, Jens Tobiska, Omar Usmani–thanks also for keeping my mail!, and Wouter Wetzels–I would have been very happy if you would have joined us in Bavaria!, for interesting discussions and nice time together, and all the best to all of you! I have also enjoyed plenty of interesting discussions and various activities with many members of other research groups including Patrice Bertet, Ruth de Boer,

Jeroen Elzerman, Silvano De Franceschi, Flavius Gligor, Marlies Goorden, Alexander ter Haar, Ronald Hanson, Florin-Ovidiu Iancu, Pablo Jarillo-Herrero, Jeong-O Lee, Adrian Lupascu, Hon Tin Man, Frank Meijer, Stefan Oberholzer, Eugen Onac, Saverio Russo, Sami Sapmaz, Erwin Slot, Lieven Vandersypen, Laurens Willems van Beveren, and Keith Williams.

After two years in Delft I have moved to Regensburg, following the appointment of Milena as a professor there. I have witnessed the exciting time of the formation of her new research group. The very kind help of our secretary Lizy Lazar has been precious to me when dealing with administrative matters. Thank you Lizy and all the best! I have appreciated Shidong Wang for being a very pleasant office mate. This has been the occasion of many instructive discussions on various topics. Thank you Shidong for these nice moments, as well as for your delicious meal at the Spring Festival, and all the best! Francesco Nesi has been one more colleague with whom I could enjoy plenty of activities beyond physics. I have admired his poetic and musical talents. Dear Francesco, thank you for these unforgettable evenings and all the best! The group has grown further and I could enjoy many interesting discussions and nice time with Georg Begemann, Andrea Donarini–it was nice to play quartet!, Martina Hentschel–many thanks for your always-at-hand comforting pralines!, Leo Mayrhofer–it was nice to play Schafkopf (another type of quartet)!, and Roman Mazurok, as well as with many members of other research groups including Giovanni Cuniberti, Dana Darau, Joachim Keller, Christian Lechner, Magdalena Marganska, Florian Otto, Emiliano Pallecchi, Pasquale Pavone, Angela Reisser, Klaus Richter, Bernhard Rieder, Peter Schlagheck, Jens Siewert, Dieter Strauch, Christoph Strunk, Elsa Thune, and Janina Zimmermann. Thank you all and all the best!

I am also very grateful to Hans van der Wielen, Fritz Wünsch, and Rudi Holzer for their very professional and friendly computer support.

Finally, I would like to add special thanks to my employer, the Foundation FOM, for having been extremely unbureaucratic and generous at the occasion of my two years' secondment in Germany. I am also grateful to the University of Regensburg for hospitality and "logistic support" during this time.

I will keep these nominal acknowledgements to the people whom I have professionally been involved with, but this should by no means hide the importance of the ones who have supported me in other ways and rendered my life so happy during this time. Especially, I am deeply grateful to all the people whom I have had the privilege and pleasure to play music with, in no less than seven countries. This has been the source of many enriching discoveries, deep exchanges, as well as valuable friendships. As always last and never least, my parents may legitimately regard this thesis as a success of their wonderful education. I am deeply indebted to them, as well as to my adored sister and brothers, grand-parents, relatives, and close friends for their hospitality at many occasions, their boundless support, and their love.

Joël Peguiron
Regensburg, August 2005

Contents

Chapter 1

Introduction

1.1 Ratchet systems

1.1.1 Classical ratchets

A ratchet system is a spatially periodic system which exhibits directed transport in the presence of unbiased external forces. Its name comes from the asymmetric toothed wheel which one finds, e.g., in the music instrument bearing the same name, in some screwdrivers and tighteners, in bicycles, and in clockworks. Another generic example of ratchet systems is provided by windmills. The wind blowing in the asymmetric sails of a windmill puts them into rotation. A mechanics converts this motion into useful work, like water pumping or grain milling. The miller has to orient the windmill in front of the wind direction.

To be more definite, we are interested in devices in which the breaking of spatial symmetry necessary for the emergence of the preferred direction of transport is intrinsic to the system, whereas the external forces furnishing the energy necessary for the transport do not induce any additional asymmetry. The emergence of work in such a situation is called the ratchet effect. For reviews, see Refs. [1, 2]. For an introductory article, see, e.g., Ref. [3].

The simplest theoretical model one can think of in order to investigate ratchet systems is a particle in a one-dimensional space. The particle of mass M is subject to a spatially periodic and asymmetric potential $V(q)$, as well as to an unbiased driving force $F(t)$. In a realistic situation, the particle can be coupled to a thermal environment. Then, it also experiences a viscous force proportional to the velocity, with viscosity coefficient η, and a stochastic force $\xi(t)$. The classical equation of motion of such a system reads

$$M\ddot{q}(t) + \eta\dot{q}(t) + \frac{\mathrm{d}}{\mathrm{d}q}V(q) = F(t) + \xi(t). \tag{1.1}$$

In this model, the release of work is manifested by a nonzero particle velocity $\dot{q}(t)$. When all forces are unbiased, the ratchet effect is characterized by the persistence of a nonzero velocity at any time t late enough after the initial time t_0 so that transients have died out. The quantity of interest for ratchet system is thus the stationary velocity

$$v^{\infty}(t) = \lim_{t \gg t_0} \dot{q}(t). \qquad (1.2)$$

In the absence of the potential $V(q)$ and of the driving force $F(t)$, equation (1.1) provides a description of Brownian motion, the incessant random motion of pollen particles suspended in water observed in 1827 by Brown [4]. As Brown himself acknowledges, this motion had been reported by others before him, among others van Leeuwenhoek in the seventeenth century. However, Brown was the first to identify the molecular origin of this motion, rather than to attribute it a biological, "animalcular", origin. The microscopic theory, developed by Einstein in one of his famous 1905 papers [5], followed by Smoluchowski [6], was verified in experiments by Perrin, which contributed to the confirmation of the existence of atoms and led to a determination of the Avogadro number. For an overview, see, e.g., Ref. [7] and references therein.

The equation of motion (1.1) comprises different kinds of ratchet systems (see Ref. [1] and references therein). First of all, the stochastic force $\xi(t)$ does not necessarily have to be of thermal nature. This applies especially to macroscopic examples. A question underlying many investigations on classical ratchets is the identification of the conditions that the stochastic force has to fulfill in order that a nonzero work can be generated.

In microscopic realizations of ratchet systems however, one is primarily interested in situations where the stochastic force $\xi(t)$ and the drag force $-\eta\dot{q}(t)$ originate from the coupling to a thermal bath. In such systems, one attempts to extract energy out of thermal fluctuations. Engines working according to this principle are also known as Brownian motors. To reach this purpose, one has to break thermal equilibrium in some way. Indeed, as shown by Smoluchowski [6] and Feynman [8, Ch. 46] (see, however, the excellent criticism given in Ref. [9]), no work can be extracted out of a ratchet system acting at thermal equilibrium. This would violate the Second Principle of Thermodynamics.

A variety of ratchet systems which have been investigated are the so-called temperature ratchets [10], where the bath temperature is periodically varied. In another variety, the flashing ratchets, the potential is periodically turned off and on again.

When the bath temperature and the potential stay constant in time, the driving force $F(t)$ is responsible for breaking the thermal equilibrium and furnishes the energy necessary to generate work. One considers a force alternating in time, and unbiased, in order not to introduce any asymmetry other than the spatial asymmetry of the potential [11]. As the effect of the force can be visualized as a rocking of the potential, one speaks of rocked ratchets. This is the model that we will study in this

thesis. A very natural case is an ac driving force of amplitude F and frequency Ω,

$$F(t) = F\cos(\Omega(t - t_0)). \tag{1.3}$$

Another case of interest is given by an unbiased bistable force switching between the values $\pm F$. This case is especially interesting in the adiabatic limit, when the switching rate of the bistable force is much slower than any other time scale of the system. Then, the particle velocity $v_{\mathrm{R}}^{\infty} = \lim_{t \gg t_0} \dot{q}(t)$ of the ratchet system can be linked to the stationary velocity $v_{\mathrm{DC}}^{\infty}(F) = \lim_{t \gg t_0} \dot{q}(t)$ in a tilted ratchet system, that is with a time-independent force of magnitude F. A tilted ratchet is not a ratchet system in the sense developed above, because a nonzero time-independent driving force is of course not unbiased. However, the ratchet effect can be investigated in such a system as well, and it manifests itself by the fact that the stationary velocity $v_{\mathrm{DC}}^{\infty}(F)$ is not an antisymmetric function of the driving F. Indeed, one has the relation

$$v_{\mathrm{R}}^{\infty} = v_{\mathrm{DC}}^{\infty}(F) + v_{\mathrm{DC}}^{\infty}(-F). \tag{1.4}$$

Instead of the stationary velocity $v^{\infty}(F)$, one often speaks in terms of the mobility $\mu(F)$, defined through the relation

$$v^{\infty}(F) = \mu(F)F. \tag{1.5}$$

The linear mobility denotes the small driving limit $\lim_{F \to 0} \mu(F)$.

Finally, we will mention a different category of ratchet systems, where the spatial asymmetry of the potential $V(q)$ is replaced by a temporal asymmetry in the driving force $F(t)$. Such time ratchets have been investigated, e.g., in Refs. [12–14].

Conceptually, the ratchet effect is linked to Parrondo's paradoxical games [15], where the alternation between two loosing games can surprisingly lead to a winning game.

1.1.2 Quantum ratchets

In the last decade, a new question has arisen, whether and how the properties of ratchet systems operating in the regime of quantum mechanics are modified with respect to their classical counterpart. An overview of existing theoretical works on quantum ratchets will be given in the next section. Some experiments will be mentioned in Chapter 2, before discussing one of them in detail.

What is expected to change for quantum ratchets in comparison to classical ratchets? To give a heuristic answer to this question, let us recall that an essential ingredient for the emergence of a nonzero particle velocity in a ratchet system is the possibility of thermal activation above the barriers of the potential, due to the exchange of energy with a bath initially at some temperature T. In the classical regime, the thermal activation rate Γ over a potential barrier of height ΔV is governed by an Arrhenius factor

$$\Gamma \propto \mathrm{e}^{-\Delta V/k_{\mathrm{B}}T}, \tag{1.6}$$

where k_B denotes Boltzmann constant. One of the major consequences is that the particle current, which is essentially proportional to the balance between the rates to the left and to the right [see, e.g., Eq. (4.39)], vanishes at zero temperature.

In the quantum regime, however, another mechanism, quantum tunneling through the potential barrier, becomes relevant in conjunction with thermal activation. Consequently, as the temperature goes to zero and the bath degrees of freedom are frozen, one may expect that the particle current tends to a nonzero value, due to the persistence of tunneling processes. This behavior has been predicted in [16] and observed in a similar experimental system [17] (see also Fig. 2.5).

Furthermore, having in mind the WKB formula for the transmission coefficient T_{tun} of a particle tunneling at energy E through a potential barrier of profile $V(q)$, between the classical turning points q_a and q_b characterized by $V(q_a) = V(q_b) = E$, which reads

$$T_{\text{tun}} = \exp\left\{ -\frac{2}{\hbar} \int_{q_a}^{q_b} \mathrm{d}q \sqrt{2M(V(q) - E)} \right\}, \qquad (1.7)$$

we expect that the rates will depend on the shape of the potential in a nontrivial way also in our more complicated case, where the particle is interacting with a bath. We put this dependence in contrast with the much simpler dependence of the Arrhenius rate (1.6), involving the barrier height ΔV only. Starting from a quantum ratchet at low temperature, we can eventually reach the classical regime by increasing the temperature, thus bridging between the two very different dependences on a same potential $V(q)$. One thus expects very nontrivial dependence of the ratchet current on the temperature. Actually, current reversals as a function of the temperature were predicted [16] and experimentally observed [18]. Due to the complex interplay of tunneling and energy exchange between the system and the bath, we can more generally expect nontrivial behavior and reversals of the particle current as a function of other parameters as well, like the parameters of the driving force or the strength of the dissipation induced by the bath. Such effects were indeed obtained in several works [12, 19–23], including ours [24–26], which are discussed in Chapters 4 and 6.

Which are the challenges posed by a theoretical description of quantum ratchets? First of all, there is the usual increase in complexity and in the size of the configuration space associated with the transfer from the number-based formulation of classical mechanics to the operator-based formulation of quantum mechanics. This includes the necessity to coherently keep track of the interferences of all past processes in the description of the system dynamics. This can become mathematically very intricate. The second challenge arises because the energy-conserving formalism of quantum mechanics applies to closed systems only. The phenomenological description of the interaction of the system with a dissipative thermal environment by including a viscous force $-\eta\dot{q}(t)$ and a stochastic force $\xi(t)$ in the equation of motion, which one uses in the classical regime, defines an open system and is not

portable in the quantum regime. Quantum ratchets thus belong to the broader issue of quantum dissipative systems [27] and provide a benchmark for their investigation.

It is possible to overcome this obstacle, provided one enlarges the system under consideration. As was already realized in the classical regime by Ullersma [28] and Zwanzig [29], an equation of motion of the form (1.1) can also be derived from a formulation involving a closed system. One again starts from a one-dimensional system, formed by the particle of mass M subject to the potential $V(q)$ and the force $F(q)$. If one bilinearly couples the coordinate q of the particle with the coordinates of a large number N_O of harmonic oscillators, solves the equations of motion for the oscillators and substitutes the solution back in the equation of motion of the particle, one obtains an equation of the form (1.1). The new degrees of freedom associated with the harmonic oscillators define what one calls the thermal bath. The total energy of the system-plus-bath is kept constant, but the description of dissipation in the system, as well as a thermal fluctuating force on the particle, are included. They take the form of a transfer of energy between the system and the bath degrees of freedom. The price paid for this description is the huge increase of the number of degrees of freedom, from 1 to $N_O + 1$.

The same procedure can be followed in a quantum formulation. It was first applied by Caldeira and Leggett [30], precisely to investigate quantum tunneling in a dissipative system. They have shown that any environment which is only weakly perturbed by the system can be described by such a bath of harmonic oscillators within linear response. This is a reasonable assumption for a small system connected to a large bath when the bath modes additionally present a large number of accessible excited states. This approach, which bears their name, is widely used to investigate quantum dissipative systems. For a review, see Ref. [27]. We will now discuss its application to quantum ratchets.

1.1.3   A model for rocked ratchets

We consider a quantum particle of mass M in a one-dimensional potential $V(q)$. The system Hamiltonian $\hat{H}_S(t) = \hat{H}_R + \hat{H}_{ext}(t)$ is made of the ratchet Hamiltonian

$$\hat{H}_R = \frac{\hat{p}^2}{2M} + V(\hat{q}), \qquad (1.8)$$

driven by a time-dependent force $F(t)$ coupling to the position operator

$$\hat{H}_{ext}(t) = -F(t)\hat{q}. \qquad (1.9)$$

We will consider an unbiased force as given, e.g., in Eq. (1.3), and a ratchet potential $V(q+L) = V(q)$ being a spatially asymmetric function of periodicity L. An example of such a potential is shown in Fig. 4.1. This combination thus defines a rocked ratchet, as discussed above.

In order to describe dissipation in the system, we let it interact with a bath. We use the Caldeira-Leggett model of a bath of harmonic oscillators whose coordinates are bilinearly coupled to the system coordinate $\hat{q}$, given by the standard Hamiltonian

$$\hat{H}_{\mathrm{B}} = \frac{1}{2} \sum_{\alpha=1}^{N_{\mathrm{O}}} \left[\frac{\hat{p}_\alpha^2}{m_\alpha} + m_\alpha \omega_\alpha^2 \left(\hat{x}_\alpha - \frac{c_\alpha}{m_\alpha \omega_\alpha^2} \hat{q} \right)^2 \right]. \tag{1.10}$$

The masses m_α, frequencies ω_α, and coupling strengths c_α of the oscillators only enter the expressions of the dynamical quantities of the system through the combination

$$J(\omega) = \frac{\pi}{2} \sum_{\alpha=1}^{N_{\mathrm{O}}} \frac{c_\alpha^2}{m_\alpha \omega_\alpha} \delta(\omega - \omega_\alpha), \tag{1.11}$$

which is called the spectral density of the bath. For more details on this result, see Appendix A.

We will consider an Ohmic spectral density, i.e. linear $J(\omega) \sim \eta\omega$ at low frequency ω. In order to avoid divergences of some dynamical quantities, one has to introduce a cutoff at large frequencies ω. The presence of a cutoff frequency physically means that the bath cannot respond arbitrarily fast to a modification in its environment [27, Ch. 3]. In this work, we will investigate two common cases: an exponential cutoff at frequency ω_{c}

$$J(\omega) = \eta\omega \mathrm{e}^{-\omega/\omega_{\mathrm{c}}}, \tag{1.12}$$

and an algebraic cutoff at frequency ω_{D}

$$J(\omega) = \frac{\eta\omega}{1 + (\omega/\omega_{\mathrm{D}})^2}, \tag{1.13}$$

known as the Drude model.

The reason for which one considers a linear spectral density can be understood from the Heisenberg equations of motion obtained from the total Hamiltonian of the system-plus-bath $\hat{H} = \hat{H}_{\mathrm{S}} + \hat{H}_{\mathrm{B}}$. The $2N_{\mathrm{O}}$ equations that one gets for the position $\hat{x}_\alpha(t)$ and momentum operators $\hat{p}_\alpha(t)$ of the bath degrees of freedom are simply the equations of motion of harmonic oscillators driven by a force $c_\alpha \hat{q}(t)$. They can be solved in terms of the system operators $\hat{q}(t)$ and $\hat{p}(t)$. After substitution of the solution in the equation of motion for the system degree of freedom, one obtains, in the limit of a large bath $N_{\mathrm{O}} \to \infty$,

$$M\ddot{\hat{q}}(t) + M \int_{t_0}^{t} \mathrm{d}t' \gamma(t - t') \dot{\hat{q}}(t') + \frac{\mathrm{d}}{\mathrm{d}q} V(\hat{q}(t)) = F(t)\hat{1} + \hat{\xi}(t), \tag{1.14}$$

with the damping kernel

$$\gamma(\tau) = \frac{2}{\pi M} \int_0^\infty \mathrm{d}\omega \frac{J(\omega)}{\omega} \cos(\omega\tau), \tag{1.15}$$

and the force

$$\hat{\xi}(t) = \sum_{\alpha=1}^{N_{\mathrm{O}}} c_\alpha \left[\left(\hat{x}_\alpha(t_0) - \frac{c_\alpha \hat{q}(t_0)}{m_\alpha \omega_\alpha^2} \right) \cos(\omega_\alpha(t - t_0)) + \frac{\hat{p}_\alpha(t_0)}{m_\alpha \omega_\alpha} \sin(\omega_\alpha(t - t_0)) \right].$$
(1.16)

Eq. (1.14) is a quantum Langevin equation for the position operator $\hat{q}(t)$. In the classical limit, the position operator may be replaced by the real-valued classical trajectory $q(t)$, yielding an equation similar to (1.1) with the memory-friction force $M \int_{t_0}^{t} dt' \gamma(t - t') \dot{q}(t')$ instead of $\eta \dot{q}(t)$. If one considers a strictly Ohmic spectral density, that is linear at low frequency and with a cutoff frequency tending to ∞, one gets the instantaneous damping kernel

$$\gamma(\tau) = \frac{2\eta}{M} \delta(\tau),$$
(1.17)

where $\delta(\tau)$ denotes Dirac's delta function. In this case, the friction force reduces to the memoryless expression $\eta \dot{q}(t)$. Thus, for a strictly Ohmic spectral density $J(\omega) = \eta \omega$, the quantum Langevin equation (1.14) reduces in the classical limit to the equation of motion (1.1) with viscous damping. The proportionality coefficient η of the Ohmic spectral density is identified with the viscosity η entering the phenomenological viscous force in (1.1). Together with the particle mass M, it defines the time scale of dissipation $\gamma^{-1} = (\eta/M)^{-1}$.

In the limit of a very large bath $N_{\mathrm{O}} \to \infty$, the force $\xi(t)$ given in (1.16) takes a stochastic character, depending on the realization of the preparation of the bath degrees of freedom at initial time t_0. Some more insight can be gained if one considers an initial preparation governed by a density matrix corresponding to thermal equilibrium at a given temperature $T = 1/k_{\mathrm{B}}\beta$,

$$\hat{\rho}_{\mathrm{B}} = \frac{\mathrm{e}^{-\beta \hat{H}_{\mathrm{B}}[q(t_0)]}}{\mathrm{Tr}_{\mathrm{B}}\, \mathrm{e}^{-\beta \hat{H}_{\mathrm{B}}[q(t_0)]}},$$
(1.18)

where, in the bath Hamiltonian $\hat{H}_{\mathrm{B}}[q(t_0)]$, the system position operator $\hat{q}$ has been replaced by a parameter $q(t_0)$ (see Section 3.2 for a more detailed discussion of this point). One can then show the properties (see, e.g., [27])

$$\langle \hat{\xi}(t) \rangle_{\mathrm{B}} = 0 \tag{1.19a}$$

$$\langle \hat{\xi}(t) \hat{\xi}(t') \rangle_{\mathrm{B}} = \hbar L(t - t'), \tag{1.19b}$$

where $\langle \cdot \rangle_{\mathrm{B}} \hat{=} \mathrm{Tr}_{\mathrm{B}}\{\hat{\rho}_{\mathrm{B}} \cdot\}$ denotes the average over the thermal density matrix (1.18), and

$$L(\tau) = \frac{1}{\pi} \int_0^\infty d\omega\, J(\omega) \left[\coth\left(\frac{\hbar\omega\beta}{2} \right) \cos(\omega\tau) - \mathrm{i}\sin(\omega\tau) \right] \tag{1.20}$$

is the bath correlation function (see also Appendix B). The first equation means that $\xi(t)$ has zero average. Taking the limit $T \to \infty$ (replacing the coth by the inverse

of its argument) together with $\omega_{\mathrm{c}} \to \infty$, the second equation reduces to $\langle \hat{\xi}(t)\hat{\xi}(t')\rangle_{\mathrm{B}} = 2\eta k_{\mathrm{B}}T\delta(t - t')$. It means that the correlations of $\xi(t)$ correspond to the ones of a stochastic force originating from a memoryless thermal bath at temperature T. This provides a justification for using the Caldeira-Leggett model in order to describe dissipative quantum systems: It is a model which has the correct classical limit.

In the quantum mechanical description, the information on the system dynamics is contained in the reduced density matrix $\hat{\rho}(t) = \mathrm{Tr}_{\mathrm{B}}\,\hat{W}(t)$, obtained from the density matrix $\hat{W}(t)$ of the system-plus-bath $\hat{H}$ by performing the trace over the bath degrees of freedom. The diagonal elements $P(q,t) = \langle q|\hat{\rho}(t)|q\rangle$ of the reduced density matrix represent the populations of a given state $|q\rangle$. They suffice in order to evaluate the evolution of the average position $\langle \hat{q}(t)\rangle = \mathrm{Tr}_{\mathrm{S}}\{\hat{q}\hat{\rho}(t)\}$. The velocity is then obtained by time differentiation, which allows the evaluation of the quantity of interest, the stationary velocity

$$v^{\infty}(t) = \lim_{t \gg t_0} \frac{\mathrm{d}}{\mathrm{d}t}\langle \hat{q}(t)\rangle. \tag{1.21}$$

Finally, we make a precision about the spatial boundary conditions. Ideally, one would like to consider an infinitely extended system, but then the total Hamiltonian would not be bounded from below, as soon as the driving force is nonzero. Practically, we consider a finite system, but large enough so that we can neglect boundary effects. Starting with a particle density localized well in the middle of the system at initial time t_0, we expect that the average velocity will be stationary at times $t \gg t_0$ after the transient dynamics has vanished, but before the particle has started to feel the effect of the boundaries. We will avoid to speak of infinitely long times, at which the particle density is spread over the entire system, and, in the presence of a time-independent force, equilibrium is reached and the velocity vanishes. In practical calculations involving the undriven system Hamiltonian H_{R}, we assume translational invariance and use periodic boundary conditions.

1.2   Existing theoretical works

In this section, we will give an overview of theoretical works on quantum ratchets prior or parallel to this thesis, and attempt to shed some light on their relations.

Most of the theoretical works on quantum ratchets are based on earlier investigations focused on dissipative tunneling, which were developed starting from the eighties. Those investigations resulted in a rather complete physical picture of the dynamics, however they were usually concerned with systems where the ratchet effect is absent. The question of rectification was addressed almost fifteen years later, with similar methods.

1.2.1   Sinusoidal potentials and other symmetric systems

The investigation of the dissipative dynamics determined by the Hamiltonian $\hat{H}$ of Section 1.1.3 with a periodic potential has been reported in 1985 already by Weiss and Grabert [31]. The method used goes as follows: By means of imaginary-time path integral techniques, the coupling to the bath degrees of freedom can be turned into a nonlocal-in-time term in the effective action for the system; The driving force is kept small enough so that the tilted potential still presents minima and maxima, and the effects of thermal activation within each potential well are neglected; The energy associated with small oscillations around the potential minima is assumed to be much smaller than the potential barrier, which corresponds to the semiclassical limit (many levels below the potential barrier); In this frame, transition rates $\Gamma^{\pm}$ between adjacent potential wells are evaluated in terms of the bounce trajectory which extremizes the action. Analytical expressions in the incoherent tunneling regime are given. The validity range of this regime is discussed in terms of the dissipation parameter $\alpha = \eta L^2 / 2\pi\hbar$, temperature T and driving amplitude F of the system of spatial periodicity L. It comprises the whole strong dissipation regime $\alpha > 1$, as well as the weak dissipation regime $\alpha < 1$ with a lower bound on the thermal energy $k_{\mathrm{B}}T$ or driving energy FL. At low temperature, within the validity range of the method, the transition rates show a power-law behavior $\Gamma \propto F^{2\alpha-1}$ as a function of the driving, whereas at zero driving a power-law $\Gamma \propto T^{2\alpha-1}$ as a function of temperature is found. The mobility as well as the diffusion coefficient are evaluated. The power-law expressions of the rates imply a behavior $\mu \propto T^{2(\alpha-1)}$ for the linear mobility, i.e., when the driving tends to zero. This expression points out a salient property of the ground state of the system, when the temperature is lowered down to zero. In the strong dissipation regime $\alpha > 1$, the linear mobility vanishes, indicating a localized ground state [region (b) in Fig. 1.1]. In the weak dissipation regime $\alpha < 1$, the linear mobility increases when the temperature is decreased, indicating rather a tendency to delocalization, before the validity of the method eventually breaks down. This delocalization to localization transition has been first derived by Schmid [32] in the case of a cosine potential.

The same formalism is used by Korshunov [34]. An analytical solution for the bounce trajectory in the overdamped limit and in the case of a cosine potential is obtained. The corresponding rates are evaluated and similar expressions are found.

In the same year 1985, the investigation of the dynamics in the case of a cosine potential by means of a different formalism, based on real-time path integral techniques, has been reported by Fisher and Zwerger [33]. Among others, this formalism is applicable beyond the semiclassical regime. It will be presented in detail in Chapters 3, 5, and 6 of this thesis. A perturbative expansion in the potential amplitude is performed, making the results particularly relevant for weakly corrugated potentials. The treatment relates the mobility μ_{WB} of the system (WB stands for weak-binding) to the mobility μ_{TB} in a dual single-band tight-binding system with nearest neighbors couplings. The spatial periodicity $\tilde{L}$ of this dual system and the periodicity L
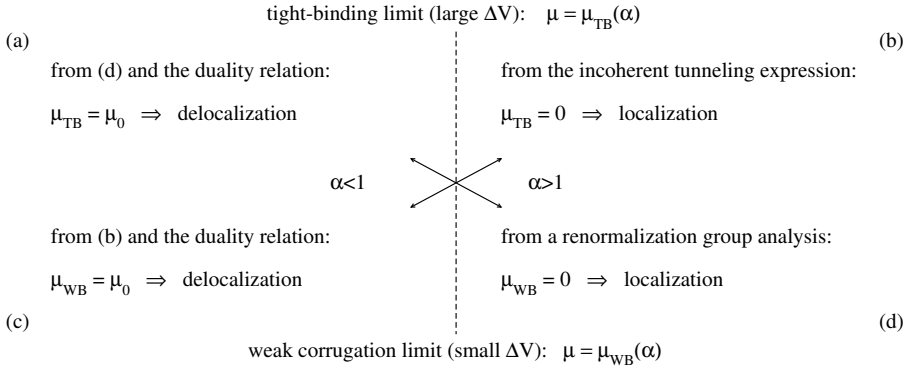
Figure 1.1: Schematic representation of the delocalization (weak dissipation $\alpha < 1$, left) to localization (strong dissipation $\alpha > 1$, right) transition of the ground state of dissipative periodic systems. It is extracted from the behavior of the linear mobility at zero temperature. In the tight-binding limit and for $\alpha > 1$ [region (b)], the incoherent tunneling expression $\mu_{\mathrm{TB}} \propto T^{2(\alpha-1)}$ of Ref. [31] can be used. The result $\mu_{\mathrm{WB}} = 0$ in the weak corrugation limit and for $\alpha > 1$ [region (d)] is obtained from a renormalization group analysis [33]. From these results, the duality relation (1.22) derived in Ref. [33] can be used to evaluate the mobility in the complementary regions (a) and (c), as symbolized by the arrows.

of the original system are connected by the simple relation $\tilde{L} = 2\pi\hbar/\eta L$, which involves dissipation through the viscosity η. As a consequence of this relation, the effective dissipation $\tilde{\alpha} = \eta \tilde{L}^2/2\pi\hbar$ in the dual system is inverted with respect to the original system, $\tilde{\alpha} = 1/\alpha$, and the energy drop per periodicity length $\tilde{\epsilon} = F\tilde{L}$ is obtained according to $\tilde{\epsilon} = \epsilon/\alpha$ from its counterpart $\epsilon = FL$. The relation between the mobilities of the two systems additionally involves the mobility $\mu_0 = 1/\eta$ in the absence of a potential, and reads

$$\mu_{\mathrm{WB}}(\alpha, \epsilon) = \mu_0 - \mu_{\mathrm{TB}}(1/\alpha, \epsilon/\alpha). \tag{1.22}$$

At the same time, this work gives an expression for the mobility $\mu_{\mathrm{TB}}(\tilde{\alpha}, \tilde{\epsilon})$ in the tight-binding model, in the incoherent tunneling regime. This expression, thus obtained by real-time path-integral techniques, coincides with the result of Ref. [31].

Although it has emerged in a perturbative framework, with respect to the potential amplitude in the weak corrugation limit, respectively to the tunneling amplitude in the tight-binding limit, the duality relation (1.22) itself holds true beyond the perturbative regimes. The indices WB and TB, which serve to distinguish between the dual systems, have thus only a historical meaning. A non-perturbative derivation of

the duality relation within the framework of linear response, obtained by means of a canonical transformation, has also been reported by Sassetti *et al.* [35].

The investigation of the linear mobility as a function of temperature, from Eq. (1.22), yields the following picture. For weak dissipation $\alpha < 1$, the dynamics at $T = 0$ corresponds essentially to the dynamics in the absence of the potential, as $\mu_{\mathrm{WB}} = \mu_0$, and the particle is delocalized [region (c) in Fig. 1.1]. Upon increasing the temperature, up to a crossover temperature T^* of the order of $\hbar^2/ML^2 k_{\mathrm{B}}$, the mobility decreases. The authors of Ref. [33] interpret this decrease by the fact that the thermal fluctuations due to the environment perturb the coherent tunneling dynamics of the particle, and speak of a regime of thermally resisted tunneling. Upon increasing the temperature further, above T^*, the mobility increases again, suggesting that thermally assisted hopping takes over as a transport mechanism. Eventually, it reaches the value μ_0 again, meaning that the thermal fluctuations are so important that the potential becomes irrelevant. For strong dissipation $\alpha > 1$, at low temperature, the incoherent tunneling expression for the tight-binding mobility $\mu_{\mathrm{TB}}(\tilde{\alpha}, \tilde{\epsilon})$ diverges and cannot be used in (1.22). However, a renormalization group analysis (see also Ref. [36]) gives $\mu_{\mathrm{WB}} = 0$ at $T = 0$ [region (d) in Fig. 1.1]. This localization means that, even at zero temperature, the influence of the environment is already strong enough to suppress tunneling. For higher temperatures, where the incoherent tunneling expression for $\mu_{\mathrm{TB}}(\tilde{\alpha}, \tilde{\epsilon})$ can be used, the mobility of the weak-binding system increases monotonically, indicating that the transport mechanism is thermally activated hopping. The value μ_0 is reached at high temperature in this case as well.

From this picture one sees, in particular, that one recovers the delocalization to localization transition as a function of the dissipation strength, at zero temperature. From the renormalization group result $\mu_{\mathrm{WB}} = 0$ at $T = 0$ for strong dissipation, by using the duality relation (1.22), one can obtain the tight-binding mobility $\mu_{\mathrm{TB}} = \mu_0$ for weak dissipation, where the incoherent tunneling expression diverges [region (a) in Fig. 1.1].

Aslangul *et al.* [37] have taken a new approach. Instead of the physical system (1.8), a single-band tight-binding Hamiltonian with nearest neighbors couplings is investigated from the very beginning. Dissipation is accounted for exactly as in the other models, by means of a bilinear coupling to a bath of harmonic oscillators. The formalism used to solve the dynamics of the system-plus-bath in order to evaluate the mobility and the diffusion coefficient is based on a polaron canonical transformation of the total Hamiltonian, which corresponds to dress the system particle with bath phonons. The expression obtained for the mobility is identical to the expression for the tight-binding mobility derived in [33] by means of real-time path integral techniques in the incoherent tunneling regime, after matching of the parameters. Moreover, the mobility and diffusion coefficient are equivalent to the results obtained by imaginary-time path integral techniques in Ref. [31], which suggests that the dynamics in the physical continuous potential is indeed reduced, in

the regime of parameters considered in that work, to a single-band tight-binding dynamics. However, the validity conditions for this reduction, as well as their interplay with the semiclassical condition required in Ref. [31], are not clear to us on the basis of these works. We will come back to this point in Section 1.3.

In a single-band tight-binding model with nearest neighbors couplings and equal on-site energies, such as the one investigated in Ref. [37], no ratchet effect is expected in the presence of temporally symmetric driving (see also Chapter 4). The ratchet current extracted from the results of Ref. [31] is zero as well, and it is therefore not discussed. This can now be understood from the fact that the parameter regime considered in that work leads to a dynamical description which corresponds to the tight-binding Hamiltonian of Ref. [37].

1.2.2   Ratchet systems

The first investigation of the quantum ratchet current, by means of imaginary-time path integral techniques, has been published in 1997 by Reimann *et al.* [16]. In this pioneering work, a rocked ratchet with adiabatic bistable driving is considered. As in Ref. [31], the driving amplitude is such that minima and maxima of the potential are still defined, and thermal activation within each well is neglected. Moderate-to-strong dissipation is invoked to exclude running solutions and justify a description in terms of incoherent tunneling rates. The semiclassical condition is given there by the requirement that the frequency $\tilde{\omega}_0$ of the damped small oscillations around a potential minimum corresponds to an energy much smaller than the potential barrier. The shape of the potential is taken into account in more detail in the evaluation of the bounce trajectory, which results in a description going beyond the effective single-band tight-binding model. In the calculation, a crossover temperature $T_c = \hbar\tilde{\omega}_0/2\pi k_B$ is identified. Above T_c, the quantum rates reduce to the classical Kramers expression $\Gamma^\pm \propto e^{-\Delta V^\pm/k_B T}$ in terms of the barriers $\Delta V^\pm$ of the tilted potential. Below T_c, the ratchet current shows an enhancement with respect to the classical result, which is attributed to tunneling. Lowering the temperature further, a current reversal is found, and the ratchet current eventually saturates to a finite value at zero temperature.

One limitation of this approach is its restriction to the situation where the dynamics is described in terms of transitions of the particle between potential minima where it is trapped. In particular, this excludes the exploration of the regime of large driving amplitudes, where the potential is expected to become irrelevant and the particle should flow at the classical velocity $v = F/\eta$. Another limitation is the semiclassical condition, which excludes the deep quantum regime where the potential wells sustain only few levels, and where one could think of deriving directly the effective tight-binding description associated with the potential considered.

The work reported by Roncaglia and Tsironis [20] one year later is based a priori on a tight-binding description. In order to get a ratchet effect, the on-site energies of

the one-band tight-binding model with nearest neighbors couplings are not any more all equal, but spatially modulated in an asymmetric pattern. The ratchet current induced by an adiabatic bistable force is evaluated, following essentially the method of Ref. [37]. The behavior as a function of driving amplitude, temperature, and dissipation, is investigated. Current reversals as a function of the driving amplitude are found. When temperature is lowered down to zero, at a finite driving amplitude, the ratchet current saturates to a finite value in the case of strong dissipation $\alpha > 1$, whereas it diverges in the weak dissipation regime $\alpha < 1$. This extends beyond the linear regime the findings of the works discussed above (see Fig. 1.1). At finite temperature and driving amplitude, another transition between two dynamical regimes, controlled by the dissipation strength, is identified. At low dissipation, the particle tends to coherent localized dynamics. At strictly zero dissipation, that is in the absence of coupling of the system to the bath, this behavior is known as Bloch oscillations or Stark localization. Upon increasing the dissipation strength, the rise of the system-bath coupling favors motion of the particle in the direction of lower energy of the system, resulting in an increase of the ratchet current. Upon further increase of the dissipation, it reaches a maximum and then decreases, reflecting the suppression of the motion due to friction.

The arbitrary character of the Hamiltonian investigated, and in particular the fact that its classical counterpart is unclear, is a serious drawback of this work.

All the approaches developed in the works discussed above have been restricted to the case of a time-independent driving force, allowing to discuss ratchet systems in the case of adiabatic bistable driving only [see Eq. (1.4)]. Hartmann *et al.* [38] have extended this formalism to the case of non-adiabatic harmonic driving. However, the Hamiltonian investigated, which is the one of Ref. [37], does not present any ratchet effect, as mentioned above. Consequently, this work does not discuss the quantum ratchet current, although it opens new possibilities for doing it.

The theoretical investigations presented in this thesis, which have been published in Refs. [24–26], pursue the development of the approaches presented above. We will profile them in the next section. Before doing so, let us mention complementary approaches which have been recently developed.

A spatially asymmetric potential, taking the form of a spatial modulation of the on-site energies, is added to the tight-binding Hamiltonian of Ref. [37] by Yukawa *et al.* [19]. This additional potential flashes in time, playing the role of the driving force in order to break thermal equilibrium. This model defines thus a flashing quantum ratchet. In this work, the coupling between the system and the bath differs from the standard bilinear form present in Eq. (1.10). Reversals of the ratchet current as a function of the temperature and the flashing frequency are reported.

Another category of ratchet systems which has been discussed in Section 1.1.1 are the time ratchets, where the spatial asymmetry of the potential is replaced by a temporal asymmetry of the driving force. The quantum regime of this category

of ratchets has been discussed by Goychuk and Hänggi [12]. Current reversals as a function of the driving parameters and the temperature have been reported. Depending on the parameters, the presence of the driving is shown to enhance or suppress diffusion.

Scheidl and Vinokur [21] have investigated the dissipative dynamics in the physical Hamiltonian $\hat{H}$ of Section 1.1.3 in the general case of a periodic potential and non-adiabatic driving forces. The amplitude of the potential as well as the one of the driving are treated perturbatively, and the nonlinear mobility is evaluated up to third order. Among the results, it is shown that the linear mobility does not present a ratchet effect, and reversals of the ratchet current as a function of driving frequency, temperature, and dissipation, are found. Interesting analytic expressions in some limits are derived. However, a clear understanding of the transport mechanisms as, e.g., in Ref. [33], is not reached. The intricacy of the obtained expressions as well as the crucial reliance of the method on the perturbation treatment limits the extension to larger potential and driving amplitudes.

In other works, dissipation is taken into account by other means than the coupling to a bath of harmonic oscillators. It can even be excluded, as in the work by Schantz *et al.* [39], where the nonzero drift velocity of wave packet reveals directed chaotic transport in a Hamiltonian system with spatial and temporal symmetry. A mixed phase space with coexisting regular and chaotic regions is identified as a necessary condition for this behavior.

Lehmann *et al.* [22], have investigated a molecular bridge between two leads as a model for quantum ratchets. The bridge is described as a single-band tight-binding model with nearest neighbors couplings and spatially asymmetric modulation of the on-site energies. Additionally, the bridge is rocked by a harmonic driving force. The first and last tight-binding sites are coupled each to a lead. The leads are modeled as large reservoirs of non-interacting electrons, kept at a given temperature. In this description, energy relaxation within the leads accounts for dissipation. Among the results, the ratchet current shows a strongly peaked structure together with reversals as a function of the driving frequency. Estimates indicate that the experimental realization of such molecular quantum ratchets is realistic.

Finally, Machura *et al.* [23] have applied a quantum Smoluchowski equation to the investigation of quantum ratchets with adiabatic bistable driving. The quantum Smoluchowski equation [40] is an effective equation for the diagonal elements of the reduced density matrix, derived in the limit of strong dissipation. The ratchet current shows reversals as a function of the temperature and driving amplitude. At large temperature or large driving amplitude, it tends to the solution obtained in the classical limit, whereas out of this parameter range, its magnitude can be larger or smaller than the one of its classical counterpart.

1.3   This thesis

In this section, we will situate our works on quantum ratchets in the theoretical context presented in the previous section, and expose the structure of this thesis. The physical model considered throughout this thesis is the one exposed in Section 1.1.3.

The aim of our first approach was to go beyond the semiclassical condition embedded in the methods developed in Refs. [16, 31], and investigate the deep quantum regime. An additional purpose was to try to understand under which conditions the dynamics can be described in terms of a tight-binding system, and derive the structure of the corresponding Hamiltonian from the original potential, instead of starting a priori from such a tight-binding description, as in Refs. [20, 37]. We have developed the following method: The Hamiltonian (1.8) of the undriven, periodic ratchet system is diagonalized by virtue of Bloch theorem, yielding expressions for the quantum states of the system, organized in energy bands; Following an analysis developed for double-well potentials [41], a parameter regime where the dynamics can be described in terms of the lowest energy bands only is considered; After a rotation to the eigenbasis of the position operator, the Hamiltonian takes the general form of a multi-band tight-binding model with non-nearest neighbors couplings and interband couplings; Invoking the localized character of the retained states, the couplings can be restricted to sites belonging to neighboring wells; The dissipative dynamics of this tight-binding system in the presence of a non-adiabatic harmonic driving force is then investigated by real-time path integral techniques as, e.g., in Ref. [38]. This method provides a theoretical description for quantum ratchets with few bands below the barrier. It has been published in Ref. [24] and is detailed in Chapter 4.

We have developed a second, complementary approach to investigate quantum ratchets, based on the duality relation developed in Ref. [33]. One notices that this formalism relies on less restrictions than other techniques. As a consequence, it is applicable in a wider range of parameters, including the deep quantum regime, and the regime of a large driving force where the classical dynamics is recovered. However, the derivation in Ref. [33] relies explicitly on the fact that the potential is a cosine function. It was not clear to us whether this is a fundamental restriction, or whether one can generalize it to any periodic potential. The purpose of our work was to answer this question. We have been able to find this generalization, which allowed us to investigate quantum ratchet systems with this powerful method. The results have been published in Ref. [25], whereas the details of the methods can be found in Ref. [26]. This work is presented in Chapter 6. Furthermore, the formalism of [33] provides the mobility only, and has not been extended to the evaluation of the diffusion coefficient. In our extension, an expression for the diffusion coefficient can be obtained, but it diverges. This has been identified as an artifact of a non-physical assumption used in the derivation, which could be relaxed in principle. This is the subject of work in progress.

We have made an attempt to confront the theoretical models developed in this thesis with an experiment based on quantum vortices in arrays of Josephson junctions, which has been performed by J. B. Majer *et al.* [11] at the Delft University of Technology. Some qualitative results of the experiment are reproduced by the model, however some others, such as the power-law dependence of the voltage-current characteristics of the array, are not understood. We have discussed the simplifications on which the model is based, and proposed directions for further investigations. This work is presented in Chapter 2.

This thesis is structured as follows: In Chapter 2, an overview of experiments on quantum ratchets complements this introduction. The experiment on quantum vortices in Josephson junction arrays on which we have collaborated is then discussed in detail. In Chapter 3, the application of real-time path integral techniques to investigate the dynamics of dissipative tight-binding systems is exposed. In Chapter 4, we report our work on quantum ratchets with few bands below the barrier, which relies on this formalism. In Chapter 5, this formalism is considered in the particular case of single-band tight-binding models, which allows further development. In Chapter 6, we report our work on the duality relation for quantum ratchets, which makes use of these developments. In the appendices, some technical material involved in the formalism is detailed.

References

[1] P. Reimann, Phys. Rep. **361**, 57 (2002).

[2] Appl. Phys. A **75**, 167 (2002), special issue on *Ratchets and Brownian motors: Basics, experiments and applications.*

[3] R. D. Astumian and P. Hänggi, Phys. Today **55**(11), 33 (2002).

[4] R. Brown, Edinb. New Philos. J. **5**, 358 (1828).

[5] A. Einstein, Ann. Phys. (Leipzig) **17**, 549 (1905).

[6] M. von Smoluchowski, Phys. Z. **13**, 1069 (1912).

[7] P. Hänggi and F. Marchesoni, Chaos **15**, 026103 (2005).

[8] R. P. Feynman, R. B. Leighton, and M. Sands, *The Feynman Lectures on Physics* (Addison-Wesley, Reading, 1963).

[9] J. M. R. Parrondo and P. Español, Am. J. Phys. **64**, 1125 (1996).

[10] P. Reimann, R. Bartussek, R. Häussler, and P. Hänggi, Phys. Lett. A **215**, 26 (1996).

[11] M. O. Magnasco, Phys. Rev. Lett. **71**, 1477 (1993).

[12] I. Goychuk and P. Hänggi, Europhys. Lett. **43**, 503 (1998).

[13] S. Flach, O. Yevtushenko, and Y. Zolotaryuk, Phys. Rev. Lett. **84**, 2358 (2000).

[14] A. V. Ustinov, C. Coqui, A. Kemp, Y. Zolotaryuk, and M. Salerno, Phys. Rev. Lett. **93**, 087001 (2004).

[15] J. M. R. Parrondo and B. Jiménez de Cisneros, cond-mat/030953, translated by P. Amengual, J. Sotelo, and D. Abbott.

[16] P. Reimann, M. Grifoni, and P. Hänggi, Phys. Rev. Lett. **79**, 10 (1997).

[17] J. B. Majer, J. Peguiron, M. Grifoni, M. Tusveld, and J. E. Mooij, Phys. Rev. Lett. **90**, 056802 (2003).

[18] H. Linke, T. E. Humphrey, A. Löfgren, A. O. Sushkov, R. Newbury, R. P. Taylor, and P. Omling, Science **286**, 2314 (1999).

[19] S. Yukawa, M. Kikuchi, G. Tatara, and H. Matsukawa, J. Phys. Soc. Jpn. **66**, 2953 (1997).

[20] R. Roncaglia and G. P. Tsironis, Phys. Rev. Lett. **81**, 10 (1998).

[21] S. Scheidl and V. M. Vinokur, Phys. Rev. B **65**, 195305 (2002).

[22] J. Lehmann, S. Kohler, P. Hänggi, and A. Nitzan, Phys. Rev. Lett. **88**, 228305 (2002).

[23] L. Machura, M. Kostur, P. Hänggi, P. Talkner, and J. Łuczka, Phys. Rev. E **70**, 031107 (2004).

[24] M. Grifoni, M. S. Ferreira, J. Peguiron, and J. B. Majer, Phys. Rev. Lett. **89**, 146801 (2002).

[25] J. Peguiron and M. Grifoni, Phys. Rev. E **71**, 010101(R) (2005).

[26] J. Peguiron and M. Grifoni, accepted in Chem. Phys.

[27] U. Weiss, *Quantum Dissipative Systems* (World Scientific, Singapore, 1999), 2nd ed.

[28] P. Ullersma, Physica **32**, 27 (1966).

[29] R. Zwanzig, J. Stat. Phys. **9**, 215 (1973).

[30] A. O. Caldeira and A. J. Leggett, Ann. Phys. **149**, 374 (1983).

[31] U. Weiss and H. Grabert, Phys. Lett. **108A**, 63 (1985).

[32] A. Schmid, Phys. Rev. Lett. **51**, 1506 (1983).

[33] M. P. A. Fisher and W. Zwerger, Phys. Rev. B **32**, 6190 (1985).

[34] S. E. Korshunov, Sov. Phys. JETP **65**, 1025 (1987).

[35] M. Sassetti, H. Schomerus, and U. Weiss, Phys. Rev. B **53**, R2914 (1996).

[36] F. Guinea, V. Hakim, and A. Muramatsu, Phys. Rev. Lett. **54**, 263 (1985).

[37] C. Aslangul, N. Pottier, and D. Saint-James, J. Physique **47**, 1671 (1986).

[38] L. Hartmann, M. Grifoni, and P. Hänggi, Europhys. Lett. **38**, 497 (1997).

[39] H. Schanz, M. F. Otto, R. Ketzmerick, and T. Dittrich, Phys. Rev. Lett. **87**, 070601 (2001).

[40] J. Ankerhold, P. Pechukas, and H. Grabert, Phys. Rev. Lett. **87**, 086802 (2001).

[41] M. Thorwart, *Tunneling and vibrational relaxation in driven multilevel systems*, Ph.D. thesis, University of Augsburg (2000).

Chapter 2

Experiments on Quantum Ratchets

The experiment presented in Section 2.2 of this chapter has been performed by J. B. Majer in collaboration with M. Tusveld, J. E. Mooij, J. Peguiron, and M. Grifoni. It has been published in Phys. Rev. Lett. **90**, 056802 (2003).

2.1   Overview

Up to date, there are only few experiments on the ratchet effect of quantum particles. The reason is the technological challenge represented by the manipulation of quantum particles and by the spatial control of their potential energy required in a ratchet experiment.

The first experiment has been reported in 1999 by Linke *et al.* [1]. It has been performed on electrons in an asymmetric conducting channel. The channel has been obtained by a lateral confinement of a two-dimensional electron gas, defined in a GaAs/AlGaAs heterostructure. The profile of the side gates responsible for the confinement has been designed asymmetric with respect to the direction of propagation. As a consequence, the electrons are subject to asymmetric potential barriers along their propagation direction. An estimate of the typical action of the electrons in this potential, yielding about 170 $\hbar$, suggests semiclassical dynamics. A nonzero ratchet current, showing reversals as a function of temperature, has been measured.

A ratchet experiment on quantum vortices in quasi one-dimensional arrays of Josephson junctions has been reported by Majer *et al.* in 2003 [2]. This experiment will be discussed in detail in Section 2.2 below.

Other experimental systems are currently emerging as potential candidates. The dynamics of fluxons in circular arrays of Josephson junctions [3] can be brought

into the quantum regime by reducing the ratio between the Josephson coupling and
the charging energy of the junctions, and by lowering the temperature. Quantum
dynamics of a single vortex has been reported [4] in ring-shaped long Josephson
junctions. By designing junctions without mirror symmetry, together with the ap-
plication of a magnetic field in the plane of the ring, the potential landscape in which
the vortex moves can be made asymmetric. Finally, cold atoms in optical lattices
provide a new class of very interesting experimental setups. The realization of a
flashing quantum ratchet in such a system has been reported in Ref. [5].

2.2   Vortices in Josephson junction arrays

In this section, we will present an experimental investigation of the quantum ratchet
effect for vortices in Josephson junction arrays [2, 6]. We will begin with a rapid
summary of some properties of single Josephson junctions, before describing the
arrays investigated. We will then discuss the dynamics of vortices in these arrays,
and its relation to the ratchet system investigated in this thesis, which is presented
in Section 1.1.3. Finally, we will present the experimental results and formulate
questions which are still open.

2.2.1   Josephson junctions

In 1962, Josephson [7] discovered that two pieces of superconducting materials sep-
arated by a weak link have striking electronic properties. A weak link can be, e.g.,
a spatial gap, a thin insulating or normal metal layer, or a constriction between the
two pieces. The first property originates from the fact that Cooper pairs can tunnel
through the weak link, carrying a superconducting current

$$I = I_{\mathrm{c}} \sin(\gamma_{21}) \tag{2.1}$$

between the two pieces, up to a critical current I_{c} depending on the characteristics
of the junction. This current is controlled by the gauge-invariant phase difference

$$\gamma_{12} = \varphi_1 - \varphi_2 - \frac{2\pi}{\Phi_0} \int_{①}^{②} \vec{A} \cdot \mathrm{d}\vec{s} \tag{2.2}$$

between the phases φ_1, φ_2 of the order parameter on the two pieces ①, ②, where $\vec{A}$
is the vector potential accounting for an externally applied magnetic field, and $\Phi_0 =
h/2e = 2.07 \times 10^{-15}$ Wb denotes the flux quantum. The meaning of this quantity
will become clear when considering loops of Josephson junctions, as one finds in
arrays.

The second property is that a variation of the phase difference $\varphi_{12} = \varphi_1 - \varphi_2$
causes a voltage

$$V = \frac{\hbar}{2e} \frac{\mathrm{d}\varphi_{12}}{\mathrm{d}t} \tag{2.3}$$

across the junction.

The energy stored in a Josephson junction may be obtained with $E = \int dt V(t) I(t)$. Combining (2.1) and (2.3), one finds at constant magnetic field

$$E = -E_J \cos(\gamma_{12}), \tag{2.4}$$

in terms of the Josephson coupling energy $E_J = \hbar I_c / 2e$.

Capacitive effects between the two pieces of superconductor can be accounted for by a capacitance C in parallel to the junction. A variation of the voltage on the capacitor will generate a displacement current $C dV/dt$. Correspondingly, an energy $CV^2/2$ is stored in the capacitor at a voltage V.

Quasiparticles tunneling between the two superconductors, or flowing through the substrate supporting the junction, carry a dissipative current which can be modeled by a resistor R in parallel to the junction. A lower bound for this resistance is the normal state resistance R_n, reached when the voltage across the junction is higher than twice the amplitude of the superconducting order parameter Δ.

All these effect are combined together in a realistic model for a Josephson junction, the so-called resistively-capacitively shunted junction (RCSJ) model. Adding the currents flowing through the parallel channels, the current through a realistic junction with parameters I_c, C, and R, is written as

$$I = I_c \sin(\gamma_{12}) + C \frac{dV}{dt} + \frac{V}{R}. \tag{2.5}$$

The conservative part of the energy in this model (thus disregarding the resistor) may be written, after use of (2.3),

$$E_{\text{tot}} = \frac{\hbar^2 C}{8e^2} \left(\frac{d\gamma_{12}}{dt} \right)^2 - E_J \cos(\gamma_{12}). \tag{2.6}$$

This can be rewritten in a Hamiltonian formalism. The conjugated variable to the phase difference γ_{12} is the excess/deficit $N = Q/2e$ of Cooper pairs on the superconductors with respect to neutrality. The charge is related to the voltage by $Q = CV$. In terms of these variables, the corresponding Hamiltonian reads

$$H = 4E_C N^2 - E_J \cos(\gamma_{12}), \tag{2.7}$$

where $E_C = e^2/2C$ denotes the charging energy of the junctions. This provides a quantum description of the junction, after replacement of the variables N and γ_{12} by operators $\hat{N}$ and $\hat{\gamma}_{12}$, which are canonically conjugated $[\hat{\gamma}_{12}, \hat{N}] = i\hat{1}$. In this Hamiltonian, one sees that the competition between the two energies E_J and $4E_C$ determines the behavior of the junction. If the Josephson energy largely dominates, the phase $\hat{\gamma}_{12}$ is the well-defined variable describing the behavior of the junction, as its quantum fluctuations become very small. If the charging energy largely dominates, it is exactly the opposite and $\hat{N}$ is the well-defined variable. When the ratio $E_J/4E_C$ is of the order of one, a detailed quantum treatment in terms of both $\hat{N}$ and $\hat{\gamma}_{12}$ is required.

2.2.2   Experimental setup

After this introduction on Josephson junctions, we will now present the quantum ratchet experiment on vortices in Josephson junction arrays. The experimental setup consists of a rectangular network of superconducting aluminum islands on a silicon substrate. Each island is weakly coupled to each of its four neighbors through a thin oxide layer defining a Josephson junction. All investigated arrays are quasi one-dimensional, having a length of $N_\mathrm{C} = 303$ cells and a width of $N_\mathrm{W} = 5$ cells. The long sides of the array are made of solid superconducting electrodes, hereafter called busbars. A scanning electron microscope picture as well as a schematic layout of one of the investigated arrays are shown in Fig. 2.1.

The coupling E_J of the junctions, as well as the spacing between them, can be tailored at will in the fabrication process. Three different arrays have been investigated. They are schematized in Fig. 2.2a. The first one (sample I) is a regular array. The length of the cells is $a = 2~\mu$m and their width $b = 0.7~\mu$m. The coupling of all junctions equals $E_\mathrm{J} = 0.43$ meV, and their capacitance is $C = 2$ fF. In the two other arrays, a periodic superstructure of three cells is built along the length of the array. In the weakly asymmetric array (sample II), only the length of the cells is varied, in ratios 0.5–1–1.5 relative to the value $a = 2~\mu$m of the regular array. In the ratchet array (sample III), the length of the cells is varied in ratios 0.5–2–0.5, and the coupling of the vertical junctions is varied in rows in ratios 1.2–1–0.8 relative to the coupling $E_\mathrm{J} = 0.43$ meV of the horizontal junctions (see Fig. 2.1). As the couplings are varied by changing the cross section of the corresponding Josephson junctions, their capacitances are expected to change in the same proportions.

For reviews on Josephson junction arrays, see, e.g., Ref. [8, 9]. In the next three sections, we will discuss some of their static and dynamic properties which are relevant for the experiment considered.

2.2.3   Statics of the array: single vortex case

A magnetic field applied perpendicularly to the plane of the array induces vortices in the discrete field formed by the phases φ_i of the superconducting order parameter of the islands. Each vortex is associated with a circular current flowing in the Josepson junctions around it, in a configuration which minimizes the total energy of the array. The magnetic flux generated by this current is exactly one flux quantum Φ_0. The number of vortices in the array is thus controlled by the ratio between the total magnetic flux Φ through the array and the flux quantum Φ_0.

The superconducting busbars tend to keep their order parameter constant and to accommodate a current flow perpendicular to them. Consequently, they repel the vortices, which are confined in the middle of the array. The dynamics of the vortices is thus essentially one-dimensional, along the length of the array.

These properties can be derived quantitatively by solving the equations obtained from the application of Kirchhoff's first law, which expresses current conservation,
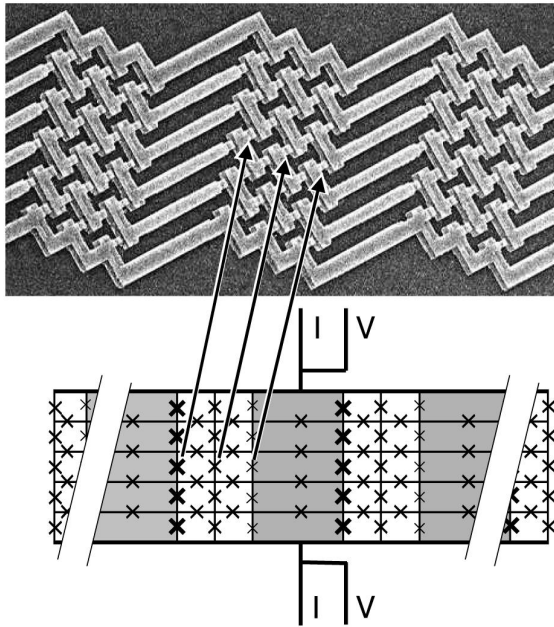
Figure 2.1: Strongly asymmetric Josephson junction array that exhibits a ratchet effect. Top: scanning electron microscope picture. Bottom: schematic layout. Josephson junctions are represented by a cross, cells are areas enclosed by four junctions. All measured arrays have a length of 303 cells and a width of 5 cells between solid superconducting electrodes (busbars). Vortices are induced by an applied magnetic field perpendicular to the array. A uniform current I imposed between the busbars exerts a force on the vortices, parallel to the busbars, whereas the voltage V arising between the busbars is proportional to the velocity of the vortices. Cell areas are 2.8 μm^2 (gray) and 0.7 μm^2 (white). Junctions indicated by arrows have areas of 240x100 nm^2, 200x100 nm^2, and 160x100 nm^2, respectively.
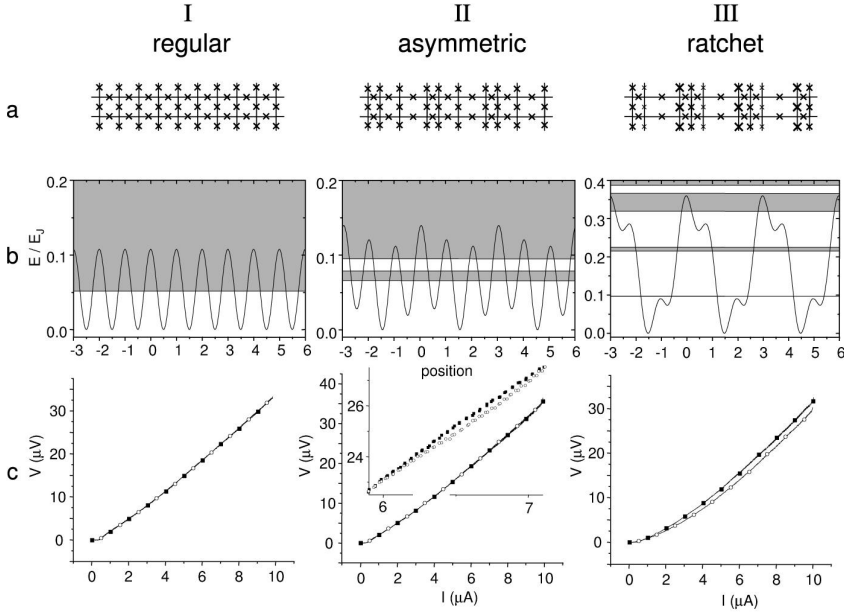
Figure 2.2: Samples and measurement results. The top row (a) indicates three supercells for each of the three arrays, row (b) the resulting potential. The calculated vortex bands are also indicated. Sample I is a regular array. It has a cosine-shaped vortex potential and one energy band that connects with a continuum. Sample II shows a weak asymmetric modulation on top of this cosine potential that leads to a gap in the spectrum with one band below the continuum. Sample III has a strongly asymmetric potential with three energy bands below the continuum. The bottom row (c) gives the measurement results for voltage (vortex current) versus bias current (vortex force), performed at 12 mK and a density s of 0.61 vortices per supercell. Open circles label the positive branch and closed squares the negative branch. Sample III shows a clear asymmetry. Sample II shows a weak asymmetry only at high bias. Inset: blow-up of the V–I curve for sample II at large bias currents showing a weak ratchet effect.

at each island of the array. Using (2.5), considering a static situation and assuming that all islands are at the same voltage, the conservation of currents flowing from an island i to any of its neighbors j may be written

$$\sum_{j \text{ neighbor of } i} I_{\text{c},ij} \sin(\gamma_{ij}) = 0, \tag{2.8}$$

where $I_{\text{c},ij}$ denotes the critical current of the junction connecting the neighboring islands i and j. The magnetic field enters via the definition (2.2) of the gauge-invariant phase difference between the phases φ_i and φ_j of the islands. In this model, the amplitude and phase of the order parameter are assumed to be constant on the whole busbar, for the sake of simplicity. In reality, the amplitude varies on a scale given by the coherence length ξ (for aluminum $\xi = 1.6 \ \mu$m), whereas one expects the phase to vary on a scale given by the Josephson penetration depth $\lambda_{\text{J}} = \sqrt{\hbar/2e\mu_0 I_{\text{c}}(2\lambda + d)}$, which depends on the London penetration depth λ and the junction thickness d. For aluminum junctions ($\lambda = 15.7$ nm) with critical current $I_{\text{c}} = 0.2 \ \mu$A and thickness $d < 30$ nm, one finds $\lambda_{\text{J}} > 4.5$ mm. All islands of the upper row of the array are connected to the upper busbar by vertical junctions. Likewise, the islands of the lower row are all connected to the lower busbar.

The solution of the set of equations (2.8) corresponds to an extremum of the function

$$E_{\text{pot}} = -\sum_{<i,j>} E_{\text{J},ij} \cos(\gamma_{ij}), \tag{2.9}$$

which represents the total potential energy of the array. The sum runs over all pairs of islands connected by a junction. Here again, the coupling of each junction is related to its critical current by $E_{\text{J},ij} = \hbar I_{\text{c},ij}/2e$.

Let us first discuss the case where the magnetic field is such that the flux through the array exactly equals one flux quantum Φ_0, and consider a completely regular array $b = a$ for simplicity. In this situation, the configuration of the phases φ_i which minimizes the energy of the array (2.9) presents a single vortex sitting in the central cell of the array, that is at the intersection of the central row with the central column. The corresponding phase and current configurations are shown in Fig. 2.3. The presence and location of a vortex is characterized via the cell vorticity n_{v}, found in the expression

$$\sum_{\text{plaquette}} \gamma_{ij} = 2\pi(n_{\text{v}} - f), \tag{2.10}$$

where the sum runs anti-clockwise over the four junctions around a given cell, the gauge-invariant phase differences γ_{ij} are taken in the interval $] - \pi, \pi]$, and $f = Ba^2/\Phi_0$ is the flux per cell in units of Φ_0. By construction [see Eq. (2.2)], the vorticity n_{v} is an integer. A vortex is characterized by $n_{\text{v}} = 1$, an antivortex by $n_{\text{v}} = -1$, and so on.

Other local minima of the array energy correspond to a vortex sitting in the middle of other cells. For positions along the central row of the array, the energy

a) phases
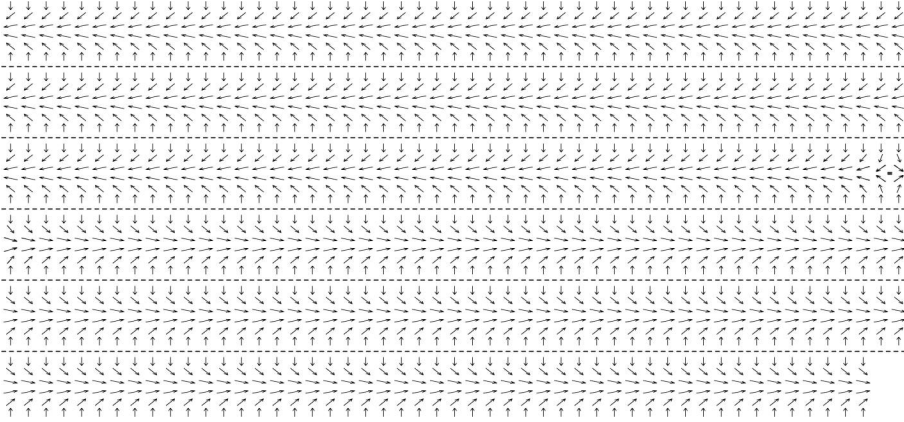
b) currents
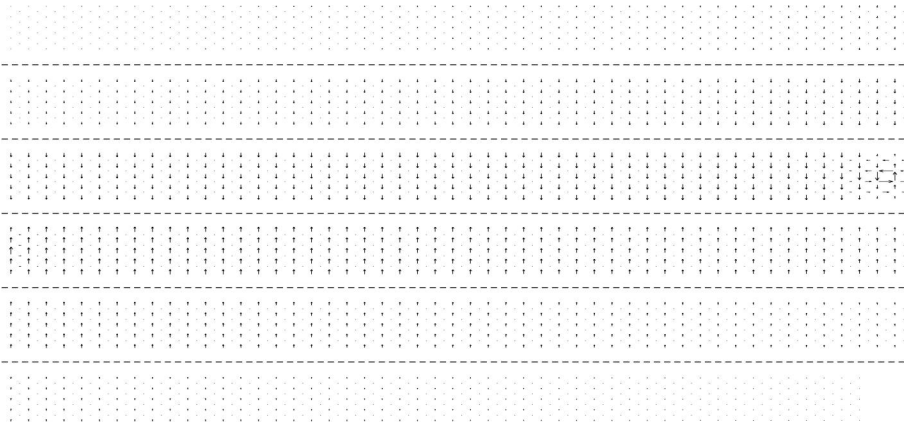
Figure 2.3: Phase (a) and current (b) configurations in the Josephson junction array. The magnetic field corresponds to one flux quantum Φ_0 through the array. A vortex sits in the central cell of the array, indicated by a black square in (a). In these representations, the array of 303x5 cells is broken in 6 pieces separated by dashed lines. The upper line corresponds to the left end of the array, whereas the lower line is its right end. The phases of the busbars are repeated all over their length. In the current configuration (b), the magnitude of the arrows is such that a current equal to the critical current I_c of the corresponding junction would be represented by an arrow with a length equal to the lattice spacing.

increases quadratically with the distance from the central cell, which corresponds to a boundary pinning energy. The difference between the phases of the busbars is found to depend linearly on the longitudinal position of the vortex, from 0 (left) to 2π (right). If the vortex is situated outside the central row, the energy is also higher, showing the repulsion of the busbars. Finally, configurations with another number of vortices present in the array, for example two vortices and one antivortex, are also local minima of the total energy. All these configurations correspond to higher energies.

A very good approximation of the phase configuration corresponding to a vortex can be obtained from the continuous limit of the set of equations (2.8), obtained by taking the limit $a \to 0$. The gauge-invariant phase difference (2.2) is replaced by a field

$$\vec{G}(x, y) = -\vec{\nabla}\varphi(x, y) - \frac{2\pi}{\Phi_0}\vec{A}(x, y) \tag{2.11}$$

on the whole array $x \in [-L_x/2, L_x/2]$, $y \in [-L_y/2, L_y/2]$. In terms of this field, the Josephson current density reads

$$\vec{\jmath}(x, y) = I_\mathrm{c}\vec{G}(x, y). \tag{2.12}$$

The current conservation equations (2.8) yield the defining equation for the field

$$\vec{\nabla} \cdot \vec{G}(x, y) = 0, \tag{2.13}$$

with boundary conditions

$$G_x(-L_x/2, y) = G_x(L_x/2, y) = 0 \tag{2.14a}$$
$$G_y(x, -L_y/2) = G_y(x, L_y/2) = 0. \tag{2.14b}$$

From Eq. (2.10), one gets

$$\oint_\mathcal{C} \vec{G}(x, y) \cdot \mathrm{d}\vec{r} = 2\pi(n_\mathcal{C} - f_\mathcal{C}), \tag{2.15}$$

where $n_\mathcal{C}$ denotes the number of vortices enclosed by a given curve $\mathcal{C}$, and $f_\mathcal{C}$ the flux through the area delimited by $\mathcal{C}$ in units of Φ_0. Finally, the energy (2.9) takes the form

$$E_\mathrm{tot} = \frac{E_\mathrm{J}}{2} \int_{-L_x/2}^{L_x/2} \mathrm{d}x \int_{-L_y/2}^{L_y/2} \mathrm{d}y \left|\vec{G}(x, y)\right|^2. \tag{2.16}$$

The solution of the differential equation (2.13) with boundary conditions (2.14), corresponding to a vortex at position $(q, 0)$ in the array, yields a phase configuration

$$\varphi(x, y) = -\arctan\left(\frac{\tan(\pi y/L_y)}{\tanh(\pi(x - q)/L_y)}\right) + \pi\theta(x - q) - 2\pi\frac{qy}{L_x L_y}, \tag{2.17}$$

in the limit where the distance between the center of the vortex at position q and the left or right boundary of the array is much bigger than L_y (or, alternatively, in the limit $L_x \to \infty$). The first two terms determine the shape of the vortex core. One sees that in the longitudinal direction, the vortex configuration decreases exponentially on the length scale L_y of the lateral confinement. The last term shows the linear dependence of the phase difference between the busbars $\varphi(x, -L_y/2) - \varphi(x, L_y/2)$ on the longitudinal position q of the vortex. For comparison, in an infinite two-dimensional array (L_x, $L_y \to \infty$), the phase configuration would be $\varphi(x,y) = -\arctan(y/x)$.

Let us now come back to the discrete array. The total energy (2.9) has local maxima when the vortex sits exactly on the junction between two islands. The difference between the energy of this maximum with the energy of the minimum reached when the vortex sits in the middle of a cell is the energy barrier that a vortex has to overcome to move from one cell to an adjacent cell. What is the shape of this potential barrier? One way to estimate it is to minimize the energy (2.9) with a constraint on the phase difference along the junction crossed by the vortex. The minimization is repeated whereas the constraint is moved from the value that this phase difference has when the vortex is in the initial cell, through the value π corresponding to the vortex sitting at the top of the barrier, until the value corresponding to the vortex in the final cell. The outcome gives the successive potential energies of the vortex. Assuming that we move the vortex along the middle row of the array, its position can be extracted from the phase difference between the busbars, and one obtains the potential $V(q)$ felt by a vortex moving along the array. Another method to get $V(q)$ is to substitute the configuration (2.17) obtained from the continuous model into the energy (2.9) of the discrete array. They give slightly different results.

The different geometries of the three samples investigated in the experiment lead to different potential landscapes for the vortices. These potentials are depicted in Fig. 2.2b. They have been evaluated by minimization of the array energy under constraint of the phase difference of the junction crossed by the vortex, as discussed above. The procedure has been done for a vortex in the center of the array, far away from the left and right boundaries, where the boundary pinning energy is minimal and stays roughly constant on several cell lengths.

For the regular array (sample I), one finds a cosine potential given by $V(q) \approx 0.05 E_{\mathrm{J}}[1 - \cos(2\pi q/a)]$, in terms of the Josephson coupling $E_{\mathrm{J}} = 0.43$ meV and the spatial periodicity $a = 2$ μm. The potentials of the superstructured array, which have a periodicity $L = 3a$, are well approximated by the three first harmonics of their Fourier expansion

$$V(q) \approx V_0 + \sum_{l=1}^{3} V_l \cos(2\pi l q/L - \psi_l). \qquad (2.18)$$

For the weakly asymmetric array (sample II), one finds the parameters

$$V_0 = 0.0663E_{\mathrm{J}}$$
$$V_1 = 0.0157E_{\mathrm{J}} \qquad\qquad \psi_1 = -2.97$$
$$V_2 = 0.0002E_{\mathrm{J}} \qquad\qquad \psi_2 = -2.11$$
$$V_3 = 0.0508E_{\mathrm{J}} \qquad\qquad \psi_3 = 3.12. \qquad (2.19)$$

One notices that the second harmonics is essentially absent. For the ratchet array (sample III), one has

$$V_0 = 0.152E_{\mathrm{J}}$$
$$V_1 = 0.153E_{\mathrm{J}} \qquad\qquad \psi_1 = -2.58$$
$$V_2 = 0.0368E_{\mathrm{J}} \qquad\qquad \psi_2 = -0.0423$$
$$V_3 = 0.0551E_{\mathrm{J}} \qquad\qquad \psi_3 = 2.82. \qquad (2.20)$$

In this last sample, $E_{\mathrm{J}} = 0.43$ meV now represents the average Josephson coupling of the junctions. In all these expressions, the constant V_0 has been chosen so that the minimum of the potential is $V(q_{\min}) = 0$, as well as an overall phase such that the barriers lie at $q_{\max} = \pm L/2$.

2.2.4 Statics of the array: multiple vortices

Let us now increase the magnetic field. One then expects as many vortices in the array as there are flux quanta Φ_0 contained in the total magnetic flux Φ through the array. This is indeed what one finds by minimizing the total energy (2.9) of the array. The configurations of lowest energy present a number of vortices equal or closest to Φ/Φ_0, which are arranged in a chain in the whole central row of the array, roughly equidistant of each other. This behavior was observed for magnetic fields corresponding to up to 61 vortices in the 303 cells long array. This means that the average distance between the vortices, when they arrange in a chain on the whole length of the array, is larger than the longitudinal core size, given by L_y. We did not investigate situations with higher magnetic fields.

For a given magnetic field, configurations with some vortices sitting outside of the central row of the array (zigzag deformation of the chain), or with a different number of vortices, e.g. additional vortex-antivortex pairs, also correspond to local minima of the energy, with a higher value than the linear chain configuration.

Such chains of vortices have been theoretically studied, e.g., in Ref. [10]. The formation of a chain indicates that the vortices repel each other. One way to understand this repulsive interaction is to realize that, when two vortices approach each other, the currents curling around their cores compete in the area between the vortices, as they flow in opposite direction. In extended two-dimensional Josephson junction arrays, the vortex-vortex interaction can be well approximated [10] by

the expression holding for vortices induced in a thin film of type II superconductor. This interaction is repulsive. When the distance r between the vortices is much shorter than the London penetration depth λ, the interaction follows a logarithmic dependance $-\ln(r/\lambda)$, whereas at large distances $r \gg \lambda$, it decays exponentially as $r^{-1/2}\mathrm{e}^{-r/\lambda}$ [11]. The London penetration depth λ is the length scale on which the circulating currents around the vortices decay. In quasi one-dimensional arrays, as we have seen, the boundaries play a crucial role, and the interaction behaves rather as $-r$ [10].

We have seen above that single vortices minimize their energy if they sit in the middle of a cell. This mechanism will compete with the repulsive vortex-vortex interaction and boundary pinning, which favor the formation of a regular chain. As a result, one can imagine that the chain of vortices will try to adapt to the underlying periodicity of the array. One can expect radically different behaviors in the vortex dynamics depending whether the periodicity of the vortex chain is commensurate or incommensurate with the one of the array. The relevant quantity is thus the vortex density in a periodicity length of the array, also named frustration. In the regular array (sample I) made of N_C columns, it is given by

$$n = \frac{\Phi}{N_\mathrm{C} a \Phi_0}. \tag{2.21}$$

In the superstructured arrays (samples II and III), where a periodicity length contains 3 cells, the relevant variable is rather the superlattice density $s = 3n$.

Experimentally, this has been investigated by measuring the small-bias resistance as a function of the magnetic field [6]. The resistance was defined as the ratio between the measured voltage V and the applied current I between the busbars. As discussed below, the current act as a force on the vortices, whereas the voltage measures their velocity. Sharp dips signaling localization have been found at commensurate situations, when $1/n$ is an integer for the regular array, and when $1/s$ is an integer for the superlattices. However, between these commensurate situations, the response behaves in good approximation linearly in the density n or s. The ratchet experiment has been performed in such an incommensurate situation, for $s = 0.61$ vortices per supercell, corresponding roughly to 62 vortices in the array.

2.2.5 Vortex dynamics

A current I flowing between the busbars through the $N_\mathrm{C} + 1$ columns of Josephson junctions adds to the current pattern associated with each vortex, and induces a force on them. Quantitatively, this can be seen as follows: In the set of equations (2.8) describing current conservation on the islands, the two equations corresponding to the busbars get an nonzero term in their right-hand-side, which is $+I$ for the busbar out of which the current is extracted, and $-I$ for the busbar in which it is injected. Accordingly, the total energy (2.9) of the array, which was introduced as the function

whose extremizing conditions are the current conservation equations (2.8), gets a new term

$$E_{\text{pot}} = - \sum_{<i,j>} E_{\text{J},ij} \cos(\gamma_{ij}) - \frac{\hbar I}{2e} \Delta \varphi_b, \qquad (2.22)$$

where $\Delta \varphi_b$ denotes the phase difference between the busbars. For the single vortex case, we have seen above that this phase difference depends linearly on the longitudinal position q of the vortex, and numerics confirms the proportionality coefficient $\Delta \varphi_b = 2\pi q / (N_{\text{C}} + 1)a$ for a discrete array. Thus, the additional term in the energy may be written $-Fq$, where

$$F = \frac{\Phi_0}{(N_{\text{C}} + 1)a} I \qquad (2.23)$$

is interpreted as a force on the vortices, pointing in the long direction of the array.

As soon as a force acts on the vortices, their motion has to be considered in the description as well. The motion of the vortices means that the phases of the islands will vary in time, and voltages arise on the junctions according to the second Josephson law (2.3). The static assumption of a constant voltage all over the array must be relaxed in this situation. The application of Kirchhoff's second law, which requires that the sum over voltage differences along any loop vanishes, yields another set of equations in addition to the current conservation (2.8). They correspond to add a kinetic term

$$E_{\text{kin}} = \sum_{<i,j>} \frac{\hbar^2 C_{ij}}{8e^2} \left(\frac{\mathrm{d}\gamma_{ij}}{\mathrm{d}t} \right)^2 \qquad (2.24)$$

to the total energy of the array (2.22), where C_{ij} denotes the capacitance between islands i and j. For a quantum description, the phase differences $\hat{\varphi}_i$ as well as the excess of Cooper pairs $\hat{N}_i \mathrel{\hat=} \hat{Q}_i / 2e$ on each island are treated as operators, as discussed in Section 2.2.1 for a single junction, and one works with the Hamiltonian

$$\hat{H} = 2e^2 \sum_{i,j} \hat{N}_i (C^{-1})_{ij} \hat{N}_j - \sum_{<i,j>} E_{\text{J},ij} \cos(\hat{\gamma}_{ij}) - \frac{\hbar I}{2e} \hat{\Delta \varphi}_b, \qquad (2.25)$$

where C^{-1} denotes the inverse of the matrix of capacitances C_{ij}.

Each island, with its pair of conjugated variables $\hat{\varphi}_i$ and $\hat{N}_i$, is one degree of freedom. In principle, the dynamics has to be solved in terms of these many degrees of freedom, which are coupled. However, one can expect that the dynamics may be described in terms of collective modes. In particular, the analysis of the statics of the array suggests vortices as natural candidates for such collective modes. One usually assumes that the vortices move in the array without change of their rest profile. By substituting the vortex configuration found in the static analysis, e.g. (2.17), into the Hamiltonian (2.25) of the array, one can derive an effective Hamiltonian in term of a single degree of freedom, being the position $\hat{q}$ of the vortex. The dynamics of

single vortices in Josephson junction arrays has been theoretically investigated, e.g., in Refs. [12–15].

The capacitive energy of the junctions acts as a kinetic energy for the vortex. The corresponding mass has been estimated [14] to

$$M \approx \frac{\Phi_0^2 C}{2a^2} = \frac{\pi^2 \hbar^2}{4E_{\mathrm{C}} a^2} \qquad (2.26)$$

for a vortex in a two-dimensional regular array of spacing a, with all capacitances equal to C. For the parameter values of the experiments, this corresponds to one thousandth of the electron mass. We also did a numerical investigation for a regular quasi one-dimensional array. We can extract the mass by rewriting the kinetic energy (2.24) as

$$E_{\mathrm{kin}} = \sum_{<i,j>} \frac{\hbar^2 C}{8e^2} \left(\frac{\mathrm{d}\gamma_{ij}}{\mathrm{d}q}\right)^2 \left(\frac{\mathrm{d}q}{\mathrm{d}t}\right)^2 = \frac{M}{2}\left(\frac{\mathrm{d}q}{\mathrm{d}t}\right)^2, \qquad (2.27)$$

The derivatives $(\mathrm{d}\gamma_{ij}/\mathrm{d}q)^2$ can be evaluated with a difference formula, from the configurations $\varphi_i(q)$ and $\varphi_i(q + \mathrm{d}q)$ obtained by minimizing the potential energy of the array for a vortex constrained at the position q, respectively $q + \mathrm{d}q$. The minimization procedure is identical to the one described above for the evaluation of the vortex potential. The mass obtained by this method is a periodic function of q, with the periodicity a of the lattice. It oscillates around a value $M \approx 0.8\pi^2\hbar^2/4E_{\mathrm{C}} a^2$, close to the two-dimensional result (2.26).

Combining this analysis of the kinetic term with the discussion of the potential term in Section 2.2.3 above, we are now in the position of writing the effective Hamiltonian for a single vortex in the array. Assuming that the vortex dynamics is restricted along the central line of the array, by invoking the repulsion from the busbars, we obtain the Hamiltonian

$$\hat{H}_{\mathrm{eff}} = \frac{\hat{p}^2}{2M} + V(\hat{q}) - F\hat{q}, \qquad (2.28)$$

in terms of the one-dimensional coordinate $\hat{q}$, representing the longitudinal position of the vortex on the central line of the array, and its conjugate momentum $\hat{p}$. The mass M is obtained from (2.26), the potential $V(\hat{q})$ from (2.18), and the force F from (2.23). In this derivation, the vortex emerges thus fundamentally as a quantum particle. The reason is that it is a collective mode of the dynamics of the phases of the superconducting islands, which in general are subject to quantum dynamics [see Eq. (2.25)]. The typical action of the vortex of mass M in the potential of periodicity L and barrier height ΔV can be estimated as $\sqrt{2M\Delta V L^2}$ (see Table 4.1). For the potential extracted for the ratchet array (sample III), which has a periodicity $L = 3a$ and a barrier height $\Delta V = 0.368 E_{\mathrm{J}}$, we get an action $\sqrt{9 \times 0.368 E_{\mathrm{J}}/8E_{\mathrm{C}}} \times h$. Substituting the ratio $E_{\mathrm{J}}/E_{\mathrm{C}} \approx 11$ obtained from the experimental parameters, this

yields an action of the order of $2.1h$. The numerical evaluation of the band structure shows that there are three bands below the potential barrier (see Section 4.2.2). The vortices may be treated as classical particles only when their action is much larger than h.

It has been shown [16] that tunneling of quasiparticles through the junctions leads to an additional capacitance $C_{qp} = 3h/64\Delta R_n$ in parallel to the junctions. For aluminum junctions at zero temperature ($\Delta = 0.1$ meV), with a normal state resistance of $R_n = 1.5$ kΩ, this additional capacitance is of the order of 1 fF.

A dissipative quasiparticle current flowing through the junctions, described by a current through the shunt resistor R in the RCSJ model, will cause energy dissipation in the array. In a phenomenological model [15] for the vortex dynamics which reproduces the estimate for the mass (2.26), this dissipation could be included as a viscous force on the vortex, with the viscosity coefficient

$$\eta \approx \frac{\Phi_0^2}{Ra^2}. \tag{2.29}$$

Combining with the mass (2.26), we get a typical dissipation time scale $\gamma^{-1} = (\eta/M)^{-1} = RC/2$ for vortices. Using the normal state resistance $R_n = 1.5$ kΩ as an estimate for R, one has $\gamma^{-1} \approx 1.5$ ps. It seems that this mechanism is not enough to explain the values of dissipation measured in Josephson junction arrays [17]. The mechanisms of dissipation relevant for the vortex motion are not well understood. It could be that the vortices loose their energy by exciting linear modes of the array, which involve small oscillations of the phases of the junctions at the plasma frequency given by $\hbar\omega_p = \sqrt{8E_J E_C}$. The corresponding energy is about 0.3 meV for the system considered.

Furthermore, in a quantum description of the vortex dynamics, dissipative effects can no longer be described with a phenomenological viscous force. Instead, a system-plus-bath formalism such as the one introduced in Section 1.1.2, where the viscosity η enters as the prefactor of the bath spectral density, can be used.

Finally, the second Josephson law (2.3) implies that a voltage

$$V = \frac{n\Phi_0}{a}v \tag{2.30}$$

arises between the busbars if vortices flow at a velocity $v = dq/dt$ parallel to them. This voltage is proportional to the density n of vortices per column of the array, given in (2.21). For the single vortex case, we can prove this expression (up to a factor $N_C/(N_C + 1) \approx 1$) by using the linear dependence of the phase difference between the busbars on the longitudinal position q of the vortex, discussed above.

2.2.6 Summary of the model

As a working model in order to confront experimental results with a theoretical description, we will use the one-particle Hamiltonian (2.28), which is discussed in

more detail in Section 1.1.3. Dissipative effects are included as a coupling to a
thermal environment. As we have seen in the previous section, the dc current I
applied between the busbars is responsible for the time-independent force F on
the vortices [see Eq. (2.23)], whereas the voltage V between the busbars measures
the vortex velocity v [see Eq. (2.30)]. Thus, the $V(I)$ characteristics of the array
is linked to the stationary particle velocity $v_{\mathrm{DC}}^{\infty}(F)$ in the model, which has been
defined in Eq. (1.21). As the force is time-independent, the model corresponds to a
tilted ratchet. However, as we discussed [see Eq. (1.4)], the ratchet current v_{R}^{∞} in a
rocked ratchet subject to an adiabatic bistable driving force of amplitude F can be
extracted from the two branches of the tilted ratchet characteristics, as

$$v_{\mathrm{R}}^{\infty} = v_{\mathrm{DC}}^{\infty}(F) + v_{\mathrm{DC}}^{\infty}(-F). \qquad (2.31)$$

We will now summarize the assumptions underlying the simplified description in
terms of the Hamiltonian (2.28), which has emerged in the previous sections. The
dynamics of the array is treated in terms of the collective modes defined by the
vortices only. The vortices are treated as independent. The argument of the linear
dependence of the small-bias resistance of the array as a function of the magnetic
field, observed experimentally in incommensurate situations, is used to justify this
assumption: This measurement tells that the response of the array depends linearly
on the number of vortices. In this line of thought, the response of the array is
modeled as the response of a single vortex multiplied by the number of vortices.
Accordingly, one works with the one-particle model (2.28). Essentially, this assump-
tion corresponds to neglect vortex-vortex interactions. However, this approximation
may be bad, as the formation of a chain of vortices, seen in the static analysis of
the array, rather indicates a strong vortex-vortex interaction. We will come back
on this point in Section 2.2.8. The repulsive interaction from the busbars on the
vortices has been taken into account as a strict restriction of the dynamics to one
dimension, along the center line of the array. Furthermore, in the one-dimensional
potential $V(q)$ for the vortices, the pinning energy from the left and right bound-
aries has been neglected. The mechanism of vortices leaving and reentering the
array, necessary for a continuous flow, has not been considered. This nucleation
mechanism has been investigated, e.g., in the classical overdamped dynamics at zero
temperature of vortices in a type-II superconductor channel [18]. Finally, a periodic
variation of the vortex mass along the array has been disregarded.

2.2.7 Experimental results

The $V(I)$ characteristics of the three different arrays, measured at a temperature $T =$
12 mK, are shown in Fig. 2.2c. The negative branch of the characteristics, for $I < 0$,
is reversed as $-V(-I)$ in order to be represented in the same quadrant as the positive
branch $V(I)$ for $I > 0$. As discussed in the previous section, the $V(I)$ characteristics
of the array is related to the stationary particle velocity $v_{\mathrm{DC}}^{\infty}(F)$ in the model. The
ratchet current (2.31) is thus given by the difference of the two branches.

The measurements show a clear ratchet effect for the strongly asymmetric sample. However, no voltage asymmetry is observed between positive and negative currents for the regular sample and for the weakly asymmetric sample at low bias currents. The symmetry for the regular array serves as a check for the validity of the experimental methods. The lack of voltage asymmetry for sample II at low currents is remarkable, however. At first, it has been interpreted as due to the fact that only the lowest Bloch band of the untilted potential participates in the dynamics. Indeed, as shown in Section 4.3, the ratchet current vanishes in a tight-binding description truncated to the lowest energy band. However, this explanation does not seem reasonable as the energy gap between the two first bands is of the same order of magnitude for samples II and III. It is a fact that the potential of sample II looks much less asymmetric than the one of sample III. The question is, in which quantitative form, through which combination of the potential parameters, does the asymmetry come into the expression for the ratchet current? The model developed in Chapter 6 provides an answer, in the case where an expansion of the ratchet current in the amplitudes of the harmonics of the potential (2.18) is rapidly converging. Then, the dominant contributions are third-order contributions, proportional to $V_1^2 V_2 \sin(\psi_2 - 2\psi_1)$ and $V_1 V_2 V_3 \sin(\psi_3 - \psi_2 - \psi_1)$. Whereas these contributions are present for the potential (2.20) characterizing the sample III, they vanish for the potential (2.19) of sample II, whose second harmonic is absent $V_2 \approx 0$. In this case, the dominant contributions to the ratchet current are only at fourth order $V_1^3 V_3 \sin(\psi_3 - 3\psi_1)$.

An even more striking result is that all three samples exhibit a power-law behavior of $V \propto I^\delta$ with exponent $\delta > 1$ for moderate-to-large currents, as shown in Fig 2.4. Strikingly, for a large range of currents, sample I and II are lying on top of each other ($\delta = 1.21$), despite the dissimilarity of the underlying potential. For sample III, different powers for the two slopes ($\delta = 1.46$ and $\delta = 1.53$), which are higher than the powers of the previous samples, are measured. The nonlinearity of the characteristics is a signature of quantum behavior. Indeed, for a classical dynamics and zero temperature, $V \propto I$ is expected above the critical current, as the vortex velocity saturates to $v = F/\eta$.

We are not aware of any theoretical explanation of this power-law behavior of the stationary velocity in such a range of driving forces. The two complementary methods that we have developed in this thesis (Chapters 4 and 6) do not solve this puzzle. In both descriptions, one obtains an expression for the stationary velocity in terms of transition rates Γ in a dissipative tight-binding model. These rates indeed present a power-law behavior $\Gamma \propto F^{2\alpha-1}$ at low temperatures $k_B T \ll FL$, with an exponent depending on the dissipation parameter $\alpha = \eta L^2 / 2\pi\hbar$. However, the description presented in Chapter 4 is applicable at low driving F only, the approximation on which it relies breaking down at a driving force corresponding to a bias current of about 0.5 μA. This excludes any confrontation with the experimental result. In the method presented in Chapter 6, the rates show a power-law, where α
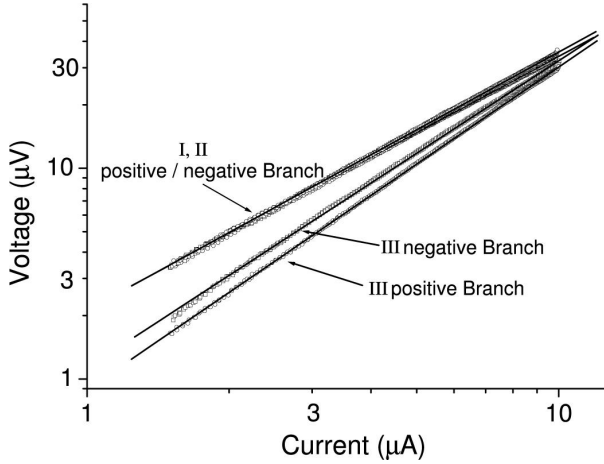
Figure 2.4: Power-law dependence of the $V(I)$ characteristics at 12 mK. All three samples exhibit a behavior $V \propto I^\delta$, with $\delta > 1$, above 1.5 μA. The two branches of sample III show larger powers than samples I and II, whose branches all collapse on the same curve. The classical behavior would correspond to linear $V(I)$ characteristics, i.e., $V \propto I$.

is replaced by $\tilde{\alpha} = \alpha^{-1}$, but their combination in the expression for the stationary velocity does not itself result in a power-law. This method, however, is applicable up to large driving F, where the classical behavior $v_{\mathrm{DC}}^\infty = F/\eta$ is recovered. This regime has not been seen in the experiment. In Fig. 2.4, it would correspond to a crossover, all curves merging on a line of slope $\delta = 1$. One notices, however, that the power-law fits of the experimental data cross each other at a bias current higher than the experimentally investigated range [19]. If observed in experiments, this linear regime would provide a direct estimation of the strength of dissipation, as the proportionality coefficient is simply $1/\eta$.

Using the value of experimental parameters to convert the measured $V(I)$ characteristics into the stationary current $v_{\mathrm{DC}}^\infty(F)$ obtained in Chapter 6, we get an agreement on the orders of magnitude for a realistic value of dissipation η (see discussion of Fig. 6.2). This conversion is also shown by alternate axes in Fig. 4.4.

The temperature dependence of the ratchet signal is shown in Fig. 2.5. On the right axis the difference V_{asymm} between the two branches is plotted for a fixed bias and density ($s = 0.38$ for sample II; $s = 0.28$ for sample III). We also include the mean of the two branches V_{symm} (plotted on the left axis) for sample III. Below 350 mK down to the base temperature of 12 mK the signals stay constant for sample III. This is a clear quantum signature. As discussed in Section 1.1.2, a classical ratchet effect, resulting from thermal activation, should decay exponentially with
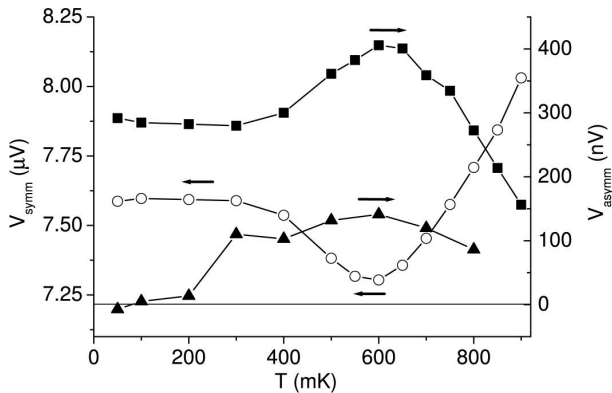
Figure 2.5: Temperature dependence of the ratchet effect. Plotted with closed symbols on the right scale (squares for sample III, triangles for sample II): V_{asymm} defined as the difference between the voltages for negative and positive currents. Plotted with open symbols (only sample III) on the left scale: V_{symm} defined as the mean of these voltages. The bias current is 6 μA for sample III, and 4 μA for sample II.

temperature. Above 350 mK the ratchet signal increases up to 650 mK and then decreases for higher temperatures. In the discussion of the temperature dependence of the ratchet current, two additional effects have to be taken into account with respect to the theoretical model. First, when the critical temperature of the superconductor is approached ($T = 1.2$ K for aluminum) the Josephson energy of the junctions decreases. This explains the decrease of the ratchet effect above 650 mK, due to the weaker potential. The fact that the mean transport simultaneously increases is consistent with that picture. In the intermediate regime (350 mK–650 mK), the increase of the thermal energy available for transport, interplays with the generation of quasiparticles, which are an additional source of friction for the vortices. In contrast, in theory one usually discusses the temperature dependence at a constant dissipation strength. The initial decrease of the mean transport with increasing temperature reminds of the regime of thermally resisted tunneling (see Ref. [20] and Section 1.2), characteristic of weak dissipation $\alpha < 1$. This behavior is not incompatible with a simultaneous increase of the ratchet current (see Fig. 6.2). Similar features are exhibited by sample II.

2.2.8 Conclusions and outlook

In conclusion, we have shown that quasi one-dimensional Josephson junction arrays provide an experimental system to investigate ratchet dynamics of quantum vortices. Rectification has been observed for asymmetric potentials. The nonlinearity of the

characteristics as well as its saturation at low temperature are clear quantum signatures. A striking result is a very clean power-law behavior of the characteristics, as well as an apparent universality of the regular and weakly asymmetric samples.

A theoretical description has been attempted, which have led to the derivation of an effective ratchet Hamiltonian for a single vortex in the array. The investigation of its dynamics by two different methods, presented in Chapters 4 and 6, accounts for rectification and for the order of magnitude of the characteristics. However, it fails to explain the power-law behavior, among others.

An analysis of the approximations on which this description is based has been presented. The treatment of the many vortices present in the array as independent particles, which is experimentally suggested by the linearity of the response of the array on the number of vortices, corresponds to neglect effects of the vortex-vortex interaction. However, it has been shown [10] that this interaction can lead to the formation of a rigid vortex chain, which is a rather strong interaction effect. Our numerical simulations confirm this behavior. We think that further investigations beyond this approximation are necessary. It could be that the effective one-particle description is simply not valid, but it could also happen that such an effective one-particle description holds in terms of other collective excitations of the array. The relevant dynamical excitation could be the motion of the entire chain of vortices. The corresponding mass, the sum of the mass of all vortices, would be much higher, possibly placing the system in the semiclassical regime. Other possible excitations could be the motion of defects of the chain, especially in incommensurate situations. In a rigid chain, these defects may behave independently, possibly leading again to an effective one-particle description, with totally different potential landscape and parameters than the one that we have derived for vortices.

One outcome of the model presented in Chapter 6 points out a very general property of such descriptions in terms of a single degree of freedom. At large driving forces, the potential becomes irrelevant for the dynamics, implying that the characteristics goes to the classical linear dependence, and the ratchet current vanishes. The experimental observation of these features would provide a clear cut in favor of such a description, as well as a direct estimation of the strength of the effective dissipation felt by this degree of freedom.

A realistic treatment of the boundaries of the array would include the boundary pinning energy as well as the mechanism of escape and reentrance of the vortices.

From a theoretical point of view, the model presented in Section 2.2.3 could be used to give analytical expressions for the modification, in superstructured arrays, of the vortex mass, shape, and dissipation, with respect to the expression derived for regular arrays. The effect of a spatially oscillating effective mass on the single vortex dynamics could also be investigated. However, we do not expect that these refinements would lead to radically new physical effects.

References

[1] H. Linke, T. E. Humphrey, A. Löfgren, A. O. Sushkov, R. Newbury, R. P. Taylor, and P. Omling, Science **286**, 2314 (1999).

[2] J. B. Majer, J. Peguiron, M. Grifoni, M. Tusveld, and J. E. Mooij, Phys. Rev. Lett. **90**, 056802 (2003).

[3] F. Falo, F. J. Martínez, J. J. Mazo, T. P. Orlando, K. Segall, and E. Trías, Appl. Phys. A **75**, 263 (2002).

[4] A. Wallraff, A. Lukashenko, J. Lisenfeld, A. Kemp, M. V. Fistul, Y. Koval, and A. V. Ustinov, Nature **425**, 155 (2003).

[5] C. Mennerat-Robilliard, D. Lucas, S. Guibal, J. Tabosa, C. Jurczak, J.-Y. Courtois, and G. Grynberg, Phys. Rev. Lett. **82**, 851 (1999).

[6] J. B. Majer, *Superconducting Quantum Circuits*, Ph.D. thesis, Delft University of Technology (2002).

[7] B. D. Josephson, Phys. Lett. **1**, 251 (1962).

[8] R. S. Newrock, C. J. Lobb, U. Geigenmüller, and M. Octavio, in *Solid State Physics*, edited by H. Ehrenreich and S. Spaepen (Academic Press, San Diego, 2000), vol. 54, p. 263.

[9] R. Fazio and H. van der Zant, Phys. Rep. **355**, 235 (2001).

[10] C. Bruder, L. I. Glazman, A. I. Larkin, J. E. Mooij, and A. van Oudenaarden, Phys. Rev. B **59**, 1383 (1999).

[11] P. G. de Gennes, *Superconductivity of Metals and Alloys* (W. A. Benjamin, New York, 1966).

[12] E. Simanek, Solid State Commun. **48**, 1023 (1983).

[13] A. I. Larkin, Y. N. Ovchinnikov, and A. Schmid, Physica B **152**, 266 (1988).

[14] U. Eckern and A. Schmid, Phys. Rev. B **39**, 6441 (1989).

[15] T. P. Orlando, J. E. Mooij, and H. S. J. van der Zant, Phys. Rev. B **43**, 10218 (1991).

[16] A. I. Larkin and Y. N. Ovchinnikov, Phys. Rev. B **28**, 6281 (1983).

[17] H. S. J. van der Zant, F. C. Fritschy, T. P. Orlando, and J. E. Mooij, Phys. Rev. Lett. **66**, 2531 (1991).

[18] T. Dröse, R. Besseling, P. Kes, and C. Morais Smith, Phys. Rev. B **67**, 064508 (2003).

[19] J. B. Majer, private communication.

[20] M. P. A. Fisher and W. Zwerger, Phys. Rev. B **32**, 6190 (1985).

Chapter 3

Path Integrals Formalism for Tight-Binding Models

3.1   Introduction

In this chapter, we will derive general results for the reduced density matrix and transition rates in driven dissipative tight-binding systems, by means of real-time path integrals techniques.

We consider a driven tight-binding Hamiltonian of the general form

$$\hat{H}_{\mathrm{S}}(t) \,\hat{=}\, \sum_{\mu} \varepsilon_{\mu} |\mu\rangle\langle\mu| + \sum_{\mu} \sum_{\nu \neq \mu} \Delta_{\nu\mu} |\nu\rangle\langle\mu| - F(t)\hat{q}. \tag{3.1}$$

The index μ stands for a set of quantum numbers labeling the tight-binding sites. The basis states $|\mu\rangle$ are chosen such that the position operator

$$\hat{q} \,\hat{=}\, \sum_{\mu} q_{\mu} |\mu\rangle\langle\mu| \tag{3.2}$$

is diagonal. The diagonal elements ε_{μ} of the undriven Hamiltonian denote the on-site energies, whereas the off-diagonal elements $\Delta_{\nu\mu}$ represent the couplings between the sites. Due to the hermiticity of the Hamiltonian, the on-site energies ε_{μ} must be real quantities, whereas the couplings $\Delta_{\nu\mu}$ must satisfy $\Delta_{\mu\nu} = \Delta_{\nu\mu}^{*}$. In general, the driving force $F(t)$ may be time-dependent.

Some examples of Hamiltonians of the form 3.1 will be encountered in the next chapters. In the single-band tight-binding Hamiltonian (5.1) considered in Chapter 5, the set of quantum numbers $\mu = l$ reduces to the single integer l denoting the position $q_l = lL$ of the tight-binding sites, arranged in a chain at distance L of each other. The on-site energies ε_l are 0, and the couplings $\Delta_{l'l} \,\hat{=}\, \Delta_m$ depend on the distance $m \,\hat{=}\, l' - l$ between the sites only.

For the multi-bands Hamiltonian (4.35) investigated in Chapter 4, the set of quantum numbers $\mu = (m, j)$ consists of a band index $m = 1, \ldots, N_B$ and a site index j taking integer values. The sites of each of the M bands are periodically positioned $q_{m,j} = q_m + jL$. The on-site energies $\varepsilon_{m,j} = \varepsilon_m$ depend on the band only.

We want to include dissipation in the tight-binding model investigated. This is done by coupling the system Hamiltonian (3.1) with a thermal environment, which is modeled by the standard Hamiltonian $\hat{H}_B$ of a bath of N_O harmonic oscillators whose coordinates are bilinearly coupled to the system coordinate $\hat{q}$ [1]

$$\hat{H}_B = \frac{1}{2} \sum_{\alpha=1}^{N_O} \left[\frac{\hat{p}_\alpha^2}{m_\alpha} + m_\alpha \omega_\alpha^2 \left(\hat{x}_\alpha - \frac{c_\alpha}{m_\alpha \omega_\alpha^2} \hat{q} \right)^2 \right]. \tag{3.3}$$

The bath is fully characterized by its spectral density

$$J(\omega) \hat{=} \frac{\pi}{2} \sum_{\alpha=1}^{N_O} \frac{c_\alpha^2}{m_\alpha \omega_\alpha} \delta(\omega - \omega_\alpha), \tag{3.4}$$

defined in terms of the masses m_α, frequencies ω_α, and coupling strengths c_α of the oscillators. We refer to Section 1.1.3 for more details.

The information on the system dynamics is contained in the reduced density matrix $\hat{\rho}(t) = \mathrm{Tr}_B \hat{W}(t)$, obtained from the density matrix $\hat{W}(t)$ of the system-plus-bath $\hat{H}(t) = \hat{H}_S(t) + \hat{H}_B$ by performing the trace over the bath degrees of freedom. The diagonal elements $P_\mu(t) = \langle \mu | \hat{\rho}(t) | \mu \rangle$ of the reduced density matrix represent the populations of the tight-binding sites μ. They suffice in order to evaluate, e.g., the evolution of the average position

$$\langle \hat{q}(t) \rangle = \mathrm{Tr}_S \{ \hat{q} \hat{\rho}(t) \} = \sum_\mu q_\mu P_\mu(t). \tag{3.5}$$

The populations $P_\mu(t)$ can be obtained by real-time path integrals techniques [1, 2]. Although these techniques are standard, we will describe them for completeness and pedagogical clarity. This is the object of the next section and Appendix A.

3.2   Path integrals expression for the populations

We want to evaluate the populations

$$P_\mu(t) = \langle \mu | \, \mathrm{Tr}_B \, \hat{W}(t) | \mu \rangle. \tag{3.6}$$

Assuming that we know the total density matrix at some initial time t_0, we obtain its evolution at time t by the formula

$$\hat{W}(t) = \mathrm{e}^{-\frac{\mathrm{i}}{\hbar} \int_{t_0}^t \mathrm{d}t' \hat{H}(t')} \hat{W}(t_0) \mathrm{e}^{\frac{\mathrm{i}}{\hbar} \int_{t_0}^t \mathrm{d}t' \hat{H}(t')}, \tag{3.7}$$

where $\hat{H}(t) = \hat{H}_{\mathrm{S}}(t) + \hat{H}_{\mathrm{B}}$ denotes the total Hamiltonian of the system-plus-bath.

In order to get an explicit expression for the populations, we have to specify the initial preparation of the system-plus-bath. From a theoretical point of view, one usually considers the particular case in which the initial density matrix $\hat{W}(t_0)$ is the tensor product of a system operator and a bath operator. By definition, these operators must then be the initial reduced density matrix of the system $\hat{\rho}(t_0)$, respectively of the bath $\hat{\rho}_{\mathrm{B}}(t_0)$,

$$\hat{W}(t_0) = \hat{\rho}(t_0) \otimes \hat{\rho}_{\mathrm{B}}(t_0). \tag{3.8}$$

Two classes of such preparations are discussed in [1, Ch. 21]. In the first case, named preparation class A, the couplings c_α between the system and the bath oscillators are supposed to be switched on at initial time t_0. Consequently, the bath is supposed to have reached a thermal equilibrium state, in terms of the uncoupled Hamiltonian $\hat{H}_{\mathrm{B}}^{(0)}$, given by (3.3) with all couplings c_α put to 0, and the temperature $T = 1/\beta k_{\mathrm{B}}$. This equilibrium state is thus independent of the system state which in general remains unspecified. The total density matrix reads then at initial time

$$\hat{W}(t_0) = \hat{\rho}(t_0) \otimes \frac{\mathrm{e}^{-\beta \hat{H}_{\mathrm{B}}^{(0)}}}{\mathrm{Tr}_{\mathrm{B}}\, \mathrm{e}^{-\beta \hat{H}_{\mathrm{B}}^{(0)}}}. \tag{3.9}$$

In the second case, the preparation class B, the system is supposed to have been constrained in some initial state $\hat{\rho}(t_0)$ during a time interval long enough, before the initial time t_0, so that the bath has reached thermal equilibrium with this system state at initial time t_0. The equilibrium state is described in terms of the Hamiltonian $\hat{H}_{\mathrm{B}}[q_0]$, given by (3.3) with the system operator $\hat{q}$ replaced by the initial position $q_0 \,\hat{=}\, \mathrm{Tr}_{\mathrm{S}}\{\hat{\rho}(t_0)\hat{q}\}$. In this case, the total density matrix reads

$$\hat{W}(t_0) = \hat{\rho}(t_0) \otimes \frac{\mathrm{e}^{-\beta \hat{H}_{\mathrm{B}}[q_0]}}{\mathrm{Tr}_{\mathrm{B}}\, \mathrm{e}^{-\beta \hat{H}_{\mathrm{B}}[q_0]}}. \tag{3.10}$$

In this thesis, we will work with this second class of initial preparations. The preparations of classes A and B are undistinguishable when $\hat{\rho}(t_0) = |0\rangle\langle 0|$, which means that, at initial time t_0, the system is in the state $|0\rangle$ of position 0, namely $\hat{q}|0\rangle = 0|0\rangle$. Indeed, this state is decoupled from the bath, as one sees in (3.3).

The product form (3.8) is usually considered because it leads to useful simplifications in the evaluation of the populations. One generally argues that the choice of a particular initial preparation should not matter as far as one is interested in the dynamics of the system at long times only, as we are. However, it is not clear whether the choice of a product form for the total density matrix, which is only a particular case of all possible density matrices, causes a loss of generality in the description of the long-time dynamics, and whether such a product matrix density can be prepared in experimental realizations. Further discussion of these questions can be found, e.g., in [3–6] and references therein.

With the initial preparation (3.10), the populations read

$$P_\mu(t) = \sum_{\mu_i, \mu_i' \in \text{TB}} \langle \mu_i | \hat{\rho}(t_0) | \mu_i' \rangle G(\mu, \mu, \mu_i, \mu_i', t), \tag{3.11}$$

with the propagating function

$$G(\mu, \mu, \mu_i, \mu_i', t) = \sum_{n, n'=0}^{\infty} \prod_{j=1}^{n-1} \left(\sum_{\nu_j \in \text{TB}} \right) \prod_{j'=1}^{n'-1} \left(\sum_{\nu_{j'}' \in \text{TB}} \right)$$

$$\times \prod_{j=1}^{n} \left(-\frac{\mathrm{i}\Delta[j]}{\hbar} \right) \prod_{j'=1}^{n'} \left(\frac{\mathrm{i}\Delta'[j']}{\hbar} \right) \int_{t_0}^{t} \mathrm{d}t_n \cdots \int_{t_0}^{t_2} \mathrm{d}t_1 \int_{t_0}^{t} \mathrm{d}t_{n'}' \cdots \int_{t_0}^{t_2'} \mathrm{d}t_1'$$

$$\times \mathrm{e}^{-\frac{\mathrm{i}}{\hbar} \int_{t_0}^{t} \mathrm{d}t' \left[E(t') - E'(t') - F(t')[q(t') - q'(t')] \right]} F_{\text{FV}}[q(t'), q'(t'), t]. \tag{3.12}$$

The calculation is sketched in Appendix A. The multiple sums and products form actually a double, discrete path integral over the tight-binding paths $q(t')$ and $q'(t')$. The path $q(t')$, named forward path, is given by

$$q(t') = q_{\mu_i} + \sum_{j=1}^{n} (q_{\nu_j} - q_{\nu_{j-1}}) \theta(t' - t_j), \tag{3.13}$$

where $\theta(t')$ denotes the step function. It presents n transitions happening at times t_j, $j = 1, \ldots, n$, and visits $n - 1$ intermediate states $|\nu_j\rangle$, $j = 1, \ldots, n - 1$, between the initial state $|\nu_0\rangle = |\mu_i\rangle$ and the final state $|\nu_n\rangle = |\mu\rangle$. Likewise, the backward path

$$q'(t') = q_{\mu_i'} + \sum_{j'=1}^{n'} (q_{\nu_{j'}'} - q_{\nu_{j'-1}'}) \theta(t' - t_{j'}'), \tag{3.14}$$

presents n' transitions at times $t_{j'}'$, $j' = 1, \ldots, n'$, and visits $n' - 1$ intermediate states $|\nu_{j'}'\rangle$ between the initial state $|\nu_0'\rangle = |\mu_i'\rangle$ and the final state $|\nu_{n'}'\rangle = |\mu\rangle$. The couplings are defined as $\Delta[j] \triangleq \Delta_{\nu_j \nu_{j-1}}$ and $\Delta'[j'] \triangleq \Delta_{\nu_{j'}' \nu_{j'-1}'}^*$, and the on-site energies given by

$$E(t') = \varepsilon_{\mu_i} + \sum_{j=1}^{n} (\varepsilon_{\nu_j} - \varepsilon_{\nu_{j-1}}) \theta(t' - t_j) \tag{3.15a}$$

$$E'(t') = \varepsilon_{\mu_i'} + \sum_{j'=1}^{n'} (\varepsilon_{\nu_{j'}'} - \varepsilon_{\nu_{j'-1}'}) \theta(t' - t_{j'}'). \tag{3.15b}$$

Finally, the influence of the dissipative bath is captured by the Feynman-Vernon influence functional

$$F_{\mathrm{FV}}[q(t'), q'(t'), t]$$

$$= \exp\left\{ -\frac{1}{\hbar} \int_{t_0}^{t} \mathrm{d}t' \int_{t_0}^{t'} \mathrm{d}t'' \left[q(t') - q'(t') \right] L_{\mathrm{R}}(t' - t'') \left[q(t'') - q'(t'') \right] \right.$$

$$- \frac{\mathrm{i}}{\hbar} \int_{t_0}^{t} \mathrm{d}t' \int_{t_0}^{t'} \mathrm{d}t'' \left[q(t') - q'(t') \right] L_{\mathrm{I}}(t' - t'') \left[q(t'') + q'(t'') \right]$$

$$- \frac{\mathrm{i}}{\hbar} M_{\mathrm{I}}(0) \int_{t_0}^{t} \mathrm{d}t' \left[q(t') - q'(t') \right] \left[q(t') + q'(t') \right]$$

$$\left. + \frac{2\mathrm{i}}{\hbar} q_0 \int_{t_0}^{t} \mathrm{d}t' \left[q(t') - q'(t') \right] M_{\mathrm{I}}(t' - t_0) \right\}, \quad (3.16)$$

which induces nonlocal-in-time Gaussian correlations between the paths. The bath enters through its temperature $T = 1/\beta k_{\mathrm{B}}$, set by the initial preparation (3.10), and its spectral density (3.4), which enter the real $L_{\mathrm{R}}(\tau)$ and imaginary part $L_{\mathrm{I}}(\tau)$ of the bath correlation function

$$L(\tau) = \frac{1}{\pi} \int_0^\infty \mathrm{d}\omega\, J(\omega) \left[\coth\left(\frac{\hbar\omega\beta}{2} \right) \cos(\omega\tau) - \mathrm{i}\sin(\omega\tau) \right]. \quad (3.17)$$

Integrating the imaginary part yields the function $M_{\mathrm{I}}(\tau) = \int_0^\infty \mathrm{d}\omega\, J(\omega) \cos(\omega\tau)/\pi\omega$. The bath correlation functions are discussed in more detail in Appendix B.

In the case of an initial preparation of class A (3.8) instead of class B (3.10), the influence functional reads

$$F_{\mathrm{FV}}^{\mathrm{A}}[q(t'), q'(t'), t]$$

$$= F_{\mathrm{FV}}^{\mathrm{B}}[q(t'), q'(t'), t] \exp\left\{ -\frac{2\mathrm{i}}{\hbar} q_0 \int_{t_0}^{t} \mathrm{d}t' \left[q(t') - q'(t') \right] M_{\mathrm{I}}(t' - t_0) \right\} \quad (3.18)$$

instead of (3.16).

3.3 Two parameterizations of the tight-binding paths

The expression for the influence functional (3.16) can be written in a simpler way. First of all, one sees that it depends on the tight-binding paths only through their difference and average

$$\xi(t') \,\hat{=}\, q(t') - q'(t') \quad (3.19\mathrm{a})$$

$$\chi(t') \,\hat{=}\, \frac{1}{2} \left[q(t') + q'(t') \right]. \quad (3.19\mathrm{b})$$

Furthermore, one can take full advantage of the step-like structure of the paths (3.13) and (3.14). One can perform two partial integrations to obtain an expression depending on the derivative and boundaries of the paths only. After use of the properties $Q(0) = 0$ and $Q(-\tau) = Q^*(\tau)$ of the twice-integrated bath correlation function (see also Appendix B)

$$Q(\tau) = \frac{1}{\pi} \int_0^\infty d\omega \frac{J(\omega)}{\omega^2} \left[\coth\left(\frac{\hbar\omega\beta}{2} \right) [1 - \cos(\omega\tau)] + i\sin(\omega\tau) \right], \qquad (3.20)$$

one has $F_{\mathrm{FV}}[q(t'), q'(t'), t] = \exp\left\{ \Phi_{\mathrm{FV}}[\xi(t'), \chi(t'), t] \right\}$ with the influence phase

$$
\begin{aligned}
\Phi_{\mathrm{FV}} & [\xi(t'), \chi(t'), t] \\
&= \frac{1}{\hbar} \int_{t_0}^t dt' \int_{t_0}^{t'} dt'' \left[\dot{\xi}(t') Q_{\mathrm{R}}(t' - t'') \dot{\xi}(t'') + 2i\dot{\xi}(t') Q_{\mathrm{I}}(t' - t'') \dot{\chi}(t'') \right] \\
&\quad - \frac{\xi(t)}{\hbar} \int_{t_0}^t dt' \left[Q_{\mathrm{R}}(t - t') \dot{\xi}(t') + 2i Q_{\mathrm{I}}(t - t') \dot{\chi}(t') \right] \\
&\quad + \frac{\xi(t_0)}{\hbar} \int_{t_0}^t dt' \dot{\xi}(t') \left[Q_{\mathrm{R}}(t' - t_0) - i Q_{\mathrm{I}}(t' - t_0) \right] \\
&\qquad\qquad\qquad - \frac{\xi(t)\xi(t_0)}{\hbar} \left[Q_{\mathrm{R}}(t - t_0) - i Q_{\mathrm{I}}(t - t_0) \right]. \quad (3.21)
\end{aligned}
$$

The two last boundary terms of this expression would be slightly different and involve $\chi(t_0)$ as well if one considers an initial preparation of class A instead of class B [see Eq. (3.18)].

In order to parameterize the forward tight-binding path (3.13) we see that the relevant quantities are the "charges" $\sigma_j \hat{=} (q_{\nu_j} - q_{\nu_{j-1}})/L$, representing the jump in position associated with the transition happening at time t_j, expressed in units of the periodicity length L of the tight-binding model. Likewise, the backward path (3.14) involves another set of charges $\sigma'_{j'} \hat{=} (q_{\nu'_{j'}} - q_{\nu'_{j'-1}})/L$. With these notations, the paths read

$$q(t') = q_{\mu_i} + L \sum_{j=1}^n \sigma_j \theta(t' - t_j) \qquad (3.22\mathrm{a})$$

$$q'(t') = q_{\mu'_i} + L \sum_{j'=1}^{n'} \sigma'_{j'} \theta(t' - t'_{j'}). \qquad (3.22\mathrm{b})$$

The boundary conditions $q(t_0) = q_{\mu_i}$, $q'(t_0) = q_{\mu_i'}$ and $q(t) = q'(t) = q_\mu$ imply the constraints

$$L \sum_{j=1}^{n} \sigma_j = q_\mu - q_{\mu_i} \tag{3.23a}$$

$$L \sum_{j'=1}^{n'} \sigma_{j'}' = q_\mu - q_{\mu_i'} \tag{3.23b}$$

on the charges. With these notations and constraints, the influence phase (3.21) takes the more compact form

$$\Phi_{\text{FV}} =$$
$$\frac{L^2}{\hbar} \left[\sum_{k=1}^{n} \sum_{j=1}^{k-1} \sigma_k \sigma_j Q(t_k - t_j) + \sum_{k'=1}^{n'} \sum_{j'=1}^{k'-1} \sigma_{k'}' \sigma_{j'}' Q^*(t_{k'}' - t_{j'}') - \sum_{k'=1}^{n'} \sum_{j=1}^{n} \sigma_{k'}' \sigma_j Q(t_{k'}' - t_j) \right]$$
$$+ \frac{L}{\hbar} (q_{\mu_i} - q_{\mu_i'}) \left[\sum_{j=1}^{n} \sigma_j Q^*(t_j - t_0) - \sum_{j'=1}^{n'} \sigma_{j'}' Q^*(t_{j'}' - t_0) \right]. \tag{3.24}$$

Likewise, the driving contribution to the propagating function (3.12) goes into

$$\Psi = \frac{\mathrm{i} L}{\hbar} \left[\sum_{j'=1}^{n'} \sigma_{j'}' \int_{t_0}^{t_{j'}'} \mathrm{d}t' F(t') - \sum_{j=1}^{n} \sigma_j \int_{t_0}^{t_j} \mathrm{d}t' F(t') \right]. \tag{3.25}$$

The succession of intermediate states $|\nu_j\rangle$ and $|\nu_{j'}'\rangle$ can be collected into the notation $\alpha_{\mu\mu\mu_i\mu_i'}^{(n,n')}$, which reminds of the number of transitions in each path and of the boundary conditions of the paths. The sum over the intermediate states can correspondingly be rewritten

$$\prod_{j=1}^{n-1} \left(\sum_{\nu_j \in \text{TB}} \right) \prod_{j'=1}^{n'-1} \left(\sum_{\nu_{j'}' \in \text{TB}} \right) \hateq \sum_{\{\alpha_{\mu\mu\mu_i\mu_i'}^{(n,n')}\}}. \tag{3.26}$$

With these notations, and upon defining the prefactor

$$\Lambda \hateq \prod_{j=1}^{n} \left(\frac{-\mathrm{i}\Delta[j]}{\hbar} \right) \prod_{j'=1}^{n'} \left(\frac{\mathrm{i}\Delta'[j']}{\hbar} \right) \tag{3.27}$$

and the on-site energy functional

$$\Delta\mathcal{E} \hateq -\frac{\mathrm{i}}{\hbar} \int_{t_0}^{t} \mathrm{d}t' \left[E(t') - E'(t') \right], \tag{3.28}$$

the propagating function (3.12) may be rewritten as

$$
G(\mu, \mu, \mu_i, \mu_i', t) = \sum_{n,n'=0}^{\infty} \sum_{\{\alpha^{(n,n')}_{\mu\mu\mu_i\mu_i'}\}} \int_{t_0}^{t} dt_n \cdots \int_{t_0}^{t_2} dt_1 \int_{t_0}^{t} dt_{n'}' \cdots \int_{t_0}^{t_2'} dt_1'
$$

$$
\times f\left[\alpha^{(n,n')}_{\mu\mu\mu_i\mu_i'}\right](t; t_n, \ldots, t_1; t_{n'}', \ldots, t_1'; t_0), \quad (3.29)
$$

in terms of the influence function which takes the compact form

$$
f\left[\alpha^{(n,n')}_{\mu\mu\mu_i\mu_i'}\right](t; t_n, \ldots, t_1; t_{n'}', \ldots, t_1'; t_0) = \Lambda \exp\{\Delta\mathcal{E} + \Phi_{\mathrm{FV}} + \Psi\}. \quad (3.30)
$$

We name this parameterization of the two tight-binding paths in terms of the charges σ_j and $\sigma_{j'}'$ the σ-σ' description. The transition times are chronologically ordered inside each path independently, $t_n > \ldots > t_1$ and $t_{n'}' > \ldots > t_1'$. As we have already seen, the difference and average paths (3.19) naturally come into play in the influence phase (3.21). Furthermore, in order to obtain certain results, it will turn out to be useful to work with a single set of chronologically ordered transitions. Altogether, it is thus natural to parameterize the couple of tight-binding paths in terms of the difference $\xi(t')$ and average $\chi(t')$ paths instead of the forward $q(t')$ and backward $q'(t')$ paths. In order to do that, we have to relabel the $N \doteq n + n'$ transition times as s_j, in chronological order, and introduce corresponding couples of charges ζ_j and κ_j. Then we may write

$$
\xi(t') = \xi_i + L \sum_{j=1}^{N} \zeta_j \theta(t' - s_j) \quad (3.31a)
$$

$$
\chi(t') = \chi_i + \frac{L}{2} \sum_{j=1}^{N} \kappa_j \theta(t' - s_j). \quad (3.31b)
$$

We have introduced the initial values $\xi_i \doteq q_{\mu_i} - q_{\mu_i'}$ and $\chi_i \doteq [q_{\mu_i} + q_{\mu_i'}]/2$ according to (3.19). Due to the final boundary conditions $\xi_f \doteq q_\mu - q_\mu = 0$ and $\chi_f \doteq [q_\mu + q_\mu]/2 = q_\mu$, the charges must satisfy the constraints

$$
L \sum_{j=1}^{N} \zeta_j = -\xi_i \quad (3.32a)
$$

$$
\frac{L}{2} \sum_{j=1}^{N} \kappa_j = q_\mu - \chi_i \quad (3.32b)
$$

We name this second parameterization the ζ-κ description. The transformation between the two equivalent descriptions is shown in Table 3.1.

ζ-κ description:								
transition time	s_1	s_2	s_3	s_4	$\ldots$	s_{N-2}	s_{N-1}	s_N
charge, difference path	ζ_1	ζ_2	ζ_3	ζ_4	$\ldots$	ζ_{N-2}	ζ_{N-1}	ζ_N
charge, average path	κ_1	κ_2	κ_3	κ_4	$\ldots$	κ_{N-2}	κ_{N-1}	κ_N
$\updownarrow$		$\updownarrow$	$\updownarrow$	$\updownarrow$	$\updownarrow$	$\updownarrow$	$\updownarrow$	$\updownarrow$
σ-σ' description:								
transition time, forward path	t_1	t_2		t_3	$\ldots$		t_n	
charge, forward path	σ_1	σ_2		σ_3	$\ldots$		σ_n	
transition time, backward path			t_1'		$\ldots$	$t_{n'-1}'$		$t_{n'}'$
charge, backward path			σ_1'		$\ldots$	$\sigma_{n'-1}'$		$\sigma_{n'}'$

Table 3.1: The relation between the two equivalent parameterizations of the tight-binding paths for an example configuration. The ζ-κ description (above) is convenient for the difference $\xi(t')$ and average path $\chi(t')$, whereas the σ-σ' description (below) is convenient for the forward $q(t')$ and backward path $q'(t')$. For the transition times, the relation between the two descriptions is given by $s_k = t_j$ or $s_k = t_j'$ when appropriate. For the charges, it is $\zeta_k=\sigma_j$ or $\zeta_k=-\sigma_j'$, and $\kappa_k=\sigma_j$ or $\kappa_k=\sigma_j'$. In the example shown, the transitions at times s_1, s_2, s_4, and s_{N-1} happen in the forward path, whereas the ones at times s_3, s_{N-2}, and s_N happen in the backward path.

With (3.31) and the constraints (3.32), the influence phase (3.21) may be rewritten as

$$\Phi_{\text{FV}} = \frac{L^2}{\hbar} \sum_{k=2}^{N} \sum_{j=1}^{k-1} [\zeta_k \zeta_j Q_{\text{R}}(s_k - s_j) + \text{i}\zeta_k \kappa_j Q_{\text{I}}(s_k - s_j)] + \frac{L}{\hbar} \xi_i \sum_{j=1}^{N} \zeta_j Q^*(s_j - t_0). \tag{3.33}$$

The driving contribution reads

$$\Psi = -\frac{\text{i}L}{\hbar} \sum_{j'=1}^{N} \zeta_j \int_{t_0}^{s_j} \text{d}t' F(t'). \tag{3.34}$$

In order to rewrite the prefactor Λ, we have to introduce a unified notation for the couplings associated with each transition. This goes like for the charges, as shown in Table 3.1,

$$\Delta''[k] \hat{=} \begin{cases} \Delta[j] & \text{if } s_k = t_j \\ -\Delta'[j'] & \text{if } s_k = t_{j'}'. \end{cases} \tag{3.35}$$

With this notation, one has

$$\Lambda = \prod_{j=1}^{N} \left(\frac{-\text{i}\Delta''[j]}{\hbar} \right). \tag{3.36}$$

The succession of intermediate states $|\nu_j\rangle$ and $|\nu'_{j'}\rangle$ visited by the two paths, ordered chronologically with respect to each other, can be collected into the notation $\beta^{(N)}_{\mu\mu\mu_i\mu'_i}$. We have to translate the integrals $\int_{t_0}^t \mathrm{d}t_n \cdots \int_{t_0}^{t_2} \mathrm{d}t_1 \int_{t_0}^t \mathrm{d}t'_{n'} \cdots \int_{t_0}^{t'_2} \mathrm{d}t'_1$ over the two sequences of chronologically ordered times, $t > t_n > \ldots > t_1 > t_0$ and $t > t'_{n'} > \ldots > t'_1 > t_0$, in terms of the single chronologically ordered sequence $t > s_N > \ldots > s_1 > t_0$. In these integrals, $(n+n')!/n!n'!$ permutations of a given ordering, say $t_n > \ldots > t_1 > t'_{n'} > \ldots > t'_1$, are visited. This is exactly compensated by the fact that one given set $\alpha^{(n,n')}_{\mu\mu\mu_i\mu'_i}$ of n ordered charges σ_j and n' ordered charges $\sigma'_{j'}$ can be combined in exactly $(n+n')!/n!n'!$ different sequences $\beta^{(N)}_{\mu\mu\mu_i\mu'_i}$ of $N = n+n'$ ordered couples of charges (ζ_j, κ_j). One can thus convince oneself of the relation

$$\sum_{n=0}^{\infty} \sum_{n'=0}^{\infty} \delta(n+n', N) \sum_{\left\{\alpha^{(n,n')}_{\mu\mu\mu_i\mu'_i}\right\}} \int_{t_0}^t \mathrm{d}t_n \ldots \int_{t_0}^{t_2} \mathrm{d}t_1 \int_{t_0}^t \mathrm{d}t'_{n'} \ldots \int_{t_0}^{t'_2} \mathrm{d}t'_1$$
$$= \sum_{\left\{\beta^{(N)}_{\mu\mu\mu_i\mu'_i}\right\}} \int_{t_0}^t \mathrm{d}s_N \ldots \int_{t_0}^{s_2} \mathrm{d}s_1. \quad (3.37)$$

Consequently, in the ζ-κ description, the propagating function (3.12) takes the form

$$G(\mu,\mu,\mu_i,\mu'_i,t) = \sum_{N=0}^{\infty} \sum_{\left\{\beta^{(N)}_{\mu\mu\mu_i\mu'_i}\right\}} \int_{t_0}^t \mathrm{d}s_N \cdots \int_{t_0}^{s_2} \mathrm{d}s_1 f\left[\beta^{(N)}_{\mu\mu\mu_i\mu'_i}\right](t; s_N, \ldots, s_1; t_0),$$
$$(3.38)$$

with the influence function defined again as

$$f\left[\beta^{(N)}_{\mu\mu\mu_i\mu'_i}\right](t; s_N, \ldots, s_1; t_0) = \Lambda \exp\left\{\Delta\mathcal{E} + \Phi_{\mathrm{FV}} + \Psi\right\}, \quad (3.39)$$

but now in terms of the expressions (3.28), (3.33), (3.34) and (3.36). Due to the chronological ordering of all transition times, this second parameterization turns out to be especially useful in order to derive a generalized master equation for the populations. This is the object of the next section.

3.4   Generalized master equation

In this section, we will discuss a generalized master equation for the populations (3.11) for a diagonal initial preparation of the system

$$\hat{\rho}(t_0) = |\mu_0\rangle\langle\mu_0|. \quad (3.40)$$

Combining with Eq. (3.38), we obtain the populations as

$$P_{\mu\mu_0}(t, t_0) = \sum_{N=0}^{\infty} \int_{t_0}^{t} \mathrm{d}s_N \cdots \int_{t_0}^{s_2} \mathrm{d}s_1 F_{\mu\mu_0}^{(N)}(s_N, \ldots, s_1), \qquad (3.41)$$

with the total influence function defined as

$$F_{\mu\mu_0}^{(N)}(s_N, \ldots, s_1) \doteq \sum_{\{\beta_{\mu\mu\mu_0\mu_0}^{(N)}\}} f\left[\beta_{\mu\mu\mu_0\mu_0}^{(N)}\right](s_N, \ldots, s_1). \qquad (3.42)$$

We added the index μ_0 and time argument t_0 to the populations $P_{\mu\mu_0}(t, t_0)$ to highlight their dependence on the initial preparation. For such a diagonal preparation, the last term in the influence phase (3.33) drops out and the whole influence function $f\left[\beta_{\mu\mu\mu_0\mu_0}^{(N)}\right](s_N, \ldots, s_1)$ does not depend explicitly on the initial and final times t_0 and t.

The structure of the populations (3.41) allows to derive the exact generalized master equation [7]

$$\frac{\mathrm{d}}{\mathrm{d}t} P_{\nu\mu_0}(t, t_0) = \int_{t_0}^{t} \mathrm{d}t' \sum_{\mu \in \mathrm{TB}} K_{\nu\mu}^{\mathrm{irred}}(t, t') P_{\mu\mu_0}(t', t_0). \qquad (3.43)$$

The derivation goes as follows. One substitutes the expression (3.41) in the generalized master equation and assumes that the kernels present an analogous structure $K_{\nu\mu}^{\mathrm{irred}}(t, t') = \sum_{N=0}^{\infty} K_{\nu\mu}^{(N),\mathrm{irred}}(t, t')$, where the Nth-order kernels are given by integrating out all intermediate times (if any) of an irreducible influence function connecting the site $|\mu\rangle$ to the site $|\nu\rangle$ in N transitions,

$$K_{\nu\mu}^{(N),\mathrm{irred}}(t, t') = \int_{t'}^{t} \mathrm{d}s_{N-1} \ldots \int_{t'}^{s_4} \mathrm{d}s_3 \int_{t'}^{s_3} \mathrm{d}s_2 F_{\nu\mu}^{(N),\mathrm{irred}}(t, s_{N-1}, \ldots, s_2, t').$$
$$(3.44)$$

After substitution in (3.41) and permutation of the integrals so that all times involved are chronologically ordered, and by comparing the two sides of the equation at each order N, one gets a set of equations which can be solved for this new influence function

$$F_{\nu\mu}^{(N),\mathrm{irred}}(s_N, \ldots, s_1) = F_{\nu\mu}^{(N)}(s_N, \ldots, s_1) - F_{\nu\mu}^{(N),\mathrm{red}}(s_N, \ldots, s_1), \qquad (3.45)$$

with the reducible contribution given by

$$F_{\nu\mu}^{(N),\mathrm{red}}(s_N, \ldots, s_1) = \sum_{k=2}^{\infty} \sum_{N_1, \ldots, N_k=2}^{\infty} \sum_{\lambda_1, \ldots, \lambda_{k-1} \in \mathrm{TB}} \delta(N_1 + \cdots + N_k, N)(-)^k$$
$$\times F_{\nu\lambda_{k-1}}^{(N_k)}(s_N, \ldots, s_{N_1+\cdots+N_{k-1}+1}) \ldots F_{\lambda_2\lambda_1}^{(N_2)}(s_{N_1+N_2}, \ldots, s_{N_1+1}) F_{\lambda_1\mu}^{(N_1)}(s_{N_1}, \ldots, s_1)$$
$$(3.46)$$

in terms of the influence functions $F_{\nu\mu}^{(N)}(s_N, \ldots, s_1)$ involved in the populations (3.41). Using relations analogous to (3.44) between the different types of kernels and influence functions and playing a bit with integral permutations, one can rewrite the relations (3.45) and (3.46) in terms of the kernels, yielding

$$K_{\nu\mu}^{(N),\mathrm{irred}}(t,t') = K_{\nu\mu}^{(N)}(t,t') - K_{\nu\mu}^{(N),\mathrm{red}}(t,t'), \tag{3.47}$$

which involves the reducible part

$$
\begin{aligned}
K_{\nu\mu}^{(N),\mathrm{red}}(t,t') = \sum_{k=2}^{\infty} \quad \sum_{N_1,\ldots,N_k=2}^{\infty} \quad & \delta(N_1 + \cdots + N_k, N)(-)^k \\
& \times K_{\nu\lambda_{k-1}}^{(N_k)}(t,s_k') \cdot \ldots \cdot K_{\lambda_2\lambda_1}^{(N_2)}(s_2'',s_2') \cdot K_{\lambda_1\mu}^{(N_1)}(s_1'',t),
\end{aligned}
\tag{3.48}
$$

with the dot-product defined as

$$K_{\nu\lambda}^{(N)}(s_4,s_3) \cdot K_{\lambda\mu}^{(N')}(s_2,s_1) \mathrel{\hat{=}} \sum_{\lambda\in\mathrm{TB}} \int_{s_1}^{s_4} \mathrm{d}s_3 \int_{s_1}^{s_3} \mathrm{d}s_2\, K_{\nu\lambda}^{(N)}(s_4,s_3) K_{\lambda\mu}^{(N')}(s_2,s_1). \tag{3.49}$$

One can ask oneself what is the utility of the generalized master equation. Indeed, the expressions (3.41) and (3.39) already allow to evaluate the populations in principle. However, as soon as one is interested in the behavior of the populations at long times $t \gg t_0$, as we are in this work, these expressions turn out to be unsuitable. When the measurement time $t - t_0$ is long, the paths involving a large number N of transitions are also relevant, therefore the influence functions $F_{\mu\mu_0}^{(N)}(s_N, \ldots, s_1)$ must be evaluated to high order N also. Unfortunately, their evaluation is intricate and becomes impracticable for N bigger than 3 or 4. On the contrary, as we will see in the next section, the master equation provides an analytical expression for the populations in the long time limit, in terms of transition rates $\Gamma_{\nu\mu}^{(N)}$ from the site $|\mu\rangle$ to the site $|\nu\rangle$ in N transitions. Furthermore, it is known [1] that considering the first orders only for the transition rates provides a good approximation in some regime of parameters.

3.5   The populations at long time

In this section, we will restrict ourselves to the case of a time-independent driving force F. We will comment on the time-dependent case in Section 3.7. We already mentioned that for the initial preparation (3.40), the partial influence function (3.39) does not depend explicitly on the initial and final times t_0 and t. The case of a time-independent driving force brings a new simplification: The partial influence function depends on the difference of its time arguments $s_N - s_{N-1}, \ldots, s_2 - s_1$ only. The total influence function $F_{\mu\mu_0}^{(N)}(s_N, \ldots, s_1)$ defined in (3.42) clearly inherits both properties.

Consequently, the populations $P_{\mu\mu_0}(t,t_0)$ and the kernels $K_{\nu\mu}^{(N)}(t,t')$ depend on the difference of their two time arguments only. The definitions $P_{\mu\mu_0}(t,t_0) \hateq P_{\mu\mu_0}(t-t_0)$ and $K_{\nu\mu}^{(N)}(t,t') \hateq K_{\nu\mu}^{(N)}(t-t')$ are thus legitimate. Using (3.48) and (3.49), one can see that the reducible part of the kernels inherits this property as well, thus so do the irreducible kernels $K_{\nu\mu}^{\mathrm{irred}}(t,t')$. With this, the generalized master equation may be rewritten

$$\frac{\mathrm{d}}{\mathrm{d}\tau}P_{\nu\mu_0}(\tau) = \int_0^\tau \mathrm{d}\tau' \sum_{\mu\in\mathrm{TB}} K_{\nu\mu}^{\mathrm{irred}}(\tau-\tau')P_{\mu\mu_0}(\tau'). \tag{3.50}$$

It has now the form of a convolution. Consequently, rewriting the generalized master equation in terms of the Laplace transform of the populations

$$\mathcal{L}P_{\mu\mu_0}(s) \hateq \int_0^\infty \mathrm{d}\tau \mathrm{e}^{-s\tau} P_{\mu\mu_0}(\tau) \tag{3.51}$$

turns the convolution into a product

$$\mathcal{L}P_{\nu\mu_0}(s) = \frac{1}{s}\left[P_{\nu\mu_0}(0) + \sum_{\mu\in\mathrm{TB}} \int_0^\infty \mathrm{d}\tau \mathrm{e}^{-s\tau} K_{\nu\mu}^{\mathrm{irred}}(\tau)\mathcal{L}P_{\mu\mu_0}(s) \right]. \tag{3.52}$$

This equation may easily be solved. The sum over the tight-binding states $|\mu\rangle$ may be seen as a matrix product between the matrix $\hat{K}^{\mathrm{irred}}(\tau)$, whose elements are the kernels $K_{\nu\mu}^{\mathrm{irred}}(\tau)$, and the vector $\vec{P}_{\mu_0}(\tau)$ containing the populations $P_{\mu\mu_0}(\tau)$, considering μ_0 as a parameter. The solution involves simply a matrix inversion

$$\mathcal{L}\vec{P}_{\mu_0}(s) = \left[s\hat{1} - \int_0^\infty \mathrm{d}\tau \mathrm{e}^{-s\tau}\hat{K}^{\mathrm{irred}}(\tau) \right]^{-1} \cdot \vec{P}_{\mu_0}(0), \tag{3.53}$$

applied on the initial populations $\vec{P}_{\mu_0}(0)$. In the small s limit, the exponential $\mathrm{e}^{-s\tau}$ may be disregarded, yielding

$$\mathcal{L}\vec{P}_{\mu_0}(s) \underset{s\to 0}{\sim} \left[s\hat{1} - \hat{\Gamma} \right]^{-1} \cdot \vec{P}_{\mu_0}(0), \tag{3.54}$$

in terms of the matrix $\hat{\Gamma}$ of transition rates

$$\Gamma_{\nu\mu} \hateq \int_0^\infty \mathrm{d}\tau K_{\nu\mu}^{\mathrm{irred}}(\tau). \tag{3.55}$$

The denomination of these quantities as transition rates will become clear below. The solution reads

$$\vec{P}_{\mu_0}(\tau) \underset{t\to\infty}{\sim} \exp\{\tau\hat{\Gamma}\} \cdot \vec{P}_{\mu_0}(0). \tag{3.56}$$

It is actually the solution of the equation

$$\frac{\mathrm{d}}{\mathrm{d}\tau}\vec{P}_{\mu_0}(\tau) = \hat{\Gamma} \cdot \vec{P}_{\mu_0}(\tau). \tag{3.57}$$

Translating this equation back in terms of the populations $P_{\mu\mu_0}(\tau)$, we obtain

$$\frac{\mathrm{d}}{\mathrm{d}\tau} P_{\nu\mu_0}(\tau) = \sum_{\mu \in \mathrm{TB}} \Gamma_{\nu\mu} P_{\mu\mu_0}(\tau). \tag{3.58}$$

If the property

$$\Gamma_{\nu\nu} = - \sum_{\mu \in \mathrm{TB},\ \mu \neq \nu} \Gamma_{\mu\nu} \tag{3.59}$$

additionally holds, one may write

$$\frac{\mathrm{d}}{\mathrm{d}\tau} P_{\nu\mu_0}(\tau) = \sum_{\mu \in \mathrm{TB},\ \mu \neq \nu} \Gamma_{\nu\mu} P_{\mu\mu_0}(\tau) - \sum_{\mu \in \mathrm{TB},\ \mu \neq \nu} \Gamma_{\mu\nu} P_{\nu\mu_0}(\tau). \tag{3.60}$$

One recognizes a master equation of Markovian form with transition rates $\Gamma_{\nu\mu}$ from the tight-binding site $|\mu\rangle$ to the site $|\nu\rangle$. We will prove the general property (3.59) with the help of the explicit expressions of the rates in the particular case studied in Chapter 5 [see Eq. (5.28)].

The physical meaning of this result is that as long as one is interested in the long-time dynamics only, a Markovian master equation is suitable even for a quantum system initially prepared as given in (3.10). The memory effects due to quantum coherence are captured in the transition rates $\Gamma_{\nu\mu}$, as long as the transient effects of the initial preparation are disregarded. The expressions for these transition rates follow from the evaluation of the diagonal elements of the reduced density matrix as presented in this chapter. As a consequence, these rates are not necessarily positive [8]. Combining the definition $K_{\nu\mu}^{\mathrm{irred}}(t,t') = \sum_{N=0}^{\infty} K_{\nu\mu}^{(N),\mathrm{irred}}(t,t')$ of the Nth-order kernels with (3.55), one can define Nth-order transition rates

$$\Gamma_{\nu\mu}^{(N)} \mathrel{\hat{=}} \int_0^\infty \mathrm{d}\tau\, K_{\nu\mu}^{(N),\mathrm{irred}}(\tau), \tag{3.61}$$

which describe coherent transitions made of N successive transitions happening in the pair of tight-binding paths. Quantum coherence during a time as long as one will can be described, provided one considers contributions up to $N \to \infty$. In a parameter regime where quantum coherence is destroyed on a short time scale, e.g. for high temperature and/or large dissipation, it is sufficient to consider the lowest orders $N = 2, 3, \ldots$ in order to evaluate the populations at long times [1]. This is one important advantage of the expression (3.56), derived from the generalized master equation, with respect to the expression (3.41).

3.6   Transition rates

In this section, we will summarize the expressions for the tight-binding transition rates obtained by combining the different equations developed in the last sections.

As the definition of the kernels (3.44), obtained from the influence function by the integration of the intermediate times, as well as the subtraction of reducible contributions, involve chronological ordering of all transition times, one sees that the natural framework to give the explicit expression of the transition rates is the ζ-κ description (see Table 3.1), where the transitions happening in the forward and backward paths are treated together. Combining (3.61) and (3.44), we get

$$\Gamma_{\nu\mu}^{(N)} = \int_{t_0}^{t} \mathrm{d}s_N \cdots \int_{t_0}^{s_2} \mathrm{d}s_1 F_{\nu\mu}^{\mathrm{irred}}(s_N, \ldots, s_1), \qquad (3.62)$$

where the irreducible influence function $F_{\nu\mu}^{\mathrm{irred}}(s_N, \ldots, s_1)$ can be obtained through Eqs. (3.45) and (3.42) from the partial contributions $f\left[\beta_{\nu\nu\mu\mu}^{(N)}\right](s_N, \ldots, s_1)$ given in (3.39).

We have seen in the preceding section that, in the case of a time-independent driving force, the influence function depends on the difference of its time arguments $s_N - s_{N-1}, \ldots, s_2 - s_1$ only. It is convenient to rewrite the time integrals in terms of the $N - 1$ time intervals $\tau_j \,\hat{=}\, s_{j+1} - s_j$, $j = 1, \ldots, N-1$, because the integrals are then disentangled. This gives

$$\Gamma_{\nu\mu}^{(N)} = \prod_{j=1}^{N-1} \left(\int_0^{\infty} \mathrm{d}\tau_j \right) F_{\nu\mu}^{(N),\mathrm{irred}}(s_N, \ldots, s_1), \qquad (3.63)$$

where $F_{\nu\mu}^{(N),\mathrm{irred}}(s_N, \ldots, s_1)$ has to be expressed in terms of the intervals τ_j as well.

In order to prove some general properties of the transition rates (see Section 5.3.1), it will turn out to be more convenient to work with the σ-σ' description (see Table 3.1). In this description, the distinction between transitions in the forward and backward paths matters, whereas their relative chronological order does not. One encounters two difficulties in order to rewrite the transition rates in terms of the partial contributions $f\left[\alpha_{\nu\nu\mu\mu}^{(n,n')}\right](t_n, \ldots, t_1; t'_{n'}, \ldots, t'_1)$ given in (3.30). Firstly, the subtraction of the reducible contributions following (3.45), which proceeds in terms of the first and last transition times, requires to make the distinction wether these times belong to the forward transition times t_j or to the backward ones $t'_{j'}$. This can lead to some intricate combinatorics. Secondly, the $N - 1$ integrals $\int_{s_1}^{\infty} \mathrm{d}s_N \cdots \int_{s_1}^{s_3} \mathrm{d}s_2$, which span all chronologically ordered configurations of the times, the last one s_N running up to ∞, whereas the first one s_1 remains unspecified, have to be translated in the σ-σ' description, where one has two sequences of chronologically ordered times, $t_n > \ldots > t_1$ and $t'_{n'} > \ldots > t'_1$, independent of each other. Following a discussion

identical to the one given above Eq. (3.37), one can derive the relation

$$\sum_{\left\{\beta_{\nu\nu\mu\mu}^{(N)}\right\}} \int_{s_1}^{\infty} ds_N \dots \int_{s_1}^{s_3} ds_2 = \sum_{n=0}^{\infty} \sum_{n'=0}^{\infty} \delta(n+n', N) \sum_{\left\{\alpha_{\nu\nu\mu\mu}^{(n,n')}\right\}}$$

$$\times \int_{-\infty}^{\infty} dt_1' \int_{t_1}^{\infty} dt_n \dots \int_{t_1}^{t_3} dt_2 \int_{t_1'}^{\infty} dt_{n'}' \dots \int_{t_1'}^{t_3'} dt_2'. \quad (3.64)$$

Exactly as for the ζ-κ description, in the case of a time-independent driving force, the influence function $f\left[\alpha_{\nu\nu\mu\mu}^{(n,n')}\right](t_n, \dots, t_1; t_{n'}', \dots, t_1')$ depends on differences of its time arguments only. Adapting the notation put forward in [8], it is convenient to rewrite the integrals in terms of the time intervals in the forward path $\rho_j \hat{=} t_{j+1} - t_j$, the time intervals in the backward path $\rho_{j'}' \hat{=} t_{j'+1}' - t_{j'}'$, as well as one variable controlling the relative position of the two chains of times, for example $\tau \hat{=} \frac{1}{n'} \sum_{j'=1}^{n'} t_{j'}' - \frac{1}{n} \sum_{j=1}^{n} t_j$. The transformation yields

$$\int_{-\infty}^{\infty} dt_1' \int_{t_1}^{\infty} dt_n \dots \int_{t_1}^{t_3} dt_2 \int_{t_1'}^{\infty} dt_{n'}' \dots \int_{t_1'}^{t_3'} dt_2'$$

$$= \int_{-\infty}^{\infty} d\tau \prod_{j=1}^{n-1} \left(\int_0^{\infty} d\rho_j\right) \prod_{j'=1}^{n'-1} \left(\int_0^{\infty} d\rho_{j'}'\right). \quad (3.65)$$

In the case where there are no transitions in the backward path $n' = 0$, respectively no transitions in the forward path $n = 0$, the integral over the variable τ is absent but there are still $n - 1 = N - 1$ integrals over the $n - 1$ intervals ρ_j, respectively $n' - 1 = N - 1$ integrals over the $n' - 1$ intervals $\rho_{j'}'$.

The rates in the σ-σ' description read thus

$$\Gamma_{\nu\mu}^{(n,n')} = \int_{-\infty}^{\infty} d\tau \prod_{j=1}^{n-1} \left(\int_0^{\infty} d\rho_j\right) \prod_{j'=1}^{n'-1} \left(\int_0^{\infty} d\rho_{j'}'\right) F_{\nu\mu}^{(n,n'),\text{irred}}(t_n, \dots, t_1; t_{n'}', \dots, t_1'),$$

$$(3.66)$$

with

$$F_{\nu\mu}^{(n,n'),\text{irred}}(t_n, \dots, t_1; t_{n'}', \dots, t_1') = \sum_{\left\{\alpha_{\nu\nu\mu\mu}^{(n,n')}\right\}} f^{\text{irred}}\left[\alpha_{\nu\nu\mu\mu}^{(n,n')}\right](t_n, \dots, t_1; t_{n'}', \dots, t_1'),$$

$$(3.67)$$

and the times rewritten in terms of the intervals ρ_j, $\rho_{j'}'$, and τ. The bridge between the two representations is given by the relation

$$\Gamma_{\nu\mu}^{(N)} = \sum_{n=0}^{\infty} \sum_{n'=0}^{\infty} \delta(n+n', N) \Gamma_{\nu\mu}^{(n,n')}. \quad (3.68)$$
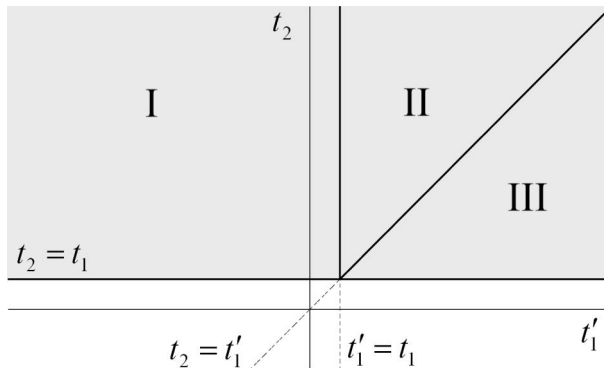
Figure 3.1: Graphical representation of the splitting of the integration domain in Eq. (3.69). The three pieces correspond to three different chronological orderings of the transition times t_1, t_2, and t_1'. The labels I, II, and III refer to the three terms in the right-hand side of Eq. (3.69) from left to right.

To one contribution to $\Gamma_{\nu\mu}^{(n,n')}$ correspond $(n+n')!/n!n'!$ contributions to $\Gamma_{\nu\mu}^{(N)}$.

For clarity, we will give an explicit example of the correspondence between the two descriptions and the relation between the domains of integration. Let us consider the contribution from a pair of paths presenting two transitions in the forward path at times t_1 and t_2, and one transition in the backward path at time t_1'. Let the charges be $\alpha_{\nu\nu\mu\mu}^{(2,1)} = \{\sigma_1, \sigma_2; \sigma_1'\}$. The three transition times may be ordered in three different ways, namely $t_2 > t_1 > t_1'$, $t_2 > t_1' > t_1$ and $t_1' > t_2 > t_1$. These three arrangements correspond to three different configurations of the charges $\beta_{\nu\nu\mu\mu}^{(3)} = \{\zeta_1, \zeta_2, \zeta_3; \kappa_1, \kappa_2, \kappa_3\}$, namely $\{-\sigma_1', \sigma_1, \sigma_2; \sigma_1', \sigma_1, \sigma_2\}$, $\{\sigma_1, -\sigma_1', \sigma_2; \sigma_1, \sigma_1', \sigma_2\}$, and $\{\sigma_1, \sigma_2, -\sigma_1'; \sigma_1, \sigma_2, \sigma_1'\}$. The integrals over the transition times may be split accordingly

$$\int_{-\infty}^{\infty} dt_1' \int_{t_1}^{\infty} dt_2 = \int_{t_1}^{\infty} dt_2 \int_{-\infty}^{t_1} dt_1' + \int_{t_1}^{\infty} dt_2 \int_{t_1}^{t_2} dt_1' + \int_{t_1}^{\infty} dt_2 \int_{t_2}^{\infty} dt_1'. \quad (3.69)$$

The three pieces of the integration domain are shown in Fig. 3.1. Each one corresponds to one of the three different configurations $\beta_{\nu\nu\mu\mu}^{(3)}$. By substituting $\tau_1 = t_1 - t_1'$, $\tau_2 = t_2 - t_1$ in the first one, $\tau_1 = t_1' - t_1$, $\tau_2 = t_2 - t_1'$ in the second one, and $\tau_1 = t_2 - t_1$, $\tau_2 = t_1' - t_2$ in the third one, all three yield $\int_0^{\infty} d\tau_2 \int_0^{\infty} d\tau_2$, which is equivalent to $\int_{s_1}^{\infty} ds_3 \int_{s_1}^{\infty} ds_2$. This demonstrates relation (3.65) for one particular subset of configurations.

3.7   The case of high-frequency ac driving

To derive the convolutive form (3.50) from the exact generalized master equation (3.43), we have used the time-independence of the Hamiltonian. What happens in the case of a time-dependent driving force $F(t')$? One particular situation of interest is the case of harmonic ac driving of amplitude F and frequency Ω, given by

$$F(t') = F \cos(\Omega(t' - t_0)). \tag{3.70}$$

It has been shown [1, 7, 9] that, when the driving frequency Ω is much bigger than all other relevant time scales in the system-plus-bath, the generalized master equation can still be brought into the convolutive form (3.50), provided that one replaces the populations $P_{\mu\mu_0}(\tau)$ and kernels $K_{\nu\mu}(\tau)$ by their average over one period of the ac driving. Consequently, this equation may still be written as in (3.60) at long times, in terms of averaged transition rates $\bar{\Gamma}_{\nu\mu}$ from the site $|\mu\rangle$ to the site $|\nu\rangle$. The second-order contributions to these averaged transition rates read [1, 7, 10]

$$\bar{\Gamma}_{\nu\mu}^{(2)} = \frac{|\Delta_{\nu\mu}|^2}{\hbar^2} \int_{-\infty}^{\infty} \mathrm{d}\tau \mathrm{e}^{-\left[(q_\mu - q_\nu)^2/\hbar\right] Q(\tau) + \mathrm{i}\left[(\varepsilon_\mu - \varepsilon_\nu)/\hbar\right]\tau} J_0\left[\frac{2F(q_\mu - q_\nu)}{\hbar\Omega} \sin\left(\frac{\Omega\tau}{2}\right)\right], \tag{3.71}$$

where the parameters of the driving force enter the zero-order Bessel function J_0.

References

[1] U. Weiss, *Quantum Dissipative Systems* (World Scientific, Singapore, 1999), 2nd ed.

[2] H. Kleinert, *Path Integrals in Quantum Mechanics, Statistics, Polymer Physics, and Financial Markets* (World Scientific, Singapore, 2004), 3rd ed.

[3] C. Morais Smith and A. O. Caldeira, Phys. Rev. A **36**, 3509 (1987).

[4] H. Grabert, P. Schramm, and G. L. Ingold, Phys. Rep. **168**, 115 (1988).

[5] P. Pechukas, Phys. Rev. Lett. **73**, 1060 (1994).

[6] K. M. Fonseca Romero, P. Talkner, and P. Hänggi, Phys. Rev. A **69**, 052109 (2004).

[7] M. Grifoni, M. Sassetti, and U. Weiss, Phys. Rev. E **53**, R2033 (1996).

[8] H. Baur, A. Fubini, and U. Weiss, Phys. Rev. B **70**, 024302 (2004).

[9] M. Grifoni and P. Hänggi, Phys. Rep. **304**, 229 (1998).

[10] L. Hartmann, M. Grifoni, and P. Hänggi, Europhys. Lett. **38**, 497 (1997).

Chapter 4

Quantum Ratchets with Few Bands below the Barrier

In collaboration with M. Grifoni, M. S. Ferreira, and J. B. Majer.

4.1   Introduction

We consider a ratchet system such as the one introduced in Chapter 1. The system Hamiltonian $\hat{H}_{\mathrm{S}}(t) = \hat{H}_{\mathrm{R}} + \hat{H}_{\mathrm{ext}}(t)$ is made of the ratchet Hamiltonian

$$\hat{H}_{\mathrm{R}} = \frac{\hat{p}^2}{2M} + V(\hat{q}), \tag{4.1}$$

driven by a time-dependent force coupling to the position operator

$$\hat{H}_{\mathrm{ext}}(t) = -F(t)\hat{q}. \tag{4.2}$$

The ratchet potential $V(q + L) = V(q)$ is a spatially asymmetric function of periodicity L. In this chapter, we will present an approach relevant for potentials which present a few Bloch bands below the barrier. An example of such a potential is shown in Fig. 4.1.

We consider a harmonic ac driving force of amplitude F and frequency Ω

$$F(t) = F \cos(\Omega(t - t_0)). \tag{4.3}$$
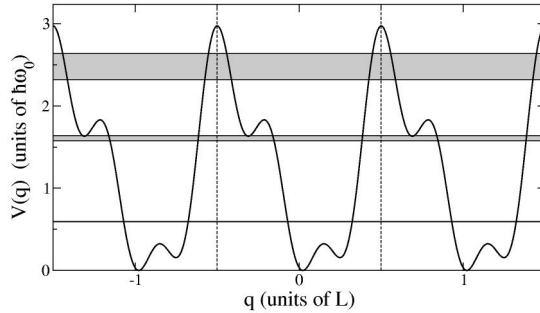
Figure 4.1: An example of a ratchet potential with three bands (shaded regions) below the barrier. The potential height is in units of the distance $\hbar\omega_0$ between the centers of the first and second band, and the length is in units of the period L.

In particular, this driving force averages to zero over a driving period, and therefore does not introduce any additional asymmetry in the system.

In order to investigate quantum Brownian motion, we let the particle interact with a dissipative thermal environment. This is modeled by the standard Hamiltonian $\hat{H}_{\mathrm{B}}$ of a bath of harmonic oscillators whose coordinates are bilinearly coupled to the system coordinate $\hat{q}$

$$\hat{H}_{\mathrm{B}} = \frac{1}{2} \sum_{\alpha=1}^{N_{\mathrm{O}}} \left[\frac{\hat{p}_\alpha^2}{m_\alpha} + m_\alpha \omega_\alpha^2 \left(\hat{x}_\alpha - \frac{c_\alpha}{m_\alpha \omega_\alpha^2} \hat{q} \right)^2 \right]. \tag{4.4}$$

The bath is fully characterized by its spectral density

$$J(\omega) = \frac{\pi}{2} \sum_{\alpha=1}^{N_{\mathrm{O}}} \frac{c_\alpha^2}{m_\alpha \omega_\alpha} \delta(\omega - \omega_\alpha), \tag{4.5}$$

defined in terms of the masses m_α, frequencies ω_α, and coupling strengths c_α of the oscillators. In this chapter, we will consider an Ohmic spectral density with a friction coefficient η and a Drude cutoff at frequency ω_{D}

$$J(\omega) = \frac{\eta\omega}{1 + (\omega/\omega_{\mathrm{D}})^2}. \tag{4.6}$$

We refer to Section 1.1.3 for the details.

We wish to evaluate the average particle velocity at long time, or ratchet current, given by

$$v = \lim_{t\to\infty} \langle \frac{\mathrm{d}}{\mathrm{d}t} \operatorname{Tr}_{\mathrm{S}}\{\hat{q}\hat{\rho}(t)\} \rangle_\Omega. \tag{4.7}$$

Here $\hat{\rho}(t) = \mathrm{Tr}_\mathrm{B}\, \hat{W}(t)$ is the reduced density matrix of the system. It is obtained by performing the trace over the bath degrees of freedom on the density matrix $\hat{W}(t)$ of the system-plus-bath $\hat{H}(t) = \hat{H}_\mathrm{S}(t) + \hat{H}_\mathrm{B}$. Finally, $\langle ... \rangle_\Omega$ denotes the time average over a driving period.

We will proceed as follows: First, we will use the Bloch theorem to diagonalize the undriven ratchet Hamiltonian and make a rotation to the eigenbasis of the position operator to write the system Hamiltonian in a tight-binding form. This will be presented in Section 4.2. Once we have obtained such a tight-binding Hamiltonian, we will only have to invoke the methods developed in Chapter 3 in order to evaluate the ratchet current. The obtained solution can be advantageously simplified in a suitable parameter regime. This will be discussed in more detail, including a numerical application, in Section 4.3.

4.2 Reduction to a tight-binding Hamiltonian

4.2.1 Bloch states

Due to the spatial periodicity of the potential $V(q + L) = V(q)$, the ratchet Hamiltonian (4.1) may be diagonalized by using Bloch theorem. Indeed, the Hamiltonian commutes with the operator performing a translation on any multiple lL of the periodicity length L, given by

$$\hat{T}(lL) = \mathrm{e}^{\mathrm{i}lL\hat{p}/\hbar}. \tag{4.8}$$

Therefore a common basis of eigenstates of $\hat{H}_\mathrm{R}$ and $\hat{T}(L)$ exists. These states are the Bloch states $|\Psi_{n,k}\rangle$ which satisfy

$$\hat{H}_\mathrm{R}|\Psi_{n,k}\rangle = E_{n,k}|\Psi_{n,k}\rangle \tag{4.9a}$$

$$\hat{T}(lL)|\Psi_{n,k}\rangle = \mathrm{e}^{\mathrm{i}klL}|\Psi_{n,k}\rangle. \tag{4.9b}$$

They are labeled by the band index n, taking integer values, and the wave-vector k, taking real values within the first Brillouin zone $k \in [-\pi/L, \pi/L]$, for a spatially infinite system. By a theorem of linear algebra, they can be chosen orthogonal and normalized, $\langle \Psi_{n',k'}|\Psi_{n,k}\rangle = \delta_{n,n'}\delta(k - k')$. In principle, these properties define them up to a phase factor which can be freely chosen, but one can restrict the possible choices if one requires that the state with opposite wave-vectors correspond to each other under time-reversal

$$\hat{\Theta}|\Psi_{n,k}\rangle = |\Psi_{n,-k}\rangle. \tag{4.10}$$

For a definition of the time-reversal operator $\hat{\Theta}$, which is the combination of a unitary operator and complex conjugation, we refer to [1, Ch. 4].

As a function of k, the eigenenergies $E_{n,k}$ are defined in the first Brillouin zone only. Accordingly, they may be written as a Fourier series. Furthermore, due to

time-reversal symmetry of the Hamiltonian $\hat{\Theta}^{-1}\hat{H}_R\hat{\Theta} = \hat{H}_R$, they must satisfy the property $E_{n,-k} = E_{n,k}$. Combining these two results, one may thus write

$$E_{n,k} = E_n + \sum_{l=1}^{\infty} \frac{\Delta_n^{(l)}}{2} \cos\left(lkL\right). \tag{4.11}$$

4.2.2   Numerical evaluation of the band structure and the wave-functions of the Bloch states

In order to numerically evaluate the parameters E_n and $\Delta_n^{(l)}$ of the band structure for a given potential $V(q)$, as well as the wave-functions $\Psi_{n,k}(q) = \langle q|\Psi_{n,k}\rangle$ of the Bloch states in the position representation, we follow the method exposed in [2, Ch. 8]. We restrict the infinite position space to an interval of length $\Lambda = N_C L$, containing a large but finite number N_C of periodicity cells of length L. Using Born-von Karman periodic boundary conditions for the wave-functions, we may write them as Fourier series

$$\Psi(q) = \sum_{k \in \mathrm{RL}} c(k)e^{ikq}. \tag{4.12}$$

The sum runs over wave-vectors k belonging to the reciprocal lattice of spacing $2\pi/\Lambda$. Using (4.9b), it is clear that only the wave-vectors $k + 2\pi l/L$ contribute to a given Bloch state $|\Psi_{n,k}\rangle$

$$\Psi_{n,k}(q) = \sum_{l=-\infty}^{\infty} c_{n,k}(k + 2\pi l/\Lambda)e^{i(k+2\pi l/\Lambda)q}. \tag{4.13}$$

Due to the restriction of the position space to the finite interval of length Λ, the possible values for the wave-vectors k of the Bloch state $|\Psi_{n,k}\rangle$ are no longer all real values in the first Brillouin zone $k \in [-\pi/L, \pi/L]$, but the N_C+1 values $k \in \{-\pi/L = -\pi N_C/\Lambda, -\pi(N_C - 2)/\Lambda, \ldots, \pi(N_C - 2)/\Lambda, \pi N_C/\Lambda = \pi/L\}$ of the reciprocal lattice comprised in the first Brillouin zone. We rewrite the potential as a Fourier series as well

$$V(q) = \sum_{l=-\infty}^{\infty} U_l e^{i(2\pi l/L)q}. \tag{4.14}$$

With these series expansions and within the so-called reduced zone scheme, the eigenvalues problem (4.9a) takes the form (see Eq. (8.41) of [2])

$$\left[\frac{\hbar^2}{2M}(k - 2\pi l/\Lambda)^2 - E_{n,k}\right] c_{n,k}(k - 2\pi l/\Lambda) + \sum_{l'=-N_C/2+1}^{N_C/2} U_{l'-l}c_{n,k}(k - 2\pi l'/\Lambda) = 0 \tag{4.15}$$

	$S(E = \Delta V)$	n
Harmonic well	$(\pi/2)\sqrt{2M\Delta V L^2}$	$(1/4\hbar)\sqrt{2M\Delta V L^2} - (1/2)$
Very deep square well	$2\sqrt{2M\Delta V L^2}$	$(1/\pi\hbar)\sqrt{2M\Delta V L^2}$
Cosine potential	$(4/\pi)\sqrt{2M\Delta V L^2}$	$-$

Table 4.1: Analytical expressions for the action $S(E = \Delta V)$ of a trajectory at the energy of the potential barrier and the number n of energy levels lying below the potential barrier for: a) A harmonic well of depth ΔV and width L; b) A very deep square well of depth $\Delta V \to \infty$ and width L; A cosine potential of amplitude ΔV and spatial periodicity L.

for a given k in the first Brillouin zone and any $l = -N_{\mathrm{C}}/2 + 1, -N_{\mathrm{C}}/2 + 2, \ldots,$ $N_{\mathrm{C}}/2 - 1, N_{\mathrm{C}}/2$. For a given k, this is a closed set of N_{C} equations for the N_{C} coefficients $c_{n,k}(k - 2\pi l/\Lambda)$, $l = -N_{\mathrm{C}}/2 + 1, -N_{\mathrm{C}}/2 + 2, \ldots, N_{\mathrm{C}}/2 - 1, N_{\mathrm{C}}/2$. They form an eigenvalues problem for a $N_{\mathrm{C}} \times N_{\mathrm{C}}$ matrix acting on the vector of coefficients. Standard methods of linear algebra can be used to solve for the eigenvalues $E_{n,k}$ and the coefficients of the eigenstates $|\Psi_{n,k}\rangle$. We fixed the free phase factor of the Bloch states by giving by convention a real positive value to $\Psi_{n,k}(q = 0)$.

This method provides information on the first N_{C} bands, $n = 1, \ldots, N_{\mathrm{C}}$, only. Ideally one should then let N_{C} tend to ∞. However, this will turn out not to be necessary. Indeed, in this work we will be interested in the deep quantum regime, where only few energy bands lie below the potential barrier ΔV. We will later restrict ourselves to a situation where the dynamics can be satisfactorily described in terms of these low lying bands only.

The number of bands lying below the barrier is controlled by the typical action $\sqrt{2M\Delta V L^2}$ depending on the particle mass M, the height of the potential barrier ΔV and its length scale L. If this typical action is large compared to the action quantum h, there will be a lot of bands below the barrier. For a very large action one reaches the classical limit. If, on the contrary, this action is of the order of h, there will be few bands below the barrier. This situation is called the deep quantum regime. In Table 4.1, one can find the relation between the action $S(E = \Delta V)$ of a trajectory at the energy of the potential barrier, the numbers of levels lying below the barrier, and the typical action $\sqrt{2M\Delta V L^2}$, for a couple of analytically solvable quantum wells. As a rule of the thumb, the number of levels lying below the barrier is the typical action $\sqrt{2M\Delta V L^2}$ divided by 3–4$\hbar$.

As an example, Fig. 4.1 shows the first three bands for the potential

$$V(q) = V_0 + \sum_{l=1}^{3} V_l \cos(2\pi l q/L - \varphi_l), \tag{4.16}$$

with the parameters

$$
\begin{aligned}
V_0 &= 1.23\hbar\omega_0 \\
V_1 &= 1.23\hbar\omega_0 & \varphi_1 &= -2.58 \\
V_2 &= 0.297\hbar\omega_0 & \varphi_2 &= -0.0423 \\
V_3 &= 0.444\hbar\omega_0 & \varphi_3 &= 2.82.
\end{aligned}
\tag{4.17}
$$

The amplitudes of the harmonics of the potential are given in units of the energy difference $\hbar\omega_0 = E_2 - E_1$ between the center of the first two bands. The mass was set to $M = 30.3\hbar/\omega_0 L^2$. This corresponds to a typical action $\sqrt{2M\Delta V L^2} = 13.4\hbar$. The parameters of the first three bands were computed for $N_C = 21$ and did not change significantly for $N_C = 26$. They read

$$
\begin{aligned}
E_1 &= 0.587\hbar\omega_0 & \Delta_1^{(1)} &= -4.43 \times 10^{-3}\hbar\omega_0 & \Delta_1^{(2)} &= 1.62 \times 10^{-5}\hbar\omega_0 \\
E_2 &= 1.59\hbar\omega_0 & \Delta_2^{(1)} &= 6.68 \times 10^{-2}\hbar\omega_0 & \Delta_2^{(2)} &= 2.60 \times 10^{-3}\hbar\omega_0 \\
E_3 &= 2.45\hbar\omega_0 & \Delta_3^{(1)} &= -3.10 \times 10^{-1}\hbar\omega_0 & \Delta_3^{(2)} &= 3.18 \times 10^{-2}\hbar\omega_0.
\end{aligned}
\tag{4.18}
$$

The parameters $\Delta_n^{(3)}$ of the next harmonics of each band n are at least two orders of magnitude smaller than the corresponding $\Delta_n^{(2)}$. We did not compute higher orders $\Delta_n^{(l)}$. The wave-functions of the corresponding Bloch states will be given in terms of the Wannier states introduced in the next section.

4.2.3   Wannier states

The Bloch states provide a natural framework to obtain information on the band structure of the Hamiltonian. From there, one would like to perform a rotation to the basis where the position operator $\hat{q}$ is diagonal, in order to map the problem onto the tight-binding system investigated in Chapter 3 [see Eqs. (3.1) and (3.2)], and use the path integrals methods developed for it. One could perform this rotation numerically in one step. However, we will gain some physical insight by going through an intermediate step involving the basis of Wannier states.

The Wannier states are defined as

$$
|\Phi_{n,j}\rangle = \sqrt{\frac{L}{2\pi}} \int_{-\pi/L}^{\pi/L} dk\, e^{-ikjL} |\Psi_{n,k}\rangle.
\tag{4.19}
$$

This Fourier transform makes typically localized Wannier states out of the typically extended Bloch states. The wave-vector k is replaced by an index j which can be interpreted as a cell index. Indeed, the property (4.9b) of the Bloch states imply

$$
\hat{T}(lL)|\Phi_{n,j}\rangle = |\Phi_{n,j+l}\rangle,
\tag{4.20}
$$
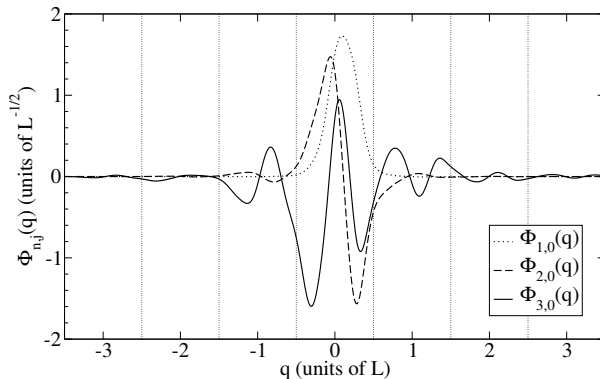
Figure 4.2: Wave-functions of the first three Wannier states $\Phi_{1,0}(q)$, $\Phi_{2,0}(q)$, and $\Phi_{3,0}(q)$ of the central cell, for the potential depicted in Fig. 4.1, and a typical action $\sqrt{2M\Delta V L^2} = 13.4\hbar$. They were computed as described in section 4.2.2 with $N_C = 31$. The vertical dotted lines indicate the location of the top of the potential barriers.

which means that the translation of $|\Phi_{n,j}\rangle$ by a length lL to the right yields $|\Phi_{n,j+l}\rangle$. The Wannier states inherit the orthogonality and normalization of the Bloch states $\langle\Phi_{n',j'}|\Phi_{n,j}\rangle = \delta_{n,n'}\delta_{j,j'}$. The time-reversal property (4.10) becomes

$$\hat{\Theta}|\Phi_{n,j}\rangle = |\Phi_{n,j}\rangle, \tag{4.21}$$

from which one can show that the wave-functions of the Wannier states are real-valued. As an example, the wave-functions of the first three bands of the potential depicted in Fig. 4.1 are shown in Fig. 4.2. Their localized character is due to the fact that the energy of the corresponding states lies below the potential barrier.

Rewritten in terms of the Wannier states, the Hamiltonian reads

$$\hat{H}_{\mathrm{R}} = \sum_{n=1}^{\infty}\left[\sum_{j=-\infty}^{\infty} E_n|\Phi_{n,j}\rangle\langle\Phi_{n,j}| + \sum_{l=1}^{\infty}\sum_{j=-\infty}^{\infty}\frac{\Delta_n^{(l)}}{4}\left(|\Phi_{n,j+l}\rangle\langle\Phi_{n,j}| + |\Phi_{n,j}\rangle\langle\Phi_{n,j+l}|\right)\right]. \tag{4.22}$$

Even more interesting is the structure of the position operator in the Wannier basis. One finds

$$\hat{q} = \sum_{n,n'=1}^{\infty}\sum_{j,j'=-\infty}^{\infty}\left(\delta_{j,j'}\delta_{n,n'}jL + \xi_{n'n}^{(j'-j)}\right)|\Phi_{n',j'}\rangle\langle\Phi_{n,j}|. \tag{4.23}$$

The first term reflects the spatial periodicity of the system. The second one is written in terms of the real-valued overlap integrals

$$\xi_{n'n}^{(j'-j)} = \langle\Phi_{n',j'-j}|\hat{q}|\Phi_{n,0}\rangle, \tag{4.24}$$

which carry information on the shape of the potential $V(q)$. One sees that the position operator is in general not diagonal in the Wannier basis.

As an example, for the potential (4.16), we find the following parameters, written in terms of the real matrices Ξ_j defined through $(\Xi_j)_{n'n} \doteq \xi_{n'n}^{(j)}$,

$$\Xi_0 = \begin{pmatrix} 1.10 \times 10^{-1}L & -1.28 \times 10^{-1}L & -6.43 \times 10^{-3}L \\ -1.28 \times 10^{-1}L & 9.28 \times 10^{-2}L & 1.60 \times 10^{-1}L \\ -6.43 \times 10^{-3}L & 1.60 \times 10^{-1}L & -1.59 \times 10^{-1}L \end{pmatrix}$$

$$\Xi_1 = \Xi_{-1}^{\mathrm{T}} = \begin{pmatrix} -1.32 \times 10^{-3}L & 5.03 \times 10^{-3}L & -6.91 \times 10^{-4}L \\ 1.46 \times 10^{-3}L & -1.82 \times 10^{-2}L & -1.02 \times 10^{-2}L \\ 1.49 \times 10^{-3}L & 8.93 \times 10^{-2}L & -1.71 \times 10^{-1}L \end{pmatrix}$$

$$\Xi_2 = \Xi_{-2}^{\mathrm{T}} = \begin{pmatrix} 1.25 \times 10^{-5}L & -4.83 \times 10^{-5}L & 1.98 \times 10^{-4}L \\ -6.33 \times 10^{-5}L & -1.15 \times 10^{-3}L & 2.53 \times 10^{-3}L \\ 5.91 \times 10^{-4}L & 1.63 \times 10^{-2}L & -1.34 \times 10^{-2}L \end{pmatrix}. \qquad (4.25)$$

We see that, due to the localized character of the Wannier states of the first three bands, the corresponding coefficients in Ξ_j decrease with increasing $|j|$. This trend goes on for $\Xi_{\pm 3}$.

4.2.4   Eigenstates of the position operator (DVR states)

We want to perform a rotation to the basis where the position operator $\hat{q}$ is diagonal, in order to map the problem onto the tight-binding system defined by Eqs. (3.1) and (3.2), and use the path integral methods developed in Chapter 3 in order to evaluate the ratchet current. The eigenbasis of the position operator is particularly convenient for two reasons: i) In this basis, only diagonal elements of the reduced density matrix of the system are needed in order to compute the current $v(t) = \mathrm{Tr}_{\mathrm{S}}\{\hat{q}\hat{\rho}(t)\}$; ii) The coupling between the system and bath coordinates is proportional to the system position operator $\hat{q}$, and it therefore assumes a simpler form in this eigenbasis, allowing for the results derived in Chapter 3. This approach originates from a numerical quasi-adiabatic propagator path integral method [3]. There, the terminology of discrete variable representation (DVR) was used for the eigenbasis of the position operator. From an analytical point of view, this method was first applied to the investigation of dissipative quantum tunneling in bistable systems in terms of multilevels in a double-well potential [4, 5].

In the Wannier basis $|\Phi_{n,j}\rangle$, the position operator is a real symmetric matrix. Therefore, there exists a real orthogonal transformation

$$|m,r\rangle = \sum_{n=1}^{\infty} \sum_{j=-\infty}^{\infty} U_{mn,rj}|\Phi_{n,j}\rangle \qquad (4.26)$$

to the eigenbasis $|m,r\rangle$ of the position operator

$$\hat{q}|m,r\rangle = q_{m,r}|m,r\rangle. \qquad (4.27)$$

The transformation mixes the bands in new pseudo-bands labeled by the index m, and the cells in new pseudo-cells labeled by the index r. Rewritten in this basis, the Hamiltonian reads

$$\hat{H}_{\mathrm{R}} = \sum_{m,m'=1}^{\infty} \sum_{r,r'=-\infty}^{\infty} H_{m'm,r'r} |m',r'\rangle\langle m,r|, \qquad (4.28)$$

with the matrix elements

$$H_{m'm,r'r} = \sum_{n=1}^{\infty} \Bigg[\sum_{j=-\infty}^{\infty} E_n U_{m'n,r'j} U_{mn,rj}$$
$$+ \sum_{l=1}^{\infty} \sum_{j=-\infty}^{\infty} \frac{\Delta_n^{(l)}}{4} \left(U_{m'n,r'j+l} U_{mn,rj} + U_{m'n,r'j} U_{mn,rj+l} \right) \Bigg]. \quad (4.29)$$

These representations of the Hamiltonian and position operator are identical to (3.1) and (3.2), provided one introduces the notation $\mu \,\hat{=}\, (m,r)$ for the quantum numbers, and $q_\mu \,\hat{=}\, q_{m,r}$, $\varepsilon_\mu \,\hat{=}\, H_{mm,rr}$ and $\Delta_{\nu\mu} \,\hat{=}\, H_{m'm,r'r}$ for the corresponding matrix elements.

Following the discussion of Chapter 3, one can write the master equation

$$\frac{\mathrm{d}}{\mathrm{d}\tau} \bar{P}_{\nu\mu_0}(\tau) = \sum_{\mu \in \mathrm{TB},\ \mu \neq \nu} \bar{\Gamma}_{\nu\mu} \bar{P}_{\mu\mu_0}(\tau) - \sum_{\mu \in \mathrm{TB},\ \mu \neq \nu} \bar{\Gamma}_{\mu\nu} \bar{P}_{\nu\mu_0}(\tau) \qquad (4.30)$$

for the populations $\bar{P}_{\mu\mu_0}(\tau) = \langle P_{\mu\mu_0}(\tau) \rangle_\Omega$ obtained from the diagonal elements of the reduced density matrix $P_{\mu\mu_0}(\tau) = \langle \mu | \hat{\rho}(t_0 + \tau) | \mu \rangle$ by averaging over a driving period. This master equation is valid at long times τ and when the averaged transition rates $\bar{\Gamma}_{\nu\mu}$ remain much smaller than the driving frequency Ω. From its solution (3.56), one extracts the ratchet current (4.7) which takes the form

$$v = \lim_{\tau \to \infty} \sum_{\mu \in \mathrm{TB}} q_\mu \dot{\bar{P}}_{\mu\mu_0}(\tau). \qquad (4.31)$$

This solves formally our problem, for the case of high-frequency ac driving. However, this solution is not very useful in practice as it requires the evaluation of infinitely many transition rates $\bar{\Gamma}_{\nu\mu}$ between the different tight-binding sites. For this reason, in the next sections we will investigate a parameter regime were the ratchet current can be expressed in terms of a few rates. We will also demonstrate the usefulness of the results by a numerical application.

4.3 Truncation to the lowest bands and tight-binding approximation

Let us consider the case where the system dynamics can be described in terms of the lowest N_{B} energy bands only. If the different energy sources for the system, that is

the energies associated with the driving amplitude FL, the driving frequency $\hbar\Omega$ and the bath temperature $k_\mathrm{B}T$, are all much smaller than the energy difference $\hbar\omega_0 = E_2 - E_1$ between the first two bands, one can argue that the probability to populate higher energy bands will be low, and that the relevant dynamical features can be captured by considering the lowest N_B bands only. If the driving frequency Ω is in or close to resonance with the separation ω_0 between the first two bands, one can argue that the dynamics will be confined to these two bands also. This even allows to soften the restrictions on the driving parameter to the regime $\Omega \lesssim \omega_0$ and $FL \lesssim \hbar\omega_0$.

We will see that considering the first band only leads to a vanishing ratchet current. So we have to consider at least two bands. Here we choose to consider the N_B bands lying below the potential barrier, because of the localized character of the corresponding Wannier states. In the example of the potential (4.16) shown in Fig. 4.1, three bands lie below the barrier, $N_\mathrm{B} = 3$. Consequently, the band index n runs from 1 to N_B in all expressions of the previous section.

The localized character of the Wannier states of the bands lying below the barrier means that the overlap between the wave-functions of Wannier states corresponding to cells at distance l from each other decays fast with increasing distance $|l|$. In other words, the matrix elements of the observables in the Wannier basis are negligible far from the diagonal. Here we choose

$$\Delta_n^{(l)} \approx 0 \quad \text{for } l \geq 2 \tag{4.32a}$$

$$\xi_{n'n}^{(l)} \approx 0 \quad \text{for } l \geq 1. \tag{4.32b}$$

Correspondingly, the Hamiltonian and position operator read in the truncated Wannier basis

$$\hat{H}_\mathrm{R} = \sum_{n=1}^{N_\mathrm{B}} \sum_{j=-\infty}^{\infty} \left[E_n |\Phi_{n,j}\rangle\langle\Phi_{n,j}| + \frac{\Delta_n^{(1)}}{4} \left(|\Phi_{n,j+1}\rangle\langle\Phi_{n,j}| + |\Phi_{n,j}\rangle\langle\Phi_{n,j+1}| \right) \right] \tag{4.33a}$$

$$\hat{q} = \sum_{n,n'=1}^{N_\mathrm{B}} \sum_{j=-\infty}^{\infty} \left(\delta_{n,n'} jL + \xi_{n'n}^{(0)} \right) |\Phi_{n',j}\rangle\langle\Phi_{n,j}|. \tag{4.33b}$$

This means that one considers up to nearest neighbors overlaps in the Hamiltonian, and on-site contributions only in the position operator. In this case, the transformation to the eigenbasis of the position operator mixes the bands within each cell

$$|m,j\rangle = \sum_{n=1}^{N_\mathrm{B}} U_{mn} |\Phi_{n,j}\rangle. \tag{4.34}$$

In this basis, the Hamiltonian operator takes the form

$$\hat{H}_{\mathrm{R}} = \sum_{j=-\infty}^{\infty} \left[\sum_{m=1}^{N_{\mathrm{B}}} \varepsilon_m |m,j\rangle\langle m,j| + \sum_{m\neq m'=1}^{N_{\mathrm{B}}} \Delta^{\mathrm{intra}}_{m'm} |m',j\rangle\langle m,j| \right.$$

$$\left. + \sum_{m,m'=1}^{N_{\mathrm{B}}} \Delta^{\mathrm{inter}}_{m'm} \left(|m',j+1\rangle\langle m,j| + |m',j\rangle\langle m,j+1| \right) \right]. \quad (4.35)$$

The diagonal elements $\varepsilon_m = \sum_{n=1}^{N_{\mathrm{B}}} E_n U_{mn} U_{mn}$ represent the on-site energies in the absence of driving. The couplings $\Delta^{\mathrm{intra}}_{m'm} = \sum_{n=1}^{N_{\mathrm{B}}} E_n U_{m'n} U_{mn}$ allow for intrawell vibrational motion, whereas the couplings $\Delta^{\mathrm{inter}}_{m'm} = \sum_{n=1}^{N_{\mathrm{B}}} (\Delta^{(1)}_n / 4) U_{m'n} U_{mn}$ account for interwell tunneling. The eigenvalues of the position operator $q_{m,j} = jL + q_m$ are periodically repeated, reflecting the periodicity of the system. The situation is depicted in Fig. 4.3 for the potential (4.16) after truncation of the dynamics to the three lowest bands. For this situation, the on-site energies, position eigenvalues, intrawell and interwell couplings read

$$\varepsilon_1 = 2.21\hbar\omega_0 \qquad\qquad q_1 = -0.244L$$
$$\varepsilon_2 = 1.13\hbar\omega_0 \qquad\qquad q_2 = 0.0240L$$
$$\varepsilon_3 = 1.27\hbar\omega_0 \qquad\qquad q_3 = 0.264L$$

$$\Delta^{\mathrm{intra}} = \begin{pmatrix} 0 & 2.20 \times 10^{-2}\hbar\omega_0 & 1.75 \times 10^{-3}\hbar\omega_0 \\ 2.20 \times 10^{-2}\hbar\omega_0 & 0 & 4.10 \times 10^{-2}\hbar\omega_0 \\ 1.75 \times 10^{-3}\hbar\omega_0 & 4.10 \times 10^{-2}\hbar\omega_0 & 0 \end{pmatrix}$$

$$\Delta^{\mathrm{inter}} = \begin{pmatrix} 3.72 \times 10^{-4}\hbar\omega_0 & 1.19 \times 10^{-4}\hbar\omega_0 & 7.78 \times 10^{-5}\hbar\omega_0 \\ 1.19 \times 10^{-4}\hbar\omega_0 & 1.05 \times 10^{-5}\hbar\omega_0 & 7.07 \times 10^{-7}\hbar\omega_0 \\ 7.78 \times 10^{-5}\hbar\omega_0 & 7.07 \times 10^{-7}\hbar\omega_0 & 5.85 \times 10^{-7}\hbar\omega_0 \end{pmatrix}. \quad (4.36)$$

If one also includes the nearest neighbors contributions $\xi^{(1)}_{n'n}$ to the position operator in the Wannier basis, instead of (4.32b), the Hamiltonian reads

$$\hat{H}_{\mathrm{R}} = \sum_{j=-\infty}^{\infty} \left[\sum_{m=1}^{N_{\mathrm{B}}} \varepsilon_m |m,j\rangle\langle m,j| + \sum_{m\neq m'=1}^{N_{\mathrm{B}}} \Delta^{\mathrm{intra}}_{m'm} |m',j\rangle\langle m,j| \right.$$

$$\left. + \sum_{m,m'=1}^{N_{\mathrm{B}}} \left(\Delta^{\mathrm{inter},f}_{m'm} |m',j+1\rangle\langle m,j| + \Delta^{\mathrm{inter},b}_{m'm} |m',j\rangle\langle m,j+1| \right) \right]. \quad (4.37)$$
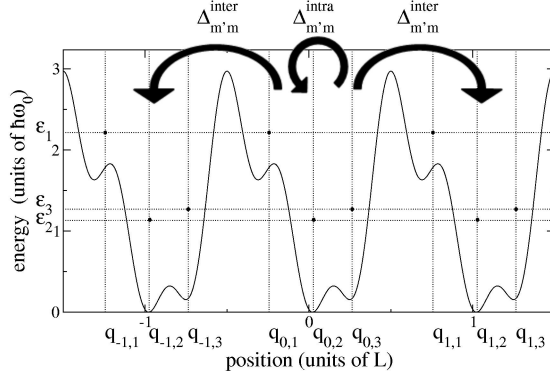
Figure 4.3:   On-site energies ε_m versus position $q_{m,l}$ of the position eigen-states $|m,l\rangle$ (black dots), for the potential (4.16) (solid line) after truncation to the $N_{\mathrm{B}} = 3$ lowest energy bands. The arrows schematically represent the intrawell and interwell couplings $\Delta^{\mathrm{intra}}_{m',m}$ and $\Delta^{\mathrm{inter}}_{m',m}$.

In this case the on-site energies, position eigenvalues and intrawell coupling change only slightly, whereas the interwell couplings get an asymmetric structure

$$\varepsilon_1 = 2.17\hbar\omega_0 \qquad\qquad q_1 = -0.250L$$
$$\varepsilon_2 = 1.14\hbar\omega_0 \qquad\qquad q_2 = 0.0285L$$
$$\varepsilon_3 = 1.30\hbar\omega_0 \qquad\qquad q_3 = 0.265L$$

$$\Delta^{\mathrm{intra}} = \begin{pmatrix} 0 & 2.30 \times 10^{-2}\hbar\omega_0 & 2.02 \times 10^{-3}\hbar\omega_0 \\ 2.30 \times 10^{-2}\hbar\omega_0 & 0 & 4.28 \times 10^{-2}\hbar\omega_0 \\ 2.02 \times 10^{-3}\hbar\omega_0 & 4.28 \times 10^{-2}\hbar\omega_0 & 0 \end{pmatrix}$$

$$\Delta^{\mathrm{inter,f}} = \left(\Delta^{\mathrm{inter,b}}\right)^T = \begin{pmatrix} 8.03 \times 10^{-5}\hbar\omega_0 & 2.28 \times 10^{-5}\hbar\omega_0 & 9.77 \times 10^{-6}\hbar\omega_0 \\ 2.35 \times 10^{-4}\hbar\omega_0 & 4.35 \times 10^{-5}\hbar\omega_0 & 1.71 \times 10^{-5}\hbar\omega_0 \\ 1.08 \times 10^{-3}\hbar\omega_0 & 1.20 \times 10^{-4}\hbar\omega_0 & 3.87 \times 10^{-5}\hbar\omega_0 \end{pmatrix}.$$

$$\tag{4.38}$$

For a Hamiltonian of the form (4.37), the master equation (4.30) may be rewrit-ten in terms of intrawell transition rates $\bar{\Gamma}^{\mathrm{intra}}_{m'm} \,\hat{=}\, \bar{\Gamma}^{jj}_{m'm}$, forward interwell transi-tion rates $\bar{\Gamma}^{\mathrm{inter,f}}_{m'm} \,\hat{=}\, \bar{\Gamma}^{j+1\,j}_{m'm}$ and backward interwell transition rates $\bar{\Gamma}^{\mathrm{inter,b}}_{m'm} \,\hat{=}\, \bar{\Gamma}^{j-1\,j}_{m'm}$, where $\bar{\Gamma}^{j'j}_{m'm}$ denote the transition rate from the state $|m,j\rangle$ to the state $|m',j'\rangle$ averaged over a driving period. Its solution yields the ratchet current

$$v = L \sum_{m,m'=1}^{N_{\mathrm{B}}} p_m^\infty \left(\bar{\Gamma}^{\mathrm{inter,f}}_{m'm} - \bar{\Gamma}^{\mathrm{inter,b}}_{m'm}\right), \tag{4.39}$$

in terms of the asymptotic population $p_m^\infty \;\hat{=}\; \lim_{\tau\to\infty} \sum_{j=-\infty}^{\infty} \bar{P}_{m,j}(\tau)$ of the band m. As an example, when the dynamics is truncated to three bands only, the asymptotic population of the first band reads

$$p_1^\infty = \frac{\bar{\Gamma}_2 \bar{\Gamma}_3 - \bar{\Gamma}_{23}\bar{\Gamma}_{32}}{\sum_{m=1}^3 \sum_{m'=m+1}^3 \left(\bar{\Gamma}_m \bar{\Gamma}_{m'} - \bar{\Gamma}_{mm'}\bar{\Gamma}_{m'm}\right)}, \tag{4.40}$$

in terms of combinations of the rates defined as $\bar{\Gamma}_{m'm} \;\hat{=}\; \bar{\Gamma}_{m'm}^{\text{inter,f}} + \bar{\Gamma}_{m'm}^{\text{inter,b}} + \bar{\Gamma}_{m'm}^{\text{intra}}$ and $\bar{\Gamma}_m \;\hat{=}\; \sum_{m'=1}^3 \bar{\Gamma}_{m'm}$. The asymptotic populations of the two other bands can be obtained by cyclic permutations of the indices. One sees that these asymptotic populations do not depend on the initial preparation.

The transition rates can be evaluated by following the lines of Chapter 3. Within an incoherent tunneling description, holding at high temperature T and/or moderate-to-strong dissipation, controlled by the dimensionless parameter $\alpha = \eta L^2/2\pi\hbar$, the lowest order in the couplings $\Delta_{m'm}^{jj} \;\hat{=}\; \Delta_{m'm}^{\text{intra}}$, $\Delta_{m'm}^{j+1j} \;\hat{=}\; \Delta_{m'm}^{\text{inter,f}}$, and $\Delta_{m'm}^{j-1j} \;\hat{=}\; \Delta_{m'm}^{\text{inter,b}}$, provides a good approximation [6]. If the driving frequency is much larger than all transition rates, they may be written (see also Section 3.7 and Refs. [6, 7])

$$\bar{\Gamma}_{m'm}^{j',j} = \frac{\left(\Delta_{m'm}^{j'j}\right)^2}{\hbar^2} \int_{-\infty}^{\infty} d\tau e^{-\left[(q_{m,j}-q_{m',j'})^2/\hbar\right]Q(\tau)+i\left[(\varepsilon_m-\varepsilon_{m'})/\hbar\right]\tau}$$
$$\times J_0\left[\frac{2F(q_{m,j}-q_{m',j'})}{\hbar\Omega}\sin\left(\frac{\Omega\tau}{2}\right)\right]. \tag{4.41}$$

The twice integrated bath correlation function $Q(\tau)$ is defined in (B.2), whereas J_0 denotes the zero-order Bessel function.

From (4.39), it is obvious that the ratchet current vanishes if one truncates the dynamics to a single band only. Indeed, in the absence of a band index m, the rates (4.41) satisfy $\bar{\Gamma}^{\text{inter,f}} = \bar{\Gamma}^{\text{inter,b}}$. When more bands are considered, the asymmetric arrangement of the position eigenvalues q_m and the richer structure of the Hamiltonian break this property. Another way to understand this result is to realize that taking a single band into account is equivalent to consider the first harmonic only of the Fourier series of the potential, which yields a cosine function, therefore spatially symmetric.

To conclude, we give a numerical application for the potential (4.16). The dynamics is truncated to the three lowest energy bands, and the parameters (4.36) are used. The ratchet current (4.39) is evaluated with the rates (4.41). The result is shown in Fig. 4.4 for $\alpha = 0.5$ and $\alpha = 2.0$, corresponding to moderate and strong dissipation. The ratchet current is plotted as a function of the driving amplitude F for different values of the driving frequency Ω. The temperature is set to $k_{\text{B}}T = 0.08\hbar\omega_0$, whereas the cutoff frequency of the Drude spectral density is set to $\omega_{\text{D}} = 0.1\omega_0$ for the case of moderate dissipation, respectively $\omega_{\text{D}} = 0.4\omega_0$ for strong dissipation.
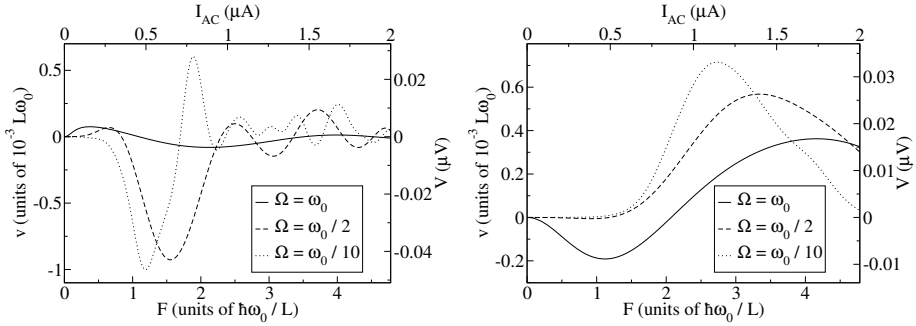
Figure 4.4: Ratchet current in the potential (4.16) after truncation to the three lowest energy bands and tight-binding approximation (4.32). The ratchet current is plotted as a function of the driving amplitude F for different driving frequencies Ω, plotted for moderate dissipation $\alpha = 0.5$ (left) and strong dissipation $\alpha = 2.0$ (right). The temperature is set to $k_B T = 0.08\hbar\omega_0$. The cutoff frequency of the Drude spectral density is set to $\omega_D = 0.1\omega_0$ (left), respectively $\omega_D = 0.4\omega_0$ (right). The alternate current-voltage scales refer to the experimental situation discussed in Chapter 2.

These curves reveal a nontrivial nonmonotonic dependence of the ratchet current on the amplitude and frequency of the driving force, and on the dissipation as well. In particular, current inversions can be tuned by changing any of these parameters. Close to these inversions, the system experiences driving-induced localization. Between them, resonances exhibit driven-assisted tunneling. For $\alpha = 2.0$, the resonances are shifted to values of the driving amplitude higher than for $\alpha = 0.5$, meaning that dissipation tends to suppress tunneling in this regime. This confirms that the system experiences moderate-to-strong dissipation. In contrast, in the weak dissipation regime, one would expect that dissipation tends to enhance tunneling. Indeed, dissipation goes with the coupling between the system and the bath, and when the system and the bath are decoupled, tunneling between states of different energy is blocked in the system.

Another important feature is the vanishing of the ratchet current in the absence of driving $F = 0$, which demonstrate that our model is free of Maxwell daemon. Indeed, in the absence of the driving force, the system is in thermal equilibrium with the bath, and a non-vanishing ratchet current would mean extracting work out of a single thermal reservoir, which is forbidden by the Second Principle of Thermodynamics.

4.4 Conclusions and outlook

In conclusion, the particle current in a dissipative quantum ratchet system in the presence of high-frequency ac driving has been calculated. The result is given in Eq. (4.31), in terms of the solution (3.56) of the master equation (4.30). It requires the evaluation of the transition rates $\bar{\Gamma}_{\nu\mu}$ in a driven dissipative tight-binding model given by the Hamiltonian (4.28).

In its complete form, this solution is of restricted practical use, as it requires the evaluation of infinitely many transition rates. For this reason, we have discussed the situation where only the $N_{\rm B}$ bands of lowest energy are taken into account. This requires that the thermal energy $k_{\rm B}T$ is much smaller than the energy difference $\hbar\omega_0 = E_2 - E_1$ between the first two bands, and that the driving parameters satisfy $\Omega \lesssim \omega_0$ and $FL \lesssim \hbar\omega_0$. We have kept the bands lying below the potential barrier. In parallel, the localized character of the corresponding Wannier states has been exploited, allowing to retain at most nearest neighbors overlaps. The result is given in Eq. (4.39). A numerical application is shown in Fig. 4.4, based on the incoherent tunneling expression (4.41) for the rates, valid at high temperature and/or large dissipation.

This method was the first to allow the evaluation of the ratchet current for a realistic system in the deep quantum regime, and was published as such [8]. The main results are: i) The occurrence of current inversions as a function of any parameter among the amplitude and frequency of the driving force, and the dissipation; ii) The absence of rectification when the dynamics is truncated to a single band.

The main drawback is its reliance on the truncation to a finite number of bands. From a practical point of view, the truncation to a small number of bands introduces strong limitations on the parameters of the driving. The driving frequency is constrained between this higher bound $\Omega \lesssim \omega_0$ and the lower bound $\Omega \gg \bar{\Gamma}_{\nu\mu}$ required in order to write the high-frequency form of the master equation. The limitation $FL \ll \hbar\omega_0$ on the driving amplitude, in the time-independent case, lies below the window reached, e.g., in state-of-the-art experimental realizations with vortices in Josephson junction arrays (see Chapter 2). From a fundamental point of view, the truncation to a finite number of bands prevents us from exploring the very interesting limit of large driving amplitude, which eventually leads to the classical limit. This was the main motivation to try developing an approach which does not rely on this restriction. Such an approach is presented in Chapter 6.

In the approach presented in this chapter, one first diagonalizes the undriven system Hamiltonian and then expresses the driving term in the obtained basis. If one would diagonalize the Hamiltonian in the presence of a time-independent force, one would obtain eigenstates arranged in Wannier-Stark ladders. It would be interesting to investigate how the dynamics in the presence of the coupling to the dissipative bath can be treated from this different starting point, and how the results are related to the ones presented in this chapter. This description would probably not require

the restriction to low driving amplitudes, as the driving would be fully embedded in the Wannier-Stark states on which it is based.

The incoherent tunneling expression (4.41) for the transition rates is the leading term in the expansion in the couplings $\Delta_{m'm}^{j'j}$. Looking at the values given in (4.38), one sees that this approximation is better for the interwell couplings than for the intrawell couplings. The intrawell dynamics is faster than the interwell dynamics. A natural improvement of the approach would thus be to treat the intrawell dynamics coherently to higher orders, while still using an incoherent tunneling description for the interwell dynamics.

References

[1] J. J. Sakurai, *Modern Quantum Mechanics* (Adison-Wesley, Redwood City, 1985).

[2] N. W. Ashcroft and N. D. Mermin, *Solid State Physics* (Harcourt, Orlando, 1976).

[3] N. Makri, in *Time-Dependent Quantum Molecular Dynamics*, edited by J. Broeckhove and L. Lathouwers (Plenum Press, New York, 1992), vol. 299 of *NATO ASI Series B: Physics.*

[4] M. Thorwart, M. Grifoni, and P. Hänggi, Phys. Rev. Lett. **85**, 860 (2000).

[5] M. Thorwart, *Tunneling and vibrational relaxation in driven multilevel systems*, Ph.D. thesis, University of Augsburg (2000).

[6] U. Weiss, *Quantum Dissipative Systems* (World Scientific, Singapore, 1999), 2nd ed.

[7] M. Grifoni, M. Sassetti, and U. Weiss, Phys. Rev. E **53**, R2033 (1996).

[8] M. Grifoni, M. S. Ferreira, J. Peguiron, and J. B. Majer, Phys. Rev. Lett. **89**, 146801 (2002).

Chapter 5

Single-Band Tight-Binding Model

5.1 Introduction

In this chapter, we will apply the formalism presented in Chapter 3 to the particular case of a single-band tight-binding model characterized by the Hamiltonian

$$\hat{H}_{\mathrm{S}} \,\hat{=}\, \sum_{m=1}^{\infty} \sum_{l=-\infty}^{\infty} \left(\Delta_m |l+m\rangle\langle l| + \Delta_m^* |l\rangle\langle l+m| \right) - F\hat{q}, \tag{5.1}$$

and position operator

$$\hat{q} \,\hat{=}\, L \sum_{l=-\infty}^{\infty} l |l\rangle\langle l|. \tag{5.2}$$

The spatial periodicity of the system is denoted by L, and the driving force by F. This system is a particular case of the one defined in Eqs. (3.1) and (3.2). Due to the presence of a single band only, the generic quantum number μ used there to label the tight-binding states is here simply replaced by an integer l specifying the position $q_l = lL$ of each state, as

$$\hat{q}|l\rangle = q_l|l\rangle. \tag{5.3}$$

Furthermore, we choose the on-site energies ε_l to be all equal. We can then set them to zero without loss of generality. We assume that the couplings $\Delta_{l'l} \,\hat{=}\, \Delta_m$ depend on the relative position $m \,\hat{=}\, l' - l$ between the coupled sites. Hermiticity of the Hamiltonian then requires $\Delta_{-m} = \Delta_m^*$. We consider a time-independent force F, for simplicity. Finally, as in Chapter 3, the system Hamiltonian (5.1) is bilinearly coupled to a bath of harmonic oscillators in order to account for dissipation (see

75

Section 1.1.3). This system is relevant for the investigation of quantum ratchets by means of the method presented in Chapter 6.

Due to translational symmetry of the model, the influence function connecting the site l to the site l', introduced in Eq. (3.42), also depends on the relative position $m = l' - l$ between the sites only. The irreducible kernels (3.44) and the transition rates (3.55) inherit this property. Therefore, we will use the notation Γ_m for the transition rate to a neighbor of order m to the right (m positive), respectively to the left (m negative).

From an analytical point of view, the particular forms of the Hamiltonian (5.1) and of the position operator (5.2) present several advantages with respect to the general system investigated in Chapter 3. As we will see in the next section, the generating function assumes a particularly simple expression at long times, which considerably simplifies the evaluation of the mobility and diffusion coefficient. Furthermore, some general properties of the transition rates are easier to extract in this framework, as shown in Section 5.3.1. Likewise, the fact that the quantum number l labeling the sites is simply an integer makes it easier to sum up all contributions to a given transition rate. This will be discussed Section 5.3.2. Most of the results presented in this chapter are not new in their essence, and can be found, e.g., in Ref. [1]. However, in contrast to that work, we also consider couplings between non-nearest neighbors, and allow them to take complex values

$$\Delta_m = |\Delta_m| \, \mathrm{e}^{\mathrm{i}\varphi_m}. \tag{5.4}$$

This will play a crucial role when a system of the form (5.1) will appear as the dual system of the continuous ratchet potential considered in Chapter 6, as a consequence of the duality relation between the two models. In particular, we will see that third-order transition rates, which are absent in the nearest-neighbors model investigated in Ref. [1], play a dominant role as soon as one is interested in the evaluation of the ratchet current. This will lead us to discuss their evaluation in Section 5.3.2, and to keep a special attention to the dependence of the rates on the phases φ_m of the couplings, as the latest will turn out to carry the information on the spatial asymmetry of the ratchet system.

5.2   Generating function

We want to evaluate the expectation value of the position operator $\langle \hat{q}(t) \rangle$ and its fluctuations $\langle \Delta \hat{q}^2(t) \rangle \hat{=} \langle \hat{q}^2(t) \rangle - \langle \hat{q}(t) \rangle^2$ at long time t. As discussed in Section 3.1, the necessary information is contained in the diagonal elements of the reduced density matrix of the system $\hat{\rho}(t)$,

$$P_l(t) \hat{=} \langle l|\hat{\rho}(t)|l \rangle, \tag{5.5}$$

which represent the populations of each site $|l\rangle$ of the tight-binding system at time t, after a preparation of the system-plus-bath according to Eq. (3.10) with $\hat{\rho}(t_0) = |l_0\rangle\langle l_0|$ at initial time t_0.

For the system considered, it turns out to be very powerful to work with the generating function, defined as

$$\tilde{P}(\lambda, t) = \sum_{l=-\infty}^{\infty} e^{\lambda q_l} P_l(t). \tag{5.6}$$

The conservation of the total population of the system implies the normalization property

$$\tilde{P}(\lambda = 0, t) = \sum_{l=-\infty}^{\infty} P_l(t) = \mathrm{Tr}_{\mathrm{S}}\{\hat{\rho}(t)\} = 1. \tag{5.7}$$

The generating function takes its name from the fact that its derivatives generate expectation values of powers of the position operator

$$\left. \frac{\partial^k \tilde{P}(\lambda, t)}{\partial \lambda^k} \right|_{\lambda=0} = \sum_{l=-\infty}^{\infty} q_l^k P_l(t) = \mathrm{Tr}_{\mathrm{S}}\{\hat{q}^k \hat{\rho}(t)\} = \langle \hat{q}^k(t) \rangle. \tag{5.8}$$

From the generalized master equation (3.50) for the populations which has been derived in Chapter 3, one can obtain a very simple expression for the generating function. Using the translational invariance of the system, which implies that the kernels depend on the relative position of the sites that they connect only, the generalized master equation takes the form

$$\frac{\mathrm{d}}{\mathrm{d}\tau} P_l(\tau) = \int_0^\tau \mathrm{d}\tau' \sum_{l'=-\infty}^{\infty} K_{l-l'}^{\mathrm{irred}}(\tau - \tau') P_{l'}(\tau'). \tag{5.9}$$

For convenience, we have momentarily replaced the time argument t of the populations by the measurement time $\tau \mathrel{\hat=} t - t_0$. Using (5.6), this equation can be rewritten in terms of the generating function, with the same convention for its time argument. This yields

$$\frac{\partial}{\partial \tau} \tilde{P}(\lambda, \tau) = \int_0^\tau \mathrm{d}\tau' \sum_{m=-\infty}^{\infty} e^{\lambda q_m} K_m^{\mathrm{irred}}(\tau - \tau') \tilde{P}(\lambda, \tau'). \tag{5.10}$$

This equation already shows the power of the generating function: This function contains all the information on the populations of the different tight-binding sites, combined in such a way that the generalized master equations (5.9), which each one of them obeys, can be written as single equation, with a new variable λ. The simplification introduced by considering a single-band tight-binding model is hidden in the property $q_l - q_{l'} = q_{l-l'}$. Introducing the Laplace transform of the generating function and following the same procedure as in Section 3.5 to solve this equation, we get

$$\mathcal{L}\tilde{P}(\lambda, s) \underset{s\to 0}{\sim} \left[s - \sum_{m=-\infty}^{\infty} e^{\lambda q_m} \Gamma_m \right]^{-1} \tilde{P}(\lambda, \tau = 0), \tag{5.11}$$

in terms of the rates $\Gamma_m \hat{=} \int_0^\infty \mathrm{d}\tau K_m^{\mathrm{irred}}(\tau)$. This yields the expression

$$\tilde{P}(\lambda, \tau) \underset{\tau \to \infty}{\sim} \exp \left\{ \tau \sum_{m=-\infty}^\infty \mathrm{e}^{\lambda q_m} \Gamma_m \right\} \tilde{P}(\lambda, \tau = 0) \tag{5.12}$$

for the generating function at long times. This expression can be written in a more convenient form by taking into account the property that the transition rates sum up to zero, or equivalently

$$\Gamma_0 = -\sum_{m \neq 0} \Gamma_m. \tag{5.13}$$

We will demonstrate this property in Section 5.4.3. Recalling the initial preparation $P_l(\tau = 0) = \delta_{l,l_0}$, which implies $\tilde{P}(\lambda, \tau = 0) = \mathrm{e}^{\lambda q_{l_0}}$, and re-establishing the original notation for the time argument, we get the result

$$\tilde{P}(\lambda, t) \underset{t \gg t_0}{\sim} \exp \left\{ (t - t_0) \sum_{m \neq 0} \left(\mathrm{e}^{\lambda q_m} - 1 \right) \Gamma_m + \lambda q_{l_0} \right\}. \tag{5.14}$$

Having this expression, it is very easy to obtain the expectation value of the position operator by using Eq. (5.8). One gets the expression

$$\langle \hat{q}(t) \rangle \underset{t \gg t_0}{\sim} (t - t_0) \sum_{m \neq 0} q_m \Gamma_m + q_{l_0}, \tag{5.15}$$

in which one reads the stationary velocity

$$v^\infty = \sum_{m \neq 0} q_m \Gamma_m. \tag{5.16}$$

The mobility is obtained by dividing by the driving amplitude, $\mu(F) = v^\infty(F)/F$.
    Likewise, one easily obtains the fluctuations of the position operator

$$\langle \Delta \hat{q}^2(t) \rangle \hat{=} \langle \hat{q}^2(t) \rangle - \langle \hat{q}(t) \rangle^2 \underset{t \gg t_0}{\sim} (t - t_0) \sum_{m \neq 0} q_m^2 \Gamma_m. \tag{5.17}$$

This shows a diffusive behavior $\langle \Delta \hat{q}^2(t) \rangle \sim 2D(t - t_0)$ with the diffusion coefficient

$$D = \frac{1}{2} \sum_{m \neq 0} q_m^2 \Gamma_m. \tag{5.18}$$

    Using the position $q_m = mL$ of the tight-binding sites, one see that the stationary velocity

$$v^\infty = L \sum_{m=1}^\infty m \Gamma_{|m|}^d \tag{5.19}$$

depends on the differences of rates $\Gamma^d_{|m|} \,\hat{=}\, \Gamma_m - \Gamma_{-m}$ only, whereas the diffusion coefficient

$$D = \frac{L}{2} \sum_{m=1}^{\infty} m^2 \Gamma^s_{|m|} \tag{5.20}$$

involves the sums $\Gamma^s_{|m|} \,\hat{=}\, \Gamma_m + \Gamma_{-m}$.

5.3 Transition rates

In the following sections, we will take advantage of the simple expressions assumed by the transition rates in the case of the single-band tight-binding Hamiltonian (5.1). We will summarize some general properties of these rates in Section 5.3.1, and give explicit expressions up to third order in tunneling in Section 5.3.2. For clarity, we will postpone the details of the formalism as well as the proofs to Section 5.4.

The expression for each transition rate Γ_m, obtained by means of the real-time path integral techniques exposed in Chapter 5, is the sum of several contributions, which can be characterized by pairs of tight-binding paths. The rates can be classified with respect to the number N of transitions happening in the pairs of tight-binding paths which they involve. This classification defines the Nth-order rates $\Gamma^{(N)}_m$. Each contribution to the rates involves at least two transitions. One has accordingly

$$\Gamma_m = \sum_{N=2}^{\infty} \Gamma^{(N)}_m. \tag{5.21}$$

In Section 3.3, we have introduced two equivalent parameterizations for the contributions to the transition rates. In the first parameterization, one distinguishes between the n transitions happening in the forward tight-binding path and the n' transitions happening in the backward path. This classification defines the rates $\Gamma^{(n,n')}_m$. From their expressions, the Nth-order rates can be recovered by summing all contributions involving $n + n' = N$ transitions

$$\Gamma^{(N)}_m = \sum_{n,n'=0}^{\infty} \delta_{n+n',N} \Gamma^{(n,n')}_m. \tag{5.22}$$

The transitions may be characterized by charges σ_j, respectively $\sigma'_{j'}$, which define a configuration

$$\alpha^{(n,n')}_m \,\hat{=}\, \{\sigma_1, \ldots, \sigma_n; \sigma'_1, \ldots, \sigma'_{n'}\}. \tag{5.23}$$

The corresponding contribution to the rate $\Gamma^{(n,n')}_m$ defines the partial rate $\gamma^{(n,n')}_m \left[\alpha^{(n,n')}_m \right]$. Summing over all possible configurations, one gets

$$\Gamma^{(n,n')}_m = \sum_{\left\{\alpha^{(n,n')}_m\right\}} \gamma^{(n,n')}_m \left[\alpha^{(n,n')}_m \right]. \tag{5.24}$$

In the second parameterization introduced in Section 3.3, the transitions in the forward and backward paths are treated at the same level, and characterized by pairs of charges ζ_j and κ_j. Each configuration

$$\beta_m^{(N)} \doteq \{\zeta_1, \kappa_1; \ldots; \zeta_N, \kappa_N\} \tag{5.25}$$

defines a contribution which is the partial rate $\gamma_m^{(N)}\left[\beta_m^{(N)}\right]$. The sum of all possible configurations yields

$$\Gamma_m^{(N)} = \sum_{\left\{\beta_m^{(N)}\right\}} \gamma_m^{(N)}\left[\beta_m^{(N)}\right]. \tag{5.26}$$

We refer to Section 5.4.1 for the details.

5.3.1   General properties of the rates

In this section, we will summarize some general properties of the transition rates which can be derived by taking advantage of the expressions assumed in the case of the single-band tight-binding Hamiltonian (5.1).

First, the transition rates are real-valued quantities

$$\Gamma_m^* = \Gamma_m. \tag{5.27}$$

This property applies to the Nth-order rates $\Gamma_m^{(N)}$ as well.

Moreover, the transition rates sum up to zero

$$\sum_{m=-\infty}^{\infty} \Gamma_m = 0. \tag{5.28}$$

This property ensures conservation of the total particle density in the system. It applies individually at each order N also.

These two properties are not specific to the particular form of the Hamiltonian (5.1). Their demonstration, presented in Section 5.4.2, respectively Section 5.4.3, can be extended to the general tight-binding system (3.1) investigated in Chapter 3.

Another property which is expected to hold in general is the parity invariance. If one reverts the direction of the position axis, one still expects to find the same physical results. This can be explicitly checked in the expressions derived in this chapter. In the Hamiltonian (5.1), reverting the position axis amounts to taking the complex conjugate of the couplings, which yields $\varphi_l \leftrightarrow -\varphi_l$, and changing the sign of the driving force, $F \leftrightarrow -F$. Furthermore, one has to compare the rate $\Gamma_{-m}(-F, \{-\varphi_l\})$ of the new system with the rate $\Gamma_m(F, \{\varphi_l\})$ obtained before the transformation. Following the procedure exposed in Section 5.4.4, one finds, as expected,

$$\Gamma_{-m}(-F, \{-\varphi_l\}) = \Gamma_m(F, \{\varphi_l\}). \tag{5.29}$$

In the case where the phases of the couplings all vanish, i.e., when all couplings are real-valued, the tight-binding Hamiltonian (5.1) is spatially symmetric in the absence of the driving force. More generally, any tight-binding Hamiltonian in which the couplings satisfy the conditions

$$|\Delta_m| \sin(\varphi_m - m\varphi_1) = 0, \qquad \forall m > 1, \tag{5.30}$$

can be brought to this situation by a phase shift of the wave-functions of the tight-binding states, and it thus corresponds to a spatially symmetric system. One notices that it is always the case for a system with nearest neighbors couplings only. When the phases vanish, Eq. (5.29) may be written as

$$\Gamma_m(-F) = \Gamma_{-m}(F), \tag{5.31}$$

giving the behavior of the rates under reversal of the driving force. From this result, one sees immediately that the sums of rates $\Gamma_{|m|}^s(F)$, respectively differences $\Gamma_{|m|}^d(F)$, introduced below Eq. (5.19), are symmetric, respectively antisymmetric, functions of the driving. As a consequence, the stationary velocity (5.19) is an antisymmetric function of the driving, meaning that the ratchet velocity (1.4) in a adiabatically rocked ratchet system based on such a Hamiltonian vanishes, as expected for a spatially symmetric system.

The last property that we will explore is detailed balance, satisfied, e.g., by the second-order tunneling rates [2]. It states that the rates $\Gamma_m^{(2)}$ and $\Gamma_{-m}^{(2)}$ are related by a factor $\mathrm{e}^{mFL/k_\mathrm{B}T}$, involving the energy drop mFL accumulated along the distance mL covered in the transition. This property has been proven at all orders for a tight-binding system with nearest neighbors couplings [1]. Following an analogous proof, presented in Section 5.4.5, we find that these relations are modified for the non-nearest-neighbors Hamiltonian (5.1). They depend explicitly on the configuration of charges, through the combination of coupling phases

$$\varphi_\Lambda \left[\alpha_m^{(n,n')} \right] \mathrel{\hat{=}} \sum_{j=1}^{n} \varphi_{\sigma_j} - \sum_{j'=1}^{n'} \varphi_{\sigma'_{j'}}, \tag{5.32}$$

and apply therefore to the partial rates only. They link the partial rates corresponding to pairs of configurations related by the transformation

$$\alpha_m^{(n,n')} \leftrightarrow \tilde{\alpha}_{-m}^{(n,n')} = \{-\sigma_n, \ldots, -\sigma_1; -\sigma'_{n'}, \ldots, -\sigma'_1\}, \tag{5.33}$$

which is a combination of charge conjugation and time reversal. One obtains the relation

$$\gamma_{-m}^{(n,n')} \left[\tilde{\alpha}_{-m}^{(n,n')} \right] = \exp \left\{ -\frac{mFL}{k_\mathrm{B}T} - 2\mathrm{i}\varphi_\Lambda \left[\alpha_m^{(n,n')} \right] \right\} \gamma_m^{(n,n')} \left[\alpha_m^{(n,n')} \right] \tag{5.34}$$

between these partial rates.

When all coupling phases are zero, however, the dependence on the configuration disappears and it becomes possible to extend this relation to the total rates Γ_m. In this case, one recovers the usual detailed balance relations

$$\Gamma_{-m} = \mathrm{e}^{-mFL/k_{\mathrm{B}}T}\Gamma_m. \tag{5.35}$$

This applies to any spatially symmetric system characterized by the conditions (5.30).

5.3.2   Explicit expressions up to third order in tunneling

In this section, we will give the explicit expression of some of the transition rates in the dissipative tight-binding model characterized by the system Hamiltonian (5.1). The derivation of these expressions is detailed in Section 5.4.6.

The contributions to the second-order transition rates $\Gamma_m^{(2)}$, for any $m \neq 0$, can be described by the single expression

$$\Gamma_m^{(2)} = \frac{|\Delta_m|^2}{\hbar^2} \int_{-\infty}^{\infty} \mathrm{d}\tau \mathrm{e}^{-m^2(L^2/\hbar)Q(\tau)+\mathrm{i}m(FL/\hbar)\tau}. \tag{5.36}$$

It involves the twice integrated bath correlation function $Q(\tau)$ defined in (B.2). For $m = 0$, one finds the relation

$$\Gamma_0^{(2)} = -\sum_{m\neq 0} \Gamma_m^{(2)}, \tag{5.37}$$

which demonstrates a particular case of the general property (5.28).

For the discussion of the third-order rates $\Gamma_m^{(3)}$, we will restrict ourselves to the case where, in the Hamiltonian (5.1), only the couplings $\Delta_{\pm 1}$, $\Delta_{\pm 2}$, respectively $\Delta_{\pm 3}$, to the first, second, respectively third-order neighbors, are nonzero. In this situation, one finds contributions to the third-order rates for $m = 0, \pm 1, \pm 2, \pm 3$ only, which can be divided into two classes

$$\Gamma_m^{(3)} = \Gamma_m^{(3)}[112] + \Gamma_m^{(3)}[123]. \tag{5.38}$$

The first class groups all contributions which involve two transitions to a nearest neighbor and one to a next-nearest neighbor, in other words twice $\Delta_{\pm 1}$ and once $\Delta_{\pm 2}$. In the expressions for the corresponding rates, the phases of the couplings always come in the combination

$$\varphi_{112} \,\hat{=}\, \varphi_2 - 2\varphi_1. \tag{5.39}$$

For $m = \pm 1, \pm 2$, these rates may be rewritten in a common expression

$$\Gamma_m^{(3)}[112] = \frac{2|\Delta_1|^2|\Delta_2|}{\hbar^3} \operatorname{Im}\left\{ \int_{-\infty}^{\infty} \mathrm{d}\tau G_{|m|}^{(3)}[112](\tau)\mathrm{e}^{\mathrm{i}m\frac{FL}{\hbar}\tau-\mathrm{i}\operatorname{sgn}(m)\varphi_{112}} \right\}, \tag{5.40}$$

with the functions

$$
G_1^{(3)}[112](\tau) = -\int_0^\infty d\rho\, e^{-\frac{2L^2}{\hbar}Q(-\rho)}
$$
$$
\times \left[e^{\frac{L^2}{\hbar}[-2Q(\tau+\rho)+Q(\tau+2\rho)]} + e^{\frac{L^2}{\hbar}[-2Q(\tau-\rho)+Q(\tau-2\rho)]} \right] \quad (5.41a)
$$
$$
G_2^{(3)}[112](\tau) = \int_0^\infty d\rho\, e^{\frac{L^2}{\hbar}[Q(\rho)-2Q(\tau+\frac{1}{2}\rho)-2Q(\tau-\frac{1}{2}\rho)]}. \quad (5.41b)
$$

The rate $\Gamma_0^{(3)}[112]$ is here again obtained by the relation

$$
\Gamma_0^{(3)}[112] = -\sum_{m\neq 0} \Gamma_m^{(3)}[112]. \quad (5.42)
$$

The contributions to the second class involve one transition of each of the three kinds, that is $\Delta_{\pm 1}$, $\Delta_{\pm 2}$, and $\Delta_{\pm 3}$. Here also, the phases of the couplings always come in the combination

$$
\varphi_{123} \hat{=} \varphi_3 - \varphi_2 - \varphi_1 = (\varphi_3 - 3\varphi_1) - (\varphi_2 - 2\varphi_1). \quad (5.43)
$$

For these rates, we find for $m = \pm 1, \pm 2, \pm 3$ the expression

$$
\Gamma_m^{(3)}[123] = \frac{2\,|\Delta_1|\,|\Delta_2|\,|\Delta_3|}{\hbar^3} \mathrm{Im}\left\{ \int_{-\infty}^\infty d\tau\, G_{|m|}^{(3)}[123](\tau) e^{im\frac{FL}{\hbar}\tau - i\,\mathrm{sgn}(m)\varphi_{123}} \right\}, \quad (5.44)
$$

with the functions

$$
G_1^{(3)}[123](\tau) = -\int_0^\infty d\rho\, e^{-\frac{6L^2}{\hbar}Q(-\rho)}
$$
$$
\times \left[e^{\frac{L^2}{\hbar}[-3Q(\tau+2\rho)+2Q(\tau+3\rho)]} + e^{\frac{L^2}{\hbar}[-3Q(\tau-2\rho)+2Q(\tau-3\rho)]} \right] \quad (5.45a)
$$
$$
G_2^{(3)}[123](\tau) = -\int_0^\infty d\rho\, e^{-\frac{3L^2}{\hbar}Q(-\rho)}
$$
$$
\times \left[e^{\frac{L^2}{\hbar}[-6Q(\tau+\frac{1}{2}\rho)+2Q(\tau+\frac{3}{2}\rho)]} + e^{\frac{L^2}{\hbar}[-6Q(\tau-\frac{1}{2}\rho)+2Q(\tau-\frac{3}{2}\rho)]} \right] \quad (5.45b)
$$
$$
G_3^{(3)}[123](\tau) = \int_0^\infty d\rho\, e^{\frac{2L^2}{\hbar}Q(\rho)}
$$
$$
\times \left[e^{\frac{L^2}{\hbar}[-6Q(\tau-\frac{1}{3}\rho)-3Q(\tau+\frac{2}{3}\rho)]} + e^{\frac{L^2}{\hbar}[-6Q(\tau+\frac{1}{3}\rho)-3Q(\tau-\frac{2}{3}\rho)]} \right]. \quad (5.45c)
$$

For $m = 0$, one has also

$$
\Gamma_0^{(3)}[123] = -\sum_{m\neq 0} \Gamma_m^{(3)}[123]. \quad (5.46)
$$

A very interesting feature of theses expressions is their explicit and simple dependence on the moduli and phases of the couplings Δ_m. In particular, this dependence has direct consequences for the ratchet current (1.4), extracted from the stationary velocity (5.19). One verifies that the second-order rates do not depend on the phases φ_m and satisfy $\Gamma_m^{(2)}(-F) = \Gamma_{-m}^{(2)}(F)$, therefore they do not contribute to the ratchet current. Likewise, one can see that the third-order contributions to the ratchet current, which are the dominant ones, are proportional to $\sin(\varphi_2 - 2\varphi_1)$ or $\sin(\varphi_3 - \varphi_2 - \varphi_1)$ [see Eqs. (6.45) and (6.46)]. Therefore, they vanish for spatially symmetric systems, characterized by the conditions (5.30).

The procedure that one has to follow in order to generalize these expressions in the presence of higher-range couplings Δ_m, $|m| > 3$, as well as to higher order $N > 3$ in tunneling, is discussed in Section 5.4.6. If we would allow the couplings $\Delta_{\pm 4}$ to be nonzero, for example, we would get additional third-order contributions involving $\Delta_{\pm 4}$ with $\Delta_{\pm 3}$ and $\Delta_{\pm 1}$, as well as contributions involving $\Delta_{\pm 4}$ and twice $\Delta_{\pm 2}$.

5.4   Proofs

5.4.1   Formalism

In this section, we will apply the mathematical expressions of the rates that we have derived in the general case in Chapter 3 to the particular system investigated in the present chapter. We recall that we have used two equivalent parameterizations to account for the numerous contributions to the rates, the σ-σ' description and the ζ-κ description, introduced in Section 3.3.

The σ-σ' description is based on the charges σ_j and $\sigma'_{j'}$, representing the jumps in the tight-binding paths (3.22). Any pair of tight-binding paths connecting the site l to the site $l + m$, whose charges satisfy the constraints

$$L \sum_{j=1}^{n} \sigma_j = L \sum_{j'=1}^{n'} \sigma'_{j'} = q_{l+m} - q_l, \tag{5.47}$$

corresponds to a contribution to the rate Γ_m.

The first simplification brought by the system (5.1) comes from the position of the sites, which takes the simple form $q_l = lL$. For this reason, the charges σ_j and $\sigma'_{j'}$ take values among nonzero integers only. Likewise, the constraints become simply

$$\sum_{j=1}^{n} \sigma_j = \sum_{j'=1}^{n'} \sigma'_{j'} = m. \tag{5.48}$$

This shows that the parameterization of the paths contributing to the rate Γ_m is independent of the position of the initial site l. Instead of the notation $\alpha_{l+m,l+m,l,l}^{(n,n')}$

used in Chapter 3, we will thus prefer

$$\alpha_m^{(n,n')} \triangleq \{\sigma_1, \ldots, \sigma_n; \sigma_1', \ldots, \sigma_{n'}'\} \tag{5.49}$$

to parameterize a pair of paths, with n transitions in the forward path, n' transitions in the backward path, and such boundary conditions.

Following the derivation of Eq. (3.66), one sees that the corresponding contributions to the transition rates may be written as

$$\Gamma_m^{(n,n')}$$
$$= \int_{-\infty}^{\infty} \mathrm{d}\tau \prod_{j=1}^{n-1} \left(\int_0^{\infty} \mathrm{d}\rho_j \right) \prod_{j'=1}^{n'-1} \left(\int_0^{\infty} \mathrm{d}\rho_{j'}' \right) F_m^{(n,n'),\mathrm{irred}}(t_n, \ldots, t_1; t_{n'}', \ldots, t_1'). \tag{5.50}$$

The integrals involve the time intervals in the forward path $\rho_j \triangleq t_{j+1} - t_j$, the time intervals in the backward path $\rho_{j'}' \triangleq t_{j'+1}' - t_{j'}'$, as well as the relative position of the two sets of times, controlled by $\tau \triangleq \frac{1}{n'} \sum_{j'=1}^{n'} t_{j'}' - \frac{1}{n} \sum_{j=1}^{n} t_j$. The irreducible influence function is obtained from

$$F_m^{(n,n')}(t_n, \ldots, t_1; t_{n'}', \ldots, t_1') = \sum_{\left\{ \alpha_m^{(n,n')} \right\}} f\left[\alpha_m^{(n,n')} \right] (t_n, \ldots, t_1; t_{n'}', \ldots, t_1'), \tag{5.51}$$

by subtracting reducible contributions according to Eq. (3.45). The configuration sum reads explicitly

$$\sum_{\left\{ \alpha_m^{(n,n')} \right\}} = \prod_{j=1}^{n-1} \left(\sum_{\sigma_j \neq 0} \right) \prod_{j'=1}^{n'-1} \left(\sum_{\sigma_{j'}' \neq 0} \right) \delta \left(\sum_{j=1}^{n} \sigma_j, m \right) \delta \left(\sum_{j'=1}^{n'} \sigma_{j'}', m \right), \tag{5.52}$$

where the charges run over all nonzero integers and the Kronecker symbols δ ensure that the constraints (5.48) are fulfilled. Bringing this sum in front of the expression (5.50), one may write

$$\Gamma_m^{(n,n')} = \sum_{\left\{ \alpha_m^{(n,n')} \right\}} \gamma_m^{(n,n')} \left[\alpha_m^{(n,n')} \right], \tag{5.53}$$

and identify the partial rate $\gamma_m^{(n,n')} \left[\alpha_m^{(n,n')} \right]$ associated with each contributing pair of paths.

The partial influence function, which has been given in Eq. (3.30), takes a slightly simpler form

$$f\left[\alpha_m^{(n,n')} \right] (t_n, \ldots, t_1; t_{n'}', \ldots, t_1') = \Lambda \exp \left\{ \Phi_{\mathrm{FV}} + \Psi \right\} \tag{5.54}$$

for the system considered in this chapter. Indeed, the on-site energy functional $\Delta\mathcal{E}$ vanishes because all on-site energies are equal in the model (5.1). The prefactor (3.27) may be rewritten explicitly in terms of the charges in this model. Indeed, the charge σ_j associated with a transition in the forward path from the site l to the site $l + m$, is simply the integer m characterizing the jump in position [see Eq. (3.22)]. Thus, the coupling $\Delta[j] = \Delta_m$ associated with this transition may be written as $\Delta[j] = \Delta_{\sigma_j}$. Likewise, the coupling $\Delta'[j'] = \Delta_m^*$ associated with a similar transition in the backward path may be written as $\Delta'[j'] = \Delta_{\sigma'_{j'}}^*$. Correspondingly, the prefactor reads

$$\Lambda = \prod_{j=1}^{n} \left(\frac{-\mathrm{i}\Delta_{\sigma_j}}{\hbar} \right) \prod_{j'=1}^{n'} \left(\frac{\mathrm{i}\Delta_{\sigma'_{j'}}^*}{\hbar} \right). \tag{5.55}$$

The last term of the Feynman-Vernon influence phase Φ_{FV} given in Eq. (3.24) vanishes when the two paths start in the same site, as it is always the case for the contributions to the transition rates. Thus one has

$$\Phi_{\mathrm{FV}} = \frac{L^2}{\hbar} \left[\sum_{k=1}^{n} \sum_{j=1}^{k-1} \sigma_k \sigma_j Q(t_k - t_j) + \sum_{k'=1}^{n'} \sum_{j'=1}^{k'-1} \sigma'_{k'} \sigma'_{j'} Q^*(t'_{k'} - t'_{j'}) \right.$$
$$\left. - \sum_{k'=1}^{n'} \sum_{j=1}^{n} \sigma'_{k'} \sigma_j Q(t'_{k'} - t_j) \right]. \tag{5.56}$$

In the situation of time-independent driving considered here, the driving term (3.25) may be slightly simplified to

$$\Psi = \frac{\mathrm{i}FL}{\hbar} \left[\sum_{j'=1}^{n'} \sigma'_{j'} t'_{j'} - \sum_{j=1}^{n} \sigma_j t_j \right], \tag{5.57}$$

using the constraints (5.48).

The same adaptation work can be done in the ζ-κ description. The charges ζ_j and κ_j on which this equivalent description is based represent the jumps in the difference and average of the two tight-binding paths, as defined in Eq. (3.31). In the system (5.1), they can take any integer value. The boundary conditions of the pairs of paths contributing to the transition rate Γ_m take the form

$$\sum_{j=1}^{N} \zeta_j = 0 \tag{5.58a}$$

$$\sum_{j=1}^{N} \kappa_j = 2m. \tag{5.58b}$$

No formal distinction is made between transitions happening in the forward or backward path. Only the total number $N = n + n'$ of transitions, happening at times s_j, matters in this description. We introduce the notation

$$\beta_m^{(N)} \triangleq \{\zeta_1, \kappa_1; \ldots; \zeta_N, \kappa_N\} \tag{5.59}$$

for the parameterization of the different contributions to the transition rates. Starting from Eq. (3.63), one may write these rates as

$$\Gamma_m^{(N)} = \prod_{j=1}^{N-1} \left(\int_0^\infty d\tau_j \right) F_m^{(N),\text{irred}}(s_n, \ldots, s_1). \tag{5.60}$$

The integrals run over the time intervals $\tau_j = s_{j+1} - s_j$. The irreducible influence function is here again obtained from

$$F_m^{(N)}(s_n, \ldots, s_1) = \sum_{\left\{\beta_m^{(N)}\right\}} f\left[\beta_m^{(N)}\right](s_n, \ldots, s_1), \tag{5.61}$$

by subtracting reducible contributions according to Eq. (3.45). The configuration sum, satisfying the constraints (5.58), now reads

$$\sum_{\left\{\beta_m^{(N)}\right\}} = \prod_{j=1}^{N-1} \left(\sum_{\zeta_j, \kappa_j = -\infty}^{\infty} \right) \delta\left(\sum_{j=1}^{N} \zeta_j, 0 \right) \delta\left(\sum_{j'=1}^{N} \kappa_j, 2m \right). \tag{5.62}$$

As above, bringing this sum in front of the expression (5.60), one can write

$$\Gamma_m^{(N)} = \sum_{\left\{\beta_m^{(N)}\right\}} \gamma_m^{(N)}\left[\beta_m^{(N)}\right], \tag{5.63}$$

and identify the partial rates $\gamma_m^{(N)}\left[\beta_m^{(N)}\right]$ associated with each contributing pair of paths.

The partial influence function (3.39) also takes the simpler form

$$f\left[\beta_m^{(N)}\right](s_n, \ldots, s_1) = \Lambda \exp\{\Phi_{\text{FV}} + \Psi\} \tag{5.64}$$

for the system (5.1). Adapting the discussion done above in the σ-σ' description for the expression (3.36), we can rewrite the prefactor as

$$\Lambda = \prod_{j=1}^{N} \left(\frac{-\operatorname{sgn}(\zeta_j \kappa_j) i \Delta_{\zeta_j}}{\hbar} \right), \tag{5.65}$$

remembering that $\Delta_m^* = \Delta_{-m}$. The phases of the couplings combine in the expression

$$\varphi_\Lambda\left[\beta_m^{(N)}\right] \triangleq \sum_{j=1}^{N} \varphi_{\zeta_j}, \tag{5.66}$$

which acts as a phase factor $\mathrm{e}^{\mathrm{i}\varphi_\Lambda}$ on the prefactor Λ. Comparing this expression with the constraint (5.58a), one sees that φ_Λ always vanishes for configurations involving two transitions $N = 2$ only. At higher orders, only combinations like $\varphi_2 - 2\varphi_1$, $\varphi_3 - 3\varphi_1, \ldots$, and linear combinations thereof, appear. Combining with the property that the transition rates are real-valued, which we will demonstrate in Section 5.4.2, we see that the rates depend on the coupling phases φ_l through trigonometric functions of these arguments only.

From the expressions (3.33) and (3.34), we obtain along the same lines as above the influence phase as

$$\Phi_{\mathrm{FV}} = \frac{L^2}{\hbar} \sum_{k=2}^{N} \sum_{j=1}^{k-1} \left[\zeta_k \zeta_j Q_{\mathrm{R}}(s_k - s_j) + \mathrm{i}\zeta_k \kappa_j Q_{\mathrm{I}}(s_k - s_j)\right], \tag{5.67}$$

and the driving term as

$$\Psi = -\frac{\mathrm{i}FL}{\hbar} \sum_{j'=1}^{N} \zeta_j s_j. \tag{5.68}$$

Finally, we recall that to one partial rate $\gamma_m^{(n,n')}\left[\alpha_m^{(n,n')}\right]$ in the σ-σ' description, there correspond $N!/n!n'!$ partial rates $\gamma_m^{(N)}\left[\beta_m^{(N)}\right]$ with $N = n + n'$ in the ζ-κ description.

This reminder of the formalism allows us now to prove the properties of the transition rates that we have summarized in Section 5.3.1.

5.4.2 Complex conjugation

Let us consider a given configuration $\alpha_m^{(n,n')}$ in the σ-σ' description and exchange the charges σ_j of the forward path with the charges $\sigma'_{j'}$ of the backward path. This transformation yields another configuration, presenting n' transitions in the forward path and n transitions in the backward path, which contributes to the same rate Γ_m, as can be seen from Eq. (5.48). Accordingly, this new configuration can be denoted $\alpha_m^{*(n',n)}$. Under this transformation

$$\alpha_m^{(n,n')} \leftrightarrow \alpha_m^{*(n',n)} = \{\sigma'_1, \ldots, \sigma'_{n'}; \sigma_1, \ldots, \sigma_n\}, \tag{5.69}$$

the prefactor (5.55) gets complex conjugated, $\Lambda \leftrightarrow \Lambda^*$. One can combine the transformation with an exchange of the transition times t_j and $t'_{j'}$ which enter the integration variables in the expression for the rates (5.50). Then, using the property $Q(-\tau) = Q^*(\tau)$ of the bath correlation function [see Eq. (B.2)], one can show

that the influence phase (5.56) also gets complex conjugated $\Phi_{\mathrm{FV}} \leftrightarrow \Phi_{\mathrm{FV}}^*$. The same happens to the driving term (5.57), $\Psi \leftrightarrow \Psi^*$, so that the partial influence function obeys

$$f\left[\alpha_m^{*(n',n)}\right](t_{n'},\ldots,t_1';t_n,\ldots,t_1) = \left(f\left[\alpha_m^{(n,n')}\right](t_n,\ldots,t_1;t_{n'},\ldots,t_1')\right)^*. \quad (5.70)$$

One can convince oneself that this property is not touched by the subtraction of reducible contributions according to Eq. (3.45). Therefore, the partial rates associated with these two configurations are also the complex conjugates of each other

$$\gamma_m^{(n',n)}\left[\alpha_m^{*(n',n)}\right] = \left(\gamma_m^{(n,n')}\left[\alpha_m^{(n,n')}\right]\right)^*. \quad (5.71)$$

To each configuration $\alpha_m^{(n,n')}$, there corresponds exactly one configuration $\alpha_m^{*(n',n)}$. In the sum (5.24), these configurations can be combined two by two, proving that $\Gamma_m^{(n,n')}$ is a real-valued quantity. Using the expressions (5.22) and (5.21), one sees that the Nth-order rate $\Gamma_m^{(N)}$ as well as the total rate Γ_m inherit this property. This demonstrates (5.27).

This property can be proven in the ζ-κ description, alternatively. There, the transformation corresponds to change the sign of the charges of the difference path, $\zeta_j \leftrightarrow -\zeta_j$. The constraints (5.58) are left unchanged by this transformation, thus

$$\beta_m^{(N)} \leftrightarrow \beta_m^{*(N)} = \{-\zeta_1, \kappa_1; \ldots; -\zeta_N, \kappa_N\}. \quad (5.72)$$

Looking at the expressions (5.65), (5.67), and (5.68), one can prove in the same way as above that the partial rates obey the relation

$$\gamma_m^{(N)}\left[\beta_m^{*(N)}\right] = \left(\gamma_m^{(N)}\left[\beta_m^{(N)}\right]\right)^*. \quad (5.73)$$

These properties, implying that the transition rates are real-valued, are not specific to the model (5.1). One can convince oneself that they hold true in the general case investigated in Chapter 3, where the tight-binding system has a more complicated structure, the nonequal on-site energies must be taken into account in the functional $\Delta\mathcal{E}$, and the driving force is time-dependent.

5.4.3   Compensation

Let us start from a configuration $\beta_m^{(N)}$ in the ζ-κ description, and revert the sign of the last charge of the average path, $\kappa_N \leftrightarrow -\kappa_N$. Looking at the constraints (5.58), one sees that this new configuration contributes to a different rate $\Gamma_{\bar{m}}$, with $\bar{m} \hat{=} m - 2\kappa_N$. We denote thus by $\bar{\beta}_{\bar{m}}^{(N)}$ the configuration obtained by this transformation,

$$\beta_m^{(N)} \leftrightarrow \bar{\beta}_{\bar{m}}^{(N)} = \{\zeta_1, \kappa_1; \ldots; \zeta_{N-1}, \kappa_{N-1}; \zeta_N, -\kappa_N\}. \quad (5.74)$$

The prefactor (5.65) simply changes its sign, $\Lambda \leftrightarrow -\Lambda$, under this transformation. The influence phase (5.67) and driving term (5.68) are left unchanged, as they do not depend on κ_N. Thus, the partial influence function obeys the relation

$$f\left[\beta_m^{(N)}\right](s_n,\ldots,s_1) = -f\left[\bar{\beta}_{\tilde{m}}^{(N)}\right](s_n,\ldots,s_1). \tag{5.75}$$

Here again, this relation is not touched by the subtraction of reducible contributions, and it can be extended to the partial rates

$$\gamma_{\tilde{m}}^{(N)}\left[\bar{\beta}_{\tilde{m}}^{(N)}\right] = -\gamma_m^{(N)}\left[\beta_m^{(N)}\right]. \tag{5.76}$$

For each configuration $\beta_m^{(N)}$, there is exactly one configuration $\bar{\beta}_{\tilde{m}}^{(N)}$, contributing to a different rate. Thus, when one sums up all transitions rates, these contributions cancel two by two, which demonstrates the property (5.28).

It would be more difficult to prove this property in the σ-σ' description, because the partial rates $\gamma_m^{(n,n')}\left[\alpha_m^{(n,n')}\right]$ do not cancel two by two. The reason for that is that the last charge in the configuration is alternatively the last charge σ_n of the forward path or the last charge $\sigma'_{n'}$ of the backward path, depending on the chronological order of the corresponding times t_n and $t'_{n'}$ in the integrals involved in (5.50). If these charges are different, $\sigma_n \neq \sigma'_{n'}$, the contributions to the partial rate coming from the different pieces of the integration domain (see also Fig. 3.1) compensate with pieces belonging to different transition rates.

On the basis of this demonstration, one can also convince oneself that this property holds true in the general case investigated in Chapter 3.

5.4.4   Parity

In order to demonstrate the parity invariance of the rates, one has to compare the rate $\Gamma_{-m}(-F, \{-\varphi_l\})$ of a new system, in which the couplings have been complex conjugated and the sign of the driving force F has been reverted, with the rate $\Gamma_m(F, \{\varphi_l\})$ obtained before the transformation. Changing the sign of all charges κ_j together with the parity transformation given by $\varphi_l \leftrightarrow -\varphi_l$ and $F \leftrightarrow -F$, and following the same procedure as in the previous section, one can easily show that these two rates are the complex conjugates of each other. Invoking the reality of the rates implied by (5.27), we obtain the relation (5.29).

5.4.5   Generalized detailed balance relations

The convenient frame for the derivation of the generalized detailed balance relations (5.34) is the σ-σ' description. Let us first write the explicit expressions of the transition times t_j and $t'_{j'}$ in terms of the time intervals $\rho_j = t_{j+1} - t_j$, $\rho'_{j'} = t'_{j'+1} - t'_{j'}$, and $\tau = \bar{t}' - \bar{t}$, where $\bar{t} \,\hat{=}\, \frac{1}{n}\sum_{j=1}^{n} t_j$, respectively $\bar{t}' \,\hat{=}\, \frac{1}{n'}\sum_{j'=1}^{n'} t'_{j'}$,

denote the center of gravity of the transition times in the forward, respectively backward, path. One has

$$t_j = \bar{t} + \sum_{k=1}^{n-1} \frac{k-n}{n} \rho_k + \sum_{k=1}^{j-1} \rho_k \tag{5.77a}$$

$$t'_{j'} = \bar{t}' + \sum_{k'=1}^{n'-1} \frac{k'-n'}{n'} \rho'_{k'} + \sum_{k'=1}^{j'-1} \rho'_{k'}. \tag{5.77b}$$

Substituting in the influence phase (5.56), one gets

$$\Phi_{\mathrm{FV}} = \frac{L^2}{\hbar} \left[\sum_{k=1}^{n} \sum_{j=1}^{k-1} \sigma_k \sigma_j Q \left(\sum_{l=j}^{k-1} \rho_l \right) + \sum_{k'=1}^{n'} \sum_{j'=1}^{k'-1} \sigma'_{k'} \sigma'_{j'} Q^* \left(\sum_{l'=j'}^{k'-1} \rho'_{l'} \right) \right.$$
$$\left. - \sum_{k'=1}^{n'} \sum_{j=1}^{n} \sigma'_{k'} \sigma_j Q \left(\tau + \sum_{l'=1}^{n'-1} \frac{l'-n'}{n'} \rho'_{l'} + \sum_{l'=1}^{k'-1} \rho'_{l'} - \sum_{l=1}^{n-1} \frac{l-n}{n} \rho_l - \sum_{l=1}^{j-1} \rho_l \right) \right]. \tag{5.78}$$

Doing the same for the driving term (5.57) and using the constraints (5.48), one obtains

$$\Psi = \frac{\mathrm{i}FL}{\hbar} \left[m\tau + m \sum_{k'=1}^{n'-1} \frac{k'-n'}{n'} \rho'_{k'} + \sum_{j'=1}^{n'} \sigma'_{j'} \sum_{k'=1}^{j'-1} \rho'_{k'} \right.$$
$$\left. - m \sum_{k=1}^{n-1} \frac{k-n}{n} \rho_k - \sum_{j=1}^{n} \sigma_j \sum_{k=1}^{j-1} \rho_k \right]. \tag{5.79}$$

Let us now consider the transformation obtained by reversing the sign and the order of the charges, given by $\sigma_j \leftrightarrow -\sigma_{n-j}$ and $\sigma'_{j'} \leftrightarrow -\sigma'_{n'-j'}$. Looking at the constraints (5.48), one sees that this transformation induces $m \leftrightarrow -m$, as desired. The inversion of the order of the charges is associated with a time reversal in the integrals in (5.50). This time reversal may be written as $t_j \leftrightarrow t + t_0 - t_{n-j+1}$ and $t'_{j'} \leftrightarrow t + t_0 - t'_{n'-j'+1}$, with respect to the reversal time $t + t_0$, so that all times remain in the interval $[t_0, t]$. It induces the transformations $\rho_j \leftrightarrow \rho_{n-j}$, $\rho'_{j'} \leftrightarrow \rho'_{n'-j'}$, and $\tau \leftrightarrow -\tau$ of the time intervals. We denote by $\tilde{\alpha}_{-m}^{(n,n')}$ the configuration obtained from $\alpha_m^{(n,n')}$ by applying this combination of charge conjugation and time reversal,

$$\alpha_m^{(n,n')} \leftrightarrow \tilde{\alpha}_{-m}^{(n,n')} = \{-\sigma_n, \ldots, -\sigma_1; -\sigma'_{n'}, \ldots, -\sigma'_1\}. \tag{5.80}$$

Under this transformation, the combination of coupling phases

$$\varphi_\Lambda \left[\alpha_m^{(n,n')} \right] \hat{=} \sum_{j=1}^{n} \varphi_{\sigma_j} - \sum_{j'=1}^{n'} \varphi_{\sigma'_{j'}}, \tag{5.81}$$

which enters the phase of the prefactor (5.55), gets its sign inverted. This can be compensated by a phase factor, yielding

$$\Lambda \leftrightarrow \exp\left\{-2\mathrm{i}\varphi_\Lambda\left[\tilde{\alpha}_{-m}^{(n,n')}\right]\right\}\Lambda. \tag{5.82}$$

With some algebra, one can show that the two first terms of the influence phase (5.78) are left unchanged, whereas in the third one the sign of the argument of the bath correlation function $Q(\tilde{\tau})$ is reverted. This can be re-established by using the property $Q(-\tilde{\tau}) = Q(\tilde{\tau} - \mathrm{i}\hbar/k_\mathrm{B}T)$ obeyed by this function [see Eq. (B.2)]. One can attribute the shift along the imaginary axis in the argument to the time interval τ and write

$$\Phi_\mathrm{FV}(\tau) \leftrightarrow \Phi_\mathrm{FV}(\tau - \mathrm{i}\hbar/k_\mathrm{B}T). \tag{5.83}$$

The driving term (5.79) is left unchanged by the transformation. However, the shift of τ necessary for the influence phase may be performed in this term as well, yielding simply

$$\Psi(\tau) \leftrightarrow \Psi(\tau - \mathrm{i}\hbar/k_\mathrm{B}T) + \frac{mFL}{k_\mathrm{B}T}. \tag{5.84}$$

To get the sign correctly on the right-hand-side, one recalls that the first term of the driving term for the configuration $\tilde{\alpha}_{-m}^{(n,n')}$ is $-\mathrm{i}m\tau FL/\hbar$.

   Altogether, we get the relation

$$
\begin{aligned}
f&\left[\alpha_m^{(n,n')}\right](\tau,\{\rho_j\},\{\rho'_{j'}\}) \\
&= \exp\left\{\frac{mFL}{k_\mathrm{B}T} - 2\mathrm{i}\varphi_\Lambda\left[\tilde{\alpha}_{-m}^{(n,n')}\right]\right\} f\left[\tilde{\alpha}_{-m}^{(n,n')}\right](\tau - \mathrm{i}\hbar/k_\mathrm{B}T,\{\rho_j\},\{\rho'_{j'}\})
\end{aligned} \tag{5.85}
$$

between the partial influence functions of the two configurations. Due to the structure of the prefactor, using the properties of the exponential function, and viewing the shift of τ as a corresponding shift of all transition times happening in the backward path, one can convince oneself that the subtraction of irreducible contributions given in Eq. (3.45) does not change this relation. It can thus be used for the partial rates

$$
\begin{aligned}
\gamma_m^{(n,n')}&\left[\alpha_m^{(n,n')}\right] \\
&= \int_{-\infty}^{\infty} \mathrm{d}\tau \prod_{j=1}^{n-1}\left(\int_0^\infty \mathrm{d}\rho_j\right)\prod_{j'=1}^{n'-1}\left(\int_0^\infty \mathrm{d}\rho'_{j'}\right) f^\mathrm{irred}\left[\alpha_m^{(n,n')}\right](\tau,\{\rho_j\},\{\rho'_{j'}\}),
\end{aligned} \tag{5.86}
$$

extracted from Eq. (5.50). To complete the proof, one has to use further properties of the bath correlation function $Q(z)$ with complex-valued argument z. One can show that this function is analytic in the stripe $0 \geq \mathrm{Im}\, z \geq -\hbar/k_\mathrm{B}T$. Furthermore, at the left and right limits of this domain, $\mathrm{Re}\, z \to \pm\infty$, its real part tends to $+\infty$

and its imaginary part to zero. Substituting τ by z in the expression for the influence phase (5.78), one can show along the same line and with the help of the constraints (5.48) that the third term always ensures an exponential suppression of the partial influence function in this limit $\operatorname{Re} z \to \pm\infty$. Combining these results with Cauchy's theorem applied to a path bordering the stripe $0 \geq \operatorname{Im} z \geq -\hbar/k_{\mathrm{B}}T$, one can demonstrate the relation

$$
\int_{-\infty}^{\infty} \mathrm{d}\tau\, f^{\mathrm{irred}} \left[\alpha_m^{(n,n')} \right] (\tau, \{\rho_j\}, \{\rho_{j'}'\})
$$
$$
= \int_{-\infty}^{\infty} \mathrm{d}\tau\, f^{\mathrm{irred}} \left[\alpha_m^{(n,n')} \right] (\tau - \mathrm{i}\hbar/k_{\mathrm{B}}T, \{\rho_j\}, \{\rho_{j'}'\}). \quad (5.87)
$$

This allows to extend the relation (5.85) to the partial partial rates (5.86). By moving the exponential factor on the other side of the relation, one completes the demonstration of (5.34).

5.4.6 Derivation of the explicit expressions for the transition rates

In this section, we will give the details of the derivation of the explicit expressions for the transition rates which have been summarized in Section 5.3.2. We will work on the basis of Eq. (5.50).

One encounters two difficulties in order to obtain a compact expression for the total rates Γ_m. The first problem is to perform the configuration sum (5.52), which implies to find all configurations of pairs of tight-binding paths involving n, respectively n', transitions, and satisfying the constraints (5.48). A graphical representation can help us in this task. Let us start from a two-dimensional lattice parameterized by pairs of integers (l, l'). Let us represent by an horizontal arrow of length m to the right a transition in the forward tight-binding path to the neighbor of order m to the right. Such a transition is characterized by a charge $\sigma = +m$. A transition to the left neighbor of order m, characterized by a charge $\sigma = -m$, is represented by an arrow of length m to the left. Likewise, we represent transitions happening in the backward path, characterized by a charge $\sigma' = +m$, respectively $\sigma' = -m$, by vertical arrows of length m, pointing downwards, respectively upwards, in our diagram. Together, the arrows corresponding to the transitions happening in the pair of tight-binding paths will draw a path in the diagram. With this representation, it is now easy to find the paths satisfying the constraints (5.48). If one starts from a diagonal site of our diagram, say at position $(0,0)$, the constraints select those paths which end up in the diagonal site (m,m). Some examples are given in Fig. 5.1.

Any contributing configuration involves at least two transitions. Each configuration yields a partial rate $\gamma_m^{(n,n')} \left[\alpha_m^{(n,n')} \right]$. Summing all configurations involving the same number n, respectively n', of transitions in the forward, respectively back-
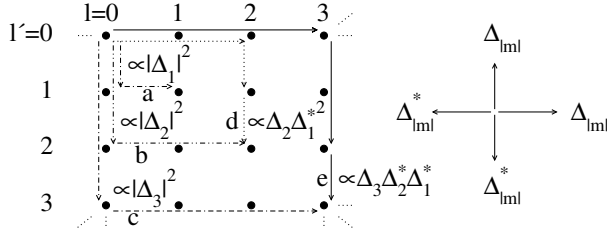
Figure 5.1: Left: Graphical representation of the pairs of tight-binding paths corresponding to some contributions to the second-order (a,b, and c) and third-order (d and e) transition rates, with the corresponding dependence on the couplings Δ_m, obtained from Eq. (5.55). Right: The couplings associated with the transitions in the forward path (horizontal) and backward path (vertical).

ward, path yields $\Gamma_m^{(n,n')}$, according to (5.24). The Nth-order rate is then obtained from (5.22).

The second difficulty is the subtraction of reducible contributions from the partial influence function, according to Eq. (3.45). However, as the kernels involve at least two transitions, the subtraction occurs for transition rates involving at least $N = 4$ transitions. Up to third order, the irreducible partial influence function f^{irred} entering the expression (5.86) equals the function f given in (5.54). In the remaining of this section, we will restrict ourselves to the second and third orders and use this property.

In order to understand the different contributions to the second-order rates $\Gamma_m^{(2)}$, let us first look at those contributions which involve only transitions to the nearest neighbors. In other words, we consider the situation described by the Hamiltonian (5.1) with $\Delta_m = 0$ for $|m| \geq 2$. In this case, the charges σ_j and $\sigma'_{j'}$ may only take the values $+1$ and -1, denoting transitions to the nearest neighbor to the right, respectively to the left. These transitions are mediated by the couplings $\Delta_{\pm 1}$.

All contributing configurations, which can be found with the help of the diagram of Fig. 5.1, are listed in Table 5.1. From there, it is clear that there is only one contribution to $\Gamma_1^{(2)}$, and only one to $\Gamma_{-1}^{(2)}$, which read

$$\Gamma_{\pm 1}^{(2)} = \frac{|\Delta_1|^2}{\hbar^2} \int_{-\infty}^{\infty} d\tau e^{-(L^2/\hbar)Q(\tau) \pm i(FL/\hbar)\tau}. \tag{5.88}$$

From the numerous contributions to $\Gamma_0^{(2)}$, we can explicitly check the relation $\Gamma_0^{(2)} = -\Gamma_1^{(2)} - \Gamma_{-1}^{(2)}$, which we have demonstrated in the general case [see Eq.(5.28)].

Let us now allow all couplings Δ_m in the Hamiltonian (5.1) to be nonzero and ask again the question: Which pairs of tight-binding paths involving two transitions

$\Gamma_m^{(n,n')}$	$\alpha_m^{(n,n')}$	Λ	Φ_{FV}	Ψ	$\beta_m^{(2)}$
		(units of $\frac{1}{\hbar^2}$)	(units of $\frac{L^2}{\hbar}$)	(units of $\frac{iFL}{\hbar}$)	
$\Gamma_1^{(1,1)}$	$\{+1;+1\}$	$|\Delta_1|^2$	$-Q(\tau)$	τ	$\{+1,+1;-1,+1\}$
					$\{-1,+1;+1,+1\}$
$\Gamma_0^{(2,0)}$	$\{+1,-1;\varnothing\}$	$-|\Delta_1|^2$	$-Q(\rho_1)$	ρ_1	$\{+1,+1;-1,-1\}$
	$\{-1,+1;\varnothing\}$	$-|\Delta_1|^2$	$-Q(\rho_1)$	$-\rho_1$	$\{-1,-1;+1,+1\}$
$\Gamma_0^{(0,2)}$	$\{\varnothing;+1,-1\}$	$-|\Delta_1|^2$	$-Q^*(\rho_1')$	$-\rho_1'$	$\{-1,+1;+1,-1\}$
	$\{\varnothing;-1,+1\}$	$-|\Delta_1|^2$	$-Q^*(\rho_1')$	ρ_1'	$\{+1,-1;-1,+1\}$
$\Gamma_{-1}^{(1,1)}$	$\{-1;-1\}$	$|\Delta_1|^2$	$-Q(\tau)$	$-\tau$	$\{-1,-1;+1,-1\}$
					$\{+1,-1;-1,-1\}$

Table 5.1: The different contributions to the rates $\Gamma_m^{(n,n')}$, obtained from (5.50), at second order $n + n' = 2$, when only transitions to the nearest neighbors, characterized by charges $\sigma_j, \sigma_{j'}' = \pm 1$, and mediated by the couplings $\Delta_{\pm 1}$, are allowed. In this situation, one obtains contributions for $m = 0, \pm 1$ only. Each contribution is specified by the configuration $\alpha_m^{(n,n')}$ of the charges, given in the second column. The next three columns give the explicit expression of the prefactor (5.55), the influence phase (5.78), and the driving term (5.79) for the corresponding contribution. The last column lists the different configurations $\beta_m^{(2)}$ in the ζ-κ description which correspond to one given contribution $\alpha_m^{(n,n')}$ in the σ-σ' description. One verifies that there are always $2!/n!n'!$ of them.

contribute to the transition rates? In the graphical representation shown in Fig. 5.1 and described above, those paths are represented by a succession of two arrows connecting the initial diagonal site $(0,0)$ with any final diagonal site (m,m). In this figure, the paths (a), (b) and (c) are examples of such configurations. It is clear that, if the first transition in any of the two tight-binding paths reaches a neighbor at distance m, the second transition must also happen between sites at the same distance m, in order to end up back in the diagonal. At second order, there will thus be no contributions to the rates combining two different couplings Δ_m and $\Delta_{m'}$. One can convince oneself that all 6 possible combinations for a given $|m|$ are similar to the ones listed in Table 5.1, with ± 1 replaced by $\pm m$ in $\alpha_m^{(n,n')}$ and $\beta_m^{(2)}$. They are proportional to $|\Delta_m|^2$ and give contributions to $\Gamma_{\pm m}^{(2)}$ and $\Gamma_0^{(2)}$. One easily sees that the general expression for the influence phase (5.78) is $\Phi_{\mathrm{FV}} = -m^2 (L^2/\hbar) Q(\tau)$, and for the driving term (5.79), $\Psi = \pm im(FL/\hbar)\tau$. Thus, the contributions to the second-order transition rates $\Gamma_m^{(2)}$, can be described by the expressions (5.36) and (5.37).

We will now investigate some contributions to the third-order rates $\Gamma_m^{(3)}$. Let us first restrict ourselves to the case where, in the Hamiltonian (5.1), only the couplings

$\Gamma_m^{(n,n')}$	$\alpha_m^{(n,n')}$	Λ	Φ_{FV} (units of $\frac{L^2}{\hbar}$)	Ψ (units of $\frac{iFL}{\hbar}$)
$\Gamma_2^{(2,1)}$	$\{+1,+1;+2\}$	λ_{112}	$Q(\rho_1) - 2Q(\tau+\frac{1}{2}\rho_1) - 2Q(\tau-\frac{1}{2}\rho_1)$	2τ
$\Gamma_2^{(1,2)}$	$\{+2;+1,+1\}$	λ_{112}^*	$Q^*(\rho_1') - 2Q(\tau+\frac{1}{2}\rho_1') - 2Q(\tau-\frac{1}{2}\rho_1')$	2τ
$\Gamma_1^{(2,1)}$	$\{-1,+2;+1\}$	$-\lambda_{112}^*$	$-2Q(\rho_1) + Q(\tau+\frac{1}{2}\rho_1) - 2Q(\tau-\frac{1}{2}\rho_1)$	$\tau - \frac{3}{2}\rho_1$
	$\{+2,-1;+1\}$	$-\lambda_{112}^*$	$-2Q(\rho_1) - 2Q(\tau+\frac{1}{2}\rho_1) + Q(\tau-\frac{1}{2}\rho_1)$	$\tau + \frac{3}{2}\rho_1$
$\Gamma_1^{(1,2)}$	$\{+1;-1,+2\}$	$-\lambda_{112}$	$-2Q^*(\rho_1') - 2Q(\tau+\frac{1}{2}\rho_1') + Q(\tau-\frac{1}{2}\rho_1')$	$\tau + \frac{3}{2}\rho_1'$
	$\{+1;+2,-1\}$	$-\lambda_{112}$	$-2Q^*(\rho_1') + Q(\tau+\frac{1}{2}\rho_1') - 2Q(\tau-\frac{1}{2}\rho_1')$	$\tau - \frac{3}{2}\rho_1'$
$\Gamma_0^{(3,0)}$	$\{+1,+1,-2;\varnothing\}$	$-\lambda_{112}$	$Q(\rho_1) - 2Q(\rho_1+\rho_2) - 2Q(\rho_2)$	$\rho_1 + 2\rho_2$
	$\{+1,-2,+1;\varnothing\}$	$-\lambda_{112}$	$-2Q(\rho_1) + Q(\rho_1+\rho_2) - 2Q(\rho_2)$	$\rho_1 - \rho_2$
	$\{-2,+1,+1;\varnothing\}$	$-\lambda_{112}$	$-2Q(\rho_1) - 2Q(\rho_1+\rho_2) + Q(\rho_2)$	$-2\rho_1 - \rho_2$
	$\{-1,-1,+2;\varnothing\}$	λ_{112}^*	$Q(\rho_1) - 2Q(\rho_1+\rho_2) - 2Q(\rho_2)$	$-\rho_1 - 2\rho_2$
	$\{-1,+2,-1;\varnothing\}$	λ_{112}^*	$-2Q(\rho_1) + Q(\rho_1+\rho_2) - 2Q(\rho_2)$	$-\rho_1 + \rho_2$
	$\{+2,-1,-1;\varnothing\}$	λ_{112}^*	$-2Q(\rho_1) - 2Q(\rho_1+\rho_2) + Q(\rho_2)$	$+2\rho_1 + \rho_2$
$\Gamma_0^{(0,3)}$	$\{\varnothing;+1,+1,-2\}$	$-\lambda_{112}^*$	$Q^*(\rho_1') - 2Q^*(\rho_1'+\rho_2') - 2Q^*(\rho_2')$	$-\rho_1' - 2\rho_2'$
	$\{\varnothing;+1,-2,+1\}$	$-\lambda_{112}^*$	$-2Q^*(\rho_1') + Q^*(\rho_1'+\rho_2') - 2Q^*(\rho_2')$	$-\rho_1' + \rho_2'$
	$\{\varnothing;-2,+1,+1\}$	$-\lambda_{112}^*$	$-2Q^*(\rho_1') - 2Q^*(\rho_1'+\rho_2') + Q^*(\rho_2')$	$2\rho_1' + \rho_2'$
	$\{\varnothing;-1,-1,+2\}$	λ_{112}	$Q^*(\rho_1') - 2Q^*(\rho_1'+\rho_2') - 2Q^*(\rho_2')$	$\rho_1' + 2\rho_2'$
	$\{\varnothing;-1,+2,-1\}$	λ_{112}	$-2Q^*(\rho_1') + Q^*(\rho_1'+\rho_2') - 2Q^*(\rho_2')$	$\rho_1' - \rho_2'$
	$\{\varnothing;+2,-1,-1\}$	λ_{112}	$-2Q^*(\rho_1') - 2Q^*(\rho_1'+\rho_2') + Q^*(\rho_2')$	$-2\rho_1' - \rho_2'$
$\Gamma_{-1}^{(2,1)}$	$\{+1,-2;-1\}$	λ_{112}	$-2Q(\rho_1) + Q(\tau+\frac{1}{2}\rho_1) - 2Q(\tau-\frac{1}{2}\rho_1)$	$-\tau + \frac{3}{2}\rho_1$
	$\{-2,+1;-1\}$	λ_{112}	$-2Q(\rho_1) - 2Q(\tau+\frac{1}{2}\rho_1) + Q(\tau-\frac{1}{2}\rho_1)$	$-\tau - \frac{3}{2}\rho_1$
$\Gamma_{-1}^{(1,2)}$	$\{-1;+1,-2\}$	λ_{112}^*	$-2Q^*(\rho_1') - 2Q(\tau+\frac{1}{2}\rho_1') + Q(\tau-\frac{1}{2}\rho_1')$	$-\tau - \frac{3}{2}\rho_1'$
	$\{-1;-2,+1\}$	λ_{112}^*	$-2Q^*(\rho_1') + Q(\tau+\frac{1}{2}\rho_1') - 2Q(\tau-\frac{1}{2}\rho_1')$	$-\tau + \frac{3}{2}\rho_1'$
$\Gamma_{-2}^{(2,1)}$	$\{-1,-1;-2\}$	$-\lambda_{112}^*$	$Q(\rho_1) - 2Q(\tau+\frac{1}{2}\rho_1) - 2Q(\tau-\frac{1}{2}\rho_1)$	-2τ
$\Gamma_{-2}^{(1,2)}$	$\{-2;-1,-1\}$	$-\lambda_{112}$	$Q^*(\rho_1') - 2Q(\tau+\frac{1}{2}\rho_1') - 2Q(\tau-\frac{1}{2}\rho_1')$	-2τ

Table 5.2: The different contributions to the rates $\Gamma_m^{(n,n')}$, obtained from (5.50), at third order $n + n' = 3$, when only transitions to the nearest neighbors and next-nearest neighbors, characterized by charges $\sigma_j, \sigma_{j'}' = \pm 1, \pm 2$, and mediated by the couplings $\Delta_{\pm 1}$ and $\Delta_{\pm 2}$, are allowed. In this situation, one obtains contributions for $m = 0, \pm 1, \pm 2$ only. Each contribution is specified by the configuration $\alpha_m^{(n,n')}$ of the charges, given in the second column. The third column gives the explicit expression of the prefactor (5.55), in terms of $\lambda_{112} \,\hat{=}\, -i\Delta_1^2 \Delta_2^*/\hbar^3$, for the corresponding contribution. The last two columns give the influence phase (5.78) and the driving term (5.79).

to the nearest neighbors $\Delta_{\pm 1}$ and next-nearest neighbors $\Delta_{\pm 2}$ are nonzero. The path (d) in Fig. 5.1 is an example of a contributing configuration. In total, one finds 24 contributions in the σ-σ' description. They are listed in Table 5.2. They all involve two transitions to a nearest neighbor and one to a next-nearest neighbor, in other words twice $\Delta_{\pm 1}$ and once $\Delta_{\pm 2}$. We will group them under the notation $\Gamma_m^{(3)}[112]$ in order to distinguish them from other contributions which will arise when we will switch on higher-order couplings Δ_m, $|m| > 2$.

Let us first look at $\Gamma_2^{(3)}[112]$. Changing the integration variable variable τ into $-\tau$ and using the property $Q(-\tau) = Q^*(\tau)$, one can verify that the second contribu-

tion $\Gamma_2^{(1,2)}$ is the complex conjugate of the first one $\Gamma_2^{(2,1)}$. Put together, they can be rewritten as

$$\Gamma_2^{(3)}[112] = \frac{2}{\hbar^3} \operatorname{Im} \left\{ \Delta_1^2 \Delta_2^* \int_{-\infty}^{\infty} \mathrm{d}\tau \int_0^{\infty} \mathrm{d}\rho e^{\frac{L^2}{\hbar}\left[Q(\rho)-2Q(\tau+\frac{1}{2}\rho)-2Q(\tau-\frac{1}{2}\rho)\right]+2i\frac{FL}{\hbar}\tau} \right\}.$$
(5.89)

Likewise, we obtain

$$\Gamma_{-2}^{(3)}[112] = \frac{2}{\hbar^3} \operatorname{Im} \left\{ \Delta_1^{*2} \Delta_2 \int_{-\infty}^{\infty} \mathrm{d}\tau \int_0^{\infty} \mathrm{d}\rho e^{\frac{L^2}{\hbar}\left[Q(\rho)-2Q(\tau+\frac{1}{2}\rho)-2Q(\tau-\frac{1}{2}\rho)\right]-2i\frac{FL}{\hbar}\tau} \right\}.$$
(5.90)

Following the same procedure, one can show that the contributions to $\Gamma_1^{(2,1)}$ are the complex conjugate of the ones to $\Gamma_1^{(1,2)}$, yielding

$$\Gamma_1^{(3)}[112] = -\frac{2}{\hbar^3} \operatorname{Im}\left\{ \Delta_1^2 \Delta_2^* \int_{-\infty}^{\infty} \mathrm{d}\tau \int_0^{\infty} \mathrm{d}\rho \right.$$
$$\times \left[e^{\frac{L^2}{\hbar}\left[-2Q(-\rho)-2Q(\tau+\frac{1}{2}\rho)+Q(\tau-\frac{1}{2}\rho)\right]+i\frac{FL}{\hbar}(\tau+\frac{3}{2}\rho)} \right.$$
$$\left. \left. + e^{\frac{L^2}{\hbar}\left[-2Q(-\rho)+Q(\tau+\frac{1}{2}\rho)-2Q(\tau-\frac{1}{2}\rho)\right]+i\frac{FL}{\hbar}(\tau-\frac{3}{2}\rho)} \right] \right\}.$$
(5.91)

Both parts of the expression can be partially merged by substituting $\tau - \frac{3}{2}\rho$ for τ in the first one, and $\tau + \frac{3}{2}\rho$ for τ in the second one. This yields

$$\Gamma_1^{(3)}[112] = -\frac{2}{\hbar^3} \operatorname{Im}\left\{ \Delta_1^2 \Delta_2^* \int_{-\infty}^{\infty} \mathrm{d}\tau \int_0^{\infty} \mathrm{d}\rho e^{-\frac{2L^2}{\hbar}Q(-\rho)+i\frac{FL}{\hbar}\tau} \right.$$
$$\left. \times \left[e^{\frac{L^2}{\hbar}[-2Q(\tau+\rho)+Q(\tau+2\rho)]} + e^{\frac{L^2}{\hbar}[-2Q(\tau-\rho)+Q(\tau-2\rho)]} \right] \right\}.$$
(5.92)

A similar expression is obtained for

$$\Gamma_{-1}^{(3)}[112] = -\frac{2}{\hbar^3} \operatorname{Im}\left\{ \Delta_1^{*2} \Delta_2 \int_{-\infty}^{\infty} \mathrm{d}\tau \int_0^{\infty} \mathrm{d}\rho e^{-\frac{2L^2}{\hbar}Q(-\rho)-i\frac{FL}{\hbar}\tau} \right.$$
$$\left. \times \left[e^{\frac{L^2}{\hbar}[-2Q(\tau+\rho)+Q(\tau+2\rho)]} + e^{\frac{L^2}{\hbar}[-2Q(\tau-\rho)+Q(\tau-2\rho)]} \right] \right\}.$$
(5.93)

Upon defining the combination

$$\varphi_{112} \stackrel{\wedge}{=} \varphi_2 - 2\varphi_1$$
(5.94)

of coupling phases, all these rates may be rewritten in a common expression, given in (5.40).

The relation (5.42) obeyed by the rate $\Gamma_0^{(3)}[112]$ can be explicitly checked with the expressions given in Table 5.2, provided that one works in the ζ-κ description. Each contribution to $\Gamma_m^{(3)}$, $m \neq 0$, corresponds to 3 contributions in the ζ-κ description, whereas each contribution to $\Gamma_0^{(3)}$ corresponds to only one. This multiplicity originates from the various chronological orderings of the transition times in the forward and backward paths, and it is in agreement with the formula $(n + n!)/n!n'!$ that we have derived. By proper substitutions in the time integrals, one can explicitly check that these 48 contributions compensate each other two by two.

Let us now allow the couplings $\Delta_{\pm 3}$ to be nonzero. One then finds 48 additional contributions in the σ-σ' description, like, e.g., the one which corresponds to the path (e) in Fig. 5.1. They all involve one transition of each of the three different kinds, therefore we group them under the notation $\Gamma_m^{(3)}[123]$. They are listed in Table 5.3. From there, applying the same procedure as for the third-order contributions involving only $\Delta_{\pm 1}$ and $\Delta_{\pm 2}$, we derive the expressions (5.44) and (5.46).

The generalization to higher-range couplings Δ_m, $|m| > 3$ becomes clear with the help of the diagram presented in Fig. 5.1. If we would allow the couplings $\Delta_{\pm 4}$ to be nonzero as well, we would get additional third-order contributions involving $\Delta_{\pm 4}$ with $\Delta_{\pm 3}$ and $\Delta_{\pm 1}$, as well as contributions involving $\Delta_{\pm 4}$ and twice $\Delta_{\pm 2}$. In order to write down explicit expressions for these contributions, one has to follow a procedure similar to what we have done here.

Going to fourth or higher order N, the procedure would also remain the same. One can see that the number of contributions increases factorially with the number of transitions. Starting from fourth order, one also has to subtract the reducible contributions in order to evaluate the transition rates.

References

[1] H. Baur, A. Fubini, and U. Weiss, Phys. Rev. B **70**, 024302 (2004).

[2] U. Weiss, *Quantum Dissipative Systems* (World Scientific, Singapore, 1999), 2nd ed.

$\Gamma_m^{(n,n')}$	$\alpha_m^{(n,n')}$	Λ	Φ_{FV} (units of $\frac{L^2}{\hbar}$)	Ψ (units of $\frac{\mathrm{i}FL}{\hbar}$)
$\Gamma_3^{(2,1)}$	$\{+1,+2;+3\}$	λ_{123}	$2Q(\rho_1) - 3Q(\tau+\frac{1}{2}\rho_1) - 6Q(\tau-\frac{1}{2}\rho_1)$	$3\tau - \frac{1}{2}\rho_1$
	$\{+2,+1;+3\}$	λ_{123}	$2Q(\rho_1) - 6Q(\tau+\frac{1}{2}\rho_1) - 3Q(\tau-\frac{1}{2}\rho_1)$	$3\tau + \frac{1}{2}\rho_1$
$\Gamma_3^{(1,2)}$	$\{+3;+1,+2\}$	λ_{123}^*	$2Q^*(\rho_1') - 6Q(\tau+\frac{1}{2}\rho_1') - 3Q(\tau-\frac{1}{2}\rho_1')$	$3\tau + \frac{1}{2}\rho_1'$
	$\{+3;+2,+1\}$	λ_{123}^*	$2Q^*(\rho_1') - 3Q(\tau+\frac{1}{2}\rho_1') - 6Q(\tau-\frac{1}{2}\rho_1')$	$3\tau - \frac{1}{2}\rho_1'$
$\Gamma_2^{(2,1)}$	$\{-1,+3;+2\}$	$-\lambda_{123}^*$	$-3Q(\rho_1) + 2Q(\tau+\frac{1}{2}\rho_1) - 6Q(\tau-\frac{1}{2}\rho_1)$	$2\tau - 2\rho_1$
	$\{+3,-1;+2\}$	$-\lambda_{123}^*$	$-3Q(\rho_1) - 6Q(\tau+\frac{1}{2}\rho_1) + 2Q(\tau-\frac{1}{2}\rho_1)$	$2\tau + 2\rho_1$
$\Gamma_2^{(1,2)}$	$\{+2;-1,+3\}$	$-\lambda_{123}$	$-3Q^*(\rho_1') - 6Q(\tau+\frac{1}{2}\rho_1') + 2Q(\tau-\frac{1}{2}\rho_1')$	$2\tau + 2\rho_1'$
	$\{+2;+3,-1\}$	$-\lambda_{123}$	$-3Q^*(\rho_1') + 2Q(\tau+\frac{1}{2}\rho_1') - 6Q(\tau-\frac{1}{2}\rho_1')$	$2\tau - 2\rho_1'$
$\Gamma_1^{(2,1)}$	$\{-2,+3;+1\}$	$-\lambda_{123}^*$	$-6Q(\rho_1) + 2Q(\tau+\frac{1}{2}\rho_1) - 3Q(\tau-\frac{1}{2}\rho_1)$	$\tau - \frac{5}{2}\rho_1$
	$\{+3,-2;+1\}$	$-\lambda_{123}^*$	$-6Q(\rho_1) - 3Q(\tau+\frac{1}{2}\rho_1) + 2Q(\tau-\frac{1}{2}\rho_1)$	$\tau + \frac{5}{2}\rho_1$
$\Gamma_1^{(1,2)}$	$\{+1;-2,+3\}$	$-\lambda_{123}$	$-6Q^*(\rho_1') - 3Q(\tau+\frac{1}{2}\rho_1') + 2Q(\tau-\frac{1}{2}\rho_1')$	$\tau + \frac{5}{2}\rho_1'$
	$\{+1;+3,-2\}$	$-\lambda_{123}$	$-6Q^*(\rho_1') + 2Q(\tau+\frac{1}{2}\rho_1') - 3Q(\tau-\frac{1}{2}\rho_1')$	$\tau - \frac{5}{2}\rho_1'$
$\Gamma_0^{(3,0)}$	$\{+1,+2,-3;\varnothing\}$	$-\lambda_{123}$	$2Q(\rho_1) - 3Q(\rho_1+\rho_2) - 6Q(\rho_2)$	$\rho_1 + 3\rho_2$
	$\{+2,-3,+1;\varnothing\}$	$-\lambda_{123}$	$-6Q(\rho_1) + 2Q(\rho_1+\rho_2) - 3Q(\rho_2)$	$2\rho_1 - \rho_2$
	$\{-3,+1,+2;\varnothing\}$	$-\lambda_{123}$	$-3Q(\rho_1) - 6Q(\rho_1+\rho_2) + 2Q(\rho_2)$	$-3\rho_1 - 2\rho_2$
	$\{+2,+1,-3;\varnothing\}$	$-\lambda_{123}$	$2Q(\rho_1) - 6Q(\rho_1+\rho_2) - 3Q(\rho_2)$	$2\rho_1 + 3\rho_2$
	$\{+1,-3,+2;\varnothing\}$	$-\lambda_{123}$	$-3Q(\rho_1) + 2Q(\rho_1+\rho_2) - 6Q(\rho_2)$	$\rho_1 - 2\rho_2$
	$\{-3,+2,+1;\varnothing\}$	$-\lambda_{123}$	$-6Q(\rho_1) - 3Q(\rho_1+\rho_2) + 2Q(\rho_2)$	$-3\rho_1 - \rho_2$
	$\{-1,-2,+3;\varnothing\}$	λ_{123}^*	$2Q(\rho_1) - 3Q(\rho_1+\rho_2) - 6Q(\rho_2)$	$-\rho_1 - 3\rho_2$
	$\{-2,+3,-1;\varnothing\}$	λ_{123}^*	$-6Q(\rho_1) + 2Q(\rho_1+\rho_2) - 3Q(\rho_2)$	$-2\rho_1 + \rho_2$
	$\{+3,-1,-2;\varnothing\}$	λ_{123}^*	$-3Q(\rho_1) - 6Q(\rho_1+\rho_2) + 2Q(\rho_2)$	$3\rho_1 + 2\rho_2$
	$\{-2,-1,+3;\varnothing\}$	λ_{123}^*	$2Q(\rho_1) - 6Q(\rho_1+\rho_2) - 3Q(\rho_2)$	$-2\rho_1 - 3\rho_2$
	$\{-1,+3,-2;\varnothing\}$	λ_{123}^*	$-3Q(\rho_1) + 2Q(\rho_1+\rho_2) - 6Q(\rho_2)$	$-\rho_1 + 2\rho_2$
	$\{+3,-2,-1;\varnothing\}$	λ_{123}^*	$-6Q(\rho_1) - 3Q(\rho_1+\rho_2) + 2Q(\rho_2)$	$3\rho_1 + \rho_2$
$\Gamma_0^{(0,3)}$	$\{\varnothing;+1,+2,-3\}$	$-\lambda_{123}^*$	$2Q^*(\rho_1') - 3Q^*(\rho_1'+\rho_2') - 6Q^*(\rho_2')$	$-\rho_1' - 3\rho_2'$
	$\{\varnothing;+2,-3,+1\}$	$-\lambda_{123}^*$	$-6Q^*(\rho_1') + 2Q^*(\rho_1'+\rho_2') - 3Q^*(\rho_2')$	$-2\rho_1' + \rho_2'$
	$\{\varnothing;-3,+1,+2\}$	$-\lambda_{123}^*$	$-3Q^*(\rho_1') - 6Q^*(\rho_1'+\rho_2') + 2Q^*(\rho_2')$	$3\rho_1' + 2\rho_2'$
	$\{\varnothing;+2,+1,-3\}$	$-\lambda_{123}^*$	$2Q^*(\rho_1') - 6Q^*(\rho_1'+\rho_2') - 3Q^*(\rho_2')$	$-2\rho_1' - 3\rho_2'$
	$\{\varnothing;+1,-3,+2\}$	$-\lambda_{123}^*$	$-3Q^*(\rho_1') + 2Q^*(\rho_1'+\rho_2') - 6Q^*(\rho_2')$	$-\rho_1' + 2\rho_2'$
	$\{\varnothing;-3,+2,+1\}$	$-\lambda_{123}^*$	$-6Q^*(\rho_1') - 3Q^*(\rho_1'+\rho_2') + 2Q^*(\rho_2')$	$3\rho_1' + \rho_2'$
	$\{\varnothing;-1,-2,+3\}$	λ_{123}	$2Q^*(\rho_1') - 3Q^*(\rho_1'+\rho_2') - 6Q^*(\rho_2')$	$\rho_1' + 3\rho_2'$
	$\{\varnothing;-2,+3,-1\}$	λ_{123}	$-6Q^*(\rho_1') + 2Q^*(\rho_1'+\rho_2') - 3Q^*(\rho_2')$	$2\rho_1' - \rho_2'$
	$\{\varnothing;+3,-1,-2\}$	λ_{123}	$-3Q^*(\rho_1') - 6Q^*(\rho_1'+\rho_2') + 2Q^*(\rho_2')$	$-3\rho_1' - 2\rho_2'$
	$\{\varnothing;-2,-1,+3\}$	λ_{123}	$2Q^*(\rho_1') - 6Q^*(\rho_1'+\rho_2') - 3Q^*(\rho_2')$	$2\rho_1' + 3\rho_2'$
	$\{\varnothing;-1,+3,-2\}$	λ_{123}	$-3Q^*(\rho_1') + 2Q^*(\rho_1'+\rho_2') - 6Q^*(\rho_2')$	$\rho_1' - 2\rho_2'$
	$\{\varnothing;+3,-2,-1\}$	λ_{123}	$-6Q^*(\rho_1') - 3Q^*(\rho_1'+\rho_2') + 2Q^*(\rho_2')$	$-3\rho_1' - \rho_2'$
$\Gamma_{-1}^{(2,1)}$	$\{+2,-3;-1\}$	λ_{123}	$-6Q(\rho_1) + 2Q(\tau+\frac{1}{2}\rho_1) - 3Q(\tau-\frac{1}{2}\rho_1)$	$-\tau + \frac{5}{2}\rho_1$
	$\{-3,+2;-1\}$	λ_{123}	$-6Q(\rho_1) - 3Q(\tau+\frac{1}{2}\rho_1) + 2Q(\tau-\frac{1}{2}\rho_1)$	$-\tau - \frac{5}{2}\rho_1$
$\Gamma_{-1}^{(1,2)}$	$\{-1;+2,-3\}$	λ_{123}^*	$-6Q^*(\rho_1') - 3Q(\tau+\frac{1}{2}\rho_1') + 2Q(\tau-\frac{1}{2}\rho_1')$	$-\tau - \frac{5}{2}\rho_1'$
	$\{-1;-3,+2\}$	λ_{123}^*	$-6Q^*(\rho_1') + 2Q(\tau+\frac{1}{2}\rho_1') - 3Q(\tau-\frac{1}{2}\rho_1')$	$-\tau + \frac{5}{2}\rho_1'$
$\Gamma_{-2}^{(2,1)}$	$\{+1,-3;-2\}$	λ_{123}	$-3Q(\rho_1) + 2Q(\tau+\frac{1}{2}\rho_1) - 6Q(\tau-\frac{1}{2}\rho_1)$	$-2\tau + 2\rho_1$
	$\{-3,+1;-2\}$	λ_{123}	$-3Q(\rho_1) - 6Q(\tau+\frac{1}{2}\rho_1) + 2Q(\tau-\frac{1}{2}\rho_1)$	$-2\tau - 2\rho_1$
$\Gamma_{-2}^{(1,2)}$	$\{-2;+1,-3\}$	λ_{123}^*	$-3Q^*(\rho_1') - 6Q(\tau+\frac{1}{2}\rho_1') + 2Q(\tau-\frac{1}{2}\rho_1')$	$-2\tau - 2\rho_1'$
	$\{-2;-3,+1\}$	λ_{123}^*	$-3Q^*(\rho_1') + 2Q(\tau+\frac{1}{2}\rho_1') - 6Q(\tau-\frac{1}{2}\rho_1')$	$-2\tau + 2\rho_1'$
$\Gamma_{-3}^{(2,1)}$	$\{-1,-2;-3\}$	$-\lambda_{123}^*$	$2Q(\rho_1) - 3Q(\tau+\frac{1}{2}\rho_1) - 6Q(\tau-\frac{1}{2}\rho_1)$	$-3\tau + \frac{1}{2}\rho_1$
	$\{-2,-1;-3\}$	$-\lambda_{123}^*$	$2Q(\rho_1) - 6Q(\tau+\frac{1}{2}\rho_1) - 3Q(\tau-\frac{1}{2}\rho_1)$	$-3\tau - \frac{1}{2}\rho_1$
$\Gamma_{-3}^{(1,2)}$	$\{-3;-1,-2\}$	$-\lambda_{123}$	$2Q^*(\rho_1') - 6Q(\tau+\frac{1}{2}\rho_1') - 3Q(\tau-\frac{1}{2}\rho_1')$	$-3\tau - \frac{1}{2}\rho_1'$
	$\{-3;-2,-1\}$	$-\lambda_{123}$	$2Q^*(\rho_1') - 3Q(\tau+\frac{1}{2}\rho_1') - 6Q(\tau-\frac{1}{2}\rho_1')$	$-3\tau + \frac{1}{2}\rho_1'$

Table 5.3: Contributions added to Table 5.2 when the couplings $\Delta_{\pm 3}$ are nonzero. In the third column, the prefactor (5.55) is given in terms of $\lambda_{123} \,\hat{=}\, -\mathrm{i}\Delta_1\Delta_2\Delta_3^*/\hbar^3$.

Chapter 6

Duality Relation for Quantum Ratchets

In collaboration with M. Grifoni.

6.1   Introduction

In this chapter, we present a generalization of an approach developed by Fisher and Zwerger [1] to investigate quantum Brownian motion in a tilted sinusoidal potential, which leads to a duality relation for the mobility of the system considered with the one of a driven dissipative tight-binding model. We will generalize this method to periodic potentials of arbitrary shape, and derive the duality relation in its most general form, in terms of a generating function out of which the average position, the mobility, and other dynamical quantities can be extracted.

We consider the model presented in Section 1.1.3. The system is given by the Hamiltonian $\hat{H}_{\mathrm{S}}$ of a quantum particle of mass M in a one-dimensional periodic potential $V(q)$ tilted by a force F,

$$\hat{H}_{\mathrm{S}} = \frac{\hat{p}^2}{2M} + V(\hat{q}) - F\hat{q}. \tag{6.1}$$

The potential can be any function of periodicity L, and is fully characterized by the amplitudes V_l and phases φ_l of its harmonics in the Fourier representation

$$V(\hat{q}) = \sum_{l=1}^{\infty} V_l \cos\left(2\pi l \hat{q}/L - \varphi_l\right). \qquad (6.2)$$

Apart from special configurations of the amplitudes and phases,

$$V_l \sin\left(\varphi_l - l\varphi_1\right) = 0, \qquad \forall l, \qquad (6.3)$$

this potential is spatially asymmetric and thus describes a ratchet system.

In order to investigate quantum Brownian motion, we let the particle interact with a dissipative thermal environment. This is modeled by the standard Hamiltonian $\hat{H}_{\mathrm{B}}$ of a bath of harmonic oscillators whose coordinates are bilinearly coupled to the system coordinate $\hat{q}$

$$\hat{H}_{\mathrm{B}} = \frac{1}{2} \sum_{\alpha=1}^{N_{\mathrm{O}}} \left[\frac{\hat{p}_{\alpha}^2}{m_{\alpha}} + m_{\alpha}\omega_{\alpha}^2 \left(\hat{x}_{\alpha} - \frac{c_{\alpha}}{m_{\alpha}\omega_{\alpha}^2}\hat{q} \right)^2 \right]. \qquad (6.4)$$

The bath is fully characterized by its spectral density

$$J(\omega) = \frac{\pi}{2} \sum_{\alpha=1}^{N_{\mathrm{O}}} \frac{c_{\alpha}^2}{m_{\alpha}\omega_{\alpha}} \delta(\omega - \omega_{\alpha}), \qquad (6.5)$$

defined in terms of the masses m_{α}, frequencies ω_{α}, and coupling strengths c_{α} of the oscillators. We consider an Ohmic spectral density, i.e. linear $J(\omega) \sim \eta\omega$ at low frequency ω. The viscosity coefficient η, together with the particle mass M, defines the time scale of dissipation $\gamma^{-1} = (\eta/M)^{-1}$.

We want to evaluate the stationary velocity

$$v^{\infty}(t) = \lim_{t \gg t_0} \frac{\mathrm{d}}{\mathrm{d}t} \langle \hat{q}(t) \rangle. \qquad (6.6)$$

As shown in Eq. (1.4), the stationary velocity in the presence of a time-independent driving force F can be used to investigate the ratchet velocity in an adiabatically rocked ratchet system based on the system (6.1).

The expectation value of the position operator, given by $\langle \hat{q}(t) \rangle = \mathrm{Tr}_{\mathrm{S}}\{\hat{q}\hat{\rho}(t)\}$, involves the reduced density matrix $\hat{\rho}(t) = \mathrm{Tr}_{\mathrm{B}}\hat{W}(t)$, obtained from the density matrix $\hat{W}(t)$ of the system-plus-bath $\hat{H} = \hat{H}_{\mathrm{S}} + \hat{H}_{\mathrm{B}}$ by performing the trace over the bath degrees of freedom. The knowledge of the diagonal elements $P(q,t) = \langle q|\hat{\rho}(t)|q\rangle$ of the reduced density matrix, called populations, suffices for its evaluation. As discussed in Section 5.2, it turns out to be very powerful to work with the generating function. For the system (6.1), which presents a continuous coordinate q, in contrast

to the discrete tight-binding system (5.1) investigated in Chapter 5, the generating function is defined as

$$\tilde{P}(\lambda, t) = \int \mathrm{d}q \mathrm{e}^{\lambda q} P(q, t), \qquad (6.7)$$

in terms of the populations. We remind that the normalization of the reduced density matrix implies the property

$$\tilde{P}(\lambda = 0, t) = 1, \qquad (6.8)$$

whereas the derivatives of this function generate expectation values of powers of the position operator

$$\left. \frac{\partial^k}{\partial \lambda^k} \tilde{P}(\lambda, t) \right|_{\lambda=0} = \langle \hat{q}^k(t) \rangle. \qquad (6.9)$$

The populations $P(q, t)$ can be obtained by real-time path integrals techniques. In order to perform the path integrals over the bath degrees of freedom, we follow the method presented in Chapter 3 and Appendix A. At initial time t_0, we assume a preparation of the form (3.10), with the system at an initial position q_0, in equilibrium with the bath at temperature $T = 1/\beta k_\mathrm{B}$. This leads to the expression

$$P(q, t) = \langle q | \hat{\rho}(t) | q \rangle = \int \mathrm{d}q_i \int \mathrm{d}q_i' \langle q_i | \hat{\rho}(t_0) | q_i' \rangle G(q, q, q_i, q_i', t) \qquad (6.10)$$

with the propagating function

$$G(q_f, q_f', q_i, q_i', t) = \int_{q_i}^{q_f} \mathcal{D}q \int_{q_i'}^{q_f'} \mathcal{D}^* q' A[q, t] A^*[q', t] F_\mathrm{FV}[q, q', t] \qquad (6.11)$$

given as a double path integral over the paths $q(t')$ and $q'(t')$. For a Hamiltonian of the form (6.1), the path integral over the continuous coordinate q stands for (see Ref. [2, Ch. 2])

$$\int_{q_i}^{q_f} \mathcal{D}q = \lim_{N_\mathrm{I} \to \infty} \left(\frac{M}{2\pi \mathrm{i}\hbar \Delta\tau} \right)^{N_\mathrm{I}/2} \int \mathrm{d}q_1 \int \mathrm{d}q_2 \dots \int \mathrm{d}q_{N_\mathrm{I}-1}, \qquad (6.12)$$

where the time interval $t - t_0$ has been sliced in N_I intervals of length $\Delta\tau = (t - t_0)/N_\mathrm{I}$ and the path $q(t')$ has been discretized into the set of values $q_k = q(t_0 + k\Delta\tau)$ for $k = 1, \dots, N_\mathrm{I} - 1$. The boundaries of the path integral remind of $q(t_0) = q_i$ and $q(t) = q_f$. The propagator $A[q, t]$ reads

$$A[q, t] = \exp \left\{ \frac{\mathrm{i}}{\hbar} \int_{t_0}^{t} \mathrm{d}t' \left[\frac{M}{2} \dot{q}(t')^2 - V(q(t')) + Fq(t') \right] \right\}. \qquad (6.13)$$

The Feynman-Vernon influence functional $F_\mathrm{FV}[q, q', t]$ is given in Eq. (3.16). It induces nonlocal-in-time Gaussian correlations between the paths $q(t')$ and $q'(t')$,

and may be conveniently rewritten in terms of the difference and average paths

$$\xi(t') \mathrel{\hat{=}} q(t') - q'(t') \tag{6.14a}$$

$$\chi(t') \mathrel{\hat{=}} \frac{1}{2}[q(t') + q'(t')]. \tag{6.14b}$$

For the influence phase, defined through $F_{\text{FV}}[q, q', t] = \exp\{\Phi_{\text{FV}}[\xi, \chi, t]\}$, this yields the expression

$$
\begin{aligned}
\Phi_{\text{FV}}[\xi, \chi, t] = &-\frac{1}{\hbar} \int_{t_0}^{t} \mathrm{d}t' \int_{t_0}^{t'} \mathrm{d}t'' \xi(t') L_{\text{R}}(t' - t'') \xi(t'') \\
&- \frac{2\mathrm{i}}{\hbar} \int_{t_0}^{t} \mathrm{d}t' \int_{t_0}^{t'} \mathrm{d}t'' \xi(t') L_{\text{I}}(t' - t'') \chi(t'') \\
&- \frac{2\mathrm{i}}{\hbar} M_{\text{I}}(0) \int_{t_0}^{t} \mathrm{d}t' \xi(t') \chi(t') + \frac{2\mathrm{i}}{\hbar} q(t_0) \int_{t_0}^{t} \mathrm{d}t' \xi(t') M_{\text{I}}(t' - t_0), \quad (6.15)
\end{aligned}
$$

which involves the bath correlation function $L(\tau)$ and its primitive $M(\tau)$ discussed in Appendix B.

Our goal is to evaluate the generating function (6.7). In general, the nonlinearity of the potential $V(q)$ prevents the evaluation of the path integrals in (6.10). However, an exact expansion of the contribution of the potential in the propagator $A[q]$ makes it feasible, as observed by Fisher and Zwerger [1] in the case of a sinusoidal potential.

In the next section, we will outline the method and present the results. We will discuss the results in Section 6.3 and apply them to the evaluation of the ratchet current in Section 6.4. For clarity, the rather technical details of the proofs are postponed to Section 6.5.

6.2   Method and results

In order to expand the contribution of the potential, we introduce a "charge" σ taking values in the set $\{\pm 1, \pm 2, \ldots\}$, and corresponding amplitudes defined as

$$\Delta_\sigma \mathrel{\hat{=}} \frac{V_\sigma}{2} \mathrm{e}^{\mathrm{i}\varphi_\sigma} \quad \text{for } \sigma > 0, \qquad\qquad \Delta_{-\sigma} \mathrel{\hat{=}} \Delta_\sigma^*. \tag{6.16}$$

This allows to rewrite the potential (6.2) as a simple sum of exponentials

$$V(q) = \sum_{\sigma = \pm 1, \pm 2, \ldots} \Delta_\sigma \mathrm{e}^{-2\pi\mathrm{i}\sigma q/L}. \tag{6.17}$$

Using this expansion, one can demonstrate that (see Section 6.5.1)

$$\exp\left\{-\frac{i}{\hbar}\int_{t_0}^{t}dt'V(q(t'))\right\} = \sum_{n=0}^{\infty}\sum_{\{\sigma_j\}}\prod_{j=1}^{n}\left(-\frac{i\Delta_{\sigma_j}}{\hbar}\right)$$

$$\times \int_{t_0}^{t}dt_n\int_{t_0}^{t_n}dt_{n-1}\ldots\int_{t_0}^{t_2}dt_1\exp\left\{-\frac{i}{\hbar}\int_{t_0}^{t}dt'\rho(t')q(t')\right\}, \quad (6.18)$$

where we have introduced n charges σ_j and corresponding times t_j, as well as the function

$$\rho(t') \triangleq \frac{2\pi\hbar}{L}\sum_{j=1}^{n}\sigma_j\delta(t'-t_j). \quad (6.19)$$

This expression can be substituted in the propagator $A[q,t]$ given in (6.13). We have to do the same for the second propagator $A^*[q',t]$, using the complex conjugate of Eq. (6.18) with a new set of n' charges $\sigma'_{j'}$ and corresponding times $t'_{j'}$, and a new function $\rho'(t')$. The product $A[q,t]A^*[q',t]$ may then be conveniently rewritten in terms of the difference $\xi(t')$, respectively average path $\chi(t')$, introduced in (6.14). This yields

$$A[q,t]A^*[q',t] = \boxed{\sum}\exp\left\{\frac{i}{\hbar}\int_{t_0}^{t}dt'\left[M\dot{\xi}(t')\dot{\chi}(t') - \chi(t')\left[\rho(t')-\rho'(t')\right]\right.\right.$$

$$\left.\left. - \xi(t')\frac{1}{2}\left[\rho(t')+\rho'(t')\right] + F\xi(t')\right]\right\}. \quad (6.20)$$

The gain of this expansion is that the paths now enter at most quadratically in the argument of the exponential. Eventually, the path integrals will become Gaussian integrals. The price paid is the emergence of a series expression. We have introduced a compact notation for the sums, products and integrals involved

$$\boxed{\sum} \triangleq \sum_{n=0}^{\infty}\sum_{n'=0}^{\infty}\sum_{\{\sigma_j\}}\sum_{\{\sigma'_{j'}\}}\prod_{j=1}^{n}\left(-\frac{i\Delta_{\sigma_j}}{\hbar}\right)\prod_{j'=1}^{n'}\left(\frac{i\Delta^*_{\sigma'_{j'}}}{\hbar}\right)$$

$$\times \int_{t_0}^{t}dt_n\int_{t_0}^{t_n}dt_{n-1}\ldots\int_{t_0}^{t_2}dt_1\int_{t_0}^{t}dt'_{n'}\int_{t_0}^{t'_{n'}}dt'_{n'-1}\ldots\int_{t_0}^{t'_2}dt'_1. \quad (6.21)$$

Performing the now Gaussian path integrals, and after a long calculation described in Sections 6.5.2–6.5.5, we obtain our main result

$$\tilde{P}(\lambda,t) \sim \boxed{\sum}'\,\mathrm{Tr_R}\left\{\hat{\rho}(t_0)e^{\lambda(\hat{q}+\hat{p}/\eta)}\right\}\exp\left\{\Phi_{\mathrm{FV}}^{\mathrm{TB}}[y_{\mathrm{sh}},x_{\mathrm{sh}},t] + \frac{iF}{\hbar}\int_{t_0}^{t}dt'y_{\mathrm{sh}}(t')\right.$$

$$\left. + \lambda\left[-\Delta\chi + \frac{F(t-t_0)}{\eta} + \frac{2ik_{\mathrm{B}}T}{\hbar}\int_{t_0}^{t}dt'y_{\mathrm{sh}}(t')\right] + \frac{\hbar\lambda^2}{2\eta^2}\left[N(t)-\frac{1}{\gamma}\dot{N}(t_0)-i\eta\right]\right\}. \quad (6.22)$$

As indicated by the relation symbol, this result is valid within some approximations, as shown in the full derivation. The validity regime is discussed in detail below Eq. (6.34). The functions

$$y_{\text{sh}}(t') \mathbin{\hat{=}} q_{\text{sh}}(t') - q'_{\text{sh}}(t') \tag{6.23a}$$

$$x_{\text{sh}}(t') \mathbin{\hat{=}} \frac{1}{2}[q_{\text{sh}}(t') + q'_{\text{sh}}(t')] \tag{6.23b}$$

denote the difference, respectively average, of the step-like paths

$$q_{\text{sh}}(t') \mathbin{\hat{=}} \tilde{L} \sum_{j=1}^{n} \sigma_j \left[\theta(t' - t_j) - 1\right] + q_{\text{sh}}(t) \tag{6.24a}$$

$$q'_{\text{sh}}(t') \mathbin{\hat{=}} \tilde{L} \sum_{j'=1}^{n'} \sigma'_{j'} \left[\theta(t' - t'_{j'}) - 1\right] + q_{\text{sh}}(t). \tag{6.24b}$$

The step heights are multiples of

$$\tilde{L} \mathbin{\hat{=}} \frac{2\pi\hbar}{\eta L}. \tag{6.25}$$

The paths end up at the same value $q_{\text{sh}}(t)$ at the final time t. Therefore, the difference path ends up at $y_{\text{sh}}(t) = 0$. The quantities

$$\Delta\xi \mathbin{\hat{=}} y_{\text{sh}}(t) - y_{\text{sh}}(t_0) = \tilde{L} \left[\sum\nolimits_{j=1}^{n} \sigma_j - \sum\nolimits_{j'=1}^{n'} \sigma'_{j'}\right] \tag{6.26a}$$

$$\Delta\chi \mathbin{\hat{=}} x_{\text{sh}}(t) - x_{\text{sh}}(t_0) = \frac{\tilde{L}}{2} \left[\sum\nolimits_{j=1}^{n} \sigma_j + \sum\nolimits_{j'=1}^{n'} \sigma'_{j'}\right] \tag{6.26b}$$

specify the initial boundary condition for the two paths. The primed sum

$$\boxed{\sum{}'} \mathbin{\hat{=}} \boxed{\sum} \delta\left(\frac{\Delta\xi}{\tilde{L}}, 0\right), \tag{6.27}$$

where δ denotes the Kronecker symbol, is thus restricted to the configurations for which the difference path starts at $y_{\text{sh}}(t_0) = 0$. The influence phase $\Phi_{\text{FV}}^{\text{TB}}[y_{\text{sh}}, x_{\text{sh}}, t]$ is defined as in (6.15), provided that the spectral density $J(\omega)$ entering the bath correlation functions $L(\tau)$ and $M_{\text{I}}(\tau)$ is replaced by the new spectral density

$$J_{\text{TB}}(\omega) \mathbin{\hat{=}} \frac{J(\omega)}{1 + (\omega/\gamma)^2}. \tag{6.28}$$

Finally, the auxiliary function $N(\tau)$ is discussed in Section 6.5.5.
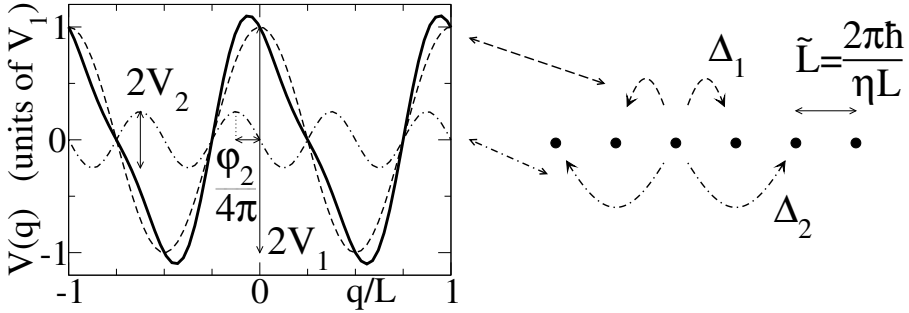
Figure 6.1: Dual relation between the dissipative ratchet system (6.1) and the tight-binding model (6.29), sketched for a two-harmonics ratchet potential (thick curve). Each harmonic (thin curves) generates couplings between neighbors of different orders in the tight-binding system, according to Eq. (6.16). The periodicity $\tilde{L}$ of the tight-binding model is determined by the relation (6.25), which involves the viscosity η in the original model.

The justification of these notations appears when one considers the generating function $\tilde{P}_{\mathrm{TB}}(\lambda, t)$ of a driven tight-binding model given by the Hamiltonian

$$\hat{H}_{\mathrm{TB}} = \sum_{m=1}^{\infty} \sum_{l=-\infty}^{\infty} \left(\Delta_m |l+m\rangle\langle l| + \Delta_m^* |l\rangle\langle l+m| \right) - F\hat{q}_{\mathrm{TB}}, \qquad (6.29)$$

which has been investigated in Chapter 5. The couplings Δ_m in this Hamiltonian are precisely the one introduced in (6.16) and involved in the boxed sum. We stress that the lth harmonic of the original potential results in a coupling to the lth-order neighbors in the dual tight-binding system, as sketched in Fig. 6.1. The phases φ_m of the harmonics of the potential are identical to the phases of the couplings. One notices that the spatial symmetry conditions for both systems, given by Eq. (6.3) and Eq. (5.30), are identical. The spatial periodicity $\tilde{L}$ of the tight-binding model, which can be read in the position operator

$$\hat{q}_{\mathrm{TB}} = \tilde{L} \sum_{l=-\infty}^{\infty} l |l\rangle\langle l|, \qquad (6.30)$$

is precisely the height unit (6.25) of the steps of the paths (6.24). This tight-binding model is bilinearly coupled to a different bath of harmonic oscillators characterized by the spectral density $J_{\mathrm{TB}}(\omega)$ given in (6.28). This spectral density is still Ohmic, with the same viscosity coefficient η, but now presents a Drude cutoff at the frequency γ set by the dissipation of the original model. The system is initially

prepared in the state $\hat{\rho}_{\mathrm{TB}}(t_0) = |l_0\rangle\langle l_0|$ with $l_0\tilde{L} = q_{\mathrm{sh}}(t_0)$. The generating function corresponding to this situation may be obtained from the definition (5.6), in terms of the populations given by the expression (3.11), discussed in Chapter 3. This expression may be simplified for the system (6.29), along the same lines as what we have done for the transition rates in Section 5.3.1. Using the notations of the present chapter, one obtains

$$\tilde{P}_{\mathrm{TB}}(\lambda, t) = \boxed{\sum\nolimits'} \exp\left\{ \Phi_{\mathrm{FV}}^{\mathrm{TB}}[y_{\mathrm{sh}}, x_{\mathrm{sh}}, t] + \frac{\mathrm{i}F}{\hbar}\int_{t_0}^{t} \mathrm{d}t'\, y_{\mathrm{sh}}(t') + \lambda\left(l_0\tilde{L} + \Delta\chi\right) \right\},$$
(6.31)

which bears a clear structural resemblance with (6.22). The λ^2-terms are absent in (6.31), but they do not play any role as far as one is interested in the average position $\langle \hat{q}(t)\rangle$ [see Eq. (6.9)]. One also notices that $\Delta\chi$ comes with an opposite sign in the two expressions.

The link between the original model (6.1) and the tight-binding model (6.29) can be pushed further. The normalization of the generating function $\tilde{P}(\lambda = 0, t) = 1$ yields the identity

$$1 = \boxed{\sum\nolimits'} \exp\left\{ \Phi_{\mathrm{FV}}^{\mathrm{TB}}[y_{\mathrm{sh}}, x_{\mathrm{sh}}, t] + \frac{\mathrm{i}F}{\hbar}\int_{t_0}^{t} \mathrm{d}t'\, y_{\mathrm{sh}}(t') \right\},$$
(6.32)

starting either from (6.22) or (6.31). Differentiating with respect to F yields the set of non-trivial identities

$$0 = \boxed{\sum\nolimits'} \left[\frac{\mathrm{i}}{\hbar}\int_{t_0}^{t} \mathrm{d}t'\, y_{\mathrm{sh}}(t')\right]^k \exp\left\{ \Phi_{\mathrm{FV}}^{\mathrm{TB}}[y_{\mathrm{sh}}, x_{\mathrm{sh}}, t] + \frac{\mathrm{i}F}{\hbar}\int_{t_0}^{t} \mathrm{d}t'\, y_{\mathrm{sh}}(t') \right\},$$
(6.33)

for any $k = 1, 2, \ldots, \infty$.

Another important result can be obtained from the relation (6.22) by evaluating the average position $\langle \hat{q}(t)\rangle$, obtained from (6.9) with $k = 1$. Using the identities (6.32) and (6.33) with $k = 1$, one gets

$$\langle \hat{q}(t)\rangle \sim \langle \hat{q}(t_0)\rangle + \frac{\langle \hat{p}(t_0)\rangle}{\eta} + \frac{F(t - t_0)}{\eta} - \langle \hat{q}_{\mathrm{TB}}(t)\rangle_{\mathrm{TB}},$$
(6.34)

where $\langle \hat{q}(t_0)\rangle = \mathrm{Tr}_{\mathrm{S}}\{\hat{q}\hat{\rho}(t_0)\}$ and $\langle \hat{p}(t_0)\rangle = \mathrm{Tr}_{\mathrm{S}}\{\hat{p}\hat{\rho}(t_0)\}$ denote the position and momentum of the initial preparation of the ratchet system. The last term of (6.34) is the average of the position operator (6.30) in the driven dissipative tight-binding model (6.29), initially prepared in the state $\hat{\rho}_{\mathrm{TB}}(t_0) = |0\rangle\langle 0|$. It can be obtained according to Eq. (6.9) with $k = 1$ as well, from the generating function (6.31) with $l_0 = 0$. It comes with a minus sign due to the minus sign in front of $\Delta\chi$ in (6.22). The duality relation for the position (6.34) is a very useful result for quantum ratchet systems. We will discuss its application in Section 6.4.

The duality relations (6.22) and (6.34) are approximate results, as denoted by the relation symbol. As derived in this chapter, they are valid when the following conditions are simultaneously met:

i) Long-time dynamics: The measurement time $t - t_0$ should be much longer than the time scale $1/\gamma$ set by dissipation. This can be easily controlled experimentally.

ii) Rare transitions limit: The terms $e^{-\gamma(t_{\text{tr}}-t_0)}$, $e^{-\gamma(t-t_{\text{tr}})}$, $e^{-\omega_{\text{B}}(t_{\text{tr}}-t_0)}$, and $e^{-\omega_{\text{B}}(t-t_{\text{tr}})}$, with $\omega_{\text{B}} = 2\pi k_{\text{B}}T/\hbar$, should be negligible with respect to 1, when t_{tr} equals any of the times $t_j, t'_{j'}$. These times, which are integration variables involved in the boxed sum, are the transition times in the double path integral representation (6.31) of the generating function of the tight-binding model. Therefore, this approximation corresponds to neglect, in the boxed sum, the contributions from the paths which involve transitions on a time scale $\max(\gamma^{-1}, \omega_{\text{B}}^{-1})$ after the initial time $t' = t_0$ or before the final time $t' = t$. It will therefore be valid when the transitions in the tight-binding model are rare on a time scale $\max(\gamma^{-1}, \omega_{\text{B}}^{-1})$. This condition is controlled by the dissipation and the temperature.

Furthermore, in our derivation we have used a strictly Ohmic spectral density $J(\omega) = \eta\omega$. In this case, the function $M_{\text{I}}(\tau)$ takes the simple form $M_{\text{I}}(\tau) = \eta\delta(\tau)$, and the divergence of $L_{\text{R}}^{\text{TB}}(0)$ allows to restrict the configuration sum to its primed version (see Appendix B). A physically more realistic situation would be to consider the Ohmic spectral density $J(\omega) = \eta\omega e^{-\omega/\omega_{\text{c}}}$ with finite cutoff frequency ω_{c}.

We do not know to which extent these restrictions are specific to the method that we have used in order to derive the duality relations. An equivalent duality relation for the mobilities [see Eq. (6.35)] has been derived in Ref. [3] in the frame of linear response for a sinusoidal potential. It is interesting to notice that the derivation presented in that work does not require the restrictions to the rare transitions limit and to a strictly Ohmic bath. A more generalized version of (6.35) has also been obtained for a much broader class of spectral densities, including sub-Ohmic and super-Ohmic ones, and in the case of time-dependent driving. We currently do not see any problem of principle in order to generalize our demonstration for a general form of the spectral density, and this is the subject of work in progress. However, we do not see how to avoid the restriction to the rare transitions limit in our derivation. Furthermore, we do not know how to generalize the identities (6.33), which we have used in our proof, for the case of time-dependent driving. These remain open questions.

6.3 Discussion

Let us now give some interpretation of the results. The duality relation (6.22) for the generating function is not very useful in itself, but very powerful in order to generate useful results. It links the dynamics of the two systems (6.1) and (6.29). The precise relation between the two systems is specified by: i) The relation (6.16) between the harmonics of the potential of the original system and the couplings in the

tight-binding system (see also Fig. 6.1); ii) The relation (6.25) between the spatial periodicities L of the original system, and $\tilde{L}$ of the tight-binding system; iii) The relation (6.28) between the spectral densities of the baths of harmonics oscillators coupled to each of the two systems. In the original system, the relevant dynamical parameters are captured by the dissipation parameter $\alpha = \eta L^2/2\pi\hbar$ and the energy drop per periodicity length $\epsilon = FL$. Due to the change of periodicity length, these parameters become $\tilde{\alpha} = 1/\alpha$ and $\tilde{\epsilon} = \epsilon/\alpha$ in the tight-binding system. Thus, weak dissipation in one system maps to strong dissipation in the other one, although the viscosity η in the spectral density does not change.

The duality relation for the average position (6.34) is an example of a useful result which can be extracted from (6.22). There, the relation between the average positions $\langle \hat{q}(t) \rangle$ and $\langle \hat{q}_{\mathrm{TB}}(t) \rangle_{\mathrm{TB}}$ in the two systems, which holds at long time, is explicit. The asymptotic dynamics covered by this result is usually described in terms of the nonlinear mobility $\mu = \lim_{t\to\infty} \langle \dot{\hat{q}}(t) \rangle/F$. Accordingly, the duality relation (6.34) may be rewritten in the form

$$\mu(\alpha, \epsilon) \sim \mu_0 - \mu_{\mathrm{TB}}(1/\alpha, \epsilon/\alpha), \qquad (6.35)$$

where $\mu_0 = 1/\eta$ is the mobility of a free system, characterized by $V(\hat{q}) \equiv 0$. In the special case of a sinusoidal potential, this relation has already been obtained in [1] for the dc mobility. As mentioned above, it has also been derived in [3] for the linear ac mobility in a sinusoidal potential.

The first three terms on the right-hand side of (6.34) reproduce exactly the classical solution for the average position $\langle q(t) \rangle$ of the free system, $V(q) \equiv 0$, at long times. In this linear case, the quantum and classical solutions should be identical, due to Ehrenfest's theorem, and they are, because the tight-binding average $\langle \hat{q}_{\mathrm{TB}}(t) \rangle_{\mathrm{TB}}$ vanishes in the absence of the potential $V(q)$. We expect the same result when the potential is present but unimportant, e.g., for large driving F and/or high temperatures T. This behavior can be observed in Fig. 6.2.

The second derivative of the generating function $\tilde{P}(\lambda, t)$ with respect to its parameter λ yields the variance $\langle \hat{q}^2(t) \rangle$, which gives information about diffusion and current noise. It would thus be natural to try to extract from (6.22) a duality relation for this quantity. However, the result diverges, because the quantity $\dot{N}(t_0)$ involved in the right-hand side diverges for the strictly Ohmic spectral density $J(\omega) = \eta\omega$ considered in the derivation. In order to get results on diffusion and current noise, we will thus have to go beyond this approximation and allow for an Ohmic bath with finite cutoff frequency. As mentioned above, we do not see any problem of principle in order to generalize our demonstration to this situation. This is the subject of work in progress.

6.4 Application: Evaluation of the ratchet current

In this section, we will discuss the application of (6.34) to evaluate the current in ratchet systems. By time-differentiation of $\langle \hat{q}(t) \rangle$, given on the left-hand side of (6.34), one obtains the stationary velocity $v_{\text{DC}}^{\infty}(F)$ in the biased situation of time-independent driving F represented by the system (6.1). As discussed above, the ratchet current in the presence of unbiased bistable driving switching adiabatically between the values $\pm F$ is obtained through the relation

$$v_{\text{R}}^{\infty}(F) = v_{\text{DC}}^{\infty}(F) + v_{\text{DC}}^{\infty}(-F). \tag{6.36}$$

Our task is thus to evaluate the right-hand side of (6.34), in particular the average of the position operator (6.30) in the driven dissipative tight-binding model (6.29), initially prepared in the state $\hat{\rho}_{\text{TB}}(t_0) = |0\rangle\langle 0|$. It can be obtained from the generating function $\tilde{P}_{\text{TB}}(\lambda, t)$ of the tight-binding system according to Eq. (6.9) with $k = 1$.

The generating function can be obtained from (6.31) with $l_0 = 0$. However, this formula is not the most suitable one in order to get the long-time behavior required in (6.34). Instead, the result

$$\tilde{P}_{\text{TB}}(\lambda, t) \underset{t \gg t_0}{\sim} \exp\left\{ (t - t_0) \sum_{m \neq 0} \Gamma_m \left(e^{\lambda m \tilde{L}} - 1 \right) \right\}, \tag{6.37}$$

developed in Section 5.2, is much more powerful. It involves the transition rates Γ_m from a site $|l\rangle$ to a site $|l + m\rangle$ in the Hamiltonian (6.29), which have been discussed in Chapter 5. From this result we derive easily

$$\langle \hat{q}_{\text{TB}}(t) \rangle \underset{t \gg t_0}{\sim} (t - t_0) \tilde{L} \sum_{m=1}^{\infty} m \Gamma_m^d. \tag{6.38}$$

in terms of the differences of transition rates

$$\Gamma_{|m|}^d \;\hat{=}\; \Gamma_m - \Gamma_{-m}. \tag{6.39}$$

Plugging this in the duality relation (6.34) and differentiating, we obtain the stationary velocity in the original model (6.1), in the presence of a driving force $+F$, respectively $-F$, as

$$v_{\text{DC}}^{\infty}(\pm F) = \pm \frac{F}{\eta} - \tilde{L} \sum_{m=1}^{\infty} m \Gamma_m^d(\pm F), \tag{6.40}$$

in terms of the transition rates $\Gamma_m(F)$, respectively $\Gamma_m(-F)$, in the system (6.29) with $\pm F$. Using (6.36), the ratchet current in the presence of adiabatic bistable driving reads accordingly

$$v_{\text{R}}^{\infty}(F) = -\tilde{L} \sum_{m=1}^{\infty} m \left[\Gamma_m^d(F) + \Gamma_m^d(-F) \right]. \tag{6.41}$$

This result shows that the ratchet current in a system characterized by the potential (6.2) is related to the transition rates in the tight-binding model (6.29) in a very simple way. As the duality relation from which it is derived, it is valid in the rare transitions limit $\Gamma_m(\pm F) \ll \min(\gamma, 2\pi k_B T/\hbar)$ and for a strictly Ohmic bath characterized by the spectral density $J(\omega) = \eta\omega$.

The evaluation of the transition rates for the model (6.29) has been discussed in Chapter 5. The numerous contributions that one obtains can be classified with respect to the number N of coherent transitions which they involve. We have denoted by $\Gamma_m^{(N)}$ the sum of all contributions involving N transitions and called it the Nth-order transition rate. The total rate follows from

$$\Gamma_m(F) = \sum_{N=2}^{\infty} \Gamma_m^{(N)}(F). \tag{6.42}$$

The complexity of the transitions rates increases with the order N. However, in tight-binding models with large dissipation parameter $\tilde{\alpha} = \eta \tilde{L}^2/2\pi\hbar$ and/or high temperature, neglecting higher orders is known to be a good approximation [4]. Besides, we will see that the second-order rates do not yield any contribution to the ratchet current. For these reasons, we will include second-order $N = 2$ and third-order $N = 3$ contributions only in the series (6.42).

In the transition rates obtained from Section 5.3.2, one may replace the couplings Δ_l by their expression (6.16) in terms of the amplitudes V_l and phases φ_l of the original potential (6.2), for the present application. One also has to substitute the periodicity length $\tilde{L}$ and the spectral density $J_{\mathrm{TB}}(\omega)$ of the tight-binding system in these expressions.

At second order, using Eq. (5.36), we find

$$\Gamma_m^{(2)}(F) = \frac{V_m^2}{4\hbar^2} \int_{-\infty}^{\infty} \mathrm{d}\tau e^{-m^2(\tilde{L}^2/\hbar)Q(\tau)+\mathrm{i}m(F\tilde{L}/\hbar)\tau}. \tag{6.43}$$

One immediately verifies that $\Gamma_m^{(2)}(-F) = \Gamma_{-m}^{(2)}(F)$, implying that these second-order rates do not contribute to the ratchet current (6.41).

For the discussion of the third-order rates, we restrict ourselves to the case where the potential (6.2) sustains at most the first three harmonics, meaning that the couplings Δ_m are all 0 for $|m| > 3$. In this situation, there are contributions to the third-order rates for $m = 0, \pm1, \pm2, \pm3$ only, which can be divided into two classes

$$\Gamma_m^{(3)}(F) = \Gamma_m^{(3)}[112](F) + \Gamma_m^{(3)}[123](F), \tag{6.44}$$

as discussed in Section 5.3.2. Rewriting the result (5.40) for the first class in terms of the differences of transition rates (6.39), one has, for $m = +1, +2$,

$$\Gamma_m^{(3),d}[112](F)$$
$$= -\frac{V_1^2 V_2}{\hbar^3} \sin(\varphi_2 - 2\varphi_1) \,\mathrm{Re}\left\{ \int_{-\infty}^{\infty} \mathrm{d}\tau G_m^{(3)}[112](\tau) \cos\left(m(F\tilde{L}/\hbar)\tau\right) \right\}, \tag{6.45}$$

with the functions $G_m^{(3)}[112](\tau)$ extracted from (5.41). For the second class (5.44), one obtains likewise, for $m = +1, +2, +3$,

$$
\begin{aligned}
\Gamma_m^{(3),d}&[123](F) \\
&= -\frac{V_1 V_2 V_3}{\hbar^3} \sin(\varphi_3 - \varphi_2 - \varphi_1) \,\mathrm{Re} \left\{ \int_{-\infty}^{\infty} \mathrm{d}\tau \, G_m^{(3)}[123](\tau) \cos\left(m(F\tilde{L}/\hbar)\tau \right) \right\},
\end{aligned}
\tag{6.46}
$$

in terms the functions $G_m^{(3)}[123](\tau)$ extracted from (5.45).

Thus, one sees that the third-order contributions to the ratchet current, which are the dominant ones, are proportional to $\sin(\varphi_2 - 2\varphi_1)$ or $\sin(\varphi_3 - \varphi_2 - \varphi_1)$. Therefore, they vanish for spatially symmetric potentials, characterized by the conditions (6.3).

The simple dependence of these transition rates on the potential parameters, which reflects itself in the stationary velocity $v_{\mathrm{DC}}^{\infty}(F)$ and ratchet current $v_{\mathrm{R}}^{\infty}(F)$, should be accessible in experimental realizations where the potential can be tailored, such as, e.g., the arrays of Josephson junctions which have been discussed in Chapter 2.

Another interesting information can be extracted from the second-order rates (6.43), which are the dominant contributions to the stationary velocity of the tight-binding system, or alternatively its mobility μ_{TB}. At zero bias $F = 0$ and in the scaling limit $\hbar\gamma \gg k_{\mathrm{B}}T$, these rates show a power-law dependence on temperature $\Gamma_m^{(2)} \propto T^{2m^2\tilde{\alpha}-1}$. The linear mobility μ_{TB} is thus dominated by the rate $\Gamma_1^{(2)}$ at low temperatures, and vanishes at $T = 0$ for $\alpha < 1$ ($\tilde{\alpha} > 1$), which corresponds to free dynamics $\mu = \mu_0$ in the dual weak-binding system, using the duality relation Eq. (6.35). We notice that, due to the behavior of the rates, the validity condition $\Gamma_m \ll \min(\gamma, 2\pi k_{\mathrm{B}}T/\hbar)$ of the duality relation can hold down to $T = 0$ for $\alpha < 1$. This suggests that the occurrence of a delocalization to localization transition at $\alpha = 1$ for the ground-state of a cosine potential [1, 5, 6] would not be affected in more general potentials.

Finally, we discuss the behavior of the stationary velocity (6.40) and ratchet current (6.41) as a function of the driving amplitude and the temperature, for a potential sustaining two harmonics only. The rates are evaluated up to third order, using the expressions (6.43) and (6.45). The outcome is shown in Fig. 6.2. With $V_1 = 4V_2$, the untilted potential, depicted in Fig. 6.1, has a barrier height $\Delta V = 2.2V_1$. We choose $\alpha = 0.2$ and $\hbar\gamma = 0.76\Delta V$. It means that the typical action is $\sqrt{2M\Delta V L^2} \approx 2\hbar$, and the dissipation rate $\gamma = \eta/M$ is about one fourth of the classical oscillation frequency $\Omega_0 = 2\pi\sqrt{V_1/ML^2}$ in the untilted potential, which corresponds to a situation of weak dissipation. In this numerical application, none of the rates exceeds 0.05γ and $0.08\omega_{\mathrm{B}}$, which means that the duality relation is valid for this system. Moreover, the third-order rates stay at least one order of magnitude below the second-order ones.
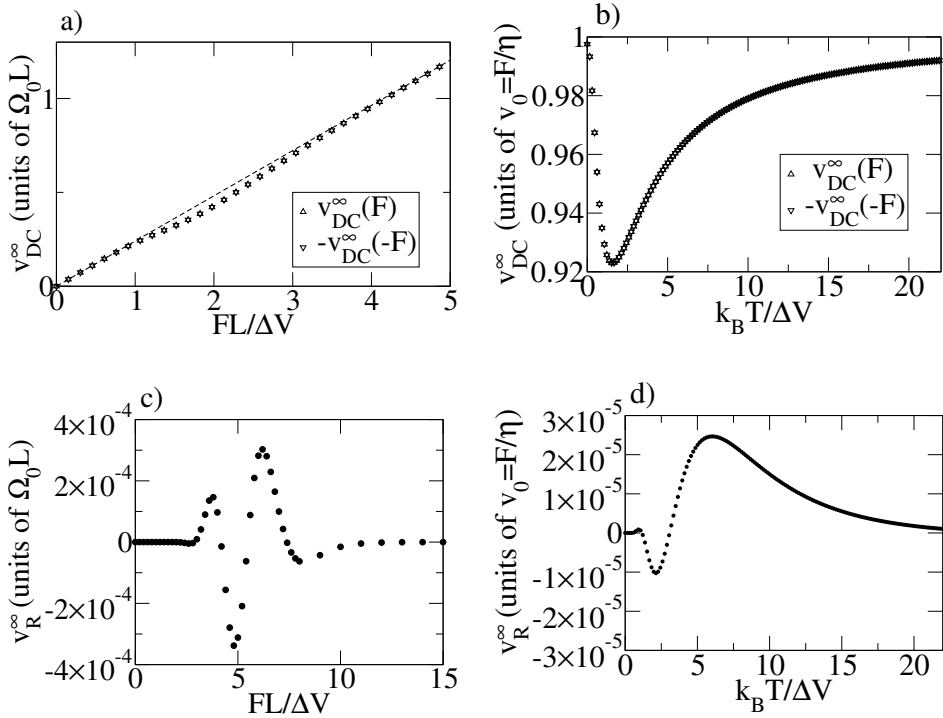
Figure 6.2: Stationary velocity (a,b) and ratchet current (c,d) as a function of the driving force (a,c) and the temperature (b,d) for the potential of amplitude ΔV depicted in Fig. 6.1. Weak dissipation is chosen with $\alpha = 0.2$ and $\hbar\gamma = 0.76\Delta V$. In (a) and (c), the temperature is fixed to $k_B T = 0.076\Delta V$, whereas in (b) and (d), the driving amplitude is set to $FL = 0.57\Delta V$. The dashed line in (a) is the classical solution in the absence of potential.

First, one observes that the ratchet current presents several reversals as a function both of the driving amplitude and the temperature.

As expected for the small values of driving and dissipation used in Fig. 6.2b, the stationary velocity is very close to the value of a free system $v_0 = F/\eta$ at $T = 0$, which corresponds to localization $v_{\mathrm{TB}}^\infty \approx 0$ in the tight-binding system. Accordingly $v_{\mathrm{R}}^\infty \approx 0$ in this regime. We obtain the opposite behavior $v_{\mathrm{TB}} \to \infty$ at low temperatures for $\alpha = 1.26$. A more detailed discussion of the behavior of the stationary velocity and ratchet current as a function of the dissipation can be found in [7].

The stationary velocity also tends to v_0 (dashed line in Fig. 6.2a) for driving amplitudes or temperatures much higher than the potential barrier, and the ratchet

current vanishes correspondingly. If observed in experiments, this linear behavior $v_{\text{DC}}^\infty(F) \sim F/\eta$ would provide a direct estimation of the dissipation strength.

Finally, let us give an order of magnitude of the scale of this curves, translated in terms of the $V(I)$ characteristics in the experiment on vortices in arrays of Josephson junctions which has been presented in Chapter 2. For a typical potential barrier $\Delta V \approx 150\ \mu\text{eV}$, and the situation of the sample III described in that chapter, a driving force given by $FL = \Delta V$ corresponds to a current $I \approx 1\ \mu\text{A}$, whereas a velocity $v = \Omega_0 L$ yields a voltage $V \approx 400\ \mu\text{V}$. The choice $\hbar\gamma = 0.76\Delta V$, which fixes the slope of the asymptotic behavior in Fig. 6.2a (dashed line), yields $\gamma \approx 170$ GHz, which corresponds to a normal-state resistance of $R_{\text{n}} \approx 6$ kΩ for the Josephson junctions [see below Eq. (2.29)]. These are realistic orders of magnitude.

6.5 Proofs

6.5.1 Expansion of the potential

First, we will demonstrate how the expansion (6.17) of the potential leads to the series expression (6.18). Using the power series representation of the exponential function, we write

$$\exp\left\{-\frac{\mathrm{i}}{\hbar}\int_{t_0}^t \mathrm{d}t'\,V(q(t'))\right\} = \sum_{n=0}^\infty \int_{t_0}^t \mathrm{d}t_n \int_{t_0}^{t_n} \mathrm{d}t_{n-1}\ldots\int_{t_0}^{t_2}\mathrm{d}t_1 \prod_{j=1}^n\left[-\frac{\mathrm{i}}{\hbar}V(q(t_j))\right]. \tag{6.47}$$

Due to the complete symmetry of the integrand in all the t_j, the n integrals have been entangled, compensating the $1/n!$ factor coming from the series expansion. We now take advantage of the representation (6.17) of the potential as a sum, introducing a charge σ_j and amplitudes Δ_{σ_j} for each term $V(q(t_j))$. For the product involved in (6.47), this yields the expression

$$\prod_{j=1}^n\left[-\frac{\mathrm{i}}{\hbar}V(q(t_j))\right] = \prod_{j=1}^n\left[-\frac{\mathrm{i}}{\hbar}\sum_{\sigma_j=\pm1,\pm2,\ldots}\Delta_{\sigma_j}e^{-2\pi\mathrm{i}\sigma_j q(t_j)/L}\right]. \tag{6.48}$$

By distributivity, product and sum can be exchanged, yielding a sum over configurations

$$\sum_{\{\sigma_j\}} \hat{=} \sum_{\sigma_1=\pm1,\pm2,\ldots}\cdots\sum_{\sigma_n=\pm1,\pm2,\ldots}, \tag{6.49}$$

which allows to write

$$\prod_{j=1}^n\left[-\frac{\mathrm{i}}{\hbar}V(q(t_j))\right] = \sum_{\{\sigma_j\}}\prod_{j=1}^n\left(-\frac{\mathrm{i}\Delta_{\sigma_j}}{\hbar}\right)\exp\left\{-\frac{2\pi\mathrm{i}}{L}\sum_{j=1}^n\sigma_j q(t_j)\right\}. \tag{6.50}$$

With the help of the function $\rho(t')$ introduced in (6.19), this can be rewritten in terms of the path $q(t')$

$$\prod_{j=1}^{n}\left[-\frac{i}{\hbar}V(q(t_j))\right] = \sum_{\{\sigma_j\}}\prod_{j=1}^{n}\left(-\frac{i\Delta_{\sigma_j}}{\hbar}\right)\exp\left\{-\frac{i}{\hbar}\int_{t_0}^{t}dt'\rho(t')q(t')\right\}. \qquad (6.51)$$

Substituting this expression in (6.47) demonstrates (6.18).

6.5.2   Evaluation of the path integrals

We now turn to the evaluation of the path integrals. We start from the expression for the propagating function (6.11). We rewrite the path integrals, defined in (6.12), in terms of the difference $\xi(t')$ and average path $\chi(t')$, introduced in (6.14). The Jacobian of this transformation is 1, therefore each pair of integrals $\int dq_k \int dq'_k$ can be replaced by $\int d\xi_k \int d\chi_k$, which we denote by replacing $\int \mathcal{D}q \int \mathcal{D}^*q'$ by $\int \mathcal{D}\xi \int \mathcal{D}^*\chi$. With this notation, the boundary conditions read $\xi_i = q_i - q'_i$, $\chi_i = (q_i + q'_i)/2$, $\xi_f = q_f - q'_f$, and $\chi_f = (q_f + q'_f)/2$. Collecting the expressions (6.15) and (6.20), we have

$$G(q_f, q'_f, q_i, q'_i, t) = \boxed{\sum} \int_{\xi_i}^{\xi_f}\mathcal{D}\xi\int_{\chi_i}^{\chi_f}\mathcal{D}^*\chi\exp\Bigg\{-S_R[\xi]-iS_I[\xi]+\frac{iF}{\hbar}\int_{t_0}^{t}dt'\xi(t')$$
$$+\frac{i}{\hbar}\int_{t_0}^{t}dt'\chi(t')\left[-M\ddot{\xi}(t')+\eta\dot{\xi}(t')-[\rho(t')-\rho'(t')]\right]$$
$$+\frac{iM}{\hbar}\left[\dot{\xi}(t)\chi_f-\dot{\xi}(t_0)\chi_i\right]+\frac{i\eta}{\hbar}\left[-\xi_f\chi_f+\xi_i\chi_i+\frac{1}{2}\xi_i^2\right]\Bigg\}, \quad (6.52)$$

with the definitions

$$S_R[\xi] = \frac{1}{\hbar}\int_{t_0}^{t}dt'\int_{t_0}^{t'}dt''\xi(t')L_R(t'-t'')\xi(t'') \qquad (6.53a)$$

$$S_I[\xi] = \frac{1}{\hbar}\int_{t_0}^{t}dt'\xi(t')\frac{1}{2}\left[\rho(t')+\rho'(t')\right]. \qquad (6.53b)$$

For the imaginary part of the integrated bath correlation function $M_I(\tau)$ (see Appendix B), we have made use of the simple form $M_I(\tau) = \eta\delta(\tau)$ assumed in the case of a strictly Ohmic bath, characterized by the spectral density $J(\omega) = \eta\omega$, that is without cutoff frequency. We also have performed a partial integration in order to remove the dependence on the derivative $\dot{\chi}(t')$ of the average path.

We discretize the paths according to the procedure described below Eq. (6.12). The integrals in the argument of the exponential are discretized as in the following

example

$$\int_{t_0}^{t} \mathrm{d}t' \chi(t') \left[-M\ddot{\xi}(t') + \eta\dot{\xi}(t') - [\rho(t') - \rho'(t')] \right]$$

$$= \sum_{k=0}^{N_{\mathrm{I}}-1} \Delta\tau \chi_k \left[-M\ddot{\xi}_k + \eta\dot{\xi}_k - [\rho_k - \rho'_k] \right], \quad (6.54)$$

and we evaluate the derivatives of the path $\xi(t')$ with the difference formulae

$$\dot{\xi}_k = \frac{\xi_{k+1} - \xi_k}{\Delta\tau} \tag{6.55a}$$

$$\ddot{\xi}_k = \frac{\xi_{k+1} - 2\xi_k + \xi_{k-1}}{\Delta\tau^2}. \tag{6.55b}$$

The terms involving χ_k form the integral

$$\int \mathrm{d}\chi_k \exp\left\{ \frac{\mathrm{i}}{\hbar} \chi_k \left[-M\ddot{\xi}_k + \eta\dot{\xi}_k - [\rho_k - \rho'_k] \right] \right\}$$

$$= 2\pi\delta\left(\frac{\mathrm{i}}{\hbar} \chi_k \left[-M\ddot{\xi}_k + \eta\dot{\xi}_k - [\rho_k - \rho'_k] \right] \right). \quad (6.56)$$

This δ-function allows to suppress the integral over ξ_k. The process is repeated for all values of $k = 1, \ldots, N_{\mathrm{I}} - 1$. Some care has to be taken with the prefactor of ξ_k in the argument of the δ-function, which will come as a denominator in front of the expression, and with the behavior of the path $\xi(t')$ and its derivatives at the boundaries. One already sees that the result of the whole process, in the limit $N_{\mathrm{I}} \to \infty$, is that the path $\xi(t')$ will be constrained to follow the solution $y(t')$ of the differential equation

$$-M\ddot{y}(t') + \eta\dot{y}(t') = \rho(t') - \rho'(t'), \tag{6.57}$$

with boundary conditions

$$y(t_0) = \xi_i, \qquad\qquad y(t) = \xi_f. \tag{6.58}$$

After having performed all integrals and taken the limit $N_{\mathrm{I}} \to \infty$, we obtain

$$G(q_f, q'_f, q_i, q'_i, t) = \frac{\eta}{2\pi\hbar(1-\varepsilon)} \boxed{\sum} \exp\left\{ -S_{\mathrm{R}}[y] - \mathrm{i}S_{\mathrm{I}}[y] + \frac{\mathrm{i}F}{\hbar} \int_{t_0}^{t} \mathrm{d}t' y(t') \right.$$

$$\left. + \frac{\mathrm{i}M}{\hbar} [\dot{y}(t)\chi_f - \dot{y}(t_0)\chi_i] + \frac{\mathrm{i}\eta}{\hbar} \left[-\xi_f\chi_f + \xi_i\chi_i + \frac{1}{2}\xi_i^2 \right] \right\}, \quad (6.59)$$

with the notation $\varepsilon = \mathrm{e}^{-\gamma(t-t_0)}$. The solution of the differential equation (6.57) with boundary conditions (6.58) can be written as $y(t') = y_{\mathrm{hom}}(t') + y_{\mathrm{part}}(t')$, in terms of a solution of the associated homogeneous differential equation

$$y_{\mathrm{hom}}(t') = \frac{\xi_i}{1-\varepsilon} \left[1 - e^{-\gamma(t-t')} \right] + \frac{\xi_f\varepsilon}{1-\varepsilon} \left[e^{\gamma(t'-t_0)} - 1 \right], \tag{6.60}$$

satisfying the boundary conditions $y_{\text{hom}}(t_0) = \xi_i$ and $y_{\text{hom}}(t) = \xi_f$, and a particular solution of the differential equation

$$
\begin{aligned}
y_{\text{part}}(t') =& \tilde{L} \sum_{j=1}^{n} \sigma_j \left[\theta(t' - t_j) \left[1 - e^{\gamma(t'-t_j)} \right] + \frac{[\varepsilon - e^{-\gamma(t_j - t_0)}][1 - e^{\gamma(t'-t_0)}]}{1 - \varepsilon} \right] \\
&- \tilde{L} \sum_{j'=1}^{n'} \sigma'_{j'} \left[\theta(t' - t'_{j'}) \left[1 - e^{\gamma(t'-t'_{j'})} \right] + \frac{[\varepsilon - e^{-\gamma(t'_{j'} - t_0)}][1 - e^{\gamma(t'-t_0)}]}{1 - \varepsilon} \right],
\end{aligned}
\tag{6.61}
$$

satisfying the boundary conditions $y_{\text{part}}(t_0) = y_{\text{part}}(t) = 0$. The periodicity length of the tight-binding model $\tilde{L} = 2\pi\hbar/\eta L$ comes into play at this stage. The derivatives of these paths at the boundaries

$$
\dot{y}_{\text{hom}}(t_0) = \frac{\gamma\varepsilon(\xi_f - \xi_i)}{1 - \varepsilon}, \qquad\qquad \dot{y}_{\text{hom}}(t) = \frac{\gamma(\xi_f - \xi_i)}{1 - \varepsilon}, \tag{6.62a}
$$

$$
\dot{y}_{\text{part}}(t_0) = \frac{\gamma(\Delta\xi_{\text{e}} - \varepsilon\Delta\xi)}{1 - \varepsilon}, \qquad\qquad \dot{y}_{\text{part}}(t) = \frac{\gamma(\Delta\xi_{\text{e}} - \Delta\xi)}{1 - \varepsilon}, \tag{6.62b}
$$

involve the quantity $\Delta\xi$ introduced in (6.26b), as well as

$$
\Delta\xi_{\text{e}} \;\hat{=}\; \tilde{L} \left[\sum_{j=1}^{n} \sigma_j e^{-\gamma(t_j - t_0)} - \sum_{j'=1}^{n'} \sigma'_{j'} e^{-\gamma(t'_{j'} - t_0)} \right]. \tag{6.63}
$$

6.5.3   Evaluation of the generating function

The result (6.59) for the propagating function can now be used to obtain the generating function (6.7). One has first to evaluate the integral $\int \mathrm{d}q e^{\lambda q} G(q, q, q_i, q'_i, t)$. Again, it will yield a δ-function for ξ_i, coming from

$$
\int \mathrm{d}q \exp\left\{ q \left[\frac{\mathrm{i}M}{\hbar} \dot{y}(t) + \lambda \right] \right\} = \frac{2\pi\hbar(1 - \varepsilon)}{\eta} \delta\left(\xi_i - \Delta\xi_{\text{e}} + \Delta\xi + \frac{\mathrm{i}\hbar(1 - \varepsilon)}{\eta}\lambda \right). \tag{6.64}
$$

The generating function reads then, after transforming the variables q_i and q'_i of the initial integrals into ξ_i and χ_i,

$$
\begin{aligned}
\tilde{P}(\lambda, t) = \boxed{\sum} \int \mathrm{d}\xi_i \delta\left(\xi_i - \Delta\xi_{\text{e}} + \Delta\xi + \frac{\mathrm{i}\hbar(1 - \varepsilon)}{\eta}\lambda \right) \\
\times \exp\left\{ -S_{\text{R}}[y] - \mathrm{i}S_{\text{I}}[y] + \frac{\mathrm{i}F}{\hbar} \int_{t_0}^{t} \mathrm{d}t' y(t') + \frac{\mathrm{i}\eta}{2\hbar}\xi_i^2 \right\} \\
\times \int \mathrm{d}\chi_i \langle \chi_i + \xi_i/2 | \hat{\rho}(t_0) | \chi_i - \xi_i/2 \rangle \exp\left\{ -\frac{\mathrm{i}M}{\hbar}\dot{y}(t_0)\chi_i + \frac{\mathrm{i}\eta}{\hbar}\xi_i\chi_i \right\}. \quad (6.65)
\end{aligned}
$$

In the position representation, an integral of the form $\int \mathrm{d}\chi_i \langle \chi_i | \cdot | \chi_i \rangle$ is a trace $\mathrm{Tr_S}\{\cdot\}$ over the system degree of freedom. With the help of the eigenstates of the momentum operator, which are described by the wave-function $\langle q | p \rangle = \mathrm{e}^{\mathrm{i}qp/\hbar}/\sqrt{2\pi\hbar}$, the expectation value in the last term of (6.65) may be rewritten as

$$\langle \chi_i + \xi_i/2 | \hat{\rho}(t_0) | \chi_i - \xi_i/2 \rangle = \langle \chi_i | e^{\mathrm{i}\xi_i \hat{p}/2\hbar} \hat{\rho}(t_0) e^{-\mathrm{i}\xi_i \hat{p}/2\hbar} | \chi_i \rangle, \qquad (6.66)$$

in terms of the momentum operator of the system. Combining with the exponential factor, using the cyclicity of the trace, the Baker-Campbell-Hausdorff formula for the product of exponentials of operators (see, e.g., [2, Ch. 2]), and the commutation relation of the position and momentum operators $[\hat{q}, \hat{p}] = \mathrm{i}\hbar \hat{1}$, one obtains the compact expression

$$\int \mathrm{d}\chi_i \langle \chi_i + \xi_i/2 | \hat{\rho}(t_0) | \chi_i - \xi_i/2 \rangle \exp\left\{ -\frac{\mathrm{i}M}{\hbar} \dot{y}(t_0)\chi_i + \frac{\mathrm{i}\eta}{\hbar} \xi_i \chi_i \right\}$$
$$= \mathrm{Tr_S}\left\{ \hat{\rho}(t_0) \exp\left[\frac{-\mathrm{i}M\dot{y}(t_0) + \mathrm{i}\eta\xi_i}{\hbar} \hat{q} + \frac{\mathrm{i}\xi_i}{\hbar} \hat{p} \right] \right\}. \quad (6.67)$$

In Eq. (6.65), the integral over ξ_i can be removed, provided that one substitutes ξ_i everywhere in the integrand by the value given in the argument of the δ-function. In the path $y(t')$, this substitution yields

$$y(t')|_{\xi_i = -\Delta\xi + \Delta\xi_\mathrm{e} - \mathrm{i}\hbar(1-\varepsilon)\lambda/\eta} = y_{\mathrm{sm},\lambda}(t'), \qquad (6.68)$$

with the definition

$$y_{\mathrm{sm},\lambda}(t') \,\hat{=}\, -\frac{\mathrm{i}\hbar\lambda}{\eta} \left[1 - \mathrm{e}^{-\gamma(t-t')} \right] + y_{\mathrm{sm}}(t'). \qquad (6.69)$$

The path $y_{\mathrm{sm}}(t') = y_{\mathrm{sm},\lambda=0}(t')$ assumes the expression

$$y_{\mathrm{sm}}(t') = \tilde{L} \sum_{j=1}^{n} \sigma_j \left[\theta(t' - t_j) - 1 \right] \left[1 - \mathrm{e}^{\gamma(t'-t_j)} \right]$$
$$- \tilde{L} \sum_{j'=1}^{n'} \sigma'_{j'} \left[\theta(t' - t'_{j'}) - 1 \right] \left[1 - \mathrm{e}^{\gamma(t'-t'_{j'})} \right], \quad (6.70)$$

which has the boundary conditions

$$y_{\mathrm{sm}}(t_0) = -\Delta\xi + \Delta\xi_\mathrm{e}, \qquad\qquad y_{\mathrm{sm}}(t) = 0, \qquad (6.71\mathrm{a})$$
$$\dot{y}_{\mathrm{sm}}(t_0) = \gamma\Delta\xi_\mathrm{e}, \qquad\qquad\qquad \dot{y}_{\mathrm{sm}}(t) = 0. \qquad (6.71\mathrm{b})$$

The index sm stands for smeared, because $y_{\mathrm{sm}}(t')$ is a step-like path whose edges are smeared on a scale $1/\gamma$, as one can see on an example drawn in Fig. 6.3a. Collecting
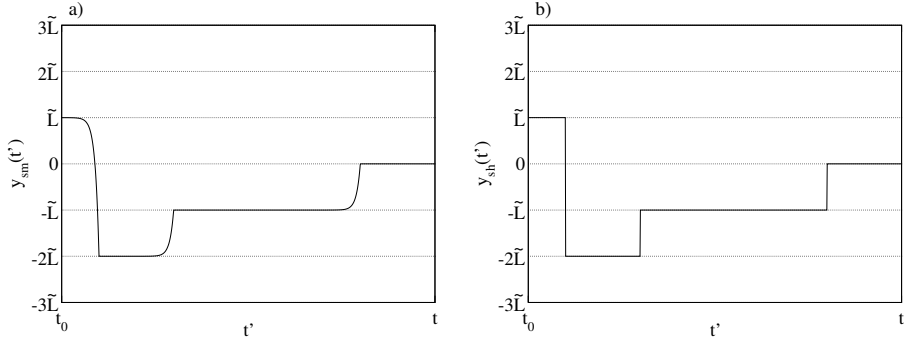
Figure 6.3: Typical smeared path $y_{\mathrm{sm}}(t')$ (left) and sharp path $y_{\mathrm{sh}}(t')$ (right), as defined in Eq. (6.70), respectively Eq. (6.23a). The height of the steps are multiples of $\tilde{L}$ and the edges of $y_{\mathrm{sm}}(t')$ are smeared on a scale $1/\gamma$.

everything, one obtains the intermediate result

$$
\begin{aligned}
\tilde{P}(\lambda, t) & \\
= \boxed{\sum} \mathrm{Tr}_{\mathrm{R}} & \left\{ \hat{\rho}(t_0) \exp\left[\left(-\frac{\mathrm{i}\eta}{\hbar}\Delta\xi + \lambda \right)\hat{q} + \left(-\frac{\mathrm{i}\eta}{\hbar}(\Delta\xi - \Delta\xi_{\mathrm{e}}) + (1-\varepsilon)\lambda \right)\frac{\hat{p}}{\eta} \right] \right\} \\
& \times \exp\left\{ -S_{\mathrm{R}}[y_{\mathrm{sm},\lambda}] - \mathrm{i}S_{\mathrm{I}}[y_{\mathrm{sm},\lambda}] + \frac{\mathrm{i}F}{\hbar}\int_{t_0}^{t}\mathrm{d}t'\, y_{\mathrm{sm},\lambda}(t') \right. \\
& \left. + \frac{\mathrm{i}\eta}{2\hbar}\left[-\Delta\xi + \Delta\xi_{\mathrm{e}} - \frac{\mathrm{i}\hbar(1-\varepsilon)}{\eta}\lambda \right]^2 \right\}. \quad (6.72)
\end{aligned}
$$

6.5.4   Identification with a tight-binding expression

The following task is to rewrite the generating function (6.72) in terms of the sharp path $y_{\mathrm{sh}}(t')$ defined in (6.23a) and represented in Fig. 6.3b. The easiest way to understand the mechanism of this transformation is to work in Fourier representation. Technically, because these paths are defined in the time interval $[t_0, t]$ only, one has first to continue them in the whole time axis by defining

$$
\bar{y}(t') \,\hat{=}\, [\theta(t' - t_0) - \theta(t' - t)]y(t'), \quad (6.73)
$$

in order to be able to use the usual Fourier transform

$$
\tilde{y}(\omega) \,\hat{=}\, \int_{-\infty}^{\infty}\mathrm{d}t'\, \bar{y}(t')\mathrm{e}^{-\mathrm{i}\omega(t' - t_0)}, \quad (6.74)
$$

and take full advantage of the usual differentiation and convolution properties. One can then demonstrate the relation

$$\tilde{y}_{\mathrm{sm},\lambda}(\omega) = \frac{\mathrm{i}\gamma}{\omega + \mathrm{i}\gamma}\left[\tilde{y}_{\mathrm{sh},\lambda}(\omega) + \frac{\Delta\xi - \Delta\xi_{\mathrm{e}}}{\gamma}\right], \qquad (6.75)$$

with the definition

$$\bar{y}_{\mathrm{sh},\lambda}(t') = -\frac{\mathrm{i}\hbar\lambda}{\eta}\left[\theta(t' - t_0) - \theta(t' - t) - \delta(t' - t_0)\frac{1 - \varepsilon}{\gamma}\right] + \bar{y}_{\mathrm{sh}}(t'). \qquad (6.76)$$

This can be done by considering the differential equation (6.57) in Fourier representation. This relation means that, up to a boundary term, the Fourier transform of the smeared and sharp paths are related by a factor $\mathrm{i}\gamma/(\omega + \mathrm{i}\gamma)$. Let us also write the real part of the influence phase $S_{\mathrm{R}}[y_{\mathrm{sm}}]$ in Fourier representation

$$S_{\mathrm{R}}[y_{\mathrm{sm}}] = \frac{1}{2\pi\hbar}\int_0^{\infty}\mathrm{d}\omega\, J(\omega)\coth\left(\hbar\omega\beta/2\right)\tilde{y}_{\mathrm{sm}}(\omega)\tilde{y}_{\mathrm{sm}}(-\omega). \qquad (6.77)$$

It can be rewritten in terms of $\tilde{y}_{\mathrm{sh}}(\omega)$ by reabsorbing the factors in a redefinition of the spectral density as in (6.28). This will additionally yield two boundary terms.

In order to rewrite the other terms of (6.72) in terms of the sharp path, it is more convenient to rewrite relation (6.75) in time domain

$$\bar{y}_{\mathrm{sm},\lambda}(t') = \int_{t'}^{\infty}\mathrm{d}t''\mathrm{e}^{\gamma(t' - t'')}\left[\gamma\bar{y}_{\mathrm{sh},\lambda}(t'') + (\Delta\xi - \Delta\xi_{\mathrm{e}})\delta(t'' - t_0)\right]. \qquad (6.78)$$

Collecting all terms, we get the still exact result

$$\begin{aligned}
&\tilde{P}(\lambda, t) \\
&= \boxed{\sum}\mathrm{Tr}_{\mathrm{R}}\left\{\hat{\rho}(t_0)\exp\left[\left(-\frac{\mathrm{i}\eta}{\hbar}\Delta\xi + \lambda\right)\hat{q} + \left(-\frac{\mathrm{i}\eta}{\hbar}(\Delta\xi - \Delta\xi_{\mathrm{e}}) + (1 - \varepsilon)\lambda\right)\frac{\hat{p}}{\eta}\right]\right\} \\
&\quad\times\exp\left\{\Phi_{\mathrm{FV}}^{\mathrm{TB}}[y_{\mathrm{sh},\lambda}, x_{\mathrm{sh}}, t] + \frac{\mathrm{i}F}{\hbar}\int_{-\infty}^{\infty}\mathrm{d}t'\bar{y}_{\mathrm{sh},\lambda}(t')\right. \\
&\quad - \frac{\Delta\xi - \Delta\xi_{\mathrm{e}}}{\hbar\gamma}\int_{-\infty}^{\infty}\mathrm{d}t'\bar{y}_{\mathrm{sh},\lambda}(t')L_{\mathrm{R}}^{\mathrm{TB}}(t' - t_0) - \frac{(\Delta\xi - \Delta\xi_{\mathrm{e}})^2}{2\hbar\gamma^2}L_{\mathrm{R}}^{\mathrm{TB}}(0) \\
&\quad\left. + \frac{\mathrm{i}F(\Delta\xi - \Delta\xi_{\mathrm{e}})}{\hbar\gamma} + \frac{\mathrm{i}\eta}{2\hbar}\left[-\Delta\xi + \Delta\xi_{\mathrm{e}} - \frac{\mathrm{i}\hbar(1 - \varepsilon)}{\eta}\lambda\right]^2\right\}. \qquad (6.79)
\end{aligned}$$

The influence phase $\Phi_{\mathrm{FV}}^{\mathrm{TB}}[y_{\mathrm{sh},\lambda}, x_{\mathrm{sh}}, t]$ is defined as in (6.15), with the correlation functions $L^{\mathrm{TB}}(\tau)$ and $M_{\mathrm{I}}^{\mathrm{TB}}(\tau)$ defined in terms of the new spectral density $J_{\mathrm{TB}}(\omega)$ given in (6.28). The average path $x_{\mathrm{sh}}(t')$ has been defined in Eq. (6.23b).

Technically, one can rewrite $\Phi_{\mathrm{FV}}^{\mathrm{TB}}[y_{\mathrm{sh},\lambda}, x_{\mathrm{sh}}, t]$ in terms of the extended path $\bar{y}_{\mathrm{sh},\lambda}(t')$ by substituting everywhere $\bar{y}_{\mathrm{sh},\lambda}(t')$ for $y_{\mathrm{sh},\lambda}(t')$ and extending the

corresponding integrals to the whole real axis. This applies to both integrals in the real part, yielding a prefactor $1/2$, and to the integrals over t' in the imaginary part.

In order to go further, we now have to exploit the simplifications valid in the regime described at the end of Section 6.2. The long-time limit yields $\varepsilon \ll 1$ and the rare transitions limit $\Delta\xi_{\mathrm{e}} \ll \Delta\xi$. Furthermore, one can see that $L_{\mathrm{R}}^{\mathrm{TB}}(0)$ diverges when the cutoff frequency ω_{c} of an Ohmic spectral density $J(\omega) = \eta\omega e^{-\omega/\omega_{\mathrm{c}}}$ tends to infinity, as in the strictly Ohmic case considered here (see Appendix B). Then, in the configuration sum, the contributions of the configurations of $\{\sigma\}$ and $\{\sigma'\}$ for which the prefactor $(\Delta\xi - \Delta\xi_{\mathrm{e}})^2/2\hbar\gamma^2$ of $L_{\mathrm{R}}^{\mathrm{TB}}(0)$ is minimal can be made as large as one will with respect to the contributions of other configurations. Therefore, combining with the rare transitions limit, we can restrict the configuration sum to configurations such that $\Delta\xi = 0$. This restricted sum is denoted with the boxed primed sum introduced in (6.27). Combining these properties, we find the much simpler expression

$$\tilde{P}(\lambda, t) \sim \boxed{\sum}' \mathrm{Tr}_{\mathrm{R}} \left\{ \hat{\rho}(t_0) e^{\lambda(\hat{q} + \hat{p}/\eta)} \right\}$$
$$\times \exp\left\{ \Phi_{\mathrm{FV}}^{\mathrm{TB}}[y_{\mathrm{sh},\lambda}, x_{\mathrm{sh}}, t] + \frac{\mathrm{i}F}{\hbar} \int_{-\infty}^{\infty} \mathrm{d}t' \bar{y}_{\mathrm{sh},\lambda}(t') - \frac{\mathrm{i}\hbar\lambda^2}{2\eta} \right\}. \quad (6.80)$$

This expression resembles already much more the one of a tight-binding generating function (6.31).

6.5.5   Extraction of the λ-dependence

The last task in order to demonstrate (6.22) is to extract explicitly the λ-dependence out of the path $y_{\mathrm{sh},\lambda}(t')$, using (6.76). For the influence phase, we find

$$\Phi_{\mathrm{FV}}^{\mathrm{TB}}[y_{\mathrm{sh},\lambda}, x_{\mathrm{sh}}, t] = \Phi_{\mathrm{FV}}^{\mathrm{TB}}[y_{\mathrm{sh}}, x_{\mathrm{sh}}, t]$$
$$+ \lambda\left[-\frac{\mathrm{i}}{\eta} \int_{t_0}^{t} \mathrm{d}t' y_{\mathrm{sh}}(t') \dot{N}(t') - \Delta\chi + \int_{t_0}^{t} \mathrm{d}t' \dot{x}_{\mathrm{sh}}(t') e^{-\gamma(t-t')} \right]$$
$$+ \frac{\hbar\lambda^2}{2\eta^2}\left[N(t) - \frac{1-\varepsilon}{\gamma} \dot{N}(t_0) \right], \quad (6.81)$$

with the auxiliary function $N(t') = \int_{t_0}^{t'} \mathrm{d}t'' \dot{N}(t'')$ given by

$$\dot{N}(t') = \int_{-\infty}^{\infty} \mathrm{d}t'' \left[\theta(t'' - t_0) - \theta(t'' - t) - \delta(t'' - t_0)\frac{1-\varepsilon}{\gamma} \right] L_{\mathrm{R}}^{\mathrm{TB}}(t' - t''). \quad (6.82)$$

Using the explicit expression of the path $y_{\mathrm{sh}}(t')$ obtained from (6.23a) and the property $y_{\mathrm{sh}}(t_0) = -\Delta\xi = 0$ satisfied by the paths over which the configuration sum

runs, one has

$$-\int_{t_0}^{t} \mathrm{d}t' y_{\mathrm{sh}}(t') \dot{N}(t') = \tilde{L} \left[\sum_{j=1}^{n} \sigma_j N(t_j) - \sum_{j'=1}^{n'} \sigma'_{j'} N(t'_{j'}) \right]. \qquad (6.83)$$

As shown in Appendix B, in the rare transitions limit one has

$$N(t_{\mathrm{tr}}) \sim -\frac{2\eta k_{\mathrm{B}} T}{\hbar} \left[t_{\mathrm{tr}} - t_0 - \frac{1}{\gamma} \right], \qquad (6.84)$$

when t_{tr} equals any of the transition times t_j, $t'_{j'}$. Therefore one may rewrite

$$-\int_{t_0}^{t} \mathrm{d}t' y_{\mathrm{sh}}(t') \dot{N}(t') = \frac{2\eta k_{\mathrm{B}} T}{\hbar} \int_{t_0}^{t} \mathrm{d}t' y_{\mathrm{sh}}(t'). \qquad (6.85)$$

Similarly, the term

$$\int_{t_0}^{t} \mathrm{d}t' \dot{x}_{\mathrm{sh}}(t') \mathrm{e}^{-\gamma(t-t')} = \tilde{L} \left[\sum_{j=1}^{n} \sigma_j \mathrm{e}^{-\gamma(t-t_j)} - \sum_{j'=1}^{n'} \sigma'_{j'} \mathrm{e}^{-\gamma(t-t'_{j'})} \right] \qquad (6.86)$$

is negligible in the rare transitions limit. Finally, for the driving contribution we obtain

$$\frac{\mathrm{i}F}{\hbar} \int_{-\infty}^{\infty} \mathrm{d}t' \bar{y}_{\mathrm{sh},\lambda}(t') = \frac{\mathrm{i}F}{\hbar} \int_{t_0}^{t} \mathrm{d}t' y_{\mathrm{sh}}(t') + \frac{\lambda F}{\eta} \left[t - t_0 - \frac{1-\varepsilon}{\gamma} \right]. \qquad (6.87)$$

The last term in the square brackets may be neglected in the long-time limit. Putting these results in (6.80) completes the proof of the duality relation (6.22).

6.6 Conclusions and outlook

In conclusion, we have developed a method yielding the duality relations (6.22) and (6.34), between the long-time dynamics in a tilted ratchet potential in the presence of dissipation, and the long-time dynamics in a driven dissipative tight-binding model. The formalism has been applied to the evaluation of the stationary velocity (6.40) in the tilted quantum ratchet system, as well as the current (6.41) in the corresponding rocked ratchet system, yielding an expressions in terms of the transition rates in the tight-binding system. In particular, the results show the explicit dependence of the ratchet current on the parameters of the ratchet potential.

This approach allows to investigate quantum ratchet systems in the weak dissipation limit, which is beyond the validity range of many of the other theoretical approaches (see Section 1.2). Weak dissipation is even a favorable situation in our approach. Indeed, the duality relation links a situation of weak dissipation in the original model with strong dissipation in the dual tight-binding model, and vice

versa. Therefore, one is brought to evaluate the tight-binding transition rates in the limit of strong dissipation, where it suffices to consider the lowest orders in the tunneling amplitude.

With respect to the perturbative approach of Ref. [8], the method reported here has the advantage that the nonlinear regime of a large driving force, eventually leading to the classical regime, can be reached. In particular, the linear dependence of the stationary velocity on the driving force in this regime provides a direct measurement of the dissipation strength.

The continuous system considered in this chapter is essentially different from the tight-binding molecular wire investigated in Ref. [9], and may thus apply to different experimental situations.

The results also indicate that the delocalization to localization transition of the ground state as a function of dissipation, put forward in Refs. [1, 5, 6] for a sinusoidal potential, is not affected by higher harmonics of the potential, and it applies thus to any periodic potential.

It is interesting to observe that the duality relation (6.35) for the mobilities has been derived, in Ref. [3], within the frame of linear response but without the restrictions to a strictly Ohmic spectral density of the bath and to the rare transitions limit. A more general duality relation is also obtained beyond adiabatic driving. It would be interesting to better understand the relation between the two approaches. As a first step, we think that the restriction to a strictly Ohmic spectral density is not essential in our derivation. An attempt to relax this condition is the subject of work in progress.

This extension would also allow to evaluate the diffusion coefficient. It can be obtained within our formalism from the duality relation (6.22) between the generating functions of the dual systems, in terms of the diffusion coefficient (5.20) evaluated from the transition rates in the dissipative tight-binding system. However, the resulting expression diverges, due to the absence of a cutoff at high frequencies in the strictly Ohmic bath considered. We think that this unphysical behavior is an artifact which would disappear, e.g., in the presence of an Ohmic bath with a finite cutoff frequency.

References

[1] M. P. A. Fisher and W. Zwerger, Phys. Rev. B **32**, 6190 (1985).

[2] H. Kleinert, *Path Integrals in Quantum Mechanics, Statistics, Polymer Physics, and Financial Markets* (World Scientific, Singapore, 2004), 3rd ed.

[3] M. Sassetti, H. Schomerus, and U. Weiss, Phys. Rev. B **53**, R2914 (1996).

[4] U. Weiss, *Quantum Dissipative Systems* (World Scientific, Singapore, 1999), 2nd ed.

[5] A. Schmid, Phys. Rev. Lett. **51**, 1506 (1983).

[6] F. Guinea, V. Hakim, and A. Muramatsu, Phys. Rev. Lett. **54**, 263 (1985).

[7] J. Peguiron and M. Grifoni, accepted in Chem. Phys.

[8] S. Scheidl and V. M. Vinokur, Phys. Rev. B **65**, 195305 (2002).

[9] J. Lehmann, S. Kohler, P. Hänggi, and A. Nitzan, Phys. Rev. Lett. **88**, 228305 (2002).

Appendix A

Evaluation of the Populations in Tight-Binding Models

We want to evaluate the populations

$$P_\mu(t) = \langle\mu| \operatorname{Tr}_B \hat{W}(t)|\mu\rangle, \tag{A.1}$$

in the tight-binding system given by the Hamiltonian (3.1), coupled to a bath described by the Hamiltonian (3.3). The system-plus-bath density matrix evolves according to (3.7) from the initial expression (3.8) or (3.10), depending on the class of initial preparation considered.

The trace over the N_O bath degrees of freedom can be written in terms of integrals over the bath coordinates x_α, namely $\operatorname{Tr}_B\{\cdot\} = \int d\vec{x}\langle\vec{x}| \cdot |\vec{x}\rangle$, with the shorthand notations $\int d\vec{x} \mathrel{\hat=} \prod_{\alpha=1}^{N_O} \int_{-\infty}^{\infty} dx_\alpha$ and $|\vec{x}\rangle \mathrel{\hat=} |x_1\rangle \otimes |x_2\rangle \otimes \cdots \otimes |x_{N_O}\rangle$. The expression for the populations can be decomposed by inserting the identity obtained from the completeness relation of the $N_O + 1$ dimensional system-plus-bath

$$\hat{1} = \sum_{\mu\in\mathrm{TB}} \int d\vec{x}|\mu, \vec{x}\rangle\langle\mu, \vec{x}| \tag{A.2}$$

between the parts of the density matrix (3.7). As the different set of states $|\mu, \vec{x}\rangle \mathrel{\hat=} |\mu\rangle \otimes |\vec{x}\rangle$ introduced through this procedure correspond to initial and final configurations, we distinguish them with additional subscripts i and f. Altogether, we have

$$P_\mu(t) = \sum_{\mu_i,\mu_i'\in\mathrm{TB}} \int d\vec{x}_i \int d\vec{x}_i' \int d\vec{x}_f$$

$$\times \langle\mu, \vec{x}_f|e^{-\frac{i}{\hbar}\int_{t_0}^t dt' \hat{H}(t')}|\mu_i, \vec{x}_i\rangle\langle\mu_i, \vec{x}_i|\hat{W}(t_0)|\mu_i', \vec{x}_i'\rangle\langle\mu_i', \vec{x}_i'|e^{\frac{i}{\hbar}\int_{t_0}^t dt' \hat{H}(t')}|\mu, \vec{x}_f\rangle. \tag{A.3}$$

We see that the propagator of the system-plus-bath

$$U(\mu_f, \vec{x}_f, t; \mu_i, \vec{x}_i, t_0) \hat{=} \langle \mu_f, \vec{x}_f | e^{-\frac{i}{\hbar} \int_{t_0}^t dt' \hat{H}(t')} | \mu_i, \vec{x}_i \rangle \tag{A.4}$$

comes naturally into play. Indeed, we may rewrite

$$P_\mu(t) = \sum_{\mu_i, \mu_i' \in TB} \int d\vec{x}_i \int d\vec{x}_i' \int d\vec{x}_f$$

$$\times U(\mu, \vec{x}_f, t; \mu_i, \vec{x}_i, t_0) \langle \mu_i, \vec{x}_i | \hat{W}(t_0) | \mu_i', \vec{x}_i' \rangle U^*(\mu, \vec{x}_f, t; \mu_i', \vec{x}_i', t_0). \tag{A.5}$$

With the initial preparations (3.8) or (3.10), the populations read

$$P_\mu(t) = \sum_{\mu_i, \mu_i' \in TB} \int d\vec{x}_i \int d\vec{x}_i' \int d\vec{x}_f$$

$$\times U(\mu, \vec{x}_f, t; \mu_i, \vec{x}_i, t_0) \langle \mu_i | \hat{\rho}(t_0) | \mu_i' \rangle \bar{U}_B(\vec{x}_i, -i\hbar\beta; \vec{x}_i', 0; q_0) U^*(\mu, \vec{x}_f, t; \mu_i', \vec{x}_i', t_0), \tag{A.6}$$

with the initial bath propagator

$$\bar{U}_B(\vec{x}_i, -i\hbar\beta; \vec{x}_i', 0; q_0) \hat{=} \langle \vec{x}_i | e^{-\beta \hat{\bar{H}}_B[q_0]} | \vec{x}_i' \rangle. \tag{A.7}$$

The bar on the Hamiltonian $\hat{\bar{H}}_B[q_0]$ denotes the fact that the couplings c_α have been replaced by other values $\bar{c}_\alpha$ which they may take during the initial preparation. This allows to describe the preparation class A (3.8), where the system is decoupled from the bath $\bar{c}_\alpha = 0$ before the initial time t_0, as well as the preparation class B (3.10), with $\bar{c}_\alpha = c_\alpha$.

The next step is the evaluation of the propagator $U(\mu, \vec{x}_f, t; \mu_i, \vec{x}_i, t_0)$. The spirit of the path integral techniques is to slice the time interval $t - t_0$ in a large number N_I of infinitesimal intervals $\Delta\tau \hat{=} (t - t_0)/N_I$. For convenience, we denote the intermediate times so introduced by $\tau_k \hat{=} t_0 + k\Delta\tau$. They have no physical meaning. The evolution operator is consequently rewritten as

$$e^{-\frac{i}{\hbar} \int_{t_0}^t dt' \hat{H}(t')} = e^{-\frac{i}{\hbar} \int_{\tau_{N_I-1}}^t dt' \hat{H}(t')} \cdot \ldots \cdot e^{-\frac{i}{\hbar} \int_{\tau_1}^{\tau_2} dt' \hat{H}(t')} e^{-\frac{i}{\hbar} \int_{t_0}^{\tau_1} dt' \hat{H}(t')}. \tag{A.8}$$

One then inserts the completeness relation (A.2) between each of the N_I exponentials. This requires the introduction of $N_I - 1$ set of states, which we chose to label chronologically $|\mu_k, \vec{x}_k\rangle = |\mu_k\rangle \otimes |\vec{x}_k\rangle$, $k = 1, \ldots, N_I - 1$. For convenience, we also introduce the notations $|\mu_0, \vec{x}_0\rangle \hat{=} |\mu_i, \vec{x}_i\rangle$ and $|\mu_{N_I}, \vec{x}_{N_I}\rangle \hat{=} |\mu, \vec{x}_f\rangle$ for the initial and final states. This yields the expression

$$U(\mu, \vec{x}_f, t; \mu_i, \vec{x}_i, t_0)$$

$$= \prod_{k=1}^{N_I-1} \left(\sum_{\mu_k \in TB} \int d\vec{x}_k \right) \prod_{k=1}^{N_I} \langle \mu_k, \vec{x}_k | e^{-\frac{i}{\hbar} \int_{\tau_{k-1}}^{\tau_k} dt' \hat{H}(t')} | \mu_{k-1}, \vec{x}_{k-1} \rangle. \tag{A.9}$$

In each of the propagators in the right-hand side, the integral in the argument of the exponential runs over an infinitesimal time interval $\Delta\tau$. Therefore one can use the approximation

$$\int_{\tau_{k-1}}^{\tau_k} \mathrm{d}t'\hat{H}(t') \underset{\Delta\tau\to 0}{\sim} \Delta\tau\hat{H}(\tau_{k-1}). \tag{A.10}$$

The argument of the exponential is thus infinitesimal, and the first term of the Taylor expansion may be used

$$\mathrm{e}^{-\frac{\mathrm{i}\Delta\tau}{\hbar}\hat{H}(\tau_{k-1})} \underset{\Delta\tau\to 0}{\sim} \hat{1} - \frac{\mathrm{i}\Delta\tau}{\hbar}\hat{H}(\tau_{k-1}). \tag{A.11}$$

The corresponding infinitesimal propagator reads

$$\langle\mu_k,\vec{x_k}|\mathrm{e}^{-\frac{\mathrm{i}}{\hbar}\int_{\tau_{k-1}}^{\tau_k}\mathrm{d}t'\hat{H}(t')}|\mu_{k-1},\vec{x}_{k-1}\rangle$$
$$\underset{\Delta\tau\to 0}{\sim} \langle\mu_k|\hat{1} - \frac{\mathrm{i}\Delta\tau}{\hbar}\hat{H}_{\mathrm{S}}(\tau_{k-1})|\mu_{k-1}\rangle\langle\vec{x_k}|\hat{1} - \frac{\mathrm{i}\Delta\tau}{\hbar}\hat{H}_{\mathrm{B}}[q(\tau_{k-1})]|\vec{x}_{k-1}\rangle, \quad \text{(A.12)}$$

where, in $\hat{H}_{\mathrm{B}}[q(\tau_{k-1})]$, the system position operator $\hat{q}$ has been replaced by the value $q(\tau_{k-1}) \,\hat{=}\, q_{\mu_{k-1}}$. In the limit $N_I \to \infty$, the sequence $q(\tau_k),\ k=0,\ldots,N_I$, builds a path $q(t')$ starting at $q(t_0) = q_{\mu_i}$ and ending at $q(t) = q_\mu$. As a consequence of (A.12), the system-plus-bath propagator factorizes in terms of a system and a bath propagators

$$U(\mu,\vec{x}_f,t;\mu_i,\vec{x}_i,t_0) = \lim_{N_I\to\infty}\sum_{\{\mu_k\}} A[q(t'),t]U_{\mathrm{B}}(\vec{x}_f,t;\vec{x}_i,t_0;q(t')). \tag{A.13}$$

The price paid for this factorization is the sum $\sum_{\{\mu_k\}} = \prod_{k=1}^{N_I-1}\left(\sum_{\mu_k\in\mathrm{TB}}\right)$ over the intermediate states $|\mu_k\rangle$. We have denoted by

$$A[q(t'),t] = \prod_{k=1}^{N_I}\langle\mu_k|\hat{1} - \frac{\mathrm{i}\Delta\tau}{\hbar}\hat{H}_{\mathrm{S}}(\tau_{k-1})|\mu_{k-1}\rangle \tag{A.14}$$

the contribution to the system propagator generated by a given configuration of the intermediate states $|\mu_k\rangle$, which define the path $q(t')$ through $q(\tau_k) \,\hat{=}\, q_{\mu_k}$. This path will thus be made of a succession of sharp steps, what we will name a tight-binding path. The sum over the intermediate states can then be seen as a discrete path integral over all possible tight-binding paths $q(t')$ connecting the initial state q_{μ_i} with the final state q_μ.

The bath propagator keeps track of the influence of the coupling with the system through its explicit dependence on the system path $q(t')$, namely

$$U_{\mathrm{B}}(\vec{x}_f,t;\vec{x}_i,t_0;q(t')) = \langle\vec{x}_i|\mathrm{e}^{-\frac{\mathrm{i}}{\hbar}\int_{t_0}^t\mathrm{d}t'\hat{H}_{\mathrm{B}}[q(t')]}|\vec{x}_i'\rangle. \tag{A.15}$$

This definition reduces to (A.7) for a constant path $q(t') = q_0$.

We want to substitute the result (A.13) in the expression (A.6) for the populations. For the second, complex conjugated, propagator $U^*(\mu, \vec{x}_f, t; \mu'_i, \vec{x}'_i, t_0)$, we have to introduce a second set of intermediate states $|\mu'_k\rangle$, which define a path $q'(t')$ through $q'(\tau_k) \, \hat{=} \, q_{\mu'_k}$, starting at $q'(t_0) = q_{\mu'_i}$ and ending at $q'(t) = q_\mu$. Altogether, we have

$$P_\mu(t) = \sum_{\mu_i, \mu'_i \in \text{TB}} \langle \mu_i | \hat{\rho}(t_0) | \mu'_i \rangle \lim_{N_I \to \infty} \sum_{\{\mu_k\}, \{\mu'_k\}} A[q(t'), t] A^*[q'(t'), t] F_{\text{FV}}[q(t'), q'(t'), t]. \tag{A.16}$$

As a consequence of (A.13), all bath contributions factorizes from the system contributions and combine into the Feynman-Vernon influence functional

$$\begin{aligned} F_{\text{FV}}[q(t'), q'(t'), t] \, \hat{=} \, \int \mathrm{d}\vec{x}_i \int \mathrm{d}\vec{x}'_i \int \mathrm{d}\vec{x}_f \\ \times \, U_{\text{B}}(\vec{x}_f, t; \vec{x}_i, t_0; q(t')) \bar{U}_{\text{B}}(\vec{x}_i, -\mathrm{i}\hbar\beta; \vec{x}'_i, 0; q_0) U^*_{\text{B}}(\vec{x}_f, t; \vec{x}'_i, t_0; q'(t')). \end{aligned} \tag{A.17}$$

In this form, it is now clear that the integrals over the bath degrees of freedom can be performed independently of the system, which only enters through the real-valued paths $q(t')$ and $q'(t')$. This step realizes the widely used expression "to trace out the bath degrees of freedom". Due to the structure of the Hamiltonian $\hat{H}_{\text{B}}[q(t')]$, the bath propagator itself factorizes

$$U_{\text{B}}(\vec{x}_f, t; \vec{x}_i, t_0; q(t')) = \prod_{\alpha=1}^{N_{\text{O}}} U_{\text{B}}^{(\alpha)}(x_f^{(\alpha)}, t; x_i^{(\alpha)}, t_0; q(t')) \tag{A.18}$$

in terms of the propagators $U_{\text{B}}^{(\alpha)}(x_f^{(\alpha)}, t; x_i^{(\alpha)}, t_0; q(t'))$ of each of the bath degrees of freedom. Each degree of freedom is a harmonic oscillator driven by the time-dependent force $c_\alpha q(t')$. Its propagator can be found in the literature [1, 2]

$$\begin{aligned} U_{\text{B}}^{(\alpha)}(x_f, t; x_i, t_0; q(t')) = \sqrt{\frac{m_\alpha \omega_\alpha}{2\pi\mathrm{i}\hbar\sin(\omega_\alpha(t-t_0))}} \\ \times \exp\Bigg\{ \frac{\mathrm{i}}{\hbar\sin(\omega_\alpha(t-t_0))} \Bigg[\frac{m_\alpha\omega_\alpha}{2}(x_f^2 + x_i^2)\cos(\omega_\alpha(t-t_0)) - m_\alpha\omega_\alpha x_f x_i \\ + c_\alpha x_f \int_{t_0}^t \mathrm{d}t' \sin(\omega_\alpha(t'-t_0))q(t') + c_\alpha x_i \int_{t_0}^t \mathrm{d}t' \sin(\omega_\alpha(t-t'))q(t') \\ - \frac{c_\alpha^2 \sin(\omega_\alpha(t-t_0))}{2m_\alpha\omega_\alpha^2} \int_{t_0}^t \mathrm{d}t' q^2(t') \\ - \frac{c_\alpha^2}{m_\alpha\omega_\alpha} \int_{t_0}^t \mathrm{d}t' \int_{t_0}^{t'} \mathrm{d}t'' \sin(\omega_\alpha(t-t'))\sin(\omega_\alpha(t''-t_0))q(t')q(t'') \Bigg] \Bigg\}. \end{aligned} \tag{A.19}$$

In this expression, the bath coordinates x_f and x_i enter at most quadratically in the argument of the exponential. One therefore sees that the three integrals involved for each bath degree of freedom in the influence functional (A.17) are Gaussian integrals and can be performed. The calculation yields

$$
\int \mathrm{d}x_i \int \mathrm{d}x_i' \int \mathrm{d}x_f
$$
$$
\times U_{\mathrm{B}}^{(\alpha)}(x_f,t;x_i,t_0;q(t'))\bar{U}_{\mathrm{B}}^{(\alpha)}(x_i,-\mathrm{i}\hbar\beta;x_i',0;q_0)U_{\mathrm{B}}^{(\alpha)^*}(x_f,t;x_i',t_0;q'(t'))
$$
$$
= \exp\Bigg\{ -\frac{c_\alpha^2}{2\hbar m_\alpha \omega_\alpha}\coth\left(\frac{\hbar\omega_\alpha\beta}{2}\right)
$$
$$
\times \int_{t_0}^{t} \mathrm{d}t' \int_{t_0}^{t'} \mathrm{d}t'' \left[q(t')-q'(t')\right]\cos(\omega_\alpha(t'-t''))\left[q(t'')-q'(t'')\right]
$$
$$
+ \frac{\mathrm{i}c_\alpha^2}{2\hbar m_\alpha \omega_\alpha} \int_{t_0}^{t} \mathrm{d}t' \int_{t_0}^{t'} \mathrm{d}t'' \left[q(t')-q'(t')\right]\sin(\omega_\alpha(t'-t''))\left[q(t'')+q'(t'')\right]
$$
$$
- \frac{\mathrm{i}c_\alpha^2}{2\hbar m_\alpha \omega_\alpha^2} \int_{t_0}^{t} \mathrm{d}t' \left[q^2(t')-q'^2(t')\right]
$$
$$
+ \frac{\mathrm{i}c_\alpha \bar{c}_\alpha q_0}{\hbar m_\alpha \omega_\alpha^2} \int_{t_0}^{t} \mathrm{d}t' \left[q(t')-q'(t')\right]\cos(\omega_\alpha(t'-t_0))\Bigg\}. \quad (\mathrm{A}.20)
$$

The last term vanishes for the preparation class A (3.8) characterized by $\bar{c}_\alpha = 0$, whereas its prefactor reads $\mathrm{i}c_\alpha^2 q_0/\hbar m_\alpha \omega_\alpha^2$ for the preparation class B (3.10). When we combine the results for all bath degrees of freedom, we see that everything can be rewritten in terms of the single combination of bath parameters

$$
J(\omega) \,\hat{=}\, \frac{\pi}{2} \sum_{\alpha=1}^{N_{\mathrm{B}}} \frac{c_\alpha^2}{m_\alpha \omega_\alpha} \delta(\omega-\omega_\alpha). \qquad (\mathrm{A}.21)
$$

This quantity is called the bath spectral density, and enters the bath correlation function $L(\tau) = L_{\mathrm{R}}(\tau)+\mathrm{i}L_{\mathrm{I}}(\tau)$ defined in (B.1). The once integrated bath correlation function $M(\tau)$ defined in (B.3) also comes into play. With these definitions, the
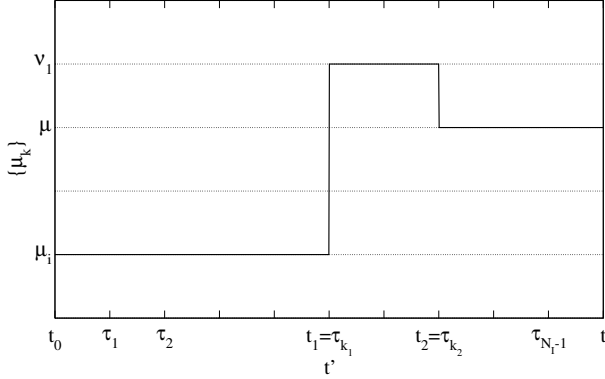
Figure A.1: Schematic representation of one possible realization of the successive states $|\mu_k\rangle$ of the system at times $\tau_k = t_0 + k\Delta\tau$. In this example, transitions happen at times $t_1 = \tau_{k_1}$ and $t_2 = \tau_{k_2}$. The system visits the intermediate state $|\nu_1\rangle$ between the initial state $|\mu_i\rangle$ and the final state $|\mu\rangle$.

influence functional finally reads

$$
\begin{aligned}
F_{\mathrm{FV}}&[q(t'), q'(t'), t] \\
&= \exp\left\{ -\frac{1}{\hbar} \int_{t_0}^{t} \mathrm{d}t' \int_{t_0}^{t'} \mathrm{d}t'' \left[q(t') - q'(t')\right] L_{\mathrm{R}}(t' - t'') \left[q(t'') - q'(t'')\right] \right. \\
&\qquad - \frac{\mathrm{i}}{\hbar} \int_{t_0}^{t} \mathrm{d}t' \int_{t_0}^{t'} \mathrm{d}t'' \left[q(t') - q'(t')\right] L_{\mathrm{I}}(t' - t'') \left[q(t'') + q'(t'')\right] \\
&\qquad - \frac{\mathrm{i}}{\hbar} M_{\mathrm{I}}(0) \int_{t_0}^{t} \mathrm{d}t' \left[q(t') - q'(t')\right] \left[q(t') + q'(t')\right] \\
&\qquad \left. + \frac{2\mathrm{i}}{\hbar} q_0 \int_{t_0}^{t} \mathrm{d}t' \left[q(t') - q'(t')\right] M_{\mathrm{I}}(t' - t_0) \right\}, \quad (A.22)
\end{aligned}
$$

for the preparation class B. For the preparation class A, the last term is absent. The last task is to evaluate the system propagator (A.14) and perform the discrete path integral $\sum_{\{\mu_k\}}$. Let us look at an example of a tight-binding path, shown in Fig. A.1. In this example, the intermediate states of the system coincide with the initial state $|\mu_i\rangle$ from the initial time $t_0 = \tau_0$ up to some time $t_1 \,\hat{=}\, \tau_{k_1}$. At time t_1, the system makes a transition from the state $|\mu_{k_1-1}\rangle = |\mu_i\rangle$ to a different state $|\mu_{k_1}\rangle = |\nu_1\rangle$, where it stays up to the time $t_2 \,\hat{=}\, \tau_{k_2}$. At this time, it makes a second transition from the state $|\mu_{k_2-1}\rangle = |\nu_1\rangle$ to the final state $|\mu_{k_2}\rangle = |\mu\rangle$, where

it stays up to the final time $t = \tau_{N_I}$. One has thus the path

$$
\mu_k = \begin{cases} \mu_i & \text{for } k = 0, \dots, k_1 - 1 \\ \nu_1 & \text{for } k = k_1, \dots, k_2 - 1 \\ \mu & \text{for } k = k_2, \dots, N_I. \end{cases} \tag{A.23}
$$

If two consecutive states $|\mu_{k-1}\rangle$ and $|\mu_k\rangle$ are identical, the corresponding contribution to the system propagator (A.14) reads

$$
\langle \nu | \hat{1} - \frac{\mathrm{i}\Delta\tau}{\hbar} \hat{H}_\mathrm{S}(\tau_{k-1}) | \nu \rangle = 1 - \frac{\mathrm{i}\Delta\tau}{\hbar} \left[\varepsilon_\nu - F(\tau_{k-1}) q_\nu \right]. \tag{A.24}
$$

On the other hand, if they are different, that is when a transition happens, one has

$$
\langle \nu' | \hat{1} - \frac{\mathrm{i}\Delta\tau}{\hbar} \hat{H}_\mathrm{S}(\tau_{k-1}) | \nu \rangle = -\frac{\mathrm{i}\Delta\tau}{\hbar} \Delta_{\nu'\nu}. \tag{A.25}
$$

For the path (A.23), the propagator (A.14) reads therefore

$$
A[q(t'), t] = \left(-\frac{\mathrm{i}\Delta\tau}{\hbar} \right)^2 \Delta_{\mu\nu_1} \Delta_{\nu_1\mu_i} \prod_{k=k_2+1}^{N_I} \left[1 - \frac{\mathrm{i}\Delta\tau}{\hbar} \left[\varepsilon_\mu - F(\tau_{k-1}) q_\mu \right] \right]
$$

$$
\times \prod_{k=k_1+1}^{k_2-1} \left[1 - \frac{\mathrm{i}\Delta\tau}{\hbar} \left[\varepsilon_{\nu_1} - F(\tau_{k-1}) q_{\nu_1} \right] \right] \prod_{k=1}^{k_1-1} \left[1 - \frac{\mathrm{i}\Delta\tau}{\hbar} \left[\varepsilon_{\mu_i} - F(\tau_{k-1}) q_{\mu_i} \right] \right]. \tag{A.26}
$$

In the limit $N_I \to \infty$, which implies $\Delta\tau \to 0$, the products may be reconstructed into exponentials [see Eq. (A.11)], yielding

$$
A[q(t'), t] \underset{N_I \to \infty}{\sim} \left(-\frac{\mathrm{i}\Delta\tau}{\hbar} \right)^2 \Delta_{\mu\nu_1} \Delta_{\nu_1\mu_i}
$$

$$
\times \mathrm{e}^{-\frac{\mathrm{i}}{\hbar} \int_{\tau_{k_2}}^{t} \mathrm{d}t' \left[\varepsilon_\mu - F(t') q_\mu \right]} \mathrm{e}^{-\frac{\mathrm{i}}{\hbar} \int_{\tau_{k_1}}^{\tau_{k_2-1}} \mathrm{d}t' \left[\varepsilon_{\nu_1} - F(t') q_{\nu_1} \right]} \mathrm{e}^{-\frac{\mathrm{i}}{\hbar} \int_{t_0}^{\tau_{k_1-1}} \mathrm{d}t' \left[\varepsilon_{\mu_i} - F(t') q_{\mu_i} \right]}. \tag{A.27}
$$

The three exponentials can be merged together. The integrals in their argument combine into a single expression if we make use of the path

$$
q(t') = \begin{cases} q_{\mu_i} & \text{for } t' \in [t_0, t_1[\\ q_{\nu_1} & \text{for } t' \in [t_1, t_2[\\ q_\mu & \text{for } t' \in [t_2, t], \end{cases} \tag{A.28}
$$

and define the on-site energy function

$$
E(t') = \begin{cases} \varepsilon_{\mu_i} & \text{for } t' \in [t_0, t_1[\\ \varepsilon_{\nu_1} & \text{for } t' \in [t_1, t_2[\\ \varepsilon_\mu & \text{for } t' \in [t_2, t]. \end{cases} \tag{A.29}
$$

The infinitesimal gaps $]\tau_{k_1-1}, \tau_{k_1}[$ and $]\tau_{k_2-1}, \tau_{k_2}[$ between the boundaries of the integrals do not matter, and one obtains

$$A[q(t'), t] \underset{N_I \to \infty}{\sim} \left(-\frac{\mathrm{i}\Delta\tau}{\hbar}\right)^2 \Delta_{\mu\nu_1} \Delta_{\nu_1\mu_i} \mathrm{e}^{-\frac{\mathrm{i}}{\hbar} \int_{t_0}^t \mathrm{d}t' \left[E(t') - F(t')q(t')\right]}. \tag{A.30}$$

This is only one example of a tight-binding path, presenting two transitions at times t_1 and t_2 and visiting a given intermediate state $|\nu_1\rangle$. If we want to sum over all possible configurations of the intermediate states $|\mu_k\rangle$ corresponding to paths presenting $n = 2$ transitions, we have to sum over all possible configurations of the transition times $t_0 < t_1 = \tau_{k_1} < t_2 = \tau_{k_2} < t$ and over all possibilities for the single intermediate state $|\nu_1\rangle$. One has

$$\sum_{\{\mu_k\},n=2} A[q(t'), t]$$

$$\underset{N_I \to \infty}{\sim} \sum_{\nu_1 \in \mathrm{TB}} \sum_{k_2=1}^{N_I-1} \sum_{k_1=1}^{k_2-1} \left(-\frac{\mathrm{i}\Delta\tau}{\hbar}\right)^2 \Delta_{\mu\nu_1} \Delta_{\nu_1\mu_i} \mathrm{e}^{-\frac{\mathrm{i}}{\hbar} \int_{t_0}^t \mathrm{d}t' \left[E(t') - F(t')q(t')\right]}. \tag{A.31}$$

In the limit $N_I \to \infty$, corresponding to $\Delta\tau \to 0$, the sums $\sum_{k_j} \Delta\tau f(\tau_{k_j} = t_0 + k_j\Delta\tau)$ are nothing but integrals over the corresponding transition times $\int \mathrm{d}t_j f(t_j)$. Thus

$$\sum_{\{\mu_k\},n=2} A[q(t'), t]$$

$$\underset{N_I \to \infty}{\sim} \sum_{\nu_1 \in \mathrm{TB}} \left(-\frac{\mathrm{i}}{\hbar}\right)^2 \Delta_{\mu\nu_1} \Delta_{\nu_1\mu_i} \int_{t_0}^t \mathrm{d}t_2 \int_{t_0}^{t_2} \mathrm{d}t_1 \mathrm{e}^{-\frac{\mathrm{i}}{\hbar} \int_{t_0}^t \mathrm{d}t' \left[E(t') - F(t')q(t')\right]}. \tag{A.32}$$

It is now clear how to generalize this expression for a path involving n transitions happening at times t_j, $j = 1, \ldots, n$, and visiting $n-1$ intermediate states $|\nu_j\rangle$, $j = 1, \ldots, n-1$. It is also clear from the above discussion that the sum over all possible configurations of the intermediate states $|\mu_k\rangle$ can be written

$$\sum_{\{\mu_k\}} A[q(t'), t] \underset{N_I \to \infty}{\sim} \sum_{n=0}^{\infty} \prod_{j=1}^{n-1} \left(\sum_{\nu_j \in \mathrm{TB}}\right) \prod_{j=1}^{n} \left(-\frac{\mathrm{i}\Delta[j]}{\hbar}\right)$$

$$\times \int_{t_0}^t \mathrm{d}t_n \cdots \int_{t_0}^{t_3} \mathrm{d}t_2 \int_{t_0}^{t_2} \mathrm{d}t_1 \mathrm{e}^{-\frac{\mathrm{i}}{\hbar} \int_{t_0}^t \mathrm{d}t' \left[E(t') - F(t')q(t')\right]}, \tag{A.33}$$

with the couplings defined as $\Delta[j] \hat{=} \Delta_{\nu_j\nu_{j-1}}$, and the path

$$q(t') = q_{\mu_i} + \sum_{j=1}^{n} (q_{\nu_j} - q_{\nu_{j-1}})\theta(t' - t_j), \tag{A.34}$$

where $\theta(t')$ denotes the step function. The conventions $\nu_0 = \mu_i$ and $\nu_n = \mu$ were used. The on-site energy reads in the same notation

$$E(t') = \varepsilon_{\mu_i} + \sum_{j=1}^{n}(\varepsilon_{\nu_j} - \varepsilon_{\nu_{j-1}})\theta(t' - t_j). \qquad (A.35)$$

We can follow the same procedure for the second propagator $A^*[q'(t')]$ and discrete path integral $\sum_{\{\mu'_k\}}$ involved in (A.16). The tight-binding path

$$q'(t') = q_{\mu'_i} + \sum_{j'=1}^{n'}(q_{\nu'_{j'}} - q_{\nu'_{j'-1}})\theta(t' - t'_{j'}) \qquad (A.36)$$

presents n' transitions at times $t'_{j'}$, $j' = 1, \ldots, n'$, and visits the $n' - 1$ intermediate states $|\nu'_{j'}\rangle$ between the initial state $|\nu'_0\rangle = |\mu'_i\rangle$ and the final state $|\nu'_{n'}\rangle = |\mu\rangle$. Introducing the couplings $\Delta'[j'] \hat{=} \Delta^*_{\nu'_{j'},\nu'_{j'-1}}$, we have

$$\sum_{\{\mu'_k\}} A^*[q'(t'),t] \underset{N_I \to \infty}{\sim} \sum_{n'=0}^{\infty} \prod_{j'=1}^{n'-1}\left(\sum_{\nu'_{j'}\in\mathrm{TB}}\right)\prod_{j'=1}^{n'}\left(\frac{\mathrm{i}\Delta'[j']}{\hbar}\right)$$

$$\times \int_{t_0}^{t}\mathrm{d}t'_{n'}\cdots\int_{t_0}^{t'_3}\mathrm{d}t'_2\int_{t_0}^{t'_2}\mathrm{d}t'_1 e^{\frac{\mathrm{i}}{\hbar}\int_{t_0}^{t}\mathrm{d}t'\left[E'(t')-F(t')q'(t')\right]}. \qquad (A.37)$$

Coming back to the populations (A.16), we obtain

$$P_\mu(t) = \sum_{\mu_i,\mu'_i\in\mathrm{TB}}\langle\mu_i|\hat{\rho}(t_0)|\mu'_i\rangle G(\mu,\mu,\mu_i,\mu'_i,t), \qquad (A.38)$$

with the propagating function

$$G(\mu,\mu,\mu_i,\mu'_i,t) = \sum_{n,n'=0}^{\infty}\prod_{j=1}^{n-1}\left(\sum_{\nu_j\in\mathrm{TB}}\right)\prod_{j'=1}^{n'-1}\left(\sum_{\nu'_{j'}\in\mathrm{TB}}\right)$$

$$\times\prod_{j=1}^{n}\left(-\frac{\mathrm{i}\Delta[j]}{\hbar}\right)\prod_{j'=1}^{n'}\left(\frac{\mathrm{i}\Delta'[j']}{\hbar}\right)\int_{t_0}^{t}\mathrm{d}t_n\cdots\int_{t_0}^{t_2}\mathrm{d}t_1\int_{t_0}^{t}\mathrm{d}t'_{n'}\cdots\int_{t_0}^{t'_2}\mathrm{d}t'_1$$

$$\times e^{-\frac{\mathrm{i}}{\hbar}\int_{t_0}^{t}\mathrm{d}t'\left[E(t')-E'(t')-F(t')[q(t')-q'(t')]\right]}F_{\mathrm{FV}}[q(t'),q'(t'),t]. \qquad (A.39)$$

This completes the demonstration of Eq.(3.12).

References

[1] H. Grabert, P. Schramm, and G. L. Ingold, Phys. Rep. **168**, 115 (1988).

[2] G. L. Ingold, Lect. Notes Phys. **611**, 1 (2002).

Appendix B

The Bath Correlation Function

B.1   Definition

The bath correlation function is defined as

$$L(\tau) \mathrel{\hat=} \frac{1}{\pi} \int_0^\infty \mathrm{d}\omega\, J(\omega) \left[\coth\left(\frac{\hbar\omega\beta}{2} \right) \cos(\omega\tau) - \mathrm{i}\sin(\omega\tau) \right]. \tag{B.1}$$

We will denote its real and imaginary parts by $L_{\mathrm{R}}(\tau)$ and $L_{\mathrm{I}}(\tau)$, respectively. The bath is characterized by its spectral function $J(\omega)$ and its temperature $T = 1/\beta k_{\mathrm{B}}$.

   The bath correlation function enters the Feynman-Vernon influence functional given, e.g., in (3.16). There, it is the kernel of a double integral involving also two paths. In a tight-binding model, these paths are step-like. Thus, when one integrates by parts, one involves the derivative of the paths, which are made of δ-functions and simplify greatly the integration. In this procedure, the twice integrated bath correlation function

$$Q(\tau) \mathrel{\hat=} \frac{1}{\pi} \int_0^\infty \mathrm{d}\omega\, \frac{J(\omega)}{\omega^2} \left[\coth\left(\frac{\hbar\omega\beta}{2} \right) [1 - \cos(\omega\tau)] + \mathrm{i}\sin(\omega\tau) \right], \tag{B.2}$$

comes into play. It satisfies $\ddot{Q}(\tau) = L(\tau)$ and $Q(0) = 0$. In some cases it is advantageous to work with the once integrated bath correlation function

$$M(\tau) \mathrel{\hat=} \frac{1}{\pi} \int_0^\infty \mathrm{d}\omega\, \frac{J(\omega)}{\omega} \left[\coth\left(\frac{\hbar\omega\beta}{2} \right) \sin(\omega\tau) + \mathrm{i}\cos(\omega\tau) \right], \tag{B.3}$$

which satisfies $\dot{M}(\tau) = L(\tau)$ and $M_{\mathrm{R}}(0) = 0$.

   We will now evaluate this correlation function for an Ohmic bath, which is characterized by a linear spectral density $J(\omega) \propto \eta\omega$ at low frequency ω. This is the case usually considered in the frame of a Caldeira-Leggett model for a system coupled to a thermal bath. The reason is that, when one takes the classical limit of the quantum Heisenberg equations of motions of this system-plus-bath, one obtains a Langevin equation for the system, with a viscous force acting on the velocity. The viscosity coefficient is precisely η. As one can also see, $L(0)$ diverges if one does not introduce a cutoff at large frequencies. The presence of a cutoff frequency physically means that the bath cannot respond arbitrarily fast to a modification in its environment [1, Ch. 3]. Here we will investigate two common cases: an exponential cutoff at frequency ω_{c}

$$J(\omega) = \eta\omega e^{-\omega/\omega_{\mathrm{c}}}, \tag{B.4}$$

and an algebraic cutoff at frequency ω_{D}

$$J(\omega) = \frac{\eta\omega}{1 + (\omega/\omega_{\mathrm{D}})^2}, \tag{B.5}$$

known as the Drude model.

B.2 Evaluation for an Ohmic bath with exponential cutoff

We want to evaluate the twice integrated bath correlation function (B.2) for the spectral density (B.4) with exponential cutoff. For the real part $Q_{\mathrm{R}}(\tau)$, following [2], we see that it is convenient to start from

$$M_{\mathrm{R}}(\tau) = \frac{\eta}{\pi} \int_0^\infty \mathrm{d}\omega \coth\left(\frac{\omega}{2\nu_{\mathrm{B}}}\right) \sin(\omega\tau) e^{-\omega/\omega_{\mathrm{c}}}, \tag{B.6}$$

where we have introduced the temperature-related frequency $\nu_{\mathrm{B}} \mathrel{\hat{=}} k_{\mathrm{B}}T/\hbar$ for convenience. Rewriting the coth and the sin in terms of exponentials, and substituting $x = \omega/\nu_{\mathrm{B}}$ in the integral, one obtains

$$M_{\mathrm{R}}(\tau) = \frac{\eta\nu_{\mathrm{B}}}{2\pi\mathrm{i}} \int_0^\infty \frac{\mathrm{d}x}{1 - e^{-x}} \left[e^{-x(\nu_{\mathrm{B}}/\omega_{\mathrm{c}} - \mathrm{i}\nu_{\mathrm{B}}\tau)} - e^{-x(\nu_{\mathrm{B}}/\omega_{\mathrm{c}} + \mathrm{i}\nu_{\mathrm{B}}\tau)} \right.$$
$$\left. + e^{-x(1 + \nu_{\mathrm{B}}/\omega_{\mathrm{c}} - \mathrm{i}\nu_{\mathrm{B}}\tau)} - e^{-x(1 + \nu_{\mathrm{B}}/\omega_{\mathrm{c}} + \mathrm{i}\nu_{\mathrm{B}}\tau)} \right]. \tag{B.7}$$

Integrals of this kind can be found in [3, formula (3.311/7)],

$$\int_0^\infty \mathrm{d}x \frac{e^{-\mu x} - e^{-\nu x}}{1 - e^{-x}} = \Psi(\nu) - \Psi(\mu), \qquad \mathrm{Re}\,\mu > 0, \mathrm{Re}\,\nu > 0. \tag{B.8}$$

Using additionally the property $\Psi(1+x) = \Psi(x) + 1/x$ of the Ψ-function, one has

$$M_{\mathrm{R}}(\tau) = \frac{\eta\nu_{\mathrm{B}}}{2\pi\mathrm{i}} \left[2\Psi\left(1 + \frac{\nu_{\mathrm{B}}}{\omega_{\mathrm{c}}} + \mathrm{i}\nu_{\mathrm{B}}\tau\right) - 2\Psi\left(1 + \frac{\nu_{\mathrm{B}}}{\omega_{\mathrm{c}}} - \mathrm{i}\nu_{\mathrm{B}}\tau\right) \right.$$
$$\left. - \left(\frac{\nu_{\mathrm{B}}}{\omega_{\mathrm{c}}} - \mathrm{i}\nu_{\mathrm{B}}\tau\right)^{-1} + \left(\frac{\nu_{\mathrm{B}}}{\omega_{\mathrm{c}}} + \mathrm{i}\nu_{\mathrm{B}}\tau\right)^{-1} \right]. \tag{B.9}$$

With the relations $\Psi(z) = \mathrm{d}\ln\Gamma(z)/\mathrm{d}z$ and $1/z = \mathrm{d}\ln(z)/\mathrm{d}z$, and the property $\Gamma(z^*) = \Gamma^*(z)$ of the Γ-function, one can rewrite this expression as

$$M_{\mathrm{R}}(\tau) = \frac{\eta}{\pi}\frac{\mathrm{d}}{\mathrm{d}\tau}\left[-\ln\left|\Gamma\left(1 + \frac{\nu_{\mathrm{B}}}{\omega_{\mathrm{c}}} + \mathrm{i}\nu_{\mathrm{B}}\tau\right)\right|^2 + \frac{1}{2}\ln\left(\frac{\nu_{\mathrm{B}}^2}{\omega_{\mathrm{c}}^2} + \nu_{\mathrm{B}}^2\tau^2\right)\right]. \tag{B.10}$$

It is then straightforward to integrate over τ in order to obtain $Q_{\mathrm{R}}(\tau)$. Remembering that $Q_{\mathrm{R}}(0) = 0$, we get

$$Q_{\mathrm{R}}(\tau) = \frac{\eta}{\pi}\left[-\ln\frac{\left|\Gamma\left(1 + \frac{\nu_{\mathrm{B}}}{\omega_{\mathrm{c}}}[1 + \mathrm{i}\omega_{\mathrm{c}}\tau]\right)\right|^2}{\left|\Gamma\left(1 + \frac{\nu_{\mathrm{B}}}{\omega_{\mathrm{c}}}\right)\right|^2} + \frac{1}{2}\ln\left(1 + \omega_{\mathrm{c}}^2\tau^2\right)\right]. \tag{B.11}$$

This expression can be somewhat simplified in the limit $\nu_{\mathrm{B}}/\omega_{\mathrm{c}} \ll 1$, which corresponds to a low temperature and/or a bath with low inertia. Using the approximations $\Gamma(1 + \varepsilon) \sim \Gamma(1) = 1$ and $|\Gamma(1 + \varepsilon[1 + \mathrm{i}x])|^2 \sim |\Gamma(1 + \mathrm{i}\varepsilon x)|^2 = \pi\varepsilon x/\sinh(\pi\varepsilon x)$ for $\varepsilon \ll 1$, we have

$$Q_{\mathrm{R}}(\tau) \sim \frac{\eta}{\pi}\left[-\ln\frac{\pi\nu_{\mathrm{B}}\tau}{\sinh(\pi\nu_{\mathrm{B}}\tau)} + \frac{1}{2}\ln\left(1 + \omega_{\mathrm{c}}^2\tau^2\right)\right], \qquad \nu_{\mathrm{B}} \ll \omega_{\mathrm{c}}. \tag{B.12}$$

For short times $\omega_{\mathrm{c}}|\tau| \ll 1$, the time-dependence is quadratic

$$Q_{\mathrm{R}}(\tau) \sim \frac{\eta}{2\pi}\omega_{\mathrm{c}}^2\tau^2, \qquad \nu_{\mathrm{B}} \ll \omega_{\mathrm{c}} \text{ and } \omega_{\mathrm{c}}|\tau| \ll 1. \tag{B.13}$$

With this expression, one also sees that $L_{\mathrm{R}}(0) = \ddot{Q}_{\mathrm{R}}(0)$ diverges quadratically when the cutoff frequency ω_{c} tends to infinity. On the other hand, at long times $\omega_{\mathrm{c}}|\tau| \gg 1$, the time-dependence is linear

$$Q_{\mathrm{R}}(\tau) \sim \eta\left[\nu_{\mathrm{B}}|\tau| - \frac{1}{\pi}\ln\left(2\pi\frac{\nu_{\mathrm{B}}}{\omega_{\mathrm{c}}}\right)\right], \qquad \nu_{\mathrm{B}} \ll \omega_{\mathrm{c}} \text{ and } \omega_{\mathrm{c}}|\tau| \gg 1. \tag{B.14}$$

This linear behavior is called the Markov form of the bath correlation function, because it is exactly what one would obtain if one would replace the bath by a memoryless Gaussian stochastic force (see also [1, Ch. 21]).
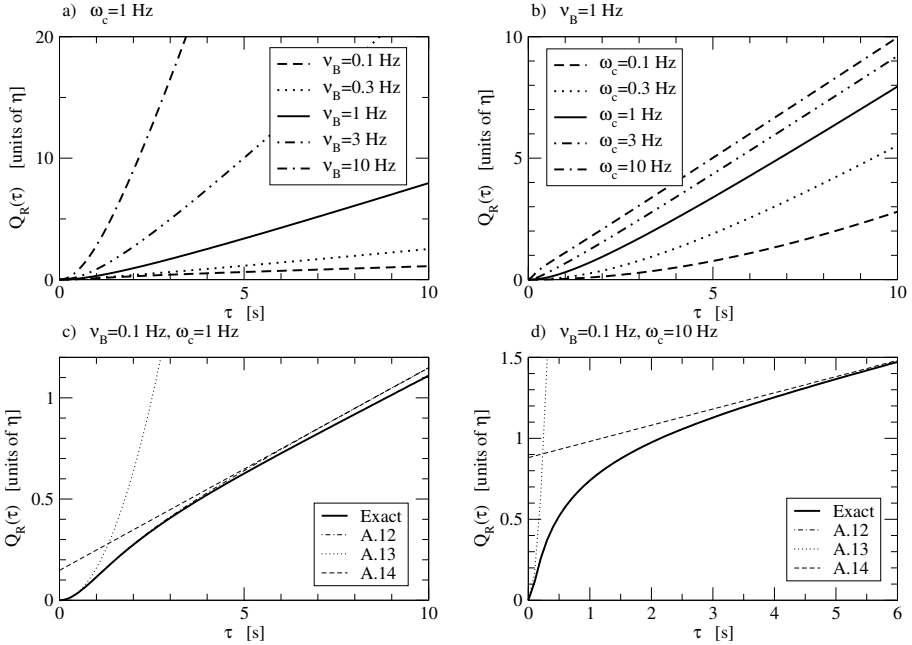
Figure B.1: The real part of the twice integrated bath correlation function for an Ohmic spectral density with exponential cutoff: a) for $\omega_c = 1$ Hz and different values of ν_B; b) for $\nu_B = 1$ Hz and different values of ω_c; c) for $\nu_B = 0.1$ Hz and $\omega_c = 1$ Hz. The dashed-dotted curve shows the approximation (B.12), valid for $\nu_B \ll \omega_c$. The dotted, respectively dashed curve shows its short-time (B.13), respectively long-time limit (B.14); d) same as c), for $\nu_B = 0.1$ Hz and $\omega_c = 10$ Hz.

The real part of the twice integrated bath correlation function as well as the approximations discussed above are shown in Fig. B.1.

The imaginary part $Q_I(\tau)$ is much easier to evaluate. There also, we start from

$$M_I(\tau) = \frac{\eta}{\pi} \int_0^\infty d\omega \cos(\omega\tau) e^{-\omega/\omega_c}. \tag{B.15}$$

The integral yields

$$M_I(\tau) = \frac{\eta}{\pi} \frac{\omega_c}{1 + \omega_c^2 \tau^2}. \tag{B.16}$$

Integrating and remembering that $Q_I(0) = 0$, we get

$$Q_I(\tau) = \frac{\eta}{\pi} \arctan(\omega_c \tau). \tag{B.17}$$

At long times $\omega_c \tau \gg 1$, this function tends to the asymptotic value $\eta/2$. It is depicted in Fig. B.3d.

B.3 Evaluation for an Ohmic bath with Drude cutoff

We now turn to the evaluation of the twice integrated bath correlation function (B.2) for the spectral density (B.5) with Drude cutoff. Here also, for the real part $Q_R(\tau)$, it is convenient to start from

$$M_R(\tau) = \frac{\eta}{\pi} \int_0^\infty \frac{d\omega}{1 + (\omega/\omega_D)^2} \coth\left(\frac{\omega}{2\nu_B}\right) \sin(\omega\tau). \tag{B.18}$$

First, we substitute $x = \omega/\omega_D$ in the integral

$$M_R(\tau) = \frac{\eta\omega_D}{\pi} \int_0^\infty \frac{dx}{1 + x^2} \coth\left(\frac{x\omega_D}{2\nu_B}\right) \sin(x\omega_D\tau). \tag{B.19}$$

This integral converges for any value of τ: At $x \to 0$, the first-order pole of $\coth(x\omega_D/2\nu_B)$ is compensated by the linear behavior of $\sin(x\omega_D\tau)$, therefore the integrand behaves as a constant; At $x \to \infty$, the integrand decays as $1/x^2$. Using the symmetry of the integrand, one can extend the integration on the whole real axis. After rewriting the sine function in terms of exponentials, one can perform the integral by using Cauchy's theorem, with some care. The result may be written in the form

$$M_R(\tau) = \eta\nu_B \, \text{sgn}(\tau) \left[1 - e^{-\omega_D|\tau|} + 2 \sum_{m=1}^\infty \frac{e^{-2\pi m\nu_B|\tau|} - e^{-\omega_D|\tau|}}{1 - (2\pi m\nu_B/\omega_D)^2} \right]. \tag{B.20}$$

The series converges uniformly in any time interval, therefore one can integrate it term-by-term to get $Q_R(\tau)$. One obtains, remembering that $Q_R(0) = 0$,

$$Q_R(\tau) = \eta \left[\nu_B|\tau| + \frac{\nu_B}{\omega_D}\left(e^{-\omega_D|\tau|} - 1\right) + \frac{2\nu_B}{\omega_D} \sum_{m=1}^\infty \frac{\frac{1 - e^{-2\pi m\nu_B|\tau|}}{2\pi m\nu_B/\omega_D} - \left(1 - e^{-\omega_D|\tau|}\right)}{1 - (2\pi m\nu_B/\omega_D)^2} \right]. \tag{B.21}$$

One can go further and get more insight with some approximations. In the limit $2\pi\nu_B|\tau| \gg 1$, the exponentials $e^{-2\pi m\nu_B|\tau|}$ can be neglected and the remaining sum performed, yielding

$$Q_R(\tau) \sim \eta\left[\nu_B|\tau| + \frac{1}{2}e^{-\omega_D|\tau|} \cot\left(\frac{\omega_D}{2\nu_B}\right) + \frac{1}{\pi}\Psi\left(\frac{\omega_D}{2\pi\nu_B}\right) + \frac{\gamma}{\pi} + \frac{\nu_B}{\omega_D} \right], \qquad 2\pi\nu_B|\tau| \gg 1, \tag{B.22}$$
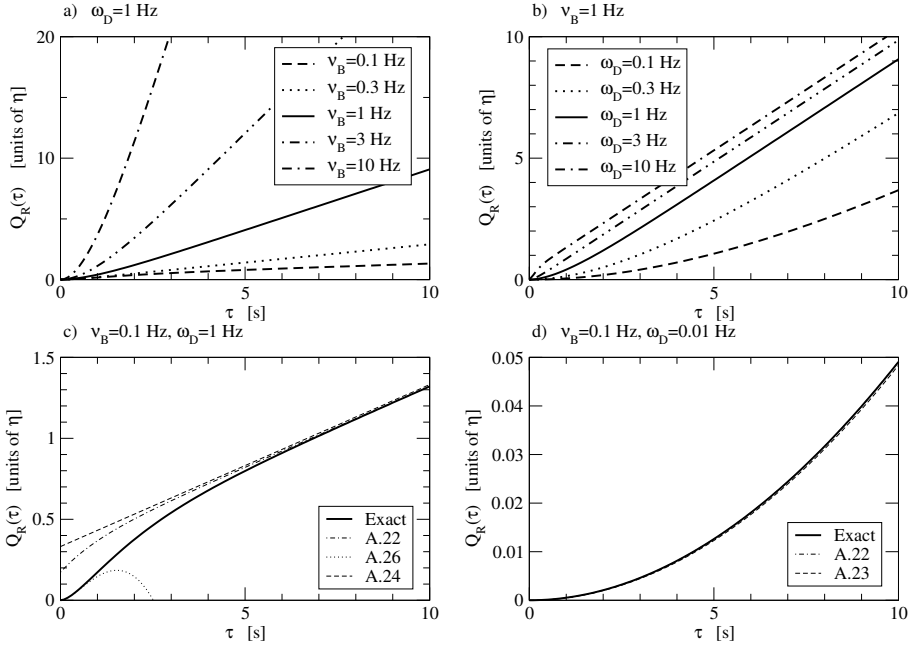
Figure B.2: The real part of the twice integrated bath correlation function for an Ohmic spectral density with Drude cutoff: a) for $\omega_\mathrm{D} = 1$ Hz and different values of ν_B; b) for $\nu_\mathrm{B} = 1$ Hz and different values of ω_D; c) for $\nu_\mathrm{B} = 0.1$ Hz and $\omega_\mathrm{D} = 1$ Hz. The dashed-dotted curve shows the long-time approximation (B.22). The dotted, respectively dashed curve shows the short-time (B.26), respectively long-time expression (B.24) valid in the regime $2\pi\nu_\mathrm{B} \ll \omega_\mathrm{D}$; d) for $\nu_\mathrm{B} = 0.1$ Hz and $\omega_\mathrm{D} = 0.01$ Hz. The dashed-dotted curve shows the long-time approximation (B.22), and the dashed curve shows its limit (B.23) in the regime $2\pi\nu_\mathrm{B} \gg \omega_\mathrm{D}$.

where $\gamma \approx 0.577$ denotes Euler's constant. One already recognizes the linear time-dependence, already found at long times for the case of an exponential cutoff [see Eq. (B.14)]. If one considers additionally the case $2\pi\nu_\mathrm{B}/\omega_\mathrm{D} \gg 1$, for which $\cot(\omega_\mathrm{D}/2\nu_\mathrm{B}) \sim 2\nu_\mathrm{B}/\omega_\mathrm{D}$ and $\Psi(\omega_\mathrm{D}/2\pi\nu_\mathrm{B}) \sim -\gamma - 2\pi\nu_\mathrm{B}/\omega_\mathrm{D}$, one finds

$$Q_\mathrm{R}(\tau) \sim \eta \left[\nu_\mathrm{B}|\tau| + \frac{\nu_\mathrm{B}}{\omega_\mathrm{D}} \left(\mathrm{e}^{-\omega_\mathrm{D}|\tau|} - 1 \right) \right], \qquad 2\pi\nu_\mathrm{B}|\tau| \gg 1 \text{ and } 2\pi\nu_\mathrm{B}/\omega_\mathrm{D} \gg 1.$$
(B.23)

In the opposite case $2\pi\nu_\mathrm{B}/\omega_\mathrm{D} \ll 1$, one uses $\Psi(\omega_\mathrm{D}/2\pi\nu_\mathrm{B}) \sim \ln(\omega_\mathrm{D}/2\pi\nu_\mathrm{B}) - \pi\nu_\mathrm{B}/\omega_\mathrm{D}$

to get

$$Q_{\mathrm{R}}(\tau) \sim \eta \left[\nu_{\mathrm{B}}|\tau| + \frac{\gamma}{\pi} + \frac{1}{\pi}\ln\left(\frac{\omega_{\mathrm{D}}}{2\pi\nu_{\mathrm{B}}}\right) \right], \qquad 2\pi\nu_{\mathrm{B}}|\tau| \gg 1 \text{ and } 2\pi\nu_{\mathrm{B}}/\omega_{\mathrm{D}} \ll 1. \tag{B.24}$$

In another limit where $2\pi\nu_{\mathrm{B}}|\tau| \ll 1$ and $2\pi\nu_{\mathrm{B}}/\omega_{\mathrm{D}} \ll 1$, the sum in Eq. (B.21) may be approximated by an integral as the summand varies only slowly with the integer m. One obtains

$$Q_{\mathrm{R}}(\tau) \sim \eta \left[-\nu_{\mathrm{B}}|\tau| + \pi\nu_{\mathrm{B}}^2\tau^2 + \frac{\nu_{\mathrm{B}}}{\omega_{\mathrm{D}}}\left(1 - \mathrm{e}^{-\omega_{\mathrm{D}}|\tau|}\right) \right.$$
$$\left. + \frac{1}{2\pi}\left[\mathrm{e}^{-\omega_{\mathrm{D}}\tau}\,\mathrm{Ei}(\omega_{\mathrm{D}}\tau) + \mathrm{e}^{\omega_{\mathrm{D}}\tau}\,\mathrm{Ei}(-\omega_{\mathrm{D}}\tau)\right] + \frac{1}{\pi}\ln(\omega_{\mathrm{D}}|\tau|) + \frac{\gamma}{\pi} \right],$$
$$2\pi\nu_{\mathrm{B}}|\tau| \ll 1 \text{ and } 2\pi\nu_{\mathrm{B}}/\omega_{\mathrm{D}} \ll 1, \quad \text{(B.25)}$$

where $\mathrm{Ei}(x) \,\hat{=}\, \wp \int_{-\infty}^{x}\mathrm{d}x\,\mathrm{e}^x/x$ denotes the Exponential Integral function. Expanding this expression up to second order in $\omega_{\mathrm{D}}\tau$, one gets

$$Q_{\mathrm{R}}(\tau) \sim \frac{\eta}{2\pi}\omega_{\mathrm{D}}^2\tau^2\left[\frac{3}{2} - \gamma - \ln(\omega_{\mathrm{D}}|\tau|)\right], \qquad \omega_{\mathrm{D}}|\tau| \ll 1 \text{ and } 2\pi\nu_{\mathrm{B}}/\omega_{\mathrm{D}} \ll 1. \tag{B.26}$$

This quadratic time-dependence at short times is very similar to the one found in case of an exponential cutoff [see Eq. (B.13)].

The real part of the twice integrated bath correlation function and its approximations are shown in Fig. B.2. A comparison between the cases of an exponential and a Drude cutoff is presented in Fig. B.3a-c.

We turn now to the imaginary part $Q_{\mathrm{I}}(\tau)$, starting again from

$$M_{\mathrm{I}}(\tau) = \frac{\eta}{\pi}\int_0^{\infty}\frac{\mathrm{d}\omega}{1 + (\omega/\omega_{\mathrm{D}})^2}\cos(\omega\tau). \tag{B.27}$$

Using Cauchy's theorem, the integral yields

$$M_{\mathrm{I}}(\tau) = \frac{\eta\omega_{\mathrm{D}}}{2}\mathrm{e}^{-\omega_{\mathrm{D}}|\tau|}. \tag{B.28}$$

Integrating and remembering that $Q_{\mathrm{I}}(0) = 0$, we get

$$Q_{\mathrm{I}}(\tau) = \frac{\eta}{2}\mathrm{sgn}(\tau)\left(1 - \mathrm{e}^{-\omega_{\mathrm{D}}|\tau|}\right). \tag{B.29}$$

At long times $\omega_{\mathrm{D}}\tau \gg 1$, this function tends to the asymptotic value $\eta/2$, exactly as in the case of an exponential cutoff [see Eq. (B.17) and Fig. B.3d].

Finally, we need to evaluate the function $N(\tau)$ necessary for the duality relation. This function was defined as [see Eq. (6.82)]

$$N(\tau) \,\hat{=}\, \int_{t_0}^{\tau}\mathrm{d}t' \int_{-\infty}^{\infty}\mathrm{d}t'' \left[\theta(t'' - t_0) - \theta(t'' - t) - \delta(t'' - t_0)\frac{1 - \mathrm{e}^{-\gamma(t-t_0)}}{\gamma}\right] L_{\mathrm{R}}(t' - t''). \tag{B.30}$$
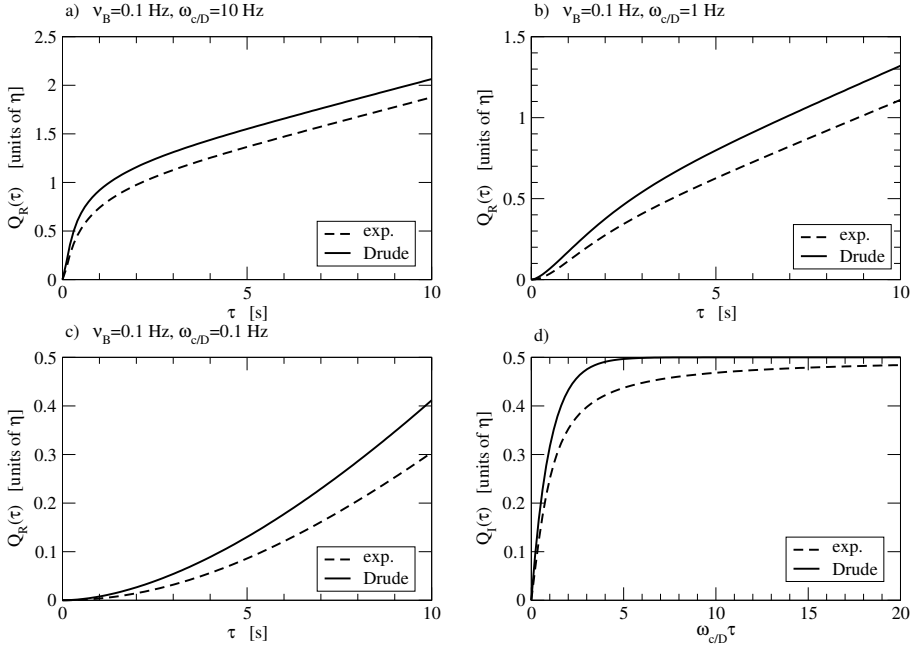
Figure B.3: Comparison between the cases of an exponential and a Drude cutoff: a) the dashed curve shows the real part of the bath correlation function for an Ohmic spectral density with an exponential cutoff, the plain curve with a Drude cutoff, for $\nu_{\mathrm{B}} = 0.1$ Hz and $\omega_{\mathrm{c/D}} = 10$ Hz; b) same as a), for $\nu_{\mathrm{B}} = 0.1$ Hz and $\omega_{\mathrm{c/D}} = 1$ Hz; c) same as a), for $\nu_{\mathrm{B}} = 0.1$ Hz and $\omega_{\mathrm{c/D}} = 0.1$ Hz; d) the dashed curve shows the imaginary part of the bath correlation function for an Ohmic spectral density with an exponential cutoff, the plain curve with a Drude cutoff.

There, t_0 and t are the beginning and the end of the measurement time, whereas γ is the dissipation frequency and also plays the role of the Drude cutoff frequency ω_{D}. Performing the integrals yields

$$N(\tau) = Q_{\mathrm{R}}(\tau - t_0) - Q_{\mathrm{R}}(t - \tau) + Q_{\mathrm{R}}(t - t_0) - \frac{1 - \mathrm{e}^{-\gamma(t - t_0)}}{\gamma} M_{\mathrm{R}}(\tau - t_0). \quad \text{(B.31)}$$

In the long-time limit (LT) characterized by $\gamma(t - t_0) \gg 1$ and $2\pi\nu_{\mathrm{B}}(t - t_0) \gg 1$, the exponentials $\mathrm{e}^{-m\gamma(t - t_0)}$ and $\mathrm{e}^{-2\pi m\nu_{\mathrm{B}}(t - t_0)}$ may be neglected in (B.21), and $Q_{\mathrm{R}}(t - t_0)$ reduces to

$$Q_{\mathrm{R}}(t - t_0) \sim \eta\nu_{\mathrm{B}} \left[t - t_0 - \frac{1}{\gamma} \right], \qquad \text{LT}. \quad \text{(B.32)}$$

More can be said when τ equals any of the transition times t_j and $t'_{j'}$, which lay between t_0 and t, and one considers the rare transitions limit (RT), where the exponentials $e^{-\gamma(\tau-t_0)}$, $e^{-\gamma(t-\tau)}$, $e^{-2\pi\nu_B(\tau-t_0)}$, and $e^{-2\pi\nu_B(t-\tau)}$ are negligible. Similarly, one then has

$$
\left.
\begin{aligned}
M_R(\tau - t_0) &\sim \eta\nu_B \\
Q_R(\tau - t_0) &\sim \eta\nu_B \left[\tau - t_0 - \tfrac{1}{\gamma}\right] \\
Q_R(t - \tau) &\sim \eta\nu_B \left[t - \tau - \tfrac{1}{\gamma}\right]
\end{aligned}
\right\}, \qquad \text{RT.} \tag{B.33}
$$

Putting everything together, we obtain the result

$$
N(\tau) \sim 2\eta\nu_B \left[\tau - t_0 - \frac{1}{\gamma}\right], \qquad \text{LT and RT,} \tag{B.34}
$$

when τ equals any of the transition times in the rare transitions limit.

References

[1] U. Weiss, *Quantum Dissipative Systems* (World Scientific, Singapore, 1999), 2nd ed.

[2] M. Thorwart, *Tunneling and vibrational relaxation in driven multilevel systems*, Ph.D. thesis, University of Augsburg (2000).

[3] I. S. Gradshteyn and I. M. Ryzhik, *Table of Integrals, Series, and Products* (Academic Press, San Diego, 2000), sixth ed.

Summary

In this thesis, ratchet systems operating in the quantum regime are investigated. A ratchet system is a periodic system presenting an intrinsic asymmetry which can be exploited to extract work out of unbiased forces. This rectification phenomenon is called the ratchet effect.

Realistic physical systems unavoidably interact with their environment. This interaction induces energy dissipation and thermal fluctuations, such as the ones that become visible in the phenomenon of Brownian motion. In ratchet systems, instead of considering fluctuations and dissipation as a nuisance which one tries to minimize, one attempts to take advantage of them in order to generate directed transport. This can be done by breaking the thermal equilibrium by means of an unbiased driving force. Such systems are thus also known as Brownian motors.

As a model for ratchet systems, we consider in this thesis the motion of a particle in a one-dimensional periodic and asymmetric potential, interacting with a thermal environment, and subject to an unbiased driving force. We seek to evaluate the velocity of the particle, which characterizes the transport.

In ratchet systems, the direction of the particle velocity depends on control parameters such as the driving force or the temperature of the environment. This feature could be exploited to sort molecules of different kinds, if one were able to find a set of parameters such that the molecules flow in opposite directions.

This thesis is focused on systems where the mass of the particle, together with the length and energy scales defined by the potential, are so small that a quantum mechanical description of the dynamics is necessary. In such quantum ratchets, intrinsic quantum fluctuations as well as the tunnel effect enrich the transport mechanisms. For systems encountered in everyday life, as well as for biological systems, these conditions are not fulfilled and a classical description of the dynamics suffices. Therefore, the investigation of quantum ratchets belongs to the frame of fundamental research.

Whereas the theoretical description of classical ratchet systems is already well developed, the case of quantum ratchets poses additional challenges which have been tackled only recently. In particular, the phenomenological description of the interaction with a thermal environment used in classical mechanics poses a problem.

It consists in the addition of a dissipative viscous force and of a stochastic force to the equation of motion of the particle and is thus not possible in the energy-conserving formalism of quantum mechanics. In this case, one has to include the full dynamics of the environment in the formalism. One then tries to eliminate the numerous degrees of freedom of the environment, in order to get an effective description of the reduced dynamics of the system of interest. The issue of the description of quantum dissipative systems has generated an active research field in the last decades. Quantum ratchets provide a benchmark for such investigations. The recent development of experimental realizations of ratchet systems operating in the quantum regime makes it possible to confront the theoretical description with experiments. In this way, one can make progress in the fundamental understanding required prior to the design of applications.

From a theoretical point of view, methods based on a path integral formalism have been developed for the description of the dynamics of quantum dissipative systems. Prior to this work, the dynamics in a continuous potential has been investigated, e.g., for the cases of a harmonic, a cubic, a double-well, and a sinusoidal potential. The dynamics in a ratchet potential has also been investigated in the semiclassical regime. Other studies have considered tight-binding models with two or more sites. In general, a tight-binding model is a collection of sites which can be occupied by the particle. The sites are arranged in a chain, which is characterized by the positions of the sites and by the on-site energies, describing the energy that the particle has when it occupies the corresponding site. Couplings between the sites enable the particle to make transitions between them. When one considers periodic tight-binding models, the values of the parameters are repeated after some periodicity cell containing n sites in an ideally infinite chain. One then says that the tight-binding model is made of n bands. In a tight-binding model, the discrete description of the motion in terms of localized sites, in contrast to the continuous character of the position in continuous systems, turns out to be very convenient in the evaluation of the velocity. It allows the derivation of an analytical expression for the stationary velocity, in terms of the transition rates between the tight-binding sites. This formalism is presented in Chapter 3 for general periodic tight-binding models. It is discussed further in Chapter 5 for the case of single-band tight-binding models not restricted to nearest neighbors coupling only.

In this thesis, we have applied and extended the path integral formalism to the investigation of quantum ratchets. Starting from a continuous ratchet potential, we have developed two approaches beyond a semiclassical description, discussed in Chapter 4 and Chapter 6, respectively, where the dynamics could be mapped onto that of an effective tight-binding model. Thus we have been able to derive the tight-binding models relevant for the description of quantum ratchets, rather than having to postulate a suitable tight-binding model as in some earlier studies.

In Chapter 4, a parameter regime is chosen such that only few low energy quantum states in each well of the periodic potential are involved in the dynamics of the

particle. These states play the role of the tight-binding sites. The resulting tight-binding model presents as many bands as there are states involved in each potential well. We discuss the mechanism and validity range of this reduction in detail. Then, using the method developed in Chapter 3, we get an analytical expression for the velocity. This quantity shows reversals as a function of the driving force and of the temperature, and it vanishes when only one band is involved.

In Chapter 6, another approach is developed. It leads to a duality relation between the original system and a single-band tight-binding model. This tight-binding model is different from the one involved in the first approach and does not have any direct physical interpretation as far as we understand. The couplings in this dual tight-binding model are related to the amplitude of the potential of the original system. The dissipation strength is opposite in the two systems. The link to a tight-binding description allows us here again to derive an analytical expression for the stationary velocity of the particle. Using further developments of the formalism which are described in Chapter 5, we are able to exhibit the explicit dependence of the velocity on the parameters of the potential. This allows us to characterize the potentials which lead to the highest rectification efficiency. The validity range of this method is different from that of the first approach, and, in particular, the classical limit can be explored.

In Chapter 2, an experimental realization based on quasi one-dimensional arrays of superconducting islands connected by Josephson junctions is discussed. Upon application of a magnetic field perpendicular to the array, one creates vortices in the field formed by the order parameter of the superconducting islands. A current applied across the width of the array acts as a force on the vortices. Their velocity can be measured as a voltage arising between the long edges of the array. The array can be designed in such a way that the vortices feel a periodic and asymmetric potential when moving along the array, and that their dynamics resides in the quantum regime. The relation between the dynamics of the vortices and the theoretical model investigated in this thesis is discussed in detail. Some qualitative results of the experiment are reproduced by the model, however some others, such as the power-law dependence of the voltage-current characteristics of the array, are not understood. We identify criticizable simplifications adopted in the model, and propose further theoretical and experimental developments.

<div style="text-align: right">

Joël Peguiron
Regensburg, July 2005

</div>

Samenvatting

In dit proefschrift worden ratelsystemen onderzocht die in het quantummechanisch regime werken. Een ratelsysteem is een periodiek systeem met een intrinsieke asymmetrie die kan worden gebruikt om arbeid te halen uit krachten die gemiddeld nul zijn (unbiased forces). Dit rectificatieverschijnsel wordt rateleffect genoemd.

Realistische natuurkundige systemen hebben onvermijdelijk wisselwerking met hun omgeving. Deze wisselwerking induceert energiedissipatie en thermische fluctuaties, zoals die die in het verschijnsel van Brownse beweging zichtbaar zijn. In ratelsystemen beschouwt men fluctuaties en dissipatie niet langer als een hinder die men probeert te minimaliseren, maar probeert men daaruit juist voordeel te trekken om gericht transport te genereren. Dit kan door het breken van het thermisch evenwicht door middel van een unbiased drijfkracht worden gedaan. Zulke systemen zijn derhalve ook als Brownse motoren bekend.

Als model voor ratelsystemen beschouwen we in dit proefschrift de beweging van een deeltje in een ééndimensionale periodieke en asymmetrische potentiaal dat wisselwerking met een thermische omgeving en een unbiased drijfkracht heeft. We proberen de snelheid van het deeltje uit te rekenen, die het transport kenmerkt.

In ratelsystemen hangt de transportrichting van controleparameters zoals de drijfkracht of de temperatuur van de omgeving af. Deze eigenschap zou kunnen worden gebruikt om moleculen van verschillende soorten te sorteren, indien een regime van parameters zou kunnen worden gevonden waar de moleculen in omgekeerde richtingen stromen.

Dit proefschrift is op systemen geconcentreerd waarbij de massa van het deeltje en de lengte- en energieschalen, die door de potentiaal bepaald zijn, zo klein zijn dat een quantummechanische beschrijving van de dynamiek nodig is. In zulke quantummechanische ratelsystemen worden de transportmechanismen door intrinsieke quantumfluctuaties en door het tunneleffect verrijkt. Voor systemen die in het alledaagse leven voorkomen, evenals voor biologische systemen, zijn deze voorwaarden niet vervuld en is een klassieke beschrijving van de dynamiek voldoende. Het onderzoek van quantummechanische ratelsystemen behoort dus tot het gebied van fundamenteel onderzoek.

   Terwijl de theoretische beschrijving van klassieke ratelsystemen al goed ontwikkeld is, stelt het geval van quantummechanische ratelsystemen extra uitdagingen die pas recentelijk zijn aangegaan. Vooral de fenomenologische beschrijving van de wisselwerking met een thermische omgeving die in de klassieke mechanica wordt gebruikt vormt een probleem. Die bestaat namelijk in het toevoegen van een dissipatieve visceuze kracht en een stochastische kracht aan de bewegingsvergelijking van het deeltje en is dus niet mogelijk in het energiebehoudend formalisme van de quantummechanica. In dit geval moet de hele dynamiek van de omgeving in het formalisme worden opgenomen. Men probeert dan de talrijke vrijheidsgraden van de omgeving te elimineren, om een effectieve beschrijving van de gereduceerde dynamiek van het systeem van belang te krijgen. Het vraagstuk van de beschrijving van quantummechanische dissipatieve systemen heeft een actief onderzoeksgebied in de afgelopen decennia veroorzaakt. Quantenmechanische ratelsystemen voorzien in een proefsysteem voor een zodanig onderzoek. De recente ontwikkeling van experimentele realisaties van ratelsystemen die in het quantummechanisch regime werken opent de mogelijkheid om de theoretische beschrijving met experimenten te vergelijken. Daardoor kunnen vorderingen worden gemaakt in het fundamenteel begrip dat nodig is voor het ontwerp van toepassingen.

   Vanuit theoretische invalshoek zijn methoden, gebaseerd op een padintegraalformalisme, voor de beschrijving van de dynamiek van quantummechanische dissipatieve systemen ontwikkeld. Voorafgaand aan dit werk is de dynamiek in een continue potentiaal onderzocht in bijvoorbeeld de gevallen van een harmonische, een kubische, een dubbelputs- en een sinusoïdale potentiaal. De dynamiek in een ratelpotentiaal is ook al in het semi-klassieke regime onderzocht. In andere onderzoeken zijn tight-binding model met twee of meer sites beschouwd. Een tight-binding model is in het algemeen een verzameling van sites die het deeltje kan bezetten. De sites vormen een ketting die gekenmerkt wordt door de plaats van de sites en de verschillende waarden van de energie die het deeltje heeft als het de desbetreffende site bezet. Koppelingen tussen de sites laten overgangen van het deeltje tussen de sites toe. In een periodiek tight-binding model worden de waarden van parameters vanaf een periodiciteitscel van n sites in een idealiter oneindige ketting gerepeteerd. Men spreekt van een tight-binding model met n banden. In een tight-binding model blijkt de discrete beschrijving van de beweging in termen van gelokaliseerde sites, in tegenstelling tot het continue kenmerk van de plaats in een continu systeem, heel geschikt voor de berekening van de snelheid te zijn. Het staat de afleiding van een analytische uitdrukking voor de stationaire snelheid in termen van de overgangssnelheden tussen de tight-binding sites toe. Dit formalisme wordt in hoofdstuk 3 voor algemene periodieke tight-binding modellen gepresenteerd. Het wordt in hoofdstuk 5 in het geval van enkelbands tight-binding modellen zonder beperking van de koppelingen tot meest nabije sites alleen verder bediscussieerd.

   In dit proefschrift hebben we het padintegraalformalisme op het onderzoek van quantummechanische ratelsystemen toegepast en uitgebreid. Uitgaande van een

continue ratelpotentiaal hebben we twee benaderingen ontwikkeld, bediscussieerd in hoofdstukken 4 en 6, die verder dan een semi-klassieke beschrijving gaan en waar de dynamiek op die van een effectief tight-binding model kon worden geprojecteerd. Het is ons dus gelukt om de tight-binding modellen die relevant zijn voor de beschrijving van quantummechanische ratelsystemen af te leiden, in plaats van een passend tight-binding model te moeten postuleren, zoals in eerdere onderzoeken.

In hoofdstuk 4 wordt een regime van parameters zodanig gekozen, dat slechts enkele quantummechanische toestanden met lage energie in ieder put in de dynamiek van het deeltje worden betrokken. Deze toestanden spelen de rol van de tight-binding sites. Het resulterende tight-binding model bevat evenveel banden als er betrokken toestanden in ieder put zijn. We bediscussiëren het mechanisme en het geldigheidsbereik van deze herleiding uitgebreid. We verkrijgen vervolgens een analytische uitdrukking voor de snelheid door gebruik te maken van de methode ontwikkeld in hoofdstuk 3. De snelheid laat omkeringen als functie van de drijfkracht en de temperatuur zien, en wordt nul als slechts één band betrokken is.

In hoofdstuk 6 wordt een andere benadering ontwikkeld. Deze leidt tot een dualiteitsrelatie tussen het oorspronkelijke systeem en een enkelbands tight-binding model. Dit tight-binding model verschilt van het tight-binding model dat betrokken is in de eerste benadering en heeft voor zover we begrijpen geen directe natuurkundige interpretatie. De koppelingen in dit duale tight-binding model zijn verbonden met de amplitude van de potentiaal van het oorspronkelijke systeem. De sterkte van dissipatie is omgekeerd in de twee systemen. De relatie met een tight-binding model staat ons hier opnieuw toe om een analytische uitdrukking voor de stationaire snelheid van het deeltje af te leiden. Met gebruikmaking van verdere ontwikkelingen van het formalisme, die in hoofdstuk 5 worden beschreven, lukt het ons om de expliciete afhankelijkheid van de snelheid van de parameters van de potentiaal te laten zien. Dit staat ons toe om de potentialen te kenmerken die het hoogste rectificatievermogen bezitten. Het geldigheidsbereik van deze methode verschilt van dat van de eerste benadering, en de klassieke limiet kan in het bijzonder worden onderzocht.

In hoofdstuk 2 wordt een experimentele realisatie bediscussieerd die gebaseerd is op een quasi-ééndimensionaal netwerk van supergeleidende eilanden die door Josephson juncties verbonden zijn. Onder het aanleggen van een magnetisch veld loodrecht op het netwerk ontstaan vortices in het veld dat wordt gevormd door de ordeparameter van de supergeleidende eilanden. Een stroom die door de breedte van het netwerk is aangelegd werkt als een kracht op de vortices. Hun snelheid kan door de spanning die tussen de lange kanten van het netwerk ontstaat worden gemeten. Het netwerk kan zodanig worden ontworpen, dat de vortices een periodieke en asymmetrische potentiaal voelen als ze zich langs het netwerk bewegen, en dat hun dynamiek in het quantummechanisch regime ligt. De relatie tussen de dynamiek van de vortices en het theoretische model dat in dit proefschrift is onderzocht wordt uitgebreid bediscussieerd. Sommige kwalitatieve resultaten van het experiment worden door het model gereproduceerd, maar andere, zoals de machtswet gevolgd door de

spanning-stroom karakteristiek van het netwerk, blijven onbegrepen. We identifice-
ren bekritiseerbare vereenvoudigingen die in het model zijn aangenomen en stellen
verdere theoretische en experimentele ontwikkelingen voor.

Joël Peguiron
Regensburg, juli 2005

Résumé

Cette thèse est consacrée à l'étude des crécelles opérant dans le régime quantique. Une crécelle, ou système à rochet, est un système périodique présentant une asymétrie qui peut être exploitée pour extraire un travail à partir de forces non biaisées. Ce phénomène de rectification est appelé l'effet crécelle.

Les systèmes physiques réalistes interagissent inévitablement avec leur environnement. Ceci cause de la dissipation d'énergie et des fluctuations thermiques comme celles qui sont visibles dans le phénomène de mouvements browniens. Dans le cas des crécelles, plutôt que de considérer les fluctuations et la dissipation comme une nuisance qu'on cherche à minimiser, on essaie d'en tirer parti afin de générer un transport dirigé. Ceci peut être réalisé en brisant l'équilibre thermique au moyen d'une force motrice non biaisée. Par conséquent, de tels systèmes sont également appelés moteurs browniens.

Dans cette thèse, nous considérons en guise de modèle pour les crécelles le mouvement d'une particule dans un potentiel unidimensionnel, périodique et asymétrique, interagissant avec un environnement thermique et soumise à une force motrice non biaisée. Nous voulons calculer la vitesse de la particule, qui caractérise le transport.

La direction de la vitesse de la particule dans ces crécelles dépend de paramètres de contrôle tels que la force motrice ou la température de l'environnement. Cette propriété pourrait être exploitée pour trier des molécules de différentes sortes, si l'on était capable de trouver un régime de paramètres où les molécules circulent dans des directions opposées.

Cette thèse se concentre sur les systèmes où la masse de la particule ainsi que les échelles de longueur et d'énergie définies par le potentiel sont si petites qu'une description au moyen de la mécanique quantique est nécessaire. Dans ces crécelles quantiques, les fluctuations quantiques intrinsèques ainsi que l'effet tunnel enrichissent les mécanismes de transport. Pour les systèmes qu'on rencontre dans la vie de tous les jours ainsi que pour les systèmes biologiques, ces conditions ne sont pas remplies et une description classique de la dynamique est suffisante. En conséquence, l'étude des crécelles quantiques s'inscrit dans le cadre de la recherche fondamentale.

Alors que la description théorique des crécelles classiques est déjà bien développée, le cas des crécelles quantiques pose des défis supplémentaires qui n'ont été relevés

que récemment. En particulier, la description phénoménologique de l'interaction avec un environnement thermique utilisée en mécanique classique pose problème. En effet, elle consiste à ajouter une force visqueuse dissipative et une force stochastique à l'équation du mouvement et n'est donc pas possible dans le formalisme de la mécanique quantique, où l'énergie est conservée. Dans ce cas, on est obligé d'inclure la dynamique complète de l'environnement au formalisme. On essaie alors d'éliminer les nombreux degrés de liberté de l'environnement afin d'obtenir une description effective de la dynamique réduite du système qui nous intéresse. Le problème de la description des systèmes dissipatifs quantiques a généré un domaine de recherche actif au cours des dernières décennies. Les crécelles quantiques fournissent un banc de test pour de telles recherches. Le récent développement de réalisations expérimentales de crécelles opérant dans le régime quantique ouvre la possibillté de confronter la description théorique avec des expériences. On peut ainsi progresser dans la compréhension fondamentale nécessaire à la conception d'applications.

D'un point de vue théorique, des méthodes basées sur un formalisme en termes d'intégrales de chemin ont été développées pour décrire les systèmes quantiques dissipatifs. Avant le présent travail, la dynamique dans un potentiel continu a été étudiée dans le cas d'un potentiel harmonique, cubique, sinusoïdal ou d'un double puits, par exemple. La dynamique dans un potentiel de crécelle a également été étudiée dans le régime semi-classique. D'autres travaux ont été consacrés à des modèles à liaison forte comprenant deux ou plusieurs sites. D'un point de vue général, un modèle à liaison forte est un ensemble de sites qui peuvent être occupés par la particule. Les sites sont arrangés en une chaîne caractérisée par la position des sites et les différentes valeurs de l'énergie que possède la particule lorsqu'elle occupe chacun des sites. Des couplages entre les sites permettent à la particule d'effectuer des transitions entre eux. Dans un modèle à liaison forte périodique, les valeurs des paramètres se répètent après une cellule de périodicité contenant n sites, dans une chaîne idéalement infinie. On parle alors d'un modèle à liaison forte à n bandes. Dans un modèle à liaison forte, la nature discrète de la description dynamique en termes de sites localisés, au contraire du caractère continu de la position dans les systèmes continus, s'avère très pratique pour l'évaluation de la vitesse. Cela nous permet de dériver une expression analytique pour la vitesse stationnaire en termes des taux de transition entre les sites du modèle à liaison forte. Ce formalisme est présenté au chapitre 3 pour des modèles à liaison forte périodiques généraux. Il est discuté en plus grand détail au chapitre 5 dans le cas d'un modèle à liaison forte à une seule bande avec des couplages non restreints aux plus proches voisins seulement.

Dans cette thèse, nous avons appliqué et étendu le formalisme des intégrales de chemin à l'étude des crécelles quantiques. A partir d'un potentiel de crécelle continu, nous avons développé deux approches dépassant une description semi-classique, présentées aux chapitres 4 et 6, où la dynamique a pu être reliée à celle d'un modèle à liaison forte effectif. Nous sommes donc parvenus à dériver les modèles à liaison forte appropriés à la description des crécelles quantiques, plutôt que de devoir postuler

un modèle à liaison forte convenable comme dans certains travaux antérieurs.

Au chapitre 4, nous choisissons un régime de paramètres tel que seuls quelques états quantiques de basse énergie dans chaque puits du potentiel périodique sont impliqués dans la dynamique de la particule. Ces états jouent le rôle des sites du modèle à liaison forte. Le système résultant présente autant de bandes qu'il y a d'états impliqués dans chaque puits de potentiel. Nous discutons en détail le mécanisme et le domaine de validité de cette réduction. En utilisant la méthode développée au chapitre 3, nous obtenons ensuite une expression analytique pour la vitesse. Elle présente des inversions en fonction de la force motrice et de la température, et elle s'annule lorsqu'il n'y a qu'une seule bande impliquée.

Au chapitre 6, nous développons une autre approche. Celle-ci conduit à une relation de dualité entre le système original et un modèle à liaison forte à une seule bande. Ce modèle à liaison forte est différent de celui qui est impliqué dans la première approche et ne présente pas d'interprétation physique directe dans l'état actuel de notre compréhension. Les couplages de ce modèle à liaison forte dual sont reliés à l'amplitude du potentiel du système original. L'intensité de la dissipation est opposée dans les deux systèmes. Ici à nouveau, le lien à une description en termes d'un modèle à liaison forte nous permet de dériver une expression analytique pour la vitesse stationnaire de la particule. En utilisant des développements supplémentaires du formalisme, présentés au chapitre 5, nous parvenons à extraire la dépendance explicite de la vitesse des paramètres du potentiel. Ceci nous permet de caractériser les potentiels qui présentent le plus grand pouvoir de rectification. Le domaine de validité de cette méthode est différent de celui de la première méthode et nous permet en particulier d'explorer la limite classique.

Au chapitre 2, nous discutons une réalisation expérimentale basée sur un réseau quasi unidimensionnel d'îlots supraconducteurs reliés par des jonctions Josephson. Par l'application d'un champ magnétique perpendiculaire au réseau, on crée des vortex dans le champ formé par le paramètre d'ordre des îlots supraconducteurs. Un courant appliqué à travers le réseau en largeur fait l'effet d'une force sur les vortex. Leur vitesse peut être mesurée par la tension générée entre les longs côtés du réseau. Le réseau peut être réalisé de telle façon que les vortex ressentent un potentiel périodique et asymétrique lorsqu'ils se déplacent le long du réseau et que leur dynamique réside dans le régime quantique. La relation entre la dynamique des vortex et le modèle théorique étudié dans cette thèse est discutée en détail. Certains résultats qualitatifs de l'expérience sont reproduits par le modèle mais d'autres, comme la dépendance en loi de puissance de la caractéristique tension-courant du réseau, restent incompris. Nous identifions des simplifications critiquables adoptées dans le modèle et proposons des développements théoriques et expérimentaux ultérieurs.

Joël Peguiron

Ratisbonne, juillet 2005

Zusammenfassung

In der vorliegenden Dissertation werden Ratschensysteme im Quantenbereich erforscht. Ein Ratschensystem ist ein periodisches System mit einer inneren Asymmetrie, die benutzt werden kann, um Arbeit aus im Zeitmittel verschwindenden Kräften zu erzeugen. Dieses Gleichrichtungsphänomen wird Ratscheneffekt genannt.

Realistische physikalische Systeme erfahren unvermeidlich Wechselwirkung mit ihrer Umgebung. Diese Wechselwirkung verursacht Energiedissipation und thermische Fluktuationen, wie diejenigen, die im Phänomen der Brownschen Bewegung zu sehen sind. In Ratschensystemen betrachtet man Fluktuationen und Dissipation nicht als eine Behinderung, die man zu minimieren versucht, sondern man versucht daraus Vorteil zu ziehen, um gerichteten Transport zu erzeugen. Das kann durch das Brechen des thermischen Gleichgewichts mittels einer im Zeitmittel verschwindenden Antriebskraft gemacht werden. Solche Systeme sind deswegen auch als Brownsche Motoren bekannt.

Als Modell für Ratschensysteme betrachten wir in dieser Dissertation die Bewegung eines Teilchens, das Wechselwirkung mit einer thermischen Umgebung und einer im Zeitmittel verschwindenden Antriebskraft erfährt, in einem eindimensionalen periodischen und asymmetrischen Potential. Wir versuchen, die Geschwindigkeit des Teilchens zu berechnen, die den Transport charakterisiert.

In Ratschensystemen hängt die Transportrichtung von Kontrollparametern wie der Antriebskraft oder der Temperatur der Umgebung ab. Diese Eigenschaft könnte benutzt werden, um Moleküle verschiedener Art zu sortieren, falls man einen Parameterbereich finden würde, in dem die Moleküle in gegensätzliche Richtungen fließen.

Diese Dissertation ist auf Systeme konzentriert, in denen die Masse des Teilchens und die durch das Potential bestimmten Länge- und Energieskalen so klein sind, dass eine quantenmechanische Beschreibung der Dynamik erforderlich ist. In solchen Quantenratschen werden die Transportmechanismen durch innere Quantenfluktuationen und durch den Tunneleffekt bereichert. Für Systeme des Alltagslebens wie für biologische Systeme sind diese Bedingungen nicht erfüllt und eine klassische Beschreibung der Dynamik reicht. Die Erforschung der Quantenratschen gehört deswegen zum Bereich der Grundlagenforschung.

Während die theoretische Beschreibung der klassischen Ratschensysteme bereits gut entwickelt wurde, stellt der Fall der Quantenratschen zusätzliche Herausforderungen, die erst kürzlich angenommen wurden. Insbesondere stellt die phänomenologische Beschreibung der Wechselwirkung mit einer thermischen Umgebung, die in der klassischen Mechanik benutzt wird, ein Problem dar. Die besteht nämlich darin, eine dissipative viskose Kraft und eine stochastische Kraft zur Bewegungsgleichung hinzuzufügen, und ist deswegen in dem energieerhaltenden Formalismus der Quantenmechanik nicht möglich. In diesem Fall muss man die ganze Dynamik der Umgebung im Formalismus einschließen. Man versucht dann, die zahlreichen Freiheitsgrade der Umgebung zu eliminieren, um eine effektive Beschreibung der reduzierten Dynamik des Systems zu erhalten. Die Frage der Beschreibung der dissipativen Quantensysteme hat in den letzten Jahrzehnten ein aktives Forschungsgebiet verursacht. Quantenratschen bieten ein Prüfsystem für eine solche Erforschung. Die neue Entwicklung von experimentellen Realisierungen von Ratschensystemen im Quantenbereich, ermöglicht den Vergleich der theoretischen Beschreibung mit Experimenten. Auf diese Weise kann man Grundverständnis gewinnen, das nötig ist, um Anwendungen zu entwerfen.

Von einem theoretischen Gesichtspunkt aus wurden auf einem Pfadintegralformalismus basierte Methoden für die Beschreibung der Dynamik der dissipativen Quantensysteme entwickelt. Vor dieser Arbeit wurde die Dynamik in kontinuierlichen Potentialen erforscht, zum Beispiel in einem harmonischen, einem kubischen, einem Doppelmulden- und einem sinusförmigen Potential. Die Dynamik in einem Ratschenpotential wurde auch bereits im semi-klassischen Bereich erforscht. In anderen Arbeiten wurden tight-binding Modelle mit zwei oder mehr Gitterpunkten betrachtet. Ein tight-binding Modell ist im allgemeinen eine Anzahl diskreter Punkte, die das Teilchen besetzen kann. Die Gitterpunkte bilden eine Kette, die durch den Ort der Gitterpunkte und die verschiedenen Energiewerte, die das Teilchen auf den entsprechenden Gitterpunkten besitzt, charakterisiert wird. Kopplungen zwischen den Gitterpunkten erlauben Übergänge des Teilchens zwischen ihnen. In einem periodischen tight-binding Modell wiederholen sich die Werte der Parameter von einer Elementarzelle von n Gitterpunkten in einer ideell unendlichen Kette. Man spricht dann von einem tight-binding Modell mit n Bändern. In einem tight-binding Modell erweist sich die diskrete Beschreibung der Bewegung, ausgedrückt durch lokalisierte Gitterpunkte, im Gegensatz zum kontinuierlichen Charakter des Ortes in kontinuierlichen Systemen, als besonders geeignet zur Berechnung der Geschwindigkeit. Sie erlaubt die Herleitung eines analytischen Ausdrucks für die stationäre Geschwindigkeit ausgedrückt durch die Übergangsraten zwischen den Gitterpunkten des tight-binding Modells. Dieser Formalismus wird im Kapitel 3 für allgemeine periodische tight-binding Modelle vorgelegt. Er wird weiter diskutiert im Kapitel 5 im Fall der Einzelband tight-binding Modelle ohne Beschränkung der Kopplungen zu den nächsten Nachbarn.

In der vorliegenden Dissertation haben wir den Pfadintegralformalismus auf die

Erforschung der Quantenratschen angewandt und weiterentwickelt. Ausgehend von einem kontinuierlichen Ratschenpotential haben wir zwei Herangehensweisen jenseits einer semi-klassischen Beschreibung entwickelt, diskutiert in den Kapiteln 4 und 6, in denen die Dynamik auf diejenige eines effektiven tight-binding Modells abgebildet werden konnte. Dadurch ist es uns gelungen, die für die Quantenratschen relevanten tight-binding Beschreibungen herzuleiten, statt wie in früheren Arbeiten ein passendes tight-binding Modell postulieren zu müssen.

Im Kapitel 4 wird der Parameterbereich so gewählt, dass nur wenige Quantenzustände niedriger Energie in jedem Topf des periodischen Potentials in der Dynamik des Teilchens beteiligt sind. Diese Zustände werden die Gitterpunkte des tight-binding Modells. Das resultierende tight-binding Modell umfasst soviel Bänder, wie es beteiligte Zustände in jedem Potentialtopf gibt. Wir diskutieren den Mechanismus sowie den Gültigkeitsbereich dieser Reduktion ausführlich. Danach erhalten wir einen analytischen Ausdruck für die stationäre Geschwindigkeit durch Anwendung der im Kapitel 3 entwickelten Methoden. Die Geschwindigkeit zeigt Vorzeichenwechsel als Funktion der Antriebskraft und der Temperatur, und verschwindet wenn nur ein Band beteiligt ist.

Im Kapitel 6 wird eine andere Methode entwickelt. Sie führt zu einer Dualitätsbeziehung zwischen dem ursprünglichen System und einem Einzelband tight-binding Modell. Dieses tight-binding Modell ist verschieden von demjenigen, das in der ersten Methode beteiligt ist, und hat soweit wir es verstehen keine direkte physikalische Interpretation. Die Kopplungen in diesem dualen tight-binding Modell sind mit der Potentialamplitude des ursprünglichen Systems verbunden. Die Intensität der Dissipation ist in beiden Systemen entgegengesetzt. Die Verbindung mit einer tight-binding Beschreibung erlaubt uns hier wieder, einen analytischen Ausdruck für die stationäre Geschwindigkeit des Teilchens herzuleiten. Durch Weiterentwicklung des Formalismus, die im Kapitel 5 beschrieben wird, gelingt es uns, die explizite Abhängigkeit der Geschwindigkeit von den Potentialparametern zu zeigen. Das erlaubt uns, die Potentiale zu charakterisieren, die das höchste Gleichrichtungsvermögen besitzen. Der Gültigkeitsbereich dieser Methode ist verschieden von demjenigen der ersten und insbesondere kann der klassische Limes erforscht werden.

Im Kapitel 2 wird eine experimentelle Realisierung diskutiert, die auf quasi-eindimensionalen Gittern von supraleitenden Inseln, mit Josephson-Kontakten verbunden, basiert ist. Durch Anlegen eines Magnetfeldes senkrecht zum Gitter entstehen Vortices im Feld, das aus dem Ordnungsparameter der supraleitenden Inseln besteht. Ein Strom, der quer zum Gitter angelegt wird, wirkt wie eine Kraft auf die Vortices. Ihre Geschwindigkeit kann durch die Spannung gemessen werden, die zwischen den langen Kanten des Gitters entsteht. Das Gitter kann derart entworfen werden, dass die Vortices ein periodisches und asymmetrisches Potential spüren, wenn sie sich das Gitter entlang bewegen, und dass ihre Dynamik sich im Quantenbereich befindet. Der Zusammenhang zwischen der Dynamik der Vortices und dem theoretischen Modell wird ausführlich diskutiert. Einige qualitative Ergebnisse des

Experiments wurden durch das Modell reproduziert, doch andere, wie das Potenz-gesetz bei der Strom-Spannungs-Charakteristik des Gitters, bleiben unverstanden. Wir identifizieren angreifbare Vereinfachungen, die im Modell angenommen wurden, und schlagen weitere theoretische und experimentelle Entwicklungen vor.

Joël Peguiron
Regensburg, Juli 2005

List of publications

1. *Quantum Ratchets with Few Bands below the Barrier*,
   M. Grifoni, M. S. Ferreira, J. Peguiron, and J. B. Majer,
   Phys. Rev. Lett. **89**, 146801 (2002), also cond-mat/0208549

2. *Quantum Ratchet Effect for Vortices*,
   J. B. Majer, J. Peguiron, M. Grifoni, M. Tusveld, and J. E. Mooij,
   Phys. Rev. Lett. **90**, 056802 (2003), also cond-mat/0301073

3. *Duality Relation for Quantum Ratchets*,
   J. Peguiron and M. Grifoni,
   Phys. Rev. E **71**, 010101(R) (2005), also cond-mat/0407759

4. *Quantum Brownian motion in ratchet potentials: duality relation and its consequences*,
   J. Peguiron and M. Grifoni,
   accepted for publication in Chem. Phys.

Curriculum Vitae

1$^{\text{st}}$ February 1978   Born in Neuchâtel (Switzerland)

8/1993 – 7/1996   High school, La Chaux-de-Fonds (Switzerland)

10/1996 – 6/2001   Study of physics, University of Neuchâtel

7/2000 – 9/2000   Trainee under the supervision of Dr. Peter Allenspach in the Laboratory for Neutron Scattering, Paul Scherrer Institut, Villigen (Switzerland)
Project: *Characterization of Mica Analyser Crystals for MARS*

10/2000 – 6/2001   Diploma thesis under the supervision of Prof. Hans Beck in the Condensed Matter Theory group, University of Neuchâtel
Subject: *Une approche à N corps du modèle de Hubbard unidimensionnel (A Many-body Approach to the One-dimensional Hubbard Model)*

7/2001 – 9/2005   Ph.D. research on *Quantum Ratchets* under the supervision of Prof. Milena Grifoni and Prof. Gerrit Bauer in the Theory group, Kavli Institute of Nanoscience, Delft University of Technology (The Netherlands)
Project supported by the Foundation for Fundamental Research on Matter (FOM), Utrecht (The Netherlands)

10/2003 – 9/2005   Guest in the Quantum Transport and Dissipation group led by Prof. Milena Grifoni, University of Regensburg (Germany)